

UC Merced

UC Merced Electronic Theses and Dissertations

Title

An Investigation into the Role of Protein-Based Viral Structural Features in Mediating the Infectivity of SARS-CoV-2

Permalink

<https://escholarship.org/uc/item/8f66f2wz>

Author

Bains, Arjan Singh

Publication Date

2023

Copyright Information

This work is made available under the terms of a Creative Commons Attribution-NonCommercial-ShareAlike License, available at <https://creativecommons.org/licenses/by-nc-sa/4.0/>

Peer reviewed|Thesis/dissertation

UNIVERSITY OF CALIFORNIA, MERCED

An Investigation into the Role of Protein-Based Viral Structural Features in Mediating the Infectivity of SARS-CoV-2

A dissertation submitted in partial satisfaction of the

requirements for the degree of

Doctor of Philosophy

in

Chemistry and Biochemistry

by

Arjan Singh Bains

Committee in charge:

Professor Michael Colvin, Chair of Advisory Committee

Professor Victor Muñoz Van Den Eynde

Professor Ramendra Saha

Professor Patricia LiWang, Supervisor

2023

Copyright  
Arjan Singh Bains, 2023  
All Rights Reserved

The dissertation of Arjan Singh Bains, titled, "An Investigation into the Role of Protein-Based Viral Structural Features in Mediating the Infectivity of SARS-CoV-2", is approved, and is acceptable in quality and form for publication on microfilm and electronically:

\_\_\_\_\_ Date \_\_\_\_\_

Professor Ramendra Saha

\_\_\_\_\_ Date \_\_\_\_\_

Professor Victor Muñoz Van Den Eynde

Supervisor \_\_\_\_\_ Date \_\_\_\_\_

Professor Patricia J. LiWang

Chair \_\_\_\_\_ Date \_\_\_\_\_

Professor Michael Colvin

University of California, Merced

2023

*Dedications*

## Table of Contents

I. List of Abbreviations.....	viii
II. List of Figures .....	xiv
III. List of Tables .....	xvi
IV. Acknowledgments .....	xvii
V. Vita for Name .....	xviii
VI. Abstract .....	xix
Chapter 1 Introduction .....	1
1.1 Introducing Coronaviruses .....	1
1.1.1 A Note on the Context of Coronavirus History .....	1
1.1.2 The Phylogeny of Coronaviruses.....	1
1.1.3 The Origin of SARS-CoV-2.....	3
1.1.4 The Recent History of the Covid-19 Pandemic .....	4
1.1.5 Lockdowns and Unexpected Coronavirus Mutations .....	5
1.2 Section 2: Features of SARS-CoV-2 Viral Infection.....	8
1.2.1 SARS-CoV-2 Viral Infection.....	8
1.3 The Role of the SARS-CoV-2 Spike Protein Dynamics in Viral Infection and Entry .....	9
1.4 References: .....	15
Chapter 2 The Effect of Select SARS-CoV-2 N-linked Glycans and Variant of Concern Spike Protein Mutations on C-Type Lectin Receptor-Mediated Infection.....	23
2.1 Abstract.....	23
2.2 Introduction .....	23
2.3 Results.....	27
2.3.1 Some, But Not All, SARS-CoV-2 Spike NTD Glycans Affect hACE2 Mediated Infectivity.....	27
2.3.2 Some SARS-CoV-2 Spike Glycans Mediate Lectin Receptor Binding and Transfer to Susceptible Cell Lines .....	30
2.3.3 Deconvoluting Trans-Infection Propensity From Direct-Infectivity Reveals Apparent Bias of DC-SIGN For N17 and N122 .....	32
2.3.4 DC-SIGN Mediated Trans-infection Is Verified By Mannan Inhibition .....	34
2.3.5 Abolishing Clusters of Glycans Severely Attenuates SARS-CoV-2 Pseudoviral Infectivity.....	35
2.3.6 Omicron BA.2 Strain May Interact with Other Cell Surface Proteins to Facilitate Trans-Infection .....	38

2.4 Discussion .....	41
2.5 Conclusions .....	47
2.6 Methods and Materials.....	48
2.6.1 Cell Lines.....	48
2.6.2 Pseudovirus Production.....	49
2.6.3 Pseudovirus Titration.....	50
2.6.4 Virus Infectivity Assays .....	51
2.7 Supplemental Figures .....	52
2.8 References .....	65
Chapter 3 The Antiviral Activity of Lectin Griffithsin Against SARS-CoV-2 Appears to be Enhanced By Interactions With Structural Proteins.....	79
3.1 Abstract.....	79
3.2 Introduction .....	80
3.3 Results.....	86
3.3.1 Wild-Type Griffithsin and M78Q Griffithsin Both Display Moderate Anti-SARS-CoV-2 Inhibitory Capabilities .....	86
3.3.2 Removing the Cross-Linking Capability of Griffithsin Does Not Appear to Affect the Inhibitory Capability of Griffithsin .....	90
3.3.3 Grft is a Moderate Inhibitor of Direct Infection, and Does Not Prevent DC-SIGN Facilitated Trans-infection .....	92
3.3.4 Additional SARS-CoV-2 structural proteins do not significantly contribute to Trans-Infection .....	99
3.3.5 Additional SARS-CoV-2 structural proteins modulate viral susceptibility to Griffithsin inhibition of hACE2 Direct Infection.....	104
3.4 Discussion .....	106
3.5 Methods and Materials.....	110
3.5.1 DNA Construction.....	110
3.5.2 Protein Production and Purification.....	111
3.5.3 Nuclear Magnetic Resonance (NMR) Spectroscopy .....	112
3.5.4 Cell Lines.....	112
3.5.5 Pseudovirus Production.....	114
3.5.6 Pseudovirus Titration.....	115
3.5.7 Virus Direct-Infectivity Assays.....	115
3.5.8 Virus Direct-Infectivity Control Assays of Raji Cells .....	116
3.5.9 Virus Raji Cell Mediated Trans-Infectivity Assays .....	117
3.5.10 Virus 3t3 Cell Mediated Trans-Infectivity Assays .....	118
3.6 Supplemental Figures .....	120

3.7 References .....	131
Chapter 4 An Investigation into SARS-CoV-2 Pseudotyped Virus Stability and the Development of Assays to Evaluate the Physical Properties of Virions.....	141
4.1 Abstract.....	141
4.2 Introduction .....	141
4.3 Results.....	145
4.3.1 Virus Survival on Various Produce Surfaces.....	145
4.3.2 Effect of Gaseous Ozone on the Surface Survival of SARS-CoV-2 .....	146
4.3.3 The Effect of Gaseous Ozone on Viral SARS-CoV-2 Spike .....	149
4.4 Discussion .....	151
4.5 Future Experiments and Preliminary Testing.....	152
4.5.1 Bio-Layer Interferometry as a Means to Measure Structural Features of Membrane-Bound Viruses- Screening for Solvents .....	152
4.5.2 Bio-Layer Interferometry as a Means to Measure Structural Features of Membrane-Bound Viruses- Screening for Virus Detection .	155
4.6 Methods and Materials.....	157
4.6.1 Pseudovirus and Plasmids Creation .....	157
4.6.2 Food Samples .....	158
4.6.3 Artificial Contamination of Produce and Treatment with Ozone ...	158
4.6.4 Generation of Ozone .....	159
4.6.5 Virus Infectivity Assays .....	159
4.6.6 Virion Capture Enzyme-Linked Immunosorbent Assay .....	160
4.6.7 Bio-Layer Interferometry .....	160
4.7 References .....	161
Chapter 5 Conclusion.....	167
5.1 Future Directions of SARS-CoV-2 Spike S1 Domain Glycan Mutation Research .....	167
5.2 Future Directions on Lectin-Based Inhibitors of SARS-CoV-2 Coronavirus	169
5.3 Future Directions on Assessing the Stability of SARS-CoV-2 Pseudotyped Lentivirions.....	171
5.4 Final Thoughts .....	171
5.5 References .....	172



## I. List of Abbreviations

3t3 cells	Spontaneously immortalized primary mouse embryonic fibroblast cells
3t3 DC-SIGN+ cells	Spontaneously immortalized primary mouse embryonic fibroblast cells transfected to permanently express DC-SIGN
B-cell	Lymphocytes that mature in the Bones marrow. They can bind to foreign antigens and initiate an antibody response.
BEI	Biodefense and Emerging Infections Research Resources Repository
BLI	Bio-Layer Interferometry
bp	Base Pair
BSL-2	Laboratory safety classification Biosafety level 2
BSA	Bovine Serum Albumin
Caco-2	Immortalized cell line originally derived from a colon carcinoma
Calu-1	Immortalized lung epithelial epidermoid carcinoma cell line
CD209	Gene encoding for DC-SIGN
CD4	Cluster of Differentiation 4
CDC	Center for Disease Control
ChVP	Chimpanzee herpesvirus
CLEC4G	C-type lectin domain family 4 member G
Covid-19	Coronavirus disease 2019
CPRG	Chlorophenol Red- $\beta$ -D-galactopyranoside
CRD	Carbohydrate Recognition Domain
Cryo-EM	Cryogenic Electron Microscopy
CTD1	C-Terminal Domain 1
CTD2	C-Terminal Domain 2
cVLP	coronavirus-like particles
CXCR4	C-X-C Chemokine receptor type 4 (originally referred to as fusin)
DC-SIGN	Dendritic Cell-Specific Intercellular adhesion molecule-3-Grabbing Non-integrin
DMEM	Dulbecco Modified Eagle Medium

DNA	Deoxynucleic Acid
dNTP	deoxyriboNucleotide TriPhosphate
E	SARS-CoV-2 Envelope structural protein
EBV	Epstein-Barr Virus
EDTA	Ethylenediaminetetraacetic acid, also known as 2-[2-bis(carboxymethyl)amino]ethyl-(carboxymethyl)amino]acetic acid
ELISA	Enzyme-Linked ImmunoSorbent Assay
ENV	HIV Envelope protein gp160
FBS	Fetal Bovine Serum
FP	Fusion Peptide
Gag	Group-specific antigen
GISAID	Global Initiative on Sharing All Influenza Data
GlcNAc	N-Acetyl-glucosamine
gp	Glycoprotein
gp120	Envelope glycoprotein 120; part of envelope protein complex on HIV surface
gp41	Envelope glycoprotein 41; part of envelope protein complex on HIV surface
Grft	Griffithsin
GLG-3A	M78Q Griffithsin – Linker – M78Q Griffithsin (D30A/D70A/D112A) Onearmed
HAV	Hepatitis A Virus
HCoV-NL63	Human Coronavirus NL63
HEK 293FT	A human embryonal kidney derived cell line transformed with the SV40 large T antigen that allows for expression from SV40 promoters and has been selected for fast growth rate
HEK 293T hACE2+	A human embryonal kidney derived cell line transformed with the SV40 large T antigen that allows for expression from SV40 promoters and has been transduced to express hACE2
HeLa	Immortalized cell line derived from cervical cancer cells
HEPES	4-(2-hydroxyethyl)-1-piperazineethanesulfonic acid

HIV	Human Immunodeficiency Virus
HR1	Heptad Repeat 1
HR2	Heptad Repeat 2
HSV-1	Herpes simplex virus 1
HSV-2	Herpes simplex virus 2
HTLV	Human T-cell leukemia-lymphoma virus (an early name for HIV)
HuH-7	Hepatocyte derived cellular carcinoma cell line
IC <sub>50</sub>	Half maximal Inhibitory Concentration
ICTV	International Committee on Taxonomy of Viruses
IgG	Immunoglobulin class G1
IPTG	Isopropyl $\beta$ -D-1-thiogalactopyranoside
KCl	Potassium Chloride
LOX-1	Lectin-Like Oxidized Low-Density Lipoprotein Receptor 1
LRRC15_1	Leucine Rich Repeat Containing 15 isoform 1
LRRC15_2	Leucine Rich Repeat Containing 15 isoform 2
L-SIGN	liver/lymph node-specific intracellular adhesion molecules-3 grabbing non-integrin
M	Membrane structural protein from SARS-CoV-2
Man	Mannose
MERS	Middle Eastern Respiratory Syndrome
MERS-CoV	MERS-related coronavirus
MIP-1 $\beta$	Macrophage Inflammatory Protein 1 beta, officially referred to as CCL4 (C-C chemokine ligand type 4)
N	Nucleocapsid structural protein from SARS-CoV-2
NaCl	Sodium Chloride
nCoV-19	Another name for Coronavirus disease 19
NCBI	National Center for Biotechnology Information

NEB	New England Biolabs
NIAID	National Institute of Allergy and Infectious Diseases
NIH	National Institutes of Health
NMR	Nuclear Magnetic Resonance
NP-40	2-[2-(4-Nonylphenoxy)ethoxy]ethanol
NRP1	Neuropilin-1
NRP2	Neuropilin-2
NSP1	nonstructural protein 1
NSP14	nonstructural protein 14
NSP16	nonstructural protein 16
NTD	N-Terminal Domain
OLR1	Gene encoding for LOX1
ORF1a	Open reading frame 1a of Nidovirus. Encodes for polyprotein 1a.
ORF1b	Open reading frame 1a of Nidovirus. Encodes for polyprotein 1ab.
ORF3a	Protein encoded for by open reading frame 3a of Nidovirus
ORF3b	Protein encoded for by open reading frame 3b of Nidovirus
ORF6	Protein encoded for by open reading frame 6 of Nidovirus
ORF7a	Protein encoded for by open reading frame 7a of Nidovirus
ORF7b	Protein encoded for by open reading frame 7b of Nidovirus
ORF8	Protein encoded for by open reading frame 8 of Nidovirus
ORF9b	Protein encoded for by open reading frame 9b of Nidovirus
ORF10	Protein encoded for by open reading frame 10 of Nidovirus
ORF14	Protein encoded for by open reading frame 14 of Nidovirus
p6	HIV-1 protein involved in the docking of several cellular and viral binding partners for HIV-1 virion release, molecular weight of 3-6 kDa (55 amino acids)
p24	HIV-1 capsid protein, molecular weight of 24 kDa
PBS	Phosphate-buffered Saline
PCR	Polymerase Chain Reaction

PDB	Protein Data Bank
Pol	Polyprotein precursor to Reverse Transcriptase, Integrase and HIV Protease
Q-Grft	M78Q Griffithsin
RANTES	Common name for CCL5 (C-C chemokine ligand type 5)
RBD	Receptor Binding Domain
RBM	Receptor Binding Motif
RNA	Ribonucleic acid
RPMI	Roswell Park Memorial Institute 1640 Medium
SARS	Severe Acute Respiratory Syndrome
SARS-CoV-1	Severe Acute Respiratory Syndrome Coronavirus 1
SARS-CoV-2	Severe Acute Respiratory Syndrome Coronavirus 2
SDS	Sodium Dodecyl Sulfate
SIV	Simian Immunodeficiency Virus
S1 domain	SARS-CoV-2 Spike protein S1 domain
S2 domain	SARS-CoV-2 Spike protein S2 domain
SIGLEC	Sialoadhesin/Sialic Acid Binding Ig Like Lectin 1
Raji WT	Immortalized cells derived from B-lymphocytes from a patient with Burkitt lymphoma; cells grow as a suspension
Raji DC-SIGN+	Immortalized cells derived from B-lymphocytes from a patient with Burkitt lymphoma transfected to express DC-SIGN; cells grow as a suspension
Tat	Trans-Activator of Transcription, transcription regulatory protein
T-cell	Lymphocytes that are processed in the Thymus and exhibit various functions related to the adaptive immune response
TEM	Transmission Electron Microscopy
TM	Transmembrane Domain
TMPRSS2	Transmembrane protease, serine 2
Tris	Tris(hydroxymethyl)aminomethane, also known as 2-Amino-2-(hydroxymethyl)-1,3-propanediol

UCM	University of California, Merced
vCCI	Viral C-C Chemokine Inhibitor
Vero E6	Immortalized cell line exhibiting epithelial morphology that was isolated from the kidney of an African green monkey
VOC	Variant of Concern
VOI	Variant of Interest
Vpr	HIV-1 protein involved in nuclear transport, molecular weight of 11.3 kDa
VSV	Vesicular Stomatitis Virus
WHO	World Health Organization
WT-Grft	Wild-Type Griffithsin
Wt	Wild type

## II. List of Figures

<b>Chapter 1</b>	
Figure 1.1: Google Analytics trend for the terms “coronavirus”	1
Figure 1.2: Classification of Coronaviridae family viruses	2, 3
Figure 1.3: Depiction of cumulative Covid-19 cases per country over 2020	5
Figure 1.4: Depiction of SARS-CoV-2 incidence by variant from sequences from patients	7
Figure 1.5: Depiction of SARS-CoV-2 infection	9
Figure 1.6: Depiction of SARS-CoV-2 Spike protein	10
Figure 1.7: Depiction of SARS-CoV-2 Infection process	11
Figure 1.8: Depiction of SARS-CoV-2 Spike RBD and RBM dynamics	12
Figure 1.9: Depiction of SARS-CoV-2 Spike RBD binding to hACE2	13
Figure 1.10: Depiction of SARS-CoV-2 Spike S2’ cut site and S2 domain elongation for fusion	14
<b>Chapter 2</b>	
Figure 1: Representation of the SARS-CoV-2 Spike gene amino acid sequence with all locations of VOC mutations	26
Figure 2: Schematic of Spike mediated infection	28-29
Figure 3: DC-SIGN Trans-infection	31-32
Figure 4: Deconvoluting signal of SARS-CoV-2 Direct- and Trans- infection	32-34
Figure 5: All SARS-CoV-2 pseudovirus Spike glycan mutations display similar susceptibilities to mannan-based Trans-inhibition	35
Figure 6: Clusters of Spike glycans can act as mutation-resistant epitopes for SARS-CoV-2 inhibitor design	36
Figure 7: Assessing if Covid-19 Strains have different infectivity	39
Figure S1: Simplified depiction of hACE2 and DC-SIGN expressing cell types in the lungs	52-53
Figure S2: Depiction of SARS-CoV-2 Spike gene mutations for key VOC strains	54
Figure S3: The glycan occupancy of the SARS-CoV-2 Spike	55
Figure S4: The glycan occupancy of the SARS-CoV-2 spike that was compiled for Figure S3	56
Figure S5: Analysis of SARS-CoV-2 Spike flexibility at N-linked glycan residues	57
Figure S6: Ensuring that Mannan had no effect on our SARS-CoV-2 pseudoviral assays	58
Figure S7: Cluster mutant strains show significantly lower raw infectivity signal	59-60
Figure S8: Demonstration of how Omicron BA.2 had the greatest hACE2-mediated infectivity	61
Figure S9: DC-SIGN is overlaid onto SARS-CoV-2 N-linked glycans N61 and N165	62-63
Figure S10: Steric clashes when DC-SIGN is overlaid onto N234	64
<b>Chapter 3</b>	
Figure 1: Wild-Type Griffithsin compared to M78Q Griffithsin	87
Figure 2: Depiction of how Grft may impede SARS-CoV-2 Spike mediated infectivity	88-89
Figure 3: Depiction, production, and antiviral assessment of the obligate dimer GLG-3A	90-91
Figure 4: DC-SIGN lectin mediated infection of Raji cells	92-93
Figure 5: DC-SIGN lectin mediated infection of 3t3 cells	95
Figure 6: Structure and glycosylation of the three SARS-CoV-2 structural proteins	97-98
Figure 7: Structural proteins enhance Direct-infection but have no effect on Trans-infection	100-101
Figure 8: Structural proteins perform variable roles in enhancing and diminishing the ability of SARS-CoV-2 pseudovirus to be inhibited by Wild-Type Griffithsin	103
Figure S1: NMR HSQC spectrum of Mono-Griffithsin	117
Figure S2: Raji cells weren’t permissible to SARS-CoV-2 pseudoviral infection	118-119
Figure S3: Representative diagrams of virions described in this chapter	120
Figure S4: Depiction of the raw hACE2-mediated Direct Infection Luciferase signal	121-122
Figure S5: Comparisons depicting pseudoviral strain susceptibility to mannan on 3t3 cell assay	123
Figure S6: Comparisons depicting pseudoviral strain propensity to undergo 3t3 DC-SIGN+ cell mediated Trans Infectivity as normalized to Direct Infection	124
<b>Chapter 4</b>	
Figure 1: Cartoon rendition of SARS-CoV-2 inactivation by ozone	136
Figure 2: Figure 2. The relative retention of infectivity of SARS-CoV-2 pseudotyped virus after being spotted onto the surface of food samples without further eradication	139
Figure 3: The sterilization of SARS-CoV-2 pseudotyped virus on the surface of produce	140-141
Figure 4: Simplified schematic representation of virion capture ELISA	142-144
Figure 5: Schematic representation of BLI	145-146
Figure 6: BLI tests of Griffithsin-mediated capture of HIV-1 gp120	147
Figure 7: Raw BLI reads for the transfected cells	149

Chapter 5

Figure 5.1: <b>Depiction of Griffithsin oriented to dock onto the glycans of the N17/61/74 cluster</b> .....	163-165
--	---------



### III. List of Tables

Chapter 3

Table 1: A summary of Wild-Type Griffithsin's antiviral capabilities against SARS-CoV-2 pseudotyped lentivirus versus coronaviral particles, as published in the literature.....	82-84
--	-------

#### **IV. Acknowledgments**

To avoid the risk of me forgetting to acknowledge someone who was incredibly important to me, I am going to err on the side of caution and not explicitly put any names here. There were already so many people that I forgot to reach out to regarding my Defense, I am certain that I will forget to acknowledge a key individual in this section. Suffice it to say that there were innumerable people who contributed in some way, shape, or form to my development over the past several years.

I want to give particular credit to those of you who were generous with your time despite the fact that I was not a peer in your lab/institution/company.

Also, I recognize those of you who put up with my lack of responsiveness- either by phone, text, email, or face-to-face contact- over the years. Thankfully, you all are gracious enough to permit me to contact you out of the blue and pick things up where we left things off.

I wish to point out that many of the people who I include in this acknowledgement are not or were not affiliated with academia or even with a university, but were members of the wider community who provided insight and advice to me.

And finally, I of course acknowledge the support of many of my fellows who worked alongside me in the lab, in the classroom, and in other contexts. Many of you trained me and served as inspirations for who I wanted to be.

Thank you to all of you.

## V. Vita for Name

### Education:

2016– TBE: Doctor of Philosophy, Chemistry and Biochemistry. U. C. Merced  
2014– 2015: Masters of Science, Medical Physiology. LUC, Stritch School of Medicine  
2010– 2014: Bachelor of Arts in Mol. & Cell Biol. (Biochemistry). U. C. Berkeley

### List of Publications:

Mortazavi M.\*, **Bains A.**\*, Afsah-Hejri L., Ehsani, R., LiWang, P. J. "SARS-CoV-2 Pseudotyped Virus Persists on the Surface of Multiple Produce but can be Inactivated with Gaseous Ozone." (2022) *Heliyon*.

\*Both authors contributed equally to this work

Guan W., Zhang N., **Bains A.**, Sadqi M., Dupureur C.M., LiWang P.J. Efficient production of fluorophore-labeled CC chemokines for biophysical studies using recombinant enterokinase and recombinant sortase. (2023) *Biopolymers*.

Guan W., Zhang N., **Bains A.**, Rodriguez A.M., LiWang, P. J. "Sustained Delivery of Antiviral Protein Griffithsin and Adhesion to A Biological Surface by A Silk Fibroin Scaffold." In Revision at *Materials*.

**Bains A.**, Guan W., LiWang, P. J. "The Effect of Select SARS-CoV-2 N-linked Glycan and Variant of Concern Spike Protein Mutations on C-Type Lectin Receptor-Mediated Infection." In Revision at *Viruses*.

### Selected Awards and Fellowships:

36th Annual Symposium of the Protein Society Poster Competition Winner (2022)

Protein Society DEI Travel Fellowship (2022)

NSF-CCBM Crest Scholar (2022)

U. C. Merced Graduate Fellowship Incentive Program Award (2020)

Rotary District 5220 Graduate School Scholarship Finalist (2020)

U. C. Merced AY 2016-2017 Chemistry and Chemical Biology Summer Fellowship (2017)

U. C. Merced Graduate Dean's Relocation Award (2016)

U. C. Merced Chancellor's Graduate Fellowship (2016)

## VI. Abstract

An Investigation into the Role of Protein-Based Viral Structural Features in Mediating the Infectivity of SARS-CoV-2

Arjan Singh Bains

Doctor of Philosophy

University of California, Merced

2023

Supervisor: Professor Patricia J. LiWang

The global pandemic caused by Severe Acute Respiratory Syndrome Coronavirus 2 (SARS-CoV-2) has underscored the urgent need for effective therapeutic strategies to inhibit viral replication and transmission. Although the severity of Coronavirus disease 2019 (Covid-19) has diminished, the SARS-CoV-2 virus is still circulating and evolving, meaning that there is still a distinct risk that a potent Variant of Concern (VOC) could arise at any time. This thesis summarizes our efforts in investigating the efficacy of several prophylactic treatments that were being investigated by the scientific community, and subsequently describes our efforts in probing the molecular mechanisms governing SARS-CoV-2 infection to identify novel vulnerabilities to exploit against the virus.

The first portion of this dissertation orients the reader in understanding the origins and features of SARS-CoV-2 and coronaviruses in general. We then move into briefly presenting key structural features of the SARS-CoV-2 virion before introducing the Spike protein and its role in facilitating infection. We cover these topics with a focus on the structural aspects of the Spike protein, including its glycosylation pattern as well as its conformational changes as it engages the human Angiotensin Converting Enzyme 2 (hACE2) receptor. We finish by describing how SARS-CoV-2 virus can interact with proteins on the surface of cells to modulate its ability to infect different kinds of cells, both *in vivo* and *in vitro*.

The second phase of the thesis focuses on summarizing our work in searching for overlooked epitopes for the development of antiviral prophylactics. Specifically, we describe our work in assessing the role of SARS-CoV-2 Spike S1 domain N-linked glycans in retaining viral infectivity and mediating viral entry into susceptible cells. In addition, we assess whether certain glycans are important in mediating viral capture and presentation by the C-type lectin receptor DC-SIGN. To quantify DC-SIGN capture, we developed a novel cell assay whereby DC-SIGN would deliver virions to susceptible cells, thereby facilitating infection-in-trans (referred to as Trans-infection in this document). Overall, our studies indicated that the glycans at N17 and N122 were important in retaining SARS-CoV-2 pseudotyped viral infectivity. On the other hand, removal of the glycan at N234 appeared to enhance viral infectivity. Drawing from insights gained in performing these assays, we then identified and tested clusters of glycans to ascertain if they were able to act as viable “cold spots” for the design and development of viral entry inhibitors. We conclude by assessing whether SARS-CoV-2

Spike protein from different strains altered the ability of Spike pseudotyped virions in infecting cells and in being captured by DC-SIGN.

We then move into assessing the efficacy of the broadly-antiviral lectin Griffithsin against SARS-CoV-2 Spike pseudotyped viruses. We tested the importance of several variables that were relevant in the context of Covid-19, including the role of the additional SARS-CoV-2 structural proteins in mediating DC-SIGN recognition, the efficacy of Griffithsin against pseudoviral strains that expressed additional structural proteins, and the differences in inhibitory capability of several Griffithsin variants.

We finish by describing several additional attempted assays that made use of our newfound expertise in SARS-CoV-2 pseudoviral production. This included several collaborations, ranging from assessing the extent to which gaseous ozone could sterilize SARS-CoV-2 pseudovirus-contaminated fomites, to troubleshooting the parameters to attempt to detect pseudotyped lentiviral binding to functionalized Biolayer Interferometry (BLI) probes.

Ultimately, this thesis contributes to the growing body of knowledge surrounding SARS-CoV-2 inhibition and prophylactic treatment by elucidating vulnerabilities in critical viral infection processes. These findings serve as the first steps to possibly develop novel prophylactic inhibitors that mitigate Covid-19 disease progression.

# Chapter 1

## Introduction

### 1.1 Introducing Coronaviruses

#### 1.1.1 A Note on the Context of Coronavirus History

Before embarking on the structural and functional features of SARS-CoV-2, the writer of this dissertation felt it prudent to add a note regarding the rationale of why he has felt it necessary to begin by examining the phylogeny and history of the virus.

Lest we forget, prior to the Covid-19 pandemic, the term “coronavirus” was effectively absent from the lexicon of most people in the modern English-speaking world (Figure 1). Anecdotally, the author encountered numerous instances where colleagues or media misunderstood aspects of coronaviruses and Covid-19. Even in the academic literature, this phenomenon still occurred to some extent. For example, an oft-cited figure for the number of Spike proteins on the surface of the SARS-CoV-2 virion was found to be incorrect in late 2020, but some papers still cited the older number [39, 41]. We do acknowledge that this is understandable, as at the start of the pandemic, we did not know much about the SARS-CoV-2 virus, and one of the core tenets of science is to update and improve our understanding of phenomena. Because coronaviruses are so new to most of us, the writer believes that a brief glimpse into the start of the coronavirus field may help to orient the rest of the dissertation.

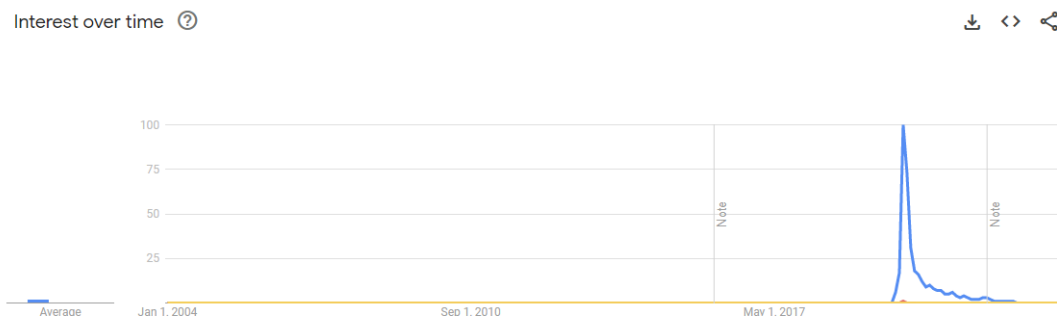


Figure 1.1: Google Analytics trend for the terms “coronavirus” (blue), “SARS” (red), “MERS” (yellow) and “zoonotic” (green, buried under the yellow line) between the years of 2004 to present.

#### 1.1.2 The Phylogeny of Coronaviruses

Within the order of enveloped, positive-stranded RNA viruses known as *Nidovirales* are eight suborders of viruses: *Abnidovirineae*, *Arnidovirineae*, *Cornidovirineae*, *Mesnidovirineae*, *Monidovirineae*, *Nanidovirinae*, *Ronidovirineae*, and *Tornidovirineae* [1]. Among these eight suborders, *Abnidovirineae* and *Monidovirineae* only contain one virus species within them [1]. Furthermore, *Abnidovirineae*, *Mesnidovirineae*, *Monidovirineae*, *Nanoviridae*, and *Ronidovirineae* do not infect mammals [2, 3, 4, 5, 6]. Between the remaining suborders, *Tornidovirineae* viruses tend

to cause gastric distress in vertebrates and are primarily transmitted through the fecal-oral route [7]. This leaves *Cornidovirineae* and *Arnidovirineae* as the two virus suborders that have members that can broadly infect mammals without relying solely on fecal-oral transmission routes [8, 9, 10].

*Cornidovirineae* suborder viruses, also colloquially referred to as Coronaviruses, attract particular interest because they are the largest known RNA viruses, with genomes as large as 25-32 kbp [12, 13]. The suborder only includes one family - called *Coronaviridae* - but the *Coronaviridae* family encompasses three subfamilies (*Orthocoronavirinae*, *Letovirinae*, and *Pitovirinae*) and numerous unclassified viral species [11]. Amongst the three subfamilies, *Letovirinae* and *Pitovirinae* viruses exclusively infect fish. On the other hand, *Orthocoronavirinae* infect a wide variety of vertebrates, including dogs, cats, pigs, birds, and humans [11]. While *Orthocoronavirinae* typically cause mild enteric or respiratory sickness, the human coronaviruses that cause Severe Acute Respiratory Syndrome (SARS) and the Middle East Respiratory Syndrome (MERS) are outliers because they cause severe respiratory disease [12]. The novel SARS-CoV-2 virus is the newest member of this cadre of *Orthocoronavirinae* outliers, as it too causes severe respiratory disease called Covid-19.

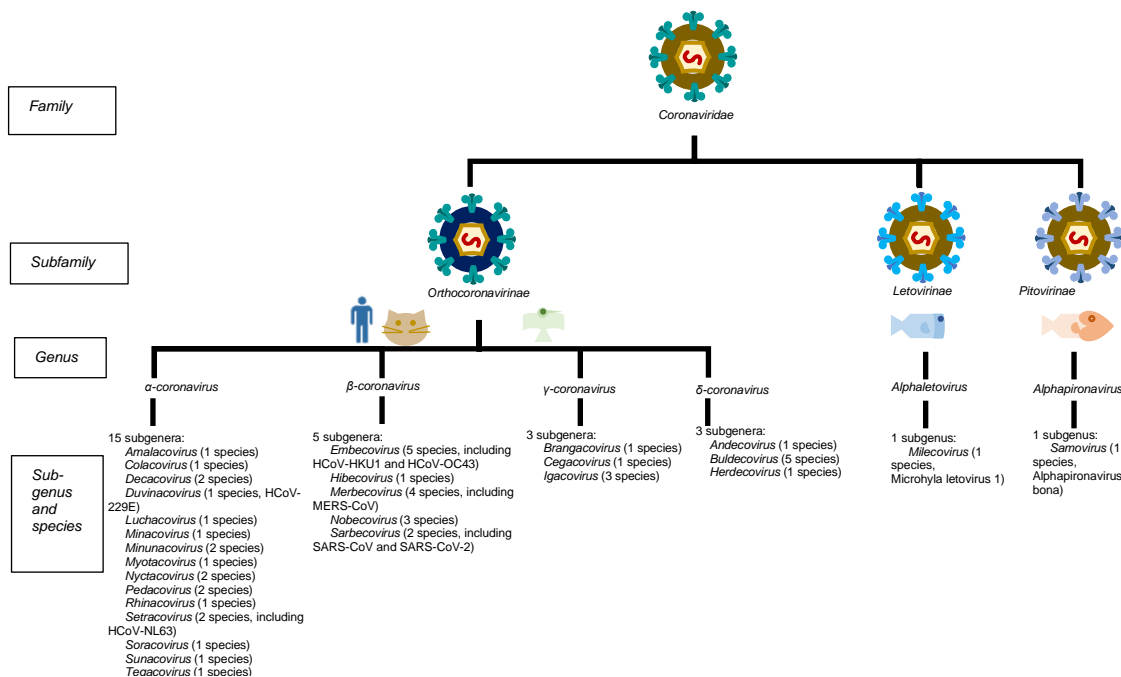


**Figure 1.2 Classification of Coronaviridae family viruses:** Out of the *Orthocoronavirinae* subfamily viruses, *Alphacoronaviruses* and *Betacoronaviruses* exclusively infect mammals, while *Gammacoronaviruses*, and *Deltacoronaviruses* primarily infect birds [13]. Indeed, it is no surprise that the three human outbreak coronaviruses (e.g. SARS-CoV-1, MERS-CoV, and SARS-CoV-2) are all closely related (in the *Betacoronaviruses* genus) [14]. The number of different species of virus under each subheading is derived from a search of the viral genera and subfamilies as decided by the International Committee on Taxonomy of Viruses (ICTV) [1]. These numbers are lower than what is displayed on the NCBI taxonomy browser, because the NCBI taxonomy browser includes organisms and viruses that have one or more protein or nucleotide sequences deposited on genetic databases (i.e. a full genome is not required for each species) [11]. In the future, we expect that some of the incomplete genomes listed on the NCBI taxonomy browser will be recognized as separate species. Likewise, some viruses with multiple strains will likely have some

strains eventually reclassified as separate species or genera. Also note that at the time of writing, ICTV classifies MERS-CoV as a member of the *Merbecovirus* genus. This is subject to change, as contemporary literature sometimes includes MERS-CoV as a member of the *Sarbecovirus* genus [14].

### 1.1.3 The Origin of SARS-CoV-2

Up until relatively recently, the consensus in scientific literature had assumed that *Coronaviridae* family viruses had only arisen approximately 10,100 years ago [13]. Given the fact that birds and bats appear to be the original hosts of coronaviruses, this dates the genesis of *Coronaviridae* viruses at an extremely young age compared to their putative hosts: both modern birds and bats are estimated to have evolved and started to diversify at least 65 million years ago [15, 16]. This is unexpected for any viral pathogen and its host species [13]. To illustrate this point, we call upon our understanding of herpes simplex virus: all primates are considered the natural hosts for their respective herpes simplex viruses (family *Herpesviridae*, subfamily *Alphaherpesvirinae*, genus *Simplexvirus*): Homo sapiens are infected with the Herpes Simplex Viruses (HSV-1 and HSV-2) and chimpanzees are infected by ChVP, for example [17]. The prevalence of these very similar herpesvirus across these two primate species implies that the common ancestor for ChVP and the human Herpes Simplex Viruses arose at the same time both primates had a common ancestor, about 6 to 8 million years ago [19, 42]. When performing a comparison of the genomes and rate of mutation from ChVP to HSV-1 and ChVP to HSV-2, it was found that the chimpanzee and human viruses were estimated to have shared a common ancestor about 2.5 million years ago (ChVP to HSV-1) to 10 million years ago (ChVP to HSV-2) [19]. This falls into the same approximate timeline for when the two host species shared a common ancestor. Ergo, it is no surprise that the timeframe of *Coronaviridae* family viruses arising ~10,000 years ago was amended when researchers found that the RNA replicase from coronaviruses, nonstructural protein 14 (NSP14), contains a unique proofreading mechanism. This grants coronaviruses a mutation rate on par with DNA viruses ( $1 \times 10^{-5}$  to  $1 \times 10^{-6}$  mutations per site per replication) as opposed to the  $1 \times 10^{-3}$  to  $1 \times 10^{-5}$  mutations per site per replication that is typical for RNA viruses [13, 43, 44]. Based off of this, it is now generally accepted that *Coronaviridae* family viruses arose 190 to 489 million years ago, which is concordant with the idea that birds and bats are the original hosts of coronaviruses [13]. Furthermore, there is evidence to suggest that zoonotic transfer of coronaviruses to human populations has happened with regularity in the past. An analysis of human genes found that the ancestors of East Asian humans likely faced strong selective pressure for the enrichment of specific mutations in 42 genes that are relevant in the context of coronavirus infection [47]. All of this serves to say that although coronaviruses as a human pathogen have gained more attention recently, the clade itself has been present and infecting humans for thousands of years.

We now go through the history of coronaviruses and SARS-CoV-2 in the context of academia. While the evolution of coronaviruses is estimated to date as far back as the Jurassic era, modern humanity only has been able to observe and analyze viruses meaningfully for just over a century [13, 45, 46]. The term “coronavirus” was first coined in the 1960s, but, coronaviruses themselves were first characterized as far back as the 1930s [20, 22, 23, 21, 24]. After formally defining the clade in the 1960s, the research groups that worked on Coronaviruses tended to be an intimate circle of people; prior to



the turn of the 21<sup>st</sup> century and the outbreak of SARS-CoV-1, much of the groundwork on human coronaviruses was laid by a moderately-sized grouping of labs and researchers [20, 21, 25-31]. The first coronavirus capable of infecting humans (hCoV-B814) was discovered in 1965 by two members included in the aforementioned grouping (Dr. D.J. Tyrrell and Dr. M.L. Bynoe), demonstrating the impact of this cluster of researchers on what would become a large and burgeoning field of research.

Interest in human coronaviruses and our capabilities to study them greatly rose during the first SARS outbreak in 2003; several scientists who would go on to become prominent Covid-19 researchers had their career start with studying SARS-CoV-1, and the and the foundations of the BSL-4 lab at the Wuhan Institute of Virology were laid during and soon after the SARS outbreak, in 2003-2005 [32, 33, 34, 35, 36]. However, in the ten years following the initial SARS, interest and research funding waned [37]. While the MERS outbreak in the mid-2010s revived some interest in human coronaviruses, the outbreak of SARS-CoV-2 7 years later would coronaviruses to the forefront of conversation [38].

#### **1.1.4 The Recent History of the Covid-19 Pandemic**

In December of 2019, a string of pneumonia cases with an unknown cause was reported in Wuhan, the capital of the Hubei Province in the People's Republic of China [48, 49]. These cases did not raise any particular concern until Dr. Zhang Jixian, the Director of the Department of Respiratory and Critical Care Medicine at the Hubei Provincial Hospital of Integrated Traditional and Western Medicine, noticed the sudden influx of patients exhibiting pneumonia symptoms, and warned authorities at the hospital on December 27, 2019 [51, 52]. An underappreciated aspect of this story is at the time that Dr. Jixian reported the pneumonia cases to hospital authorities, she had seen only 7 patients exhibiting symptoms [52]. Wuhan City is one of the most populous cities in the world, with a modern and urbanized populace and infrastructure, meaning it could have been easy to dismiss such a low number of cases in a city with about 11 million inhabitants [50]. But Dr. Jixian may have been particularly suited to notice the implications of the sudden influx of patients exhibiting respiratory symptoms- Dr. Jixian was not only the head of respiratory care at the hospital, but also she had been a mid-career doctor who was entrusted with monitoring several hospitals in Wuhan during the SARS outbreak in the early 2000s [52].

The pneumonia cases spread rapidly: by New Year's Day, the isolation beds at the Hubei Provincial Hospital of Integrated Traditional and Western Medicine were fully occupied and the daily number of outpatients in the Respiratory Department was double what they typically had [52]. By January 1, 2021, city officials in Wuhan closed down a seafood market that several of the initial patients had ties to [53]. Less than a week later, a paper was submitted for publication where a sample of bronchoalveolar lavage fluid from a patient who was admitted to the Central Hospital of Wuhan on December 27, 2020 revealed that a new coronaviral agent was responsible for the rapidly-spreading pneumonia cases [54]. Less than a month later, the novel coronavirus had already been detected outside of China, as a tourist in Thailand was found to be infected on January 13, 2020 [58]. On February 11, 2020, a preprint from the ICTV named the novel coronavirus SARS-CoV-2 [55, 56]. By March, a publication in the New England Journal of Medicine reported that the novel SARS coronavirus had been detected in the United

States of America as far back as on January 20, 2020, indicating the remarkable pathogenicity and contagiousness of SARS-CoV-2 [57]. It further provided strong evidence that the SARS-CoV-2 virion may be far more widespread than what in-person testing and monitoring symptomatic individuals would suggest. Perhaps due to the release of the New England Journal of Medicine manuscript, the World Health Organization (WHO) released a statement on March 11, 2020 formally declaring Covid-19 was a pandemic [59, 60]. At this point in time- a mere 3 months after Covid-19 had first been detected- it had already spread to 114 countries, with at least 118,000 cases and 4291 deaths formally attributed to the disease [59, 60]. In reality, these values probably underestimate the true number of deaths caused by Covid-19 [61].

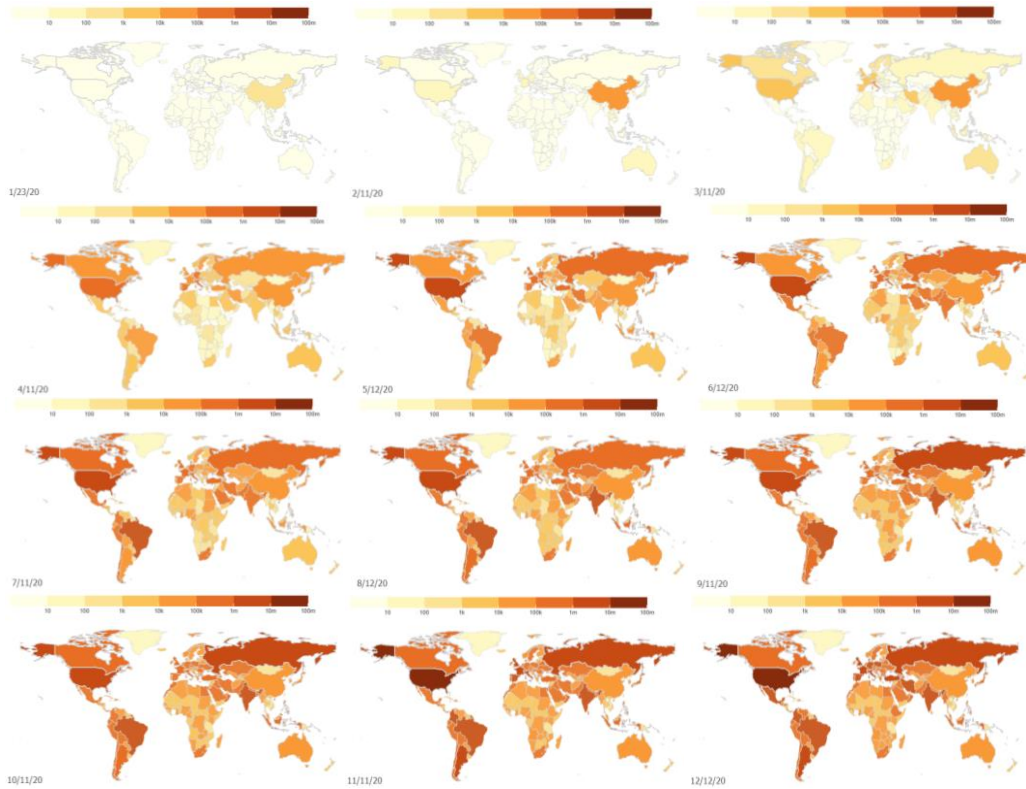


**Figure 1.3 Depiction of cumulative Covid-19 cases per country over 2020:** Each step in the color gradation scale indicates an order of magnitude more cases. This figure is adapted from interactive data available on the Johns Hopkins University of Medicine Coronavirus Research Center [62].

### 1.1.5 Lockdowns and Unexpected Coronavirus Mutations

Soon after the doctors in Wuhan realized the agent responsible for the pneumonia-like symptoms in patients was a novel SARS-like coronavirus, they implemented preventative measures that were initially implemented during the SARS-CoV-1 outbreak. The city of Wuhan was placed under strict lockdown on January 23, 2020, less than 2 weeks after the gene sequence of SARS-CoV-2 was reported [54, 59, 60, 63]. The rest of the world soon followed suit, with a global lockdown largely in place in March of 2020, after the WHO declared that Covid-19 was officially a pandemic [63].

However, lockdown protocols varied from country to country. For example, while the Scandinavian countries Norway, Denmark and Sweden share many similarities in their healthcare systems and general approach to social policy, only Norway and Denmark implemented strong social distancing rules, while Sweden implemented comparatively few if any restrictions on its populace [64, 65].

By mid-March of 2020, scientists and health professionals in Europe, Oceania, and the East Coast of the USA started to report that SARS-CoV-2 sequences in Covid-19 patients had started to display a higher and higher incidence of a D614G mutation in the gene of a SARS-CoV-2 protein (called the Spike protein) [66]. While this was somewhat surprising given the low mutation rate of the coronaviral RNA replicase, health professionals quickly rationalized that the high contagiousness and sheer number of people infected with SARS-CoV-2 provided the virus ample opportunity to acquire mutations with fitness advantages [66, 67]. This moment was pivotal in the timeline of the Covid-19 pandemic in that it fomented the idea that SARS-CoV-2 mutant strains would become a major aspect of combating Covid-19 [66, 67].

Now, several years into the pandemic, many people are inured to the news that the SARS-CoV-2 virus can mutate. To date, there are over 15 million sequences on the GISAID Covid-19 database, each representing a unique SARS-CoV-2 sample from an infected human [68-70]. Although many of these sequences did not gain enough fitness from said mutations to become classified as new SARS-CoV-2 strain, there are still nonetheless over 934 recognized SARS-CoV-2 strains as of Summer 2023 [71, 72]. As the Covid-19 pandemic progressed, various vaccines were created, and humanity gained herd immunity to certain strains of SARS-CoV-2; the virus itself mutated and different variants gained prominence. A brief representation of this process is depicted below (Figure 1.4).



**Figure 1.4 Depiction of SARS-CoV-2 incidence by variant from sequences from patients in select countries:** Data were available starting from March 2021 to July 2023. Time points were selected based on relatively large changes in SARS-CoV-2 variants' incidence. These time lapse images show the rise and fall of several SARS-CoV-2 strains, including Alpha being supplanted by Gamma, before both were rapidly outcompeted by Delta, which was then outcompeted by Omicron. Since mid-2022, several Omicron lineages have been competing for dominance. Please note that although the number of infection is quite low at the moment (1,977 data points on the graph for the United States on July 17, 2023), it only takes the development of a novel infectious strain to lead to a surge in infections (see how the United States went from 19,311 data points on June 21, 2021 to over 100,000 on November 8, 2021 when the Delta strain arose).

## 1.2 Section 2: Features of SARS-CoV-2 Viral Infection

### 1.2.1 SARS-CoV-2 Viral Infection

The SARS-CoV-2 virus, like other members of the family *Orthocoronaviridae*, is a membrane-encapsulated positive-strand RNA virus about 100-160 nm in diameter (although evidence shows SARS-CoV-2 tends to stay on the smaller side of that distribution, staying close to 80-100 nm in diameter) [41, 74, 76]. As mentioned previously, the RNA genome of the viruses in this family are among the largest known, with the SARS-CoV-2 genome measuring 29800 to 29900 base pairs [75].

The genome of SARS-CoV-2 encodes for several different proteins, including 4 structural proteins (called N, M, E, and S), 16 non-structural proteins that are involved in genome transcription and replication (NSP1 to NSP16, expressed as two large polyproteins called ORF1a and ORF1b from the genes *ORF1a* and *ORF1ab*, respectively; the polyproteins are cleaved to release the NSP proteins), and 9 accessory proteins (ORF3a, ORF3d, ORF6, ORF7a, ORF7b, ORF8, ORF9b, ORF14, and ORF10) [76, 77]. In general, *Orthocoronaviridae* viruses encode for these same proteins in their genomes, although there is extremely high variability in the number of accessory proteins retained in other coronaviruses: some viruses in this family dispense of all but 2 of the accessory proteins [75]. In the case of SARS-CoV-2, accessory proteins ORF3b, ORF9b, and ORF10 are not highly expressed. From what we can tell, none of the individual accessory protein genes is conserved across all members of the *Orthocoronaviridae* family, calling into question their necessity in ensuring productive SARS-CoV-2 infection [75].

Out of all of these proteins, only the structural proteins are incorporated into the mature SARS-CoV-2 virion [41, 78, 79]. Thus, these four proteins are the ones that have the greatest effect on the physical characteristics of SARS-CoV-2, such as its cold resistance [76, 79, 80]. Among the structural proteins, arguably the most important factor in determining SARS-CoV-2 tropism is the S protein, also called the Spike protein [76]. The Spike protein is responsible for binding to the SARS-CoV-2 entry receptor, the human Angiotensin Converting Enzyme 2 (hACE2). hACE2 serves as the entry receptor for the SARS-CoV-1 virion, but the Spike protein from the SARS-CoV-2 virion appears to show 10-20 times greater affinity to the receptor than the SARS-CoV-1 virus, possibly providing one explanation for why SARS-CoV-2 is more pathogenic than SARS-CoV-1 [76]. We will go into more detail regarding the Spike protein, but a simplified diagram showing the importance of the Spike protein in dictating virus entry is below (Figure 1.5).

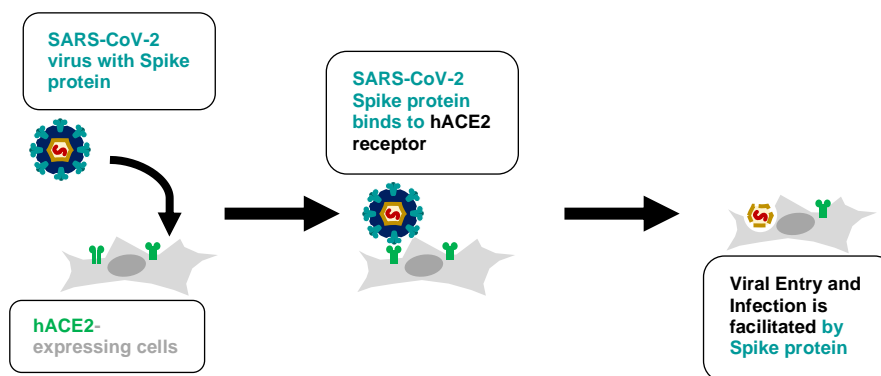


**Figure 1.5 Depiction of SARS-CoV-2 infection:** To orient the reader, this is a simplified depiction of how the SARS-CoV-2 Spike protein mediates infection and viral entry. The SARS-CoV-2 virion requires one of its spike trimer to bind to the hACE2 receptor in order to facilitate viral entry and infection.

### 1.3 The Role of the SARS-CoV-2 Spike Protein Dynamics in Viral Infection and Entry

The SARS-CoV-2 Spike protein is a 1273 amino acid (approximately 141 kDa) homotrimeric membrane-embedded glycoprotein [75]. The Spike protein encompasses three different domains: the Signal Sequence at the N-terminus which is usually cleaved off of the spike in reported PDB structures (residues 1-13), the S1 domain (residues 14-685), and the C-terminal S2 domain (residues 686-1273) [81]. Within the S1 domain, it is further subdivided into the N-terminal Domain (NTD, residues 14-305) and the Receptor-Binding Domain (RBD, residues 319-541) [81]. The remaining C-terminal portions of the S1 domain are subdivided into two C-Terminal Domains: C-Terminal Domain 1 (CTD1, residues 527 to 591) and C-Terminal Domain 2 (CTD2, residues 591 to 685). Similarly, the S2 domain is further subdivided into the fusion peptide domain (FP, residues 788-806), the heptapeptide repeat sequence 1 (HR1, residues 912-984), heptapeptide repeat sequence 2 (HR2, residues 1163-1213), the transmembrane domain (TM, residues 1213-1237), and the cytoplasm domain (residues 1237-1273) [81].

The SARS-CoV-2 Spike protein has been shown to adopt two conformations: the down/closed conformation-whereby the RBD lies against the surface of the Spike trimer- and the open/up conformation (Figure 1.8) [83]. In order to bind to the hACE2 receptor and propagate efficient infection, the Spike protein must be in the up/open conformation, as the surface that interacts with the hACE2 receptor (called the Receptor Binding Motif, RBM, residues 424-494) is buried and inaccessible when the Spike is in the down/closed conformation (Figure 1.9) [74, 83, 84].

A unique feature of the SARS-CoV-2 Spike protein when compared to the Spike protein of other closely related coronaviruses is the existence of a four-residue R-R-A-R furin cleavage site at the residues 682 to 685 between the S1 and S2 domains [81, 82]. Cleavage at this S1/S2 junction allows the Spike protein to gain the ability to open/flip “up” the RBD with a hinge-like movement,

thereby revealing the buried residues of the Receptor Binding Motif, along with allowing N501 to form a favorable stabilizing hydrogen bond with the backbone of another loop of the Spike S1 domain [83, 85, 86]. These RBM residues are responsible for binding to hACE2, which is the first step in mediating viral entry and infection [86].

In order for the SARS-CoV-2 virus to fuse with the host membrane, it must further undergo cleavage at the S2' cut site, located between R815 and S816 in the S2 domain [81, 87, 88]. Cleavage at the S2' site is typically performed by Transmembrane protease, serine 2 (TMPRSS2) proteases on the surface of target hACE2-expressing cells, although it is also possible for Cathepsin L proteases to cut the S2' site if the virion is endocytosed by the target cell [87].

After the S2' undergoes cleavage, the SARS-CoV-2 Spike S1 domain is thought to dissociate from the spike protein (Figure 1.10) [89]. The remaining details of the membrane fusion process is thought to mimic the process of membrane fusion characterized for class I fusion proteins [89]. In the case of SARS-CoV-2, the S2 domain elongates and inserts its FP into the host membrane. The HR2 domain is assumed to fold back onto the HR1 domain to form a 6-helix bundle which pulls the viral membrane and host cell membrane close to each other, thereby allowing for the formation of a fusion pore and the release of the viral genome into the cytosol [89].

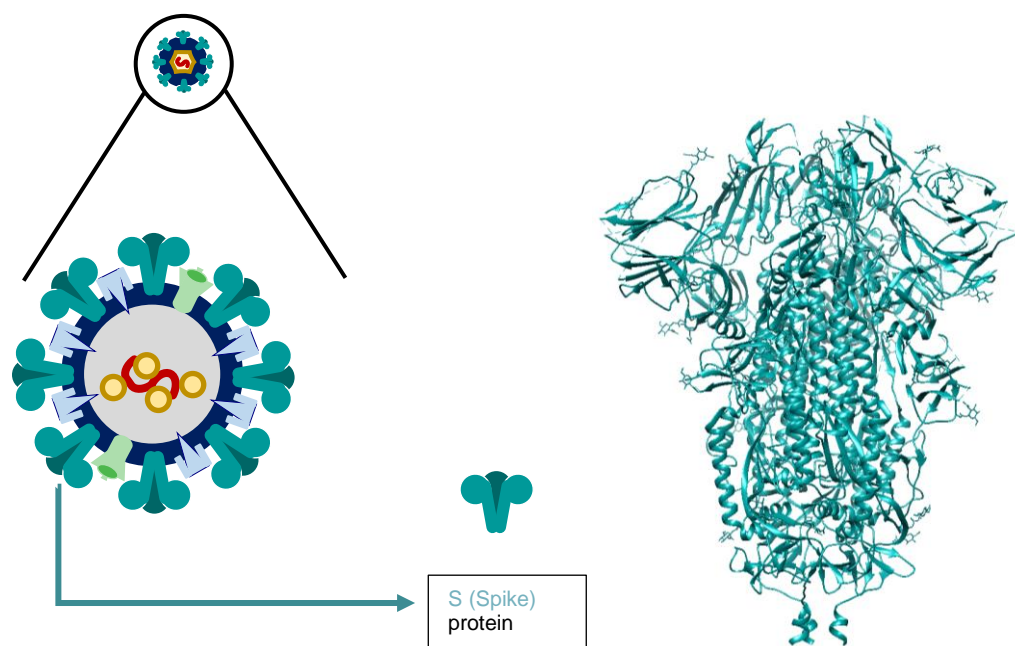


**Figure 1.6 Depiction of SARS-CoV-2 Spike protein:** On the left, we have added more detail to our representation of the SARS-CoV-2 Spike Virion. The trimeric Spike protein (teal blue), Membrane protein (sky blue), Envelope protein (mint green), and Nucleocapsid protein (gold and yellow) are depicted along with the RNA genome (dark red). On the right is a ribbon structure of the SARS-CoV-2 spike, in teal to match the color of our graphical representation and to help orient the reader in preparation for the next figures (PDB ID: 6VXX).

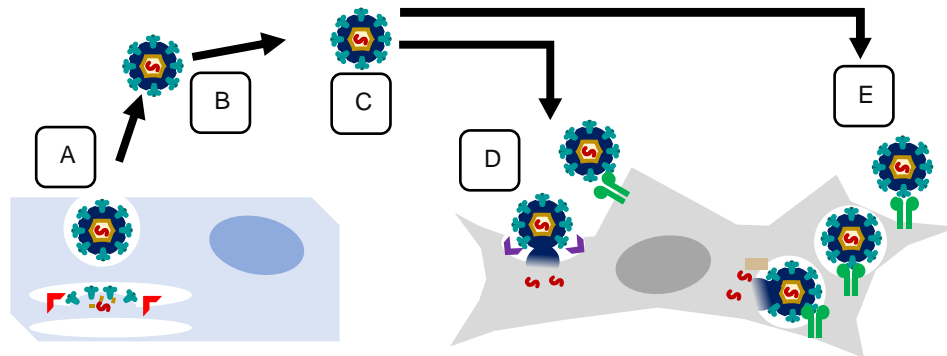


**Figure 1.7 Depiction of SARS-CoV-2 Infection process:** **(A)** The SARS-CoV-2 virion is formed by budding into the luminal space of the Endoplasmic Reticulum/Golgi Apparatus. N protein is shown as gold specks around the RNA genome (again depicted in dark red). It is thought that the Cytoplasm domain in the S2 domain of the Spike protein interacts with the RNA-bound N protein, allowing for the SARS-CoV-2 RNA genome to be packaged into the viral particle [90]. As the viral particle is forming, host furin-like proteases (bright red angle shapes) cleave the Spike proteins at the furin cleavage site at the S1/S2 junction. **(B)** The SARS-CoV-2 virion is released from the infected cell. **(C)** The SARS-CoV-2 virion can undergo two hACE2-mediated infection pathways, provided that the Spike RBD can bind to hACE2 (green shapes on grey cell surface). **(D)** The SARS-CoV-2 virus is processed at the S2' cleavage site by Transmembrane protease, serine 2 (TMPRSS2) proteases (purple chevron shapes) at the cell surface. This allows for virus-host fusion and the delivery of the SARS-CoV-2 RNA into the cell. **(E)** Alternatively, the virion can be endocytosed by the target cell fast enough that the S2' site is not cleaved by surface proteases. The lysosomal protease Cathepsin L (tan rectangle) can then cleave the S2' site, allowing for virus-host fusion and the delivery of the SARS-CoV-2 RNA into the cell.



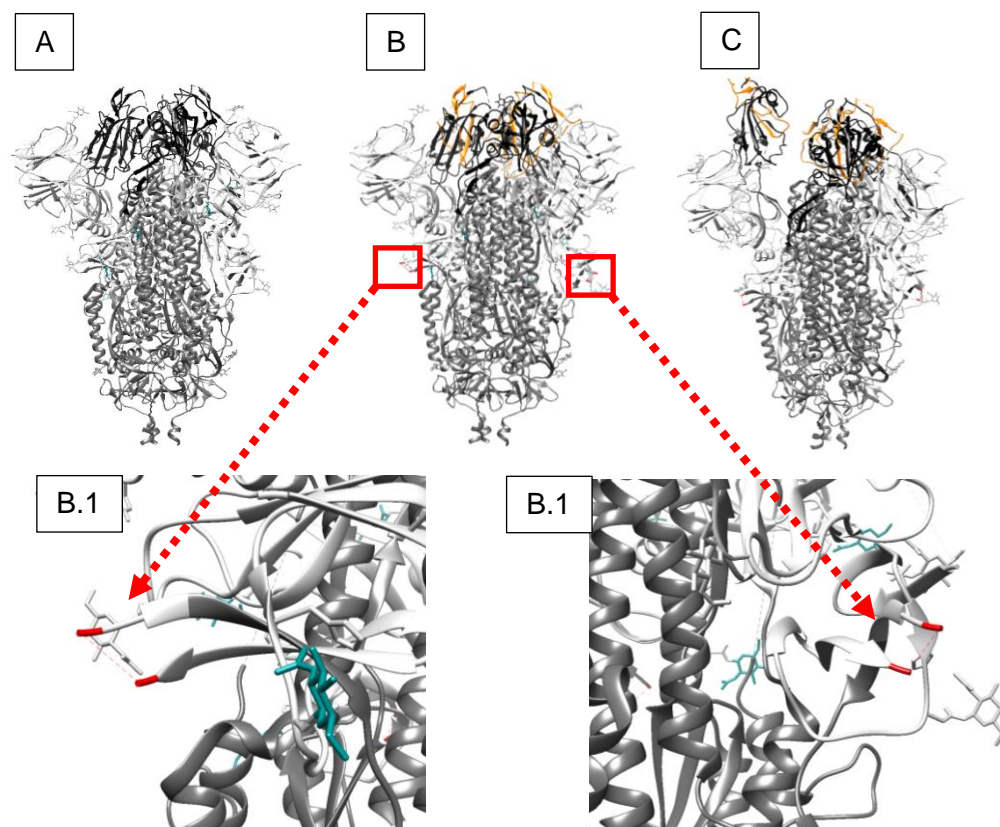


**Figure 1.8 Depiction of SARS-CoV-2 Spike RBD and RBM dynamics:** **(A)** On the left is a recolored depiction of the SARS-CoV-2 Spike protein in the down/closed conformation, from Figure 1.5 (PDB ID: 6VXX). The S1 domain is in light grey, except for the region of the S1 domain that is encompassed by the RBD: the RBD is depicted in black. The S2 domain is depicted in dark grey. **(B)** The same image as in A. is shown again, except the RBM within the RBD has been recolored orange. We can see that there is significant steric hindrance preventing easy access to the orange region of the S1 domain. Furthermore, the S1/S2 junction/furin cleavage site is boxed in red. The furin cleavage site is on a flexible loop that is not resolved on most PDB structures. Ergo, the site is depicted with a red dashed line. These furin cleavage sites are zoomed in and enhanced in figures labeled **B.1**. **(C)** The SARS-CoV-2 Spike protein is again depicted with the same color coding as in parts A. and B., but this time one of the monomers of the spike trimer is in the open/up conformation (PDB ID: 6VYB). We can clearly see that the RBM of the open/up monomer is far more accessible.

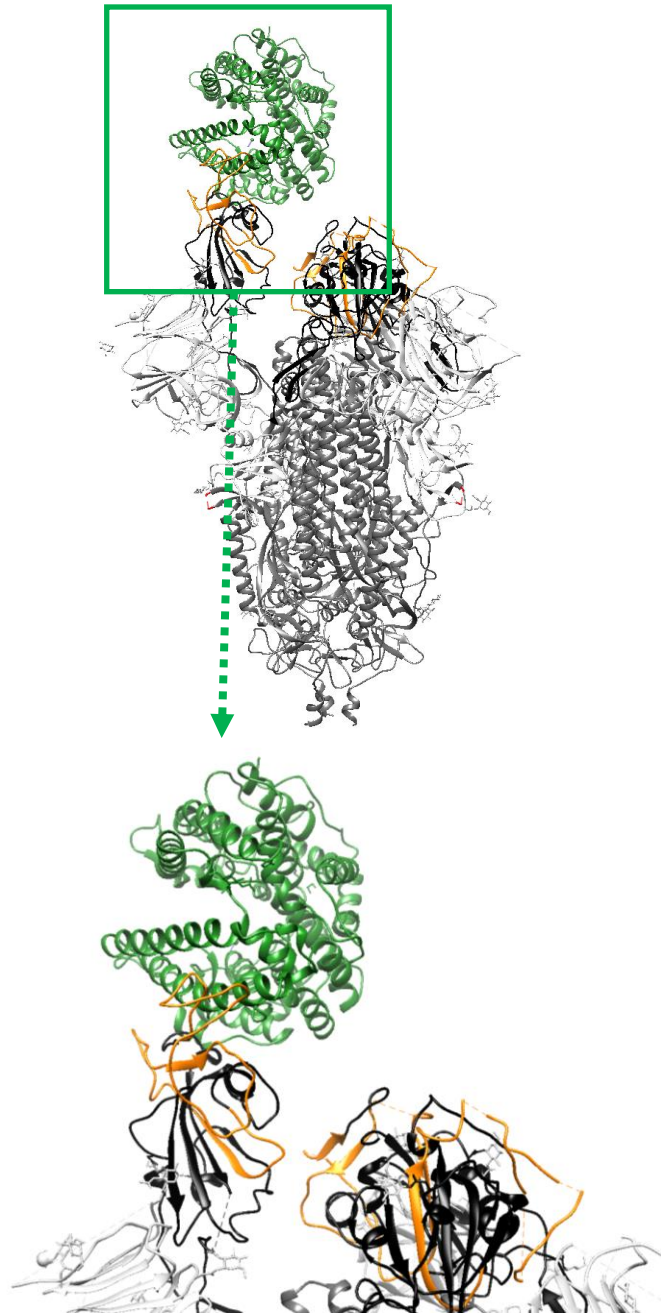


**Figure 1.9 Depiction of SARS-CoV-2 Spike RBD binding to hACE2:** The human Angiotensin Converting Enzyme extracellular domain is depicted in green. The PBD structure of the RBD binding to hACE2 (PDB ID: 6VW1) was overlaid onto the PDB structure of the SARS-CoV-2 Spike with one monomer in the up/open conformation (PDB ID: 6VYB). The Spike protein was color coded as above: S1 not including RBD in light grey, RBD not in black, RBM in orange, and S2 domain in dark grey. We can see that the residues starting from A475 to S494 clearly is in close proximity to the alpha helix containing residues S19 to A36 of the hACE2 protein.

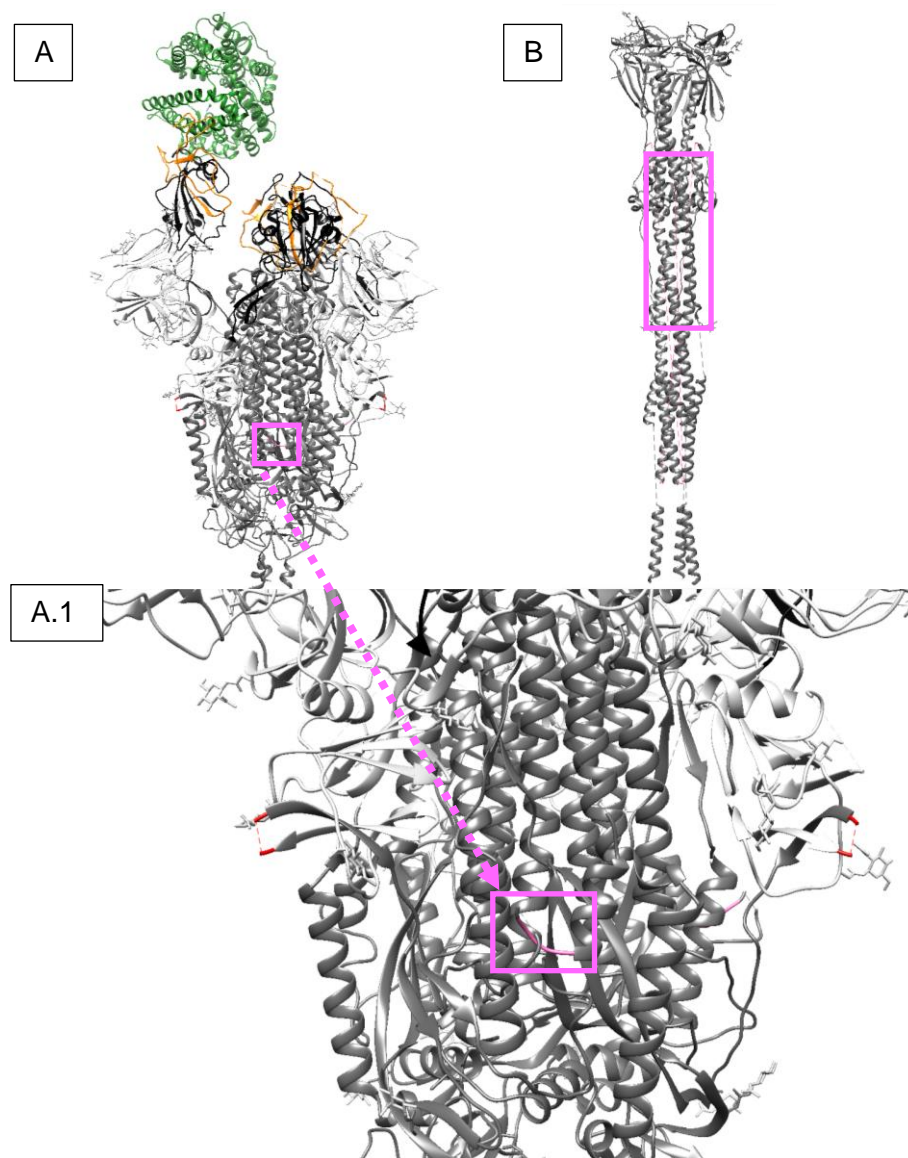


**Figure 1.10 Depiction of SARS-CoV-2 Spike S2' cut site and S2 domain elongation for fusion:** **(A)** Depiction of the SARS-CoV-2 Spike protein in the one-up conformation bound to hACE2, as described above ((PDB ID: 6VW1 overlaid onto PDB ID: 6VYB). The S2' cut site is boxed and color coded pink. The S2' cut site is zoomed in on figure **(A.1)**. Please note that the S1/S2 furin cleavage sites are still shown in red, but they are not boxed. The author does find it intriguing that the S1/S2 cut site is located close to the S2' cut site, leading him to wonder whether a protease could cleave both sites at the same time. **(B)** A depiction of the S2 domain in the post-fusion conformation, after the S1 domain has dissociated from the Spike protein. Since large stretches of the structure did not have resolution, the S2' cut site is estimated to be within the area boxed in pink. (PDB ID: 7E9T).

#### 1.4 References:

- [1]: "International Committee on Taxonomy of Viruses (ICTV)". [talk.ictvonline.org](http://talk.ictvonline.org). Retrieved 2020-06-08. Accessed 2023-08-08.
- [2]: Bukhari, K.; Mulley, G.; Gulyaeva, A. A.; Zhao, L.; Shu, G.; Jiang, J; Neuman, B. W. Description and initial characterization of metatranscriptomic nidovirus-like genomes from the proposed new family Abysoviridae, and from a sister group to the Coronavirinae, the proposed genus Alphaletovirus. *Virology*. 2018 Sep; 524: 160–171. doi:10.1016/j.virol.2018.08.010.
- [3]: Sadeghi M, Popov V, Guzman H, Phan TG, Vasilakis N, Tesh R, Delwart E. Genomes of viral isolates derived from different mosquitos species. *Virus Res*. 2017 Oct 15;242:49-57. doi: 10.1016/j.virusres.2017.08.012. Epub 2017 Sep 21. PMID: 28855097; PMCID: PMC5665172.
- [4]: Saberi, A.; Gulyaeva, A. A.; Brubacher, J. L.; Newmark, P. A.; Gorbalenya, A. E. A planarian nidovirus expands the limits of RNA genome size. *PLOS Pathogens*. 2018;(14)11: e1007314. doi:10.1371/journal.ppat.1007314.
- [5]: Thomas JE, Gronenborn B, Harding RM, Mandal B, Grigoras I, Randles JW, Sano Y, Timchenko T, Vetten HJ, Yeh HH, Ziebell H, Ictv Report Consortium. ICTV Virus Taxonomy Profile: Nanoviridae. *J Gen Virol*. 2021 Mar;102(3):001544. doi: 10.1099/jgv.0.001544. Epub 2021 Jan 12. PMID: 33433311; PMCID: PMC8515864.
- [6]: King, A. M. Q.; Adams, M. J.; Carstens, E. B.; Lefkowitz, E. J., eds. "Order - Nidovirales". *Virus Taxonomy*. 2012: 784–794, Elsevier. doi:10.1016/B978-0-12-384684-6.00066-5.
- [7]: Koopmans, M., Herrewegh, A., & Horzinek, M. C. Diagnosis of torovirus infection. *Lancet*. 1991; 337(8745): 859. [https://doi.org/10.1016/0140-6736\(91\)92573-k](https://doi.org/10.1016/0140-6736(91)92573-k)
- [8]: Mohammadi H, Sharif S, Rowland RR, Yoo D. The lactate dehydrogenase-elevating virus capsid protein is a nuclear-cytoplasmic protein. *Arch Virol*. 2009;154(7):1071-80. doi: 10.1007/s00705-009-0410-0. Epub 2009 Jun 11. PMID: 19517211; PMCID: PMC7087266.
- [9]: Warren, Cody J.; Yu, Shuiqing; Peters, Douglas K.; Barbachano-Guerrero, Arturo; Yang, Qing; Burris, Bridget L.; Worwa, Gabriella; Huang, I.-Chueh; Wilkerson, Gregory K.; Goldberg, Tony L.; Kuhn, Jens H.; Sawyer, Sara L. Primate hemorrhagic fever-causing arteriviruses are poised for spillover to humans. *Cell*. Oct 2022;185 (21): 3980–3991.e18. doi:10.1016/j.cell.2022.09.022. ISSN 0092-8674. PMC 9588614. PMID 36182704.
- [10]: Vlasova AN, Wang Q, Jung K, Langel SN, Malik YS, Saif LJ. Porcine Coronaviruses. *Emerging and Transboundary Animal Viruses*. 2020 Feb 23:79–110. doi: 10.1007/978-981-15-0402-0\_4. PMCID: PMC7123000.
- [11]: Taxonomy Browser. NCBI. Accessed August 11, 2023. <https://www.ncbi.nlm.nih.gov/Taxonomy/Browser/wwwtax.cgi?p=7&id=2499399>

- [12]: Payne, S. Family Coronaviridae. *Viruses*. 2017:149–58. doi: 10.1016/B978-0-12-803109-4.00017-9. Epub 2017 Sep 1. PMID: PMC7149805.
- [13]: Wertheim, J. O.; Chu, D. K. W.; Peiris, J. S. M.; Kosakovsky Pond, S. L.; Poon, L. L. M. Poon. A Case for the Ancient Origin of Coronaviruses. *Journal of Virology*. Vol. 87, No. 12. DOI: <https://doi.org/10.1128/jvi.03273-12>
- [14]: Singh, D., Yi, S.V. On the origin and evolution of SARS-CoV-2. *Exp Mol Med* 53, 537–547 (2021). <https://doi.org/10.1038/s12276-021-00604-z>
- [15]: Claramunt, S.; Cracraft, J. A new time tree reveals Earth history's imprint on the evolution of modern birds. *Sci Adv*. 2015 Dec 11;1(11):e1501005. doi: 10.1126/sciadv.1501005. PMID: 26824065; PMID: PMC4730849.
- [16]: Tsagkogeorga, G.; Parker, J.; Stupka, E.; Cotton, J. A.; Rossiter, S. J. Phylogenomic Analyses Elucidate the Evolutionary Relationships of Bats. *Current Biology*. Volume 23, Issue 22, 18 November 2013, Pages 2262-2267
- [17]: Eberle, R.; Jones-Engel, L. Understanding Primate Herpesviruses. *J Emerg Dis Virol*. 2017 Mar;3(1):10.16966/2473-1846.127. doi: 10.16966/2473-1846.127. Epub 2017 Jan 31. PMID: 29607423; PMID: PMC5878061.
- [18]: Hurst, C.J.; Adcock, N.J. Relationship Between Humans and Their Viruses. *Viral Ecology*. 2000:519–48. doi: 10.1016/B978-012362675-2/50015-X. Epub 2007 May 9. PMID: PMC7150212.
- [19]: Wertheim, J.O.; Smith, M.D.; Smith, D.M.; Scheffler, K.; Kosakovsky Pond, S.L. Evolutionary origins of human herpes simplex viruses 1 and 2. *Mol Biol Evol*. 2014 Sep;31(9):2356-64. doi: 10.1093/molbev/msu185. Epub 2014 Jun 10. PMID: 24916030; PMID: PMC4137711.
- [20]: Tyrrell, D.A.; Bynoe, M.L. Cultivation of a novel type of common-cold virus in organ cultures. *Br Med J* 1965; 1(5448): 1467-70.
- [21]: Almeida, J.D.; Berry, D.M.; Cunningham, C.H.; Hamre, D.; Hofstad, M.S.; Mallucci, L.; McIntosh, K.; Tyrrell, D.A.J. *Virology: Coronaviruses*. *Nature* 1968; 220(5168): 650.
- [22]: Schalk, A.F.; Hawn, M.C. An apparently new respiratory disease of baby chicks. *J Am Vet Med Assoc* 1931; 78: 413-23.
- [23]: Bushnell, L.D.; Brandly, C.A. Laryngotracheitis in chicks. *Poultry Science* 1933; 12(1): 55-60.
- [24]: Beach, J.R.; Schalm, O.W. A filterable virus, distinct from that of laryngotracheitis, the cause of a respiratory disease of chicks. *Poultry Sci* 1936; 15(3): 199-206.
- [25]: McIntosh, K. "Coronaviruses: a comparative review." *Current topics in microbiology and immunology/Ergebnisse der Mikrobiologie und Immunitätsforschung* (1974): 85-129.
- [26]: Hamre, D.; Kindig, D.A.; Mann, J. Growth and intracellular development of a new respiratory virus. *J Virol*. 1967 Aug;1(4):810-6. doi: 10.1128/JVI.1.4.810-816.1967. PMID: 4912236; PMID: PMC375356.

- [27]: Macnaughton, M.R.; Madge, M.H. The genome of human coronavirus strain 229E. *J Gen Virol.* 1978 Jun;39(3):497-504. doi: 10.1099/0022-1317-39-3-497. PMID: 660165.
- [28]: Bradburne, A.F.; Tyrrell, D.A. The propagation of "coronaviruses" in tissue-culture. *Arch Gesamte Virusforsch.* 1969;28(2):133-50. doi: 10.1007/BF01249379. PMID: 4984061; PMCID: PMC7086760.
- [29]: Becker, W.B.; McIntosh, K.; Dees, J.H.; Chanock, R.M. Morphogenesis of avian infectious bronchitis virus and a related human virus (strain 229E). *J Virol.* 1967 Oct;1(5):1019-27. doi: 10.1128/JVI.1.5.1019-1027.1967. PMID: 5630226; PMCID: PMC375381.
- [30]: Kaye, H.S.; Ong, S.B.; Dowdle, W.R. Detection of coronavirus 229E antibody by indirect hemagglutination. *Appl Microbiol.* 1972 Nov;24(5):703-7. doi: 10.1128/am.24.5.703-707.1972. PMID: 4674373; PMCID: PMC380648.
- [31]: Zakstel'skaia, Lia.; Sheboldov, A.V.; Berezina, O.N.; Zhdanov, V.M. Poluchenie mechennykh izotopami preparatov koronavirusa OC43 pri razmnozhenii v mozge mysheĭ-sosunkov [Production of isotope-labeled coronavirus OC43 preparations through multiplication in the brain of suckling mice]. *Vopr Virusol.* 1973 Nov-Dec;18(6):738-41. Russian. PMID: 4789993.
- [32]: WHO (18 May 2004). "China's latest SARS outbreak has been contained, but biosafety concerns remain – Update 7". World Health Organization. Archived from the original on 12 February 2020. Retrieved 14 February 2020.
- [33]: Li, F.; Li, W.; Farzan, M.; Harrison, S. C. Harrison. Structure of SARS coronavirus spike receptor-binding domain complexed with receptor. *Science.* 2005;309.5742: 1864-1868.
- [34]: Li, Wendong; Shi, Zhengli; Yu, Meng; Ren, Wuze; Smith, Craig; Epstein, Jonathan H; Wang, Hanzhong; Cramer, Gary; Hu, Zhihong; Zhang, Huajun; Zhang, Jianhong; McEachern, Jennifer; Field, Hume; Daszak, Peter; Eaton, Bryan T; Zhang, Shuyi; Wang, Lin-Fa (28 October 2005). "Bats Are Natural Reservoirs of SARS-Like Coronaviruses". *Science.* 310 (5748): 676–679. doi:10.1126/science.1118391.
- [35]: Boyd Y.; Curtis, K. M.; Fritz, E. A.; Hensley, L. E.; Jahrling, P. B.; Prentice, E.; Denison, M. R.; Geisbert, T. W.; Baric, R. S. Reverse genetics with a full-length infectious cDNA of severe acute respiratory syndrome coronavirus. *PNAS.* 2003: 100 (22) 12995-13000.
- [36]: Cyranoski, D. (23 February 2017). "Inside the Chinese lab poised to study world's most dangerous pathogens". *Nature.* 542 (7642): 399–400.
- [37]: Hixenbaugh, M. "Scientists were close to a coronavirus vaccine years ago. Then the money dried up." < <https://www.nbcnews.com/health/health-care/scientists-were-close-coronavirus-vaccine-years-ago-then-money-dried-n1150091>>. CBS News. March 5, 2020. Accessed 8/11/2023.
- [38]: Morrison, J. S.; Ayotte, K.; Gerberding, J. "Ending the Cycle of Crisis and Complacency in U.S. Global Health Security: A Report of the CSIS Commission on Strengthening America's Health Security." Center for Strategic and International Studies.

November 2019. < [https://csis-website-prod.s3.amazonaws.com/s3fs-public/publication/191122\\_EndingTheCycle\\_GHSC\\_WEB\\_FULL\\_11.22.pdf](https://csis-website-prod.s3.amazonaws.com/s3fs-public/publication/191122_EndingTheCycle_GHSC_WEB_FULL_11.22.pdf)>

[39]: Bar-On, Y. M.; Flamholz, A.; Phillips, R.; Milo, R. Science Forum: SARS-CoV-2 (COVID-19) by the numbers. *eLife*. 2020;9:e57309

[40]: Pinals, R. L.; Ledesma, F.; Yang, D.; Navarro, N.; Jeong, S.; Pak, J. E.; Kuo, L.; Chuang, Y-C.; Cheng, Y-W.; Sun, H-Y.; Landry, M. P. Rapid SARS-CoV-2 Spike Protein Detection by Carbon Nanotube-Based Near-Infrared Nanosensors. *Nano Lett*. 2021; (21)5; 2272–2280. <https://doi.org/10.1021/acs.nanolett.1c00118>

[41]: Yao H, Song Y, Chen Y, Wu N, Xu J, Sun C, Zhang J, Weng T, Zhang Z, Wu Z, Cheng L, Shi D, Lu X, Lei J, Crispin M, Shi Y, Li L, Li S. Molecular Architecture of the SARS-CoV-2 Virus. *Cell*. 2020 Oct 29;183(3):730-738.e13. doi: 10.1016/j.cell.2020.09.018. Epub 2020 Sep 6. PMID: 32979942; PMCID: PMC7474903.

[42]: Suntsova, M.V., Buzdin, A.A. Differences between human and chimpanzee genomes and their implications in gene expression, protein functions and biochemical properties of the two species. *BMC Genomics* 21 (Suppl 7), 535 (2020). <https://doi.org/10.1186/s12864-020-06962-8>

[43]: Eckerle LD, Becker MM, Halpin RA, Li K, Venter E, Lu X, Scherbakova S, Graham RL, Baric RS, Stockwell TB, Spiro DJ, and Denison MR. 2010. Infidelity of SARS-CoV Nsp14-exonuclease mutant virus replication is revealed by complete genome sequencing. *PLoS Pathog*. 6:e1000896.

[44]: Duffy S, Shackelton LA, and Holmes EC. 2008. Rates of evolutionary change in viruses: patterns and determinants. *Nat. Rev. Genet*. 9:267–276.

[45]: Holgado, B.; Suñer, M. Palaeodiversity and evolution in the Mesozoic world. *J Iber Geol*. 2018;44; 1–5. <https://doi.org/10.1007/s41513-018-0058-2>

[46]: Smith, D. R. “Chapter 1 - The application of iPSCs to questions in virology: a historical perspective.” *iPSCs for Studying Infectious Diseases: Volume 8 in Advances in Stem Cell Biology*. Edited by: Alexander Birbrair, Academic Press, 2021, pages 1-30.

[47]: Souilmi Y, Lauterbur ME, Tobler R, Huber CD, Johar AS, Moradi SV, Johnston WA, Krogan NJ, Alexandrov K, Enard D. An ancient viral epidemic involving host coronavirus interacting genes more than 20,000 years ago in East Asia. *Curr Biol*. 2021 Aug 23;31(16):3504-3514.e9. doi: 10.1016/j.cub.2021.05.067. Epub 2021 Jun 24. Erratum in: *Curr Biol*. 2021 Aug 23;31(16):3704. PMID: 34171302; PMCID: PMC8223470.

[48]: Sun J, He WT, Wang L, Lai A, Ji X, Zhai X, Li G, Suchard MA, Tian J, Zhou J, Veit M, Su S. COVID-19: Epidemiology, Evolution, and Cross-Disciplinary Perspectives. *Trends Mol Med*. 2020 May;26(5):483-495. doi: 10.1016/j.molmed.2020.02.008. Epub 2020 Mar 21. PMID: 32359479; PMCID: PMC7118693.

[49]: Huang C, Wang Y, Li X, Ren L, Zhao J, Hu Y, Zhang L, Fan G, Xu J, Gu X, Cheng Z, Yu T, Xia J, Wei Y, Wu W, Xie X, Yin W, Li H, Liu M, Xiao Y, Gao H, Guo L, Xie J, Wang G, Jiang R, Gao Z, Jin Q, Wang J, Cao B. Clinical features of patients infected with 2019 novel coronavirus in Wuhan, China. *Lancet*. 2020 Feb 15;395(10223):497-506. doi: 10.1016/S0140-6736(20)30183-5. Epub 2020 Jan 24. Erratum in: *Lancet*. 2020 Jan 30;: PMID: 31986264; PMCID: PMC7159299.

- [50]: "Illuminating China's Provinces, Municipalities & Autonomous Regions."  
<http://www.china.org.cn/english/features/43585.htm> Accessed August 12, 2023.
- [51]: Yu, G.; Yanfeng, P.; Rui, Y.; Yuding, F.; Danmeng, M.; Murphy, F.; Wei, H.; Shen, T. (29 February 2020). "In Depth: How Early Signs of a SARS-Like Virus Were Spotted, Spread, and Throttled". Caixin Global. Accessed August 12, 2023.
- [52]: 体育总局：防控疫情，取消举办体育六艺系列活动之乐动冰雪\_中国政库\_澎湃新闻-The Paper. Thepaper.cn. n.d. Archived from the original on 23 January 2020. Accessed August 12, 2023.
- [53]: 武汉华南海鲜市场休市整治：多数商户已关门停业(图). January 2020.  
<<https://finance.sina.com.cn/china/gncj/2020-01-01/doc-iihnzhfz9652655.shtml>>  
Archived from the original on 2 January 2020. Accessed August 12, 2023.
- [54]: Wu F, Zhao S, Yu B, Chen YM, Wang W, Song ZG, Hu Y, Tao ZW, Tian JH, Pei YY, Yuan ML, Zhang YL, Dai FH, Liu Y, Wang QM, Zheng JJ, Xu L, Holmes EC, Zhang YZ. A new coronavirus associated with human respiratory disease in China. *Nature*. 2020 Mar;579(7798):265-269. doi: 10.1038/s41586-020-2008-3. Epub 2020 Feb 3. Erratum in: *Nature*. 2020 Apr;580(7803):E7. PMID: 32015508; PMCID: PMC7094943.
- [55]: Gorbalenya, A. E.; Baker, S. C.; Baric, R. S.; de Groot, R. J.; Drosten, C.; Gulyaeva, A. A.; Haagmans, B. L.; Lauber, C.; Leontovich, A. M.; Neuman, B. W.; Penzar, D.; Perlman, S.; Poon, L. L. M.; Samborskiy, D.; Sidorov, I. A.; Sola, I.; Ziebuhr, J. Severe acute respiratory syndrome-related coronavirus: The species and its viruses – a statement of the Coronavirus Study Group. *bioRxiv* 2020.02.07.937862; doi: <https://doi.org/10.1101/2020.02.07.937862>
- [56]: Coronaviridae Study Group of the International Committee on Taxonomy of Viruses. The species Severe acute respiratory syndrome-related coronavirus: classifying 2019-nCoV and naming it SARS-CoV-2. *Nat Microbiol* 5, 536–544 (2020).  
<https://doi.org/10.1038/s41564-020-0695-z>
- [57]: Holshue, M.L.; DeBolt, C.; Lindquist, S.; Lofy, K.H.; Wiesman, J.; Bruce, H. First case of 2019 novel coronavirus in the United States. *N Engl J Med*. 2020 Jan 31 doi: 10.1056/NEJMoa2001191.
- [58]: Smith, D.R. Review a brief history of coronaviruses in Thailand. *J Virol Methods*. 2021 Mar;289:114034. doi: 10.1016/j.jviromet.2020.114034. Epub 2020 Dec 4. PMID: 33285189; PMCID: PMC7831773.
- [59]: CDC Museum COVID-19 timeline. <https://www.cdc.gov/museum/timeline/covid19.html> Accessed August 12, 2023
- [60]: WHO Director-General's opening remarks at the media briefing on COVID-19 - 11 March 2020. < <https://www.who.int/director-general/speeches/detail/who-director-general-s-opening-remarks-at-the-media-briefing-on-covid-19---11-march-2020>>. Accessed August 12, 2023.
- [61]: Chow, C.C.; Chang, J.C.; Gerkin, R.C.; Vattikuti, S. Global prediction of unreported SARS-CoV2 infection from observed COVID-19 cases. *medRxiv* [Preprint]. 2020 May 5:2020.04.29.20083485. doi: 10.1101/2020.04.29.20083485. PMID: 32510525; PMCID: PMC7239078.



[62]: “CUMULATIVE CASES OVER TIME: Where COVID-19 cases have been reported across the globe.” Johns Hopkins University of Medicine Coronavirus Research Center, Thursday, March 16, 2023. < <https://coronavirus.jhu.edu/data/animated-world-map> > Accessed August 12, 2023.

[63]: Onyeaka, H.; Anumudu, C.K.; Al-Sharify, Z.T.; Egele-Godswill, E.; Mbaegbu, P. COVID-19 pandemic: A review of the global lockdown and its far-reaching effects. *Science Progress*. 2021;104(2). doi:10.1177/00368504211019854

[64]: Pillai, S.; Siddika, N.; Hoque, A. E.; Kabir, R. COVID-19: Situation of European Countries so Far. *Arch Med Res*. 2020 Oct;51(7):723-725. doi: 10.1016/j.arcmed.2020.05.015. Epub 2020 May 22. PMID: 32475614; PMCID: PMC7242919.

[65]: Juul, F.E.; Jodal, H.C.; Barua, I.; Refsum, E.; Olsvik, Ø.; Helsingen, L.M.; Løberg, M.; Bretthauer, M.; Kalager, M.; Emilsson, L. Mortality in Norway and Sweden during the COVID-19 pandemic. *Scand J Public Health*. 2022 Feb;50(1):38-45. doi: 10.1177/14034948211047137. Epub 2021 Oct 5. PMID: 34609261; PMCID: PMC8807990.

[66]: Korber, B.; Fischer, W.M.; Gnanakaran, S.; Yoon, H.; Theiler, J.; Abfalterer, W.; Hengartner, N.; Giorgi, E.E.; Bhattacharya, T.; Foley, B.; Hastie, K.M.; Parker, M.D.; Partridge, D.G.; Evans CM, Freeman TM, de Silva TI; Sheffield COVID-19 Genomics Group; McDanal C, Perez LG, Tang H, Moon-Walker A, Whelan SP, LaBranche CC, Saphire EO, Montefiori DC. Tracking Changes in SARS-CoV-2 Spike: Evidence that D614G Increases Infectivity of the COVID-19 Virus. *Cell*. 2020 Aug 20;182(4):812-827.e19. doi: 10.1016/j.cell.2020.06.043. Epub 2020 Jul 3. PMID: 32697968; PMCID: PMC7332439.

[67]: Dawood, A. A. Mutated COVID-19 may foretell a great risk for mankind in the future. *New Microbes and New Infections*. 2020 May; 35, 100673.

[68]: Khare, S., et al (2021) GISAID's Role in Pandemic Response. *China CDC Weekly*, 3(49): 1049-1051. doi: 10.46234/ccdcw2021.255 PMCID: 8668406

[69]: Elbe, S. and Buckland-Merrett, G. (2017) Data, disease and diplomacy: GISAID's innovative contribution to global health. *Global Challenges*, 1:33-46. doi: 10.1002/gch2.1018 PMCID: 31565258

[70]: Shu, Y. and McCauley, J. (2017) GISAID: from vision to reality. *EuroSurveillance*, 22(13) doi: 10.2807/1560-7917.ES.2017.22.13.30494 PMCID: PMC5388101

[71]: O'Toole, Á.; Scher, E.; Underwood, A.; Jackson, B.; Hill, V.; McCrone, J. T.; Colquhoun, R.; Ruis, C.; Abu-Dahab, K.; Taylor, B.; Yeats, C.; Du Plessis, L.; Maloney, D.; Medd, N.; Attwood, S. W.; Aanensen, D. M.; Holmes, E. C.; Pybus, O. G.; Rambaut, A. Assignment of epidemiological lineages in an emerging pandemic using the pangolin tool. *Virus Evolution*. 2021. DOI:10.1093/ve/veab064

[72]: Rambaut A, Holmes EC, O'Toole Á, Hill V, McCrone JT, Ruis C, du Plessis L & Pybus OG. A dynamic nomenclature proposal for SARS-CoV-2 lineages to assist genomic epidemiology. (2020) *Nature Microbiology* DOI:10.1038/s41564-020-0770-5

- [73]: Mathieu, E.; Ritchie, H.; Rodés-Guirao, L.; Appel, C.; Giattino, C.; Hasell, J.; Macdonald, B.; Dattani, S.; Beltekian, D.; Ortiz-Ospina, E.; Roser, M. (2020) - "Coronavirus Pandemic (COVID-19)". Published online at OurWorldInData.org. Retrieved from: '<https://ourworldindata.org/coronavirus>' [Online Resource]
- [74]: Cui, J.; Li, F.; Shi, Z.L. Origin and evolution of pathogenic coronaviruses. *Nat Rev Microbiol* 17, 181–192 (2019). <https://doi.org/10.1038/s41579-018-0118-9>
- [75]: Khailany RA, Safdar M, Ozaslan M. Genomic characterization of a novel SARS-CoV-2. *Gene Rep.* 2020 Jun;19:100682. doi: 10.1016/j.genrep.2020.100682. Epub 2020 Apr 16. PMID: 32300673; PMCID: PMC7161481.
- [76]: Yadav R, Chaudhary JK, Jain N, Chaudhary PK, Khanra S, Dhamija P, Sharma A, Kumar A, Handu S. Role of Structural and Non-Structural Proteins and Therapeutic Targets of SARS-CoV-2 for COVID-19. *Cells.* 2021 Apr 6;10(4):821. doi: 10.3390/cells10040821. PMID: 33917481; PMCID: PMC8067447.
- [77]: Zhang, J.; Ejikemeuwa, A.; Gerzanich, V.; Nasr, m.; Tang, Q.; Simard, J. M.; Zhao, R. Y. Understanding the Role of SARS-CoV-2 ORF3a in Viral Pathogenesis and COVID-19. *Front. Microbiol.*, 09 March 2022. Volume 13 – 2022. <https://doi.org/10.3389/fmicb.2022.854567>
- [78]: Payne S. Family Coronaviridae. *Viruses.* 2017:149–58. doi: 10.1016/B978-0-12-803109-4.00017-9. Epub 2017 Sep 1. PMCID: PMC7149805.
- [79]: Satarker S, Nampoothiri M. Structural Proteins in Severe Acute Respiratory Syndrome Coronavirus-2. *Arch Med Res.* 2020 Aug;51(6):482-491. doi: 10.1016/j.arcmed.2020.05.012. Epub 2020 May 25. PMID: 32493627; PMCID: PMC7247499.
- [80]: Isachenko V, Isachenko E, Mallmann P, Rahimi G. High cryo-resistance of SARS-CoV-2 virus: Increased risk of re-contamination at transplantation of cryopreserved ovarian tissue after COVID-19 pandemic. *Cryobiology.* 2021 Dec;103:1-6. doi: 10.1016/j.cryobiol.2021.09.009. Epub 2021 Sep 25. PMID: 34571024; PMCID: PMC8463116.
- [81]: Huang, Y., Yang, C., Xu, X-F. et al. Structural and functional properties of SARS-CoV-2 spike protein: potential antiviral drug development for COVID-19. *Acta Pharmacol Sin* 41, 1141–1149 (2020). <https://doi.org/10.1038/s41401-020-0485-4>
- [82]: Chan, Y. A.; Zhan, S. H. The Emergence of the Spike Furin Cleavage Site in SARS-CoV-2, *Molecular Biology and Evolution*, Volume 39, Issue 1, January 2022, msab327, <https://doi.org/10.1093/molbev/msab327>
- [83]: Shang, J.; Wan, Y.; Luo, C.; Ye, G.; Geng, Q.; Auerbach, A.; Li, F. Cell entry mechanisms of SARS-CoV-2. *PNAS.* 2020 May: 117 (21) 11727-11734.
- [84]: Sun, J.; He, W.T.; Wang, L.; Lai, A.; Ji, X.; Zhai, X.; Li, G.; Suchard, M.A.; Tian, J.; Zhou, J.; Veit, M.; Su, S. COVID-19: Epidemiology, Evolution, and Cross-Disciplinary Perspectives. *Trends Mol Med.* 2020 May;26(5):483-495. doi: 10.1016/j.molmed.2020.02.008. Epub 2020 Mar 21. PMID: 32359479; PMCID: PMC7118693.

- [85]: Lan, J.; Ge, J.; Yu, J.; Shan, S.; Zhou, H.; Fan, S.; Zhang, Q.; Shi, X.; Wang, Q.; Zhang, L.; Wang, X. Structure of the SARS-CoV-2 spike receptor-binding domain bound to the ACE2 receptor. *Nature* 581, 215–220 (2020). <https://doi.org/10.1038/s41586-020-2180-5>
- [86]: Shang, J., Ye, G., Shi, K. et al. Structural basis of receptor recognition by SARS-CoV-2. *Nature* 581, 221–224 (2020). <https://doi.org/10.1038/s41586-020-2179-y>
- [87]: Takeda, M. Proteolytic activation of SARS-CoV-2 spike protein. *Microbiol Immunol.* 2022 Jan;66(1):15-23. doi: 10.1111/1348-0421.12945. Epub 2021 Oct 12. PMID: 34561887; PMCID: PMC8652499.
- [88]: Coutard, B.; Valle, C.; de Lamballerie, X.; B. Canard, Seidah, N.G.; E. Decroly. The spike glycoprotein of the new coronavirus 2019-nCoV contains a furin-like cleavage site absent in CoV of the same clade. *Antiviral Research.* Volume 176, April 2020, 104742
- [89]: Li, X.; Yuan, H.; Li, X.; Wang, H. Spike protein mediated membrane fusion during SARS-CoV-2 infection. *J Med Virol.* 2023 Jan;95(1):e28212. doi: 10.1002/jmv.28212. Epub 2022 Oct 25. PMID: 36224449; PMCID: PMC9874878.
- [90]: Hardenbrook, N.J.; Zhang, P. A structural view of the SARS-CoV-2 virus and its assembly. *Current Opinion in Virology.* 2022 Feb; 52: 123-134.

## Chapter 2

### **The Effect of Select SARS-CoV-2 N-linked Glycans and Variant of Concern Spike Protein Mutations on C-Type Lectin Receptor-Mediated Infection**

This chapter is in submission with minor modifications at *Viruses*, manuscript ID: viruses-2557296

#### **2.1 Abstract**

The SARS-CoV-2 virion has shown remarkable resilience, capable of mutating to escape immune detection and re-establishing infectious capabilities despite new vaccine rollouts. Therefore, there is a critical need to identify relatively immutable epitopes on the SARS-CoV-2 virion that are resistant to future mutations the virus may accumulate. While hACE2 has been identified as the receptor that mediates SARS-CoV-2 susceptibility, it is only modestly expressed in the lung tissue. C-type lectin receptors like DC-SIGN can act as attachment sites to enhance SARS-CoV-2 infection of cells with moderate or low hACE2 expression. We developed an easy-to-implement assay system that allows for the testing of SARS-CoV-2 Trans-infection. Using our assay, we assessed how SARS-CoV-2 Spike S1 domain glycans and Spike proteins from different strains affected the ability of pseudotyped lentivirions to undergo DC-SIGN mediated Trans-infection. Through our experiments with 7 glycan point mutants, 2 glycan cluster mutants, and four strains of SARS-CoV-2 Spike, we found that glycans N17 and N122 appear to have significant roles in maintaining Covid-19's infectious capabilities. We further found the virus cannot retain infectivity upon the loss of multiple glycosylation sites, and that the Omicron BA.2 strain pseudovirions may have an increased ability to bind to other non-lectin receptor proteins on the surface of cells. Taken together, our work opens the door to the development of new therapeutics that can target overlooked epitopes of the SARS-CoV-2 virion to prevent C-type lectin receptor mediated Trans-infection in the lung tissue.

#### **2.2 Introduction**

Despite the rapid development and wide dissemination of SARS-CoV-2 vaccines, for the past 2 years the winter season has culminated in a surge in coronavirus infections [1]. These surges coincided with the rise of new variants that could evade detection by the immune system: the Variants of Concern (VOC) B.1.1.7 (Alpha), B.1.135 (Beta), B.1.525 (Eta), B.1.617.1 (Delta) and P.1/B.1.1.28.1 (Gamma) were all identified in the late Fall to Winter of 2020-2021 [2, 3]. B.1.1.529 (Omicron) was identified in several countries in November of 2021, and currently various Omicron subvariants have developed and display increased vaccine evasion. Out of these new variants, Omicron XBB.1.5 is rapidly taking over the proportion of Covid-19 cases globally and appears to reliably establish breakthrough infections in patients who had been vaccinated more than three times (including patients who have received bivalent boosters) [3-6].

The consistent ability of SARS-CoV-2 to avoid recognition by the immune system and establish breakthrough infections despite vaccine rollouts has led to numerous members of the medical community to concede that Covid-19 is here to stay. Much like the seasonal flu, annual or even biannual booster shots are commonplace and necessary to combat the latest variants of the virus [7, 8]. Even though the mutation rate

of the polymerase for SARS-CoV-2 is an order of magnitude or so lower than for human immunodeficiency virus (HIV)-1, the ease of infection, relatively broad tropism, and long course of infection allows for sufficient rates of mutations for the SARS-CoV-2 genome to escape immune detection and eventually establish breakthrough infection [9, 10, 11]. The evidence that Covid-19 will likely continue to mutate is perhaps best exemplified by how globally, Delta strains were the dominant variant of SARS-CoV-2 for about 6 months between June and December of 2021, with nearly 100% of Covid-19 cases worldwide testing as the Delta variant for the latter 5 months of that period [6]. And yet, despite this dominance, Omicron is now the prevalent variant with almost triple the number of spike mutations as Delta [7]. While initial selective pressure on the Omicron strain favored immune escape, it appears that Omicron strains are now undergoing mutations to increase their pathogenic activity, as shown by the increased transmissibility of Omicron BA.2 and BA.3 when compared to BA.1, and the increased fusogenic activity of more recent strains like Omicron XBB.1.5, CA.3.1 and CH.1.1 when compared to BA.2 [4, 10-15].

The SARS-CoV-2 genome is approximately 29,900 nucleotides long and encodes 16 nonstructural, 4 structural, and up to 6 accessory proteins [16]. Since the 16 nonstructural proteins are involved with replication and transcription, and the 6 accessory proteins are not incorporated into the mature virion (although they are hypothesized to impede the host immune system signaling or otherwise aid in viral pathogenesis), this leaves the 4 structural proteins as the key factors that can affect virion architecture, determine virus infectivity, and act as antigen recognition sites for the host immune system [16-18]. Of these 4 structural proteins, one of them- the N protein- associates with the viral RNA genome on the interior of the virion [16]. The other three proteins are expressed on the surface of the viral particle, and are called S (Spike protein), M (Membrane protein), and E (Envelope protein). Perhaps the most clinically relevant protein out of the three surface proteins is the Spike protein, since it directs recognition and fusion mediated via the human Angiotensinogen Converting Enzyme 2 (hACE2) receptor on the surface of target cells [16]. Nearly all antibodies that display neutralizing ability against SARS-CoV-2 bind to the Spike protein, particularly the S1 domain [19-22]. Furthermore, RNA vaccines (Moderna mRNA-1273 and Pfizer-BioNTech BNT162b2/Comirnaty), adenoviral vaccines (Astrazeneca-Oxford ChAdOx1-S and Janssen Biologics B.V./Janssen Pharmaceutica NV COVID-19 Vaccine Janssen) and novel mosaic/nanoparticle vaccines raise antibodies against the Spike protein, further highlighting that Covid-19 breakthrough infections are largely determined by epitope modification of the Spike protein [23-27]. Ergo, there is an urgent need to identify immutable locations (also known as “cold spots”) on the SARS-CoV-2 Spike protein and use these to create variant-proof Covid-19 vaccines and prophylactics [28-30].

The S protein is a trimeric transmembrane glycoprotein comprised of two domains: the S1 domain, which is responsible for attachment to target cells via the hACE2 receptor, and the S2 domain, which contains the fusion peptide and orchestrates membrane fusion and viral infection [21, 31]. The S1 domain is further subdivided into an N-terminal Domain (NTD), two C-terminal Domains (CTD1 and CTD2), and a

Receptor Binding Domain (RBD) which contains a surface called the Receptor Binding Motif (RBM). The RBM is a 69 amino acid loop that contains the 17 residues that contact 20 residues in the hACE2 N-terminal helix and are integral in dictating SARS-CoV-2 tropism [31-33]. The Spike protein can adopt two conformations: a “down” or “closed” position where the RBM is inaccessible to the hACE2 receptor, and an “up” or “open” position where the RBD opens and reveals the RBM for binding to the hACE2 receptor [31-33].

The SARS-CoV-2 S protein also has 22 N-linked glycosylation sites and 2 O-linked glycosylation sites [34-37]. Glycans on viral spike proteins perform several functions, including being recognized by receptors on host cells, maintaining protein stability, and shielding viral spike epitopes from the host immune system [34, 38-40]. In the case of SARS-CoV-2, it has been shown that lectin receptors such as Dendritic Cell-Specific Intercellular adhesion molecule-3-Grabbing Non-integrin (DC-SIGN), Liver/lymph node-specific intracellular adhesion molecules-3 grabbing non-integrin (L-SIGN), C-type lectin domain family 4 member G (CLEC4G) and sialic acid binding Ig like lectin 1 (SIGLEC1) can bind to the glycans on the surface of the S protein and “hold” the virus in close proximity to cells, thereby facilitating more efficient infection [41-45]. This is particularly pertinent for the progression of Covid-19 since SARS-CoV-2 virions are transmitted via airborne routes and infection initiates in the proximal airways [42, 46]. While lung tissue acts as the point-of-entry for SARS-CoV-2 virions, the respiratory system only modestly express hACE2. It has been shown that lectin receptor-mediated Trans-infection- whereby a cell type that expresses a lectin receptor facilitates the transfer and entry of SARS-CoV-2 virions to cells that mildly express hACE2- is the primary process by which Covid-19 initiates infection in the lungs [42, 45, 47-49]. This is further supported by the fact that lung tissue is highly patrolled by the innate immune system, with DC-SIGN+ dendritic cells being found throughout the lung interstitium and in the airways (Figure S1) [43]. Most significantly, in contrast to other viruses like HIV and Ebola virus, almost none of the SARS-CoV-2 Variants of Concern (VOC) have displayed any alteration at the key Asparagines where N-linked glycosylation is found on the SARS-CoV-2 Spike [41, 50-53]. Considering the number of mutation sites across all SARS-CoV-2 VOC (Figure 1)- 109 mutations in the 1273 aa long Spike- and the fact that mutations are detectable in patients as early as 4 days of Covid-19 infection, the immutability of the SARS-CoV-2 Spike glycans is remarkable [54].

Composite Locations of SARS-CoV-2 Spike Mutations for All VOIs and VOCs June 2023

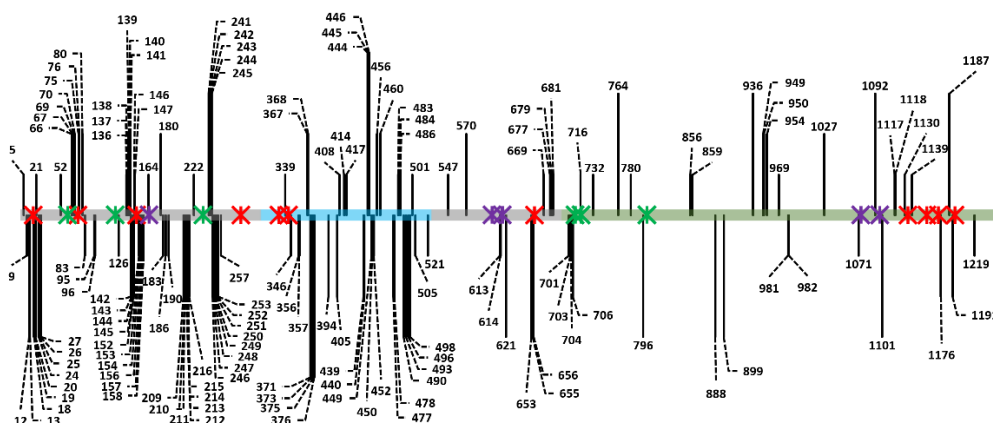


**Figure 1. Representation of the SARS-CoV-2 Spike gene amino acid sequence with all locations of VOC mutations.** S1 domain is depicted in grey (residues 14 to 685), which is further subdivided into 4 domains: the N-Terminal Domain (NTD, residues 14 to 306), the Receptor Binding Domain (RBD, residues 319 to 527, depicted in teal), and two C-Terminal Domains, C-Terminal Domain 1 (CTD1, residues 527 to 591) and C-Terminal Domain 2 (CTD2, residues 591 to 685). Within the Receptor Binding Domain is the Receptor Binding Motif (RBM, residues 438 to 506) which encompasses the key amino acids that mediate SARS-CoV-2 Spike protein binding to the host hACE2 receptor. The S2 domain is depicted in grey-green and ranges from residues 686 to 1273. Black lines indicate locations of point mutations across VOCs (for a list of the specific VOCs summarized here, see Figure S2). Red, Green, and Purple ✂ crosses depict locations of N-linked glycans. Red crosses indicate complex glycans, green crosses indicate high-mannose glycans, and purple crosses depict hybrid glycans and glycans that were inconsistently identified as being complex or high-mannose, as based on an analysis of existing literature (Figure S3, Figure S4). While mutations have occurred in VOC's immediately adjacent to glycan sites, there have been no variants that have mutations at the Asparagine residues where N-linked glycosylation is present [41, 52, 53].

In the following work, key glycans that are necessary for maintaining the functionality of the SARS-CoV-2 Spike in facilitating both hACE2-mediated Direct-infection and DC-SIGN mediated Trans-infection were identified. If specific glycan mutations diminished the infectivity of the virus, then there is likely a strong selective pressure for those glycans to be preserved no matter what possible mutations may occur in future variants of SARS-CoV-2. This would provide key epitope locations that could act as “cold spots” for the development of a variant-proof vaccine or prophylactic [42, 50]. Particular focus was given to those Spike glycans that were in close proximity to the RBD, since it was hypothesized that impairing the conformational dynamics of the Receptor Binding Domain would have the highest likelihood of preventing infection. Indeed, this is likely why numerous vaccines currently in development make use of the RBD as the antigen rather than the full-length Spike [10, 25, 55, 56]. However, since the eventual goal of this work is to identify SARS-CoV-2 Spike protein epitopes beyond what current therapeutics target, N-linked glycans that were proximal to the Spike RBD- but not directly on it- were selected. In this study, the glycans at N17, N61, N74, N122, N149, N165, and N234 were assessed.

In addition to evaluating the importance of S1 domain glycans, we also assessed how Spike glycoproteins from certain VOC strains affected the infectivity of SARS-CoV-2 pseudotyped virions. The impact of how Spike proteins from some Covid-19 strains alter Direct-infectivity has already been tested *in vitro*, but to our knowledge, no *in vitro* lectin receptor-mediated Trans-infection tests have been performed to compare the susceptibility of different strains of SARS-CoV-2 [4, 10, 11, 14, 15, 57, 58, 59]. We report the differences in DC-SIGN-mediated Trans-infection for Wuhan CoV-19, D614G, Delta, and Omicron BA.2 pseudovirions on our assay system.

## 2.3 Results

### 2.3.1 Some, But Not All, SARS-CoV-2 Spike NTD Glycans Affect hACE2 Mediated Infectivity

To investigate the role of N-linked glycans in mediating infection by SARS-CoV-2, the 7 N-linked glycans proximal to the RBD were investigated: N17, N61, N74, N122, N149, N165, and N234 (Figure 2A, 2B). Most of these sites are predicted to be fairly well-occupied by high-mannose or hybrid glycans, thereby increasing the likelihood that C-type lectin receptors like DC-SIGN would bind and facilitate Trans-infection (Figure 2, Figure S3, Figure S4). Based on an analysis of nearly all PDB SARS-CoV-2 Cryo-EM structures as of June 30, 2023, the N17, N74, N149, and N165 glycans are present on highly flexible domains of the SARS-CoV-2 Spike, which suggests that these glycans are on regions of the spike that are solvent-exposed or are more likely to undergo allosteric changes that could further modulate the ability of the SARS-CoV-2 Spike to mediate infectivity (Figure S5). Previous literature has further predicted that glycans N165 and N234 assist in maintaining the SARS-CoV-2 Spike in the RBD-up conformation, which is necessary for interaction with ACE-2 and infection [61].



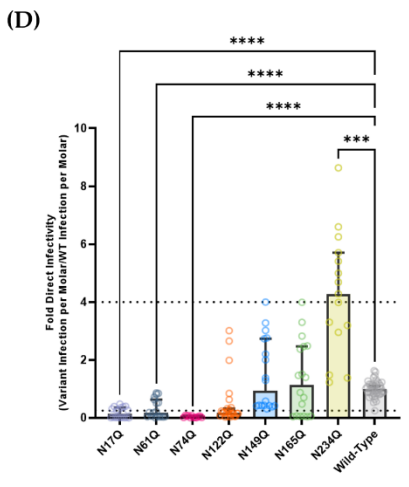
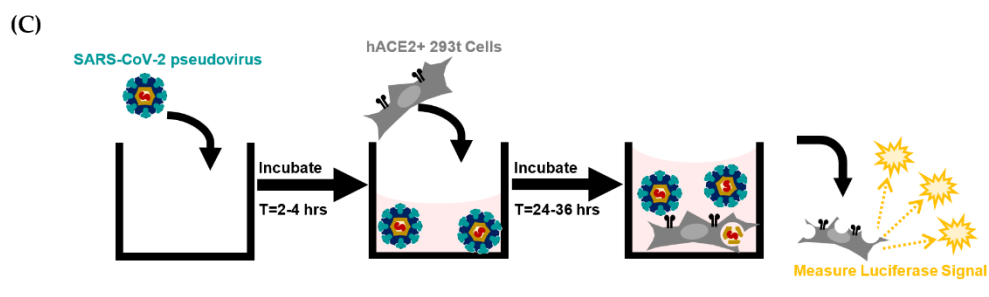
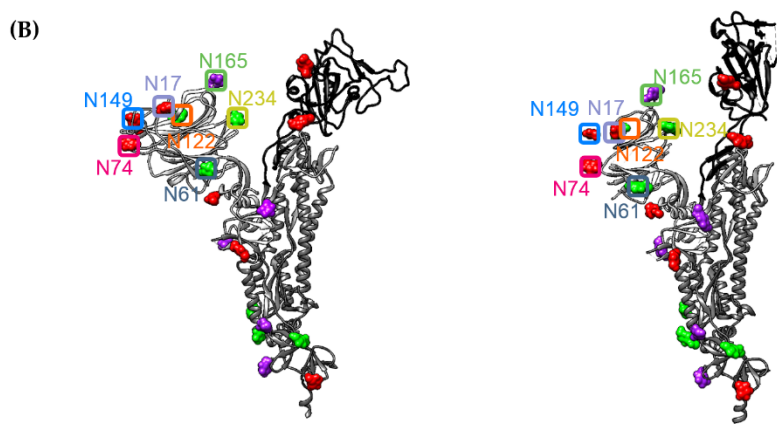
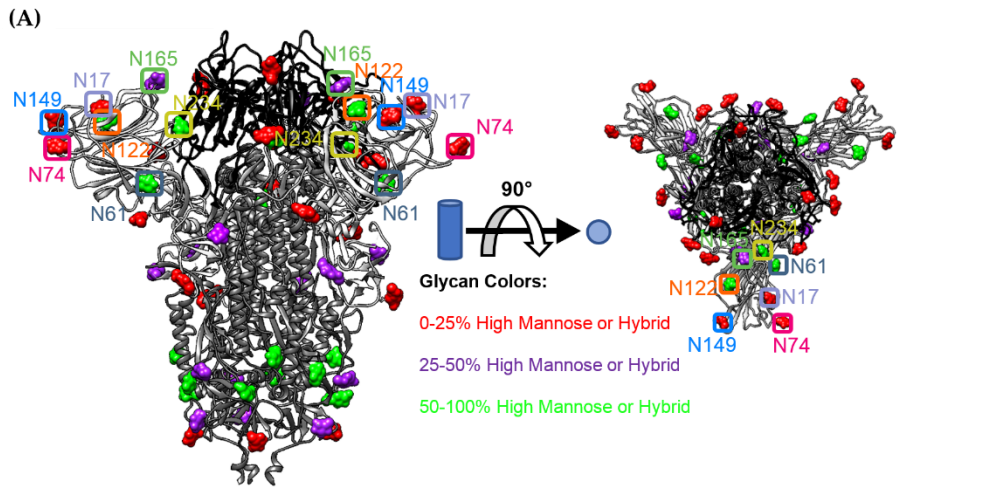


**Figure 2. Schematic of Spike mediated infection. (A)** Depiction of the trimeric SARS-CoV-2 Spike with glycans. The amino acid backbone is represented as a ribbon structure: S2 domain is dark gray, S1 Receptor Binding Domain is black, and the remainder of the S1 domain outside of the RBD is light grey. The locations of N-linked glycans are depicted as space-filling models of a representative monosaccharide. High-mannose glycans are depicted in green. Complex glycans are depicted in red. Hybrid glycans or glycans that have less than 50% consensus between high-mannose and complex based on existing literature are depicted in purple. The left side of the picture is a side profile of the trimeric spike protein. The right side is a top view of the trimeric spike protein. The RBD closed conformation structures are adapted from PDB ID: 7NT9 by Rosa, A. et. al. **(B)** Depiction of the SARS-CoV-2 Spike monomer. The RBD down/closed conformation is on the left while the RBD up/open conformation is on the right. Glycans are depicted and color coded as in 2A. The RBD closed conformation structures are all from PDB ID: 7NT9 by Rosa, A. The RBD up subunit is from PDB ID: 6VYB by Walls, A.C. et. al. **(C)** Simplified depiction of the Direct-infection process utilized for experiments. Viral samples were incubated in wells for 2-4 hours before adding cells to viral suspensions. This was done to more closely mimic the incubation step of the Trans-infection procedure (Figure 3). **(D)** Direct-Infectivity of selected SARS-CoV-2 Spike S1 domain N-linked glycosylation mutants. The infectivity for each mutant strain was normalized to Wild-Type nCov-19 Wuhan strain SARS-CoV-2 Spike pseudovirus. Dashed lines depict a four-fold difference in viral infectivity (threshold of significance based off of Li, Q. et. al.) [62]. Graphs depict median relative infectivity per strain with 95% confidence interval. Statistical analysis is a Welch ANOVA of Direct-infection with an Alpha value of 0.05. \* indicates a P-value < 0.1. \*\* indicates a P-value < 0.01. \*\*\* indicates a P-value < 0.001. \*\*\*\* indicates a P-value < 0.0001.

To study the functional role of the glycosylation proximal to the SARS-CoV-2 Spike RBD, we created mutated SARS-CoV-2 Spike genes whereby the Asparagine (N) residues at the aforementioned glycan sites were changed to Glutamine (Q) residues. All glycan mutants were created using a SARS-CoV-2 Wuhan 2019-nCoV Spike (Genbank NC\_045512) vector as the parent sequence. The resulting vectors were used to functionalize lentiviral pseudovirus that were then tested on a luciferase-based infectivity assay (Figure 2C) [60].

To determine the effect of these mutations on Direct-infection, each pseudovirus containing a Spike variant was used to infect 293t cells transduced to stably express high levels of hACE2 (Figure 2C, 2D). Results showed that N17Q, N61Q, and N74Q glycans had significantly reduced infectivity when compared to Wild-Type Spike lentiviral pseudovirus, displaying nearly an order of magnitude lower signal. This is largely in accordance with previous literature, where these glycan mutations tended to decrease infectivity by about 2- to 4- fold when compared to Wild-Type SARS-CoV-2 Spike pseudotyped virions [62, 63]. The more pronounced decrease in infectivity that we observed for these mutant strains- and particularly for the N74Q strain- could be explained by the fact that other systems utilized Vesicular stomatitis virus (VSV) pseudovirions (which have higher spike expression on their surface) or tested viral infectivity on different hACE2-expressing cell lines [62, 63].

Oddly, the N234Q pseudovirus showed increased infectivity compared to Wild-Type spike lentivirus, which appears to disagree with its hypothesized role in propping the RBD in an open conformation to facilitate more efficient Spike-hACE2 recognition [61]. Although unexpected, N234Q SARS-CoV-2 pseudotyped virus has been shown to have modestly decreased infectivity in the previous literature, indicating that its role as a glycan gate may not alter RBD-hACE2 recognition as much as previously thought [63, 64].

In contrast, the N122Q, N149Q and N165Q mutants do not demonstrate any significant alteration in infectivity when compared to the Wild-Type SARS-CoV-2 Spike. Granted, even though N122Q had too large of a spread to definitively state that it caused lower infectivity, the median and mean infectivity signal for the N122Q strain did tend to be about 4-fold lower than Wild-Type signal. Still, these infectivity signals are largely in accordance with previous literature: either moderately decreasing infectivity (N122Q) or falling somewhere between slightly enhancing infectivity to moderately attenuating infectivity (N149Q, N165Q) [62, 63].

### **2.3.2 Some SARS-CoV-2 Spike Glycans Mediate Lectin Receptor Binding and Transfer to Susceptible Cell Lines**

DC-SIGN is a human lectin receptor that has already been demonstrated to bind to recombinant SARS-CoV-2 Spike protein and facilitate infection-in-trans *in vitro* [42, 43, 45, 64,]. DC-SIGN is expressed on the surface of several immune cell subsets in the respiratory system (Figure S1). Due to the wide expression of DC-SIGN on various cell types within the respiratory system, it is accepted that DC-SIGN is a key attachment factor that allows for efficient SARS-CoV-2 infection of modestly-hACE2-expressing cells of the lungs (Figure 3A) [42, 43, 45].

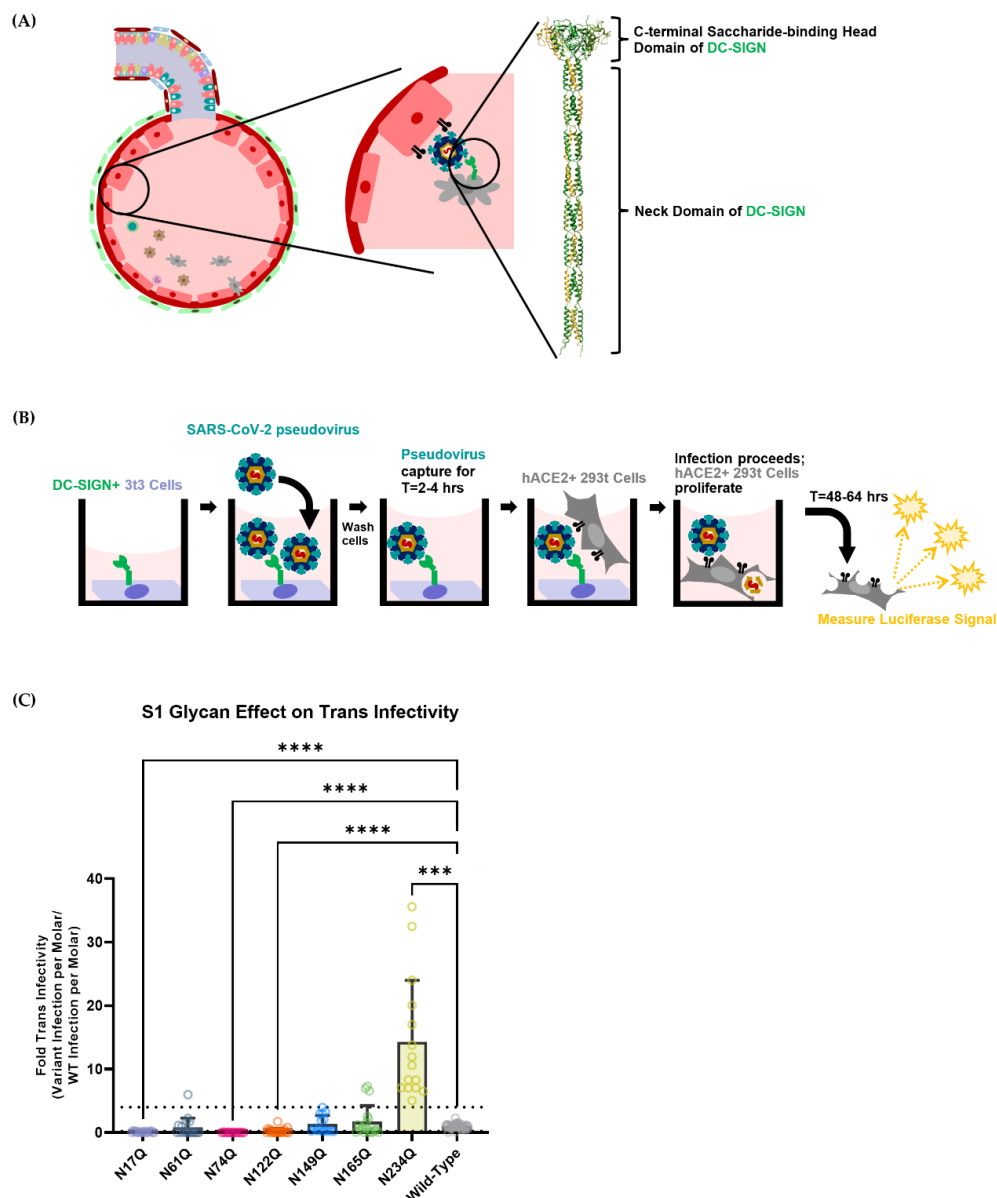


**Figure 3. DC-SIGN Trans-infection.** (A) Schematic diagram of how DC-SIGN could mediate infection-in-trans within the alveoli in vivo. On the right is an AlphaFold structure prediction of the DC-SIGN protein's extracellular domain [65, 66]. The structure was chosen by selecting the closest prediction to a previously constructed structure from Tabarani, G. et. al. [67]. DC-SIGN extracellular domain is a homotetramer that is comprised of a long neck domain and a C-terminal sugar-binding head domain. (B) Schematic diagram of the DC-SIGN Mediated Trans-Infection assay. In brief, 3t3 murine fibroblast cells expressing DC-SIGN were seeded into wells of a 96-well plate. After allowing cells to adhere, cells were incubated with SARS-CoV-2 Spike pseudotyped virions for several hours before being washed. HEK-293t hACE2+ cells were then seeded over the top, allowing captured virus to be delivered to susceptible cells, thereby modeling DC-SIGN facilitated Trans-infection. After allowing 293t hACE2+ cells to undergo infection for 48-64 hours, cells were lysed and luciferase activity was measured. (C) Trans-Infectivity of selected SARS-CoV-2 Spike S1 Domain N-linked glycosylation mutants. Trans-infection procedure was carried out as depicted in Figure 4A. Graphs depict median relative infectivity per strain with 95% confidence interval. Dashed lines show a 4-fold difference in infectivity, as inspired by existing literature [62].

Statistical analysis is a Welch ANOVA of Trans-infection with an Alpha value of 0.05. \* indicates a P-value < 0.1. \*\* indicates a P-value < 0.01. \*\*\* indicates a P-value < 0.001. \*\*\*\* indicates a P-value < 0.0001.

In light of the importance of viral capture in facilitating the spread of Covid-19, the SARS-CoV-2 S1 domain glycans analyzed in Figure 2 were then assessed to measure how they contributed to DC-SIGN mediated Trans-infection. To do so, an *in vitro* assay was developed to isolate the process of viral capture and transfer to a permissible hACE2-expressing cell. A murine 3t3 cell fibroblast line that had been transduced with the human lectin receptor DC-SIGN (3t3 DC-SIGN+) was used to capture SARS-CoV-2 pseudotyped lentivirus and mediate infection-in-trans (Figure 3B).

Each strain broadly followed the same trend for their Trans-infection signal as for Direct-infection: glycans N17, N61, N74, and N122 showed decreased infectivity while N234 showed enhanced infectivity when compared to Wild-Type nCoV-19 SARS-CoV-2 Spike (Figure 3C). Like N122Q for Direct-infectivity, the N61Q strain had too large of a spread to claim that it had significantly lower Trans-infectivity than Wild-Type virus. Although comparing the Trans-infection signal of each strain to the Wild-Type strain gave some idea of how the glycans contribute to DC-SIGN recognition, this information does not specify whether the decrease in infectivity is due to decreased SARS-CoV-2 Spike capture by DC-SIGN, or whether the decrease in infectivity is due to lower hACE2-mediated Direct-infection.

### 2.3.3 Deconvoluting Trans-Infection Propensity From Direct-Infectivity Reveals Apparent Bias of DC-SIGN For N17 and N122

To disentangle the effect of each glycan mutant on hACE2 entry from their effect on DC-SIGN binding, Trans-infection signal was normalized to Direct-infection signal for each SARS-CoV-2 pseudovirus strain to obtain each strain's propensity for Trans-infection (Figure 4A, 4B). This depicts each strain's potential to undergo DC-SIGN mediated infection-in-trans independent of the ability of each strain to bind to the hACE2 receptor.

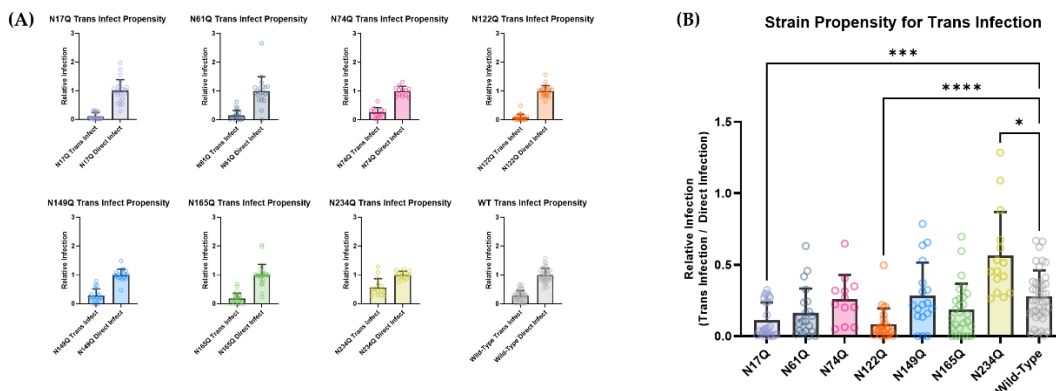


**Figure 4.** Deconvoluting signal of SARS-CoV-2 Direct- and Trans- infection reveals that S1 domain Spike glycans are important in mediating Trans-infection. **(A)** Direct- and Trans- infection signal for each pseudovirus glycan variant. **(B)** Each variant's Propensity for Trans-infection, whereby the signal of Trans-infection was normalized to each variants' hACE2 mediated Direct-infection. Statistical analysis is a Welch ANOVA with an Alpha value of 0.05. \* indicates a P-value < 0.1. \*\* indicates a P-value < 0.01. \*\*\* indicates a P-value < 0.001. \*\*\*\* indicates a P-value < 0.0001.

Wild-Type SARS-CoV-2 pseudotyped virus yielded a Trans-infectivity of about 28.1% the signal of Direct-infection. The mutations that removed accessible glycans moderately distal to the RBD (N17Q, N122Q) significantly decreased the Trans-infectivity of SARS-CoV-2 pseudotyped virions, indicating that DC-SIGN appears to primarily utilize these glycans to facilitate Trans-infection. This is perhaps because these glycans are far enough away from the viral membrane to allow for efficient DC-SIGN/Spike protein recognition but also ensure that hACE2-RBD interactions are not sterically hindered by the carbohydrate-recognition domain of DC-SIGN itself.

Conversely, the removal of glycans that were adjacent to the RBD (N165, N61) did not appear to impede Trans-infectivity. Structural analysis suggests that the DC-SIGN Carbohydrate Recognition Domain (CRD) cannot easily access the N61 glycan because of a possible clash with the 620-641 loop region of the S2 domain of the adjacent SARS-CoV-2 spike monomer. Likewise, the DC-SIGN CRD cannot access the N165 glycan due to a possible clash with the 466-491 loop within the Receptor Binding Motif. Since sterically impeding the RBM region of the SARS-CoV-2 Spike would drastically impair the ability of the virion to efficiently bind to hACE2, it is therefore highly unlikely that DC-SIGN is able to mediate Trans-infection by binding to N165. In short, DC-SIGN has a low likelihood of binding to glycans N61 or N165, so their removal does not significantly alter these variants' ability to undergo Trans-infection.

Interestingly, notable exceptions to this were N74 and N149: even though these glycans were distal to the SARS-CoV-2 spike RBD, the N74Q and N149Q pseudoviral mutants did not display attenuated DC-SIGN-mediated Trans-infectivity, with Trans-infection signals at 26.0% and 28.4% of Direct-infection signal respectively. This could be explained by the fact that DC-SIGN has a strong bias to bind to high-mannose sugars [42, 43]. The consensus in the literature is that when SARS-CoV-2 spike expressed in mammalian cells, N74 and N149 are predominantly occupied by complex glycans, suggesting that DC-SIGN would not have high affinity for these sites and thus would not rely on these glycans to capture SARS-CoV-2 virions (Figure S3).

Removal of N234 appeared to not only increase viral hACE2-mediated Direct-infectivity (Figure 2D), but also appeared to significantly increase the propensity of SARS-CoV-2 pseudotyped virus to undergo DC-SIGN mediated Trans-infection, with about two-fold higher calculated Trans-infection propensity than the Wild-type strain (Figure 4A, 4B). Even though N234 is highly occupied by mannose sugars (Figure S3)-thereby making it a favorable target for DC-SIGN binding- it is not as accessible as the other glycans, being almost completely obscured when an adjacent Spike is in the down conformation. Ergo, it is probably not accessible enough to act as a reliable epitope for DC-SIGN binding. While this provides some explanation for why removal of N234 doesn't impair SARS-CoV-2 pseudoviral infection-in-trans, it does not explain the increased propensity of SARS-CoV-2 Spike for infection.

At this point the differences in Trans-infection propensity could be explained by a multitude of factors, ranging from viral instability, to virion capture by other 3t3 cell surface receptors, to DC-SIGN binding to SARS-CoV-2 Spike glycans with different binding pockets [68]. Thus, it was necessary to verify that SARS-CoV-2 Spike glycan recognition by DC-SIGN was the causative factor in mediating Trans-infection.

### 2.3.4 DC-SIGN Mediated Trans-infection Is Verified By Mannan Inhibition

To verify that the observed differences in Trans-infection were indeed due to DC-SIGN's interaction with sugar moieties on the surface of the SARS-CoV-2 virion, the Trans-infection assay was performed in the presence of a competitive inhibitor of DC-SIGN binding. Mannan is a general term for a polymer of mannose sugars that can act as a competitive inhibitor of glycan-DC-SIGN binding (Figure 5A). Due to its low cost and high potency, mannan is a convenient control to validate whether the observed variations in Trans-infectivity for the glycan mutant pseudoviral strains was being mediated solely by DC-SIGN binding to the viral surface S1 glycans.

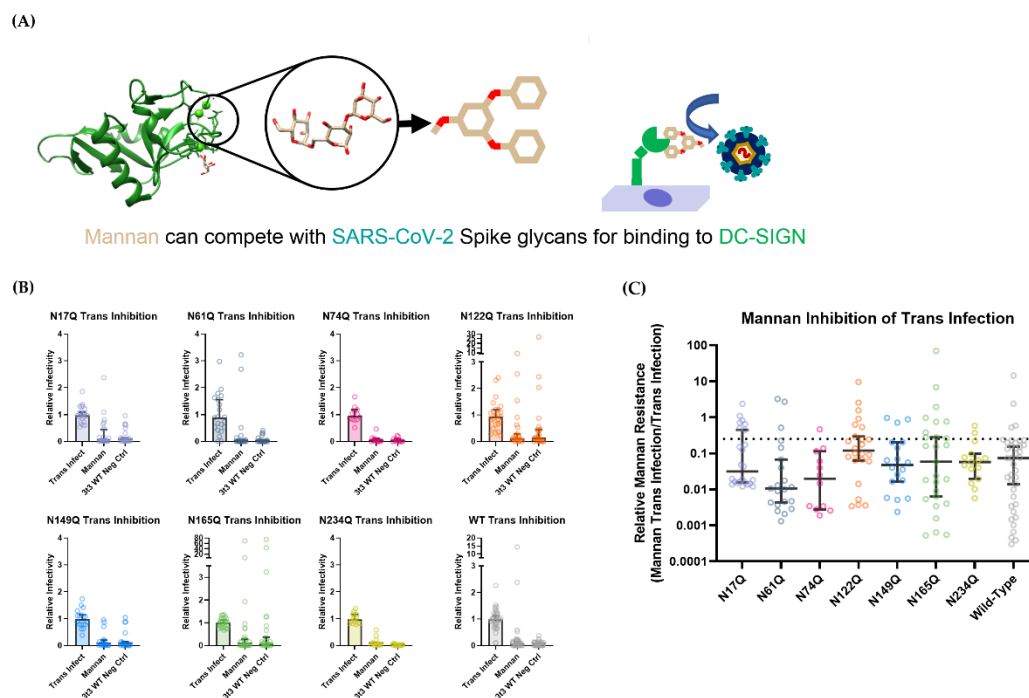


**Figure 5.** All SARS-CoV-2 pseudovirus Spike glycan mutations display similar susceptibilities to mannan-based Trans-inhibition. **(A)** Depiction of mannan (tan/red) acting as a competitive inhibitor of DC-SIGN (green) binding to sugars. Structure of DC-SIGN C-terminal domain is PDB: 1SL4 by Guo et. al. **(B)** Depiction of mannan inhibition of Trans-infection when compared to negative controls where 3t3 cells did not express DC-SIGN and to Trans-infection assays without mannan. **(C)** Depiction of how efficiently mannan inhibited Trans-infection for each glycan mutant strain. Dashed line depicts a signal 4-fold decrease in infectivity, as inspired by previous literature [62]. Wild-Type virus, when exposed to mannan, had Trans-infectivity reduced by 90%. A Welch and Brown-Forsythe Anova with an Alpha value of 0.05 demonstrated that there was no significant difference in mannan inhibition between any of the strains.

First it was verified that a concentration range of 0  $\mu\text{g/mL}$  to 185  $\mu\text{g/mL}$  of mannan did not significantly affect the ability of SARS-CoV-2 pseudovirions to undergo hACE2-mediated infection (Figure S8). After verifying that mannan did not appear to alter SARS-CoV-2 spike interaction with hACE2, 20  $\mu\text{g/mL}$  was used to inhibit Trans-infection for all SARS-CoV-2 glycan mutants.

All SARS-CoV-2 pseudovirus Spike mutant strains appeared to show identical susceptibility to mannan-based inhibition of Trans-infection, with about 90-95% diminishment of signal (Figure 5C). This provided strong evidence that the pseudoviral strains were captured by DC-SIGN and the variations in Trans-infection propensity observed in Figure 5 were indeed due to how glycan knockouts affected interactions with the DC-SIGN receptor. Ergo, our data suggests that the N-linked glycans at N17 and N122 have the highest propensity to act as binding sites for DC-SIGN to facilitate SARS-CoV-2 infection-in-trans.

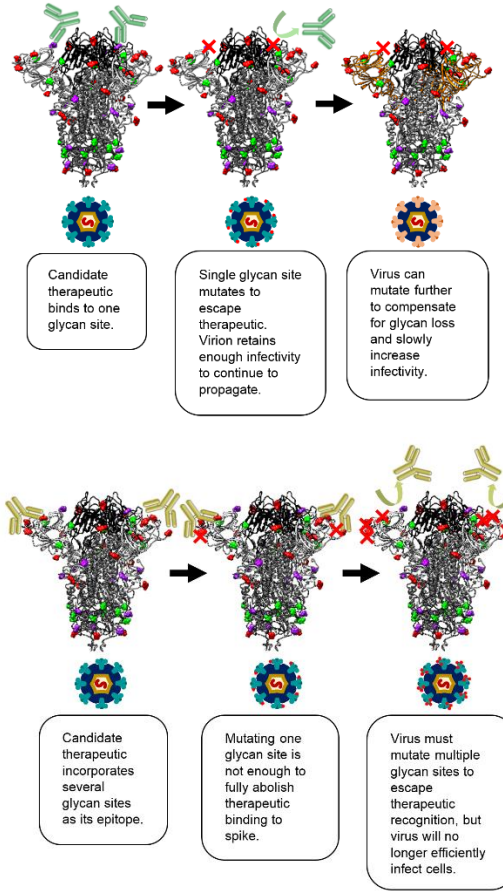
Given glycan 234's role in keeping the SARS-CoV-2 spike in the open/up conformation, it could be possible that the N234Q strain's increased propensity for Trans-infection is due to a bias for DC-SIGN to bind to the closed conformation of the SARS-CoV-2 Spike [61]. This could be because of slight steric occlusion of other glycans (like N122 and N165) when the Spike is in the RBD-up conformation. However, this does not explain the observed increased activity of the N234Q strain in Direct-infectivity assays. Like N234, N165 is also theorized to assist in keeping the SARS-CoV-2 Spike RBD in the up/open conformation [61]. While in our hands N165Q did not make a significant change on Direct-infectivity, previous literature found that in some instances, N165Q increased the hACE2-mediated-infectivity of SARS-CoV-2 pseudovirus by 20% on Calu1-hACE2+ cells [63]. Regardless of the reason, more research is needed to ascertain how the removal of these glycans is responsible for causing greater infectivity.

### **2.3.5 Abolishing Clusters of Glycans Severely Attenuates SARS-CoV-2 Pseudoviral Infectivity**

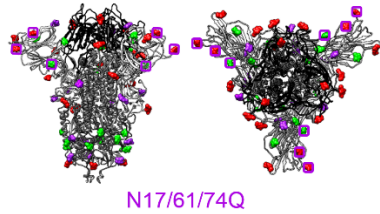
As noted, several SARS-CoV-2 Spike N-terminal domain glycan mutants showed significantly attenuated pseudoviral infectivity (N17, N61, and N74 for Direct-infectivity and N17, N61 and N122 for Trans-infectivity). These glycan sites would likely constitute "cold spots" that would be conserved due to evolutionary pressure to retain viral infectivity. Rather than relying on merely one glycan site to serve as an epitope for a broad, variant-proof SARS-CoV-2 treatment, targeting S1 domain glycans as clusters could serve as more robust epitopes for Covid-19 vaccines and prophylactic treatments (Figure 6A). To test this strategy, two pseudoviral strains with deletions of a glycan cluster (i.e. multiple glycosylation sites in close proximity) were created: a strain with N17Q, N61Q, N74Q mutations (called N17/61/74Q) and another with N122Q, N149Q, N234Q mutations (called N122/149/234Q) (Figure 6B, 6C). Although glycan N234 is not easily accessible, this particular glycan was removed to assess whether the removal of other glycans could compensate for the increased infectivity the N234Q mutant strain displayed previously. For the purposes of our assessment, we considered a viable "cold spot" to be a glycan cluster variant that exhibits 2 orders of magnitude lower infectivity than Wild-Type virus. This is based on existing work that shows that SARS-CoV-2 can mutate to breakthrough prophylactics and antibodies that attenuate infectivity by 1 to 1.5 orders of magnitude [5, 15, 20, 68, 69]. Thus, we posit that an epitope site that reduces viral infectivity by more than 2 orders of magnitude to be under sufficiently strong evolutionary pressure to not mutate.



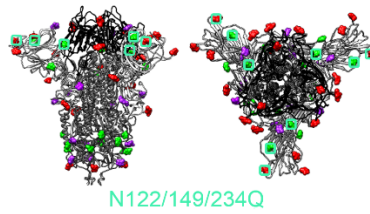
(A)



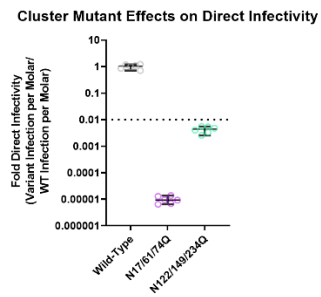
(B)



(C)



(D)



(E)

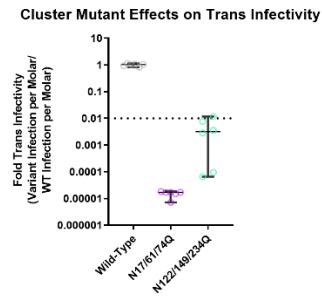


**Figure 6.** Clusters of Spike glycans can act as mutation-resistant epitopes for SARS-CoV-2 inhibitor design. **(A)** Schematic display of SARS-CoV-2 mutation and immune escape. Since glycans are heavily conserved on the SARS-CoV-2 Spike, it implies that they can act as robust “cold spots” for the development of therapeutics. However, SARS-CoV-2 Omicron strains have mutated significantly to escape immune detection, which implies they could further mutate to compensate for the loss of a single glycan site. Thus, it is necessary to identify clusters of glycans that will effectively eliminate viral infectivity if they are removed from the Spike protein, making it far less likely for prophylactics against glycan clusters from losing efficacy against further mutated SARS-CoV-2 strains. **(B), (C)** Depiction of the two cluster strains that were designed: N17/61/74Q and N122/149/234Q. **(D)** Direct-infectivity of cluster N-linked glycosylation mutants normalized to Wild-Type/Wuhan strain SARS-CoV-2 spike pseudovirus. **(E)** Trans-infectivity of cluster N-linked glycosylation mutants normalized to Wild-Type/Wuhan strain SARS-CoV-2 Spike pseudovirus. The infectivity signal from the N17/61/74Q strain was so poor that the Trans-infectivity signal was at the lower limit of detection for our plate reader/instrumentation (Figure S7). **(A), (B), (C).** SARS-CoV-2 Spike structures are adapted from PDB ID: 7NT9 by Rosa, A.

In a Direct-infectivity assay, both cluster mutant pseudoviral strains showed significantly reduced signal, not only compared to Wild-Type Wuhan nCoV-19 strain SARS-CoV-2 pseudovirus, but also when compared to single mutant strains (Figure 1, Figure 6A). The N17Q and N74Q strains exhibited the greatest attenuation of infectivity amongst single glycan mutants on our Direct-infectivity assay, with signals of 17.9% and 3.97% of Wild-Type, respectively (Figure 1). As was expected, the cluster mutant strain N17/61/74Q- which encompassed both the N17Q and N74Q mutations- displayed a greatly diminished Direct-infectivity signal, at about 5 orders of magnitude lower than the Wild-Type pseudovirus (0.00098% of Wild-Type) (Figure 6D). For strain N122/149/234Q, the anticipated loss in infectivity from the N122Q mutation was expected to be offset to some extent by an increase in infectivity from N234Q. Ultimately, N122/149/234Q displayed more than 100-fold higher Direct-infectivity than N17/61/74Q, with a signal of 0.424% of Wild-Type. However, this was still about an order of magnitude lower than the infectivity of the least infectious single glycan mutant strain (N74Q) (Figure 1), and about three orders of magnitude lower infectivity than the Wild-Type strain (Figure 6D), demonstrating that even though the N149Q and N234Q mutations did not impede hACE2-mediated infectivity, the removal of clusters of glycans had a combinatorial effect on attenuating SARS-CoV-2 infection. Thus, both the N17/61/74Q and N122/149/234Q glycan cluster epitopes could serve as a feasible target for anti-SARS-CoV-2 hACE2 prophylaxis.

In terms of raw Trans-infectivity, the cluster mutants N17/61/74Q and N122/149/234Q exhibited a signal of 0.00152% and 0.432% of the Wild-Type strain, respectively (Figure 6E). But, as in Figure 3, these data needed to be normalized to the Direct-infectivity signal in order to ascertain the propensity for viral strains to be captured by DC-SIGN and undergo Trans-infection.

Figure S7D shows each cluster mutant had about the same relative signal for Trans-infection as Direct-infection. Thus, each mutant appeared to have the same propensity to undergo DC-SIGN-mediated Trans-infection as the Wild-Type strain pseudovirus: N17/61/74Q and N122/149/234Q strains displayed a Trans-infection propensity of median = 48.1% (avg 43.0%) and median = 35.4% (avg 48.0%) of Direct-infection, respectively. For comparison, the Wild-Type strain exhibited a Trans-infection propensity of median = 33.8% (avg 37.0%) of Direct-infection.

For the N122/149/234Q strain, this behavior was expected; the increased DC-SIGN recognition observed in the N234Q single glycan mutant strain appeared to be

counteracted by the removal of some other glycan density in the N-terminal domain, perhaps bringing its Trans-infection propensity down to match the Wild-Type strain. In contrast, the N17/61/74Q strain displayed such a diminished luciferase signal that its Trans-infection luciferase reads were beneath the threshold of detection for the instrumentation (Figure S8A, S8B). This means that this strain could have had a significantly lower propensity for DC-SIGN mediated Trans-infection, but it simply could not be measured. At the very least, the N17/61/74Q cluster mutation did not enhance the propensity for DC-SIGN mediated Trans-infection.

Overall, these results indicate that future SARS-CoV-2 VOC strains are unlikely to mutate clusters of S1 domain glycans since doing so would drastically diminish hACE2-mediated infectivity. Based off of the aforementioned 2-orders of magnitude threshold for infectivity, N122/149/234 and especially the N17/61/74 glycan clusters likely will work as robust “cold spots” to develop strain-resistant antiviral treatments for Covid-19. Specifically, we believe that a multivalent or engineered inhibitor designed to bind to N17, N61, and N74 in concert will exhibit reliable inhibitory capabilities against numerous potential SARS-CoV-2 strains that appear in the future.

### **2.3.6 Omicron BA.2 Strain May Interact with Other Cell Surface Proteins to Facilitate Trans-Infection**

Over the course of the Covid-19 pandemic, the vast number of cases globally has allowed for ample opportunity for mutations to arise in the SARS-CoV-2 genome despite the relatively low mutation rate of the polymerase [10]. The GISAID database shows that every amino acid in the SARS-CoV-2 Spike protein sequence has mutated at some point. While most of the mutations were not beneficial- as evidenced by their low incidence and persistence- some of these changes led to drastically increased viral fitness, typically by allowing increased infectivity or facilitating immune escape [46, 71, 72]. These strains were labeled as “Variants of Interest” (VOI) or “Variants of Concern” (VOC) to highlight their clinical relevance and importance in terms of public health.

The initial Omicron SARS-CoV-2 BA.1 strain became a Variant of Concern primarily due to its ability to avoid detection by the host immune system [69, 73, 74]. It showed milder infectious characteristics in vivo when compared with other strains: Omicron BA.1 led to less damage to the alveolar spaces, spread more slowly through the lung bronchioles, and had a peak viral load in the lungs 2 days later than other strains [72]. When the Omicron BA.2 strain rapidly overtook the BA.1 strain to become the dominant VOC in mid-2022, it was further mutated to ameliorate some of the initial Omicron characteristics: Omicron BA.2 exhibited greater infectivity in the upper airways and bronchial tissues than even Wild-Type or Delta-strain SARS-CoV-2 virus [75].

To investigate whether this drastic increase of Omicron BA.2 in lung tissue penetration could be attributed solely to greater hACE2 mediated infection, or if increased DC-SIGN binding contributed in part to the increased infectivity, Omicron BA.2 lentiviral pseudovirus was assessed in both Direct- and Trans-infectivity assay systems. The infectivity of Omicron BA.2 Spike pseudotyped virus was compared to several strains of Covid-19 lentiviral pseudovirus: Wild-Type nCoV-19 Wuhan, Wild-Type nCov-19 Wuhan virus with the D614G mutation, and Delta strain pseudovirus [76].

Omicron BA.2 demonstrated significantly higher hACE2-mediated infectivity per molar compared to Wild-Type and D614G, with approximately 6-fold more luciferase

signal per molar than Wild-type virus. The Delta strain displayed such a range of infectivity per molar that it was difficult to make a conclusive statistically significant statement about its propensity to undergo Direct-infection (Figure 7A). This is perhaps more easily depicted by comparing the raw luciferase reads for each strain to the virus titer (Figure S8). These data are largely in accordance with expectations, since, as mentioned above, Omicron BA.2 appears to infect respiratory tissue more efficiently than Wild-Type and Delta SARS-CoV-2 [75].

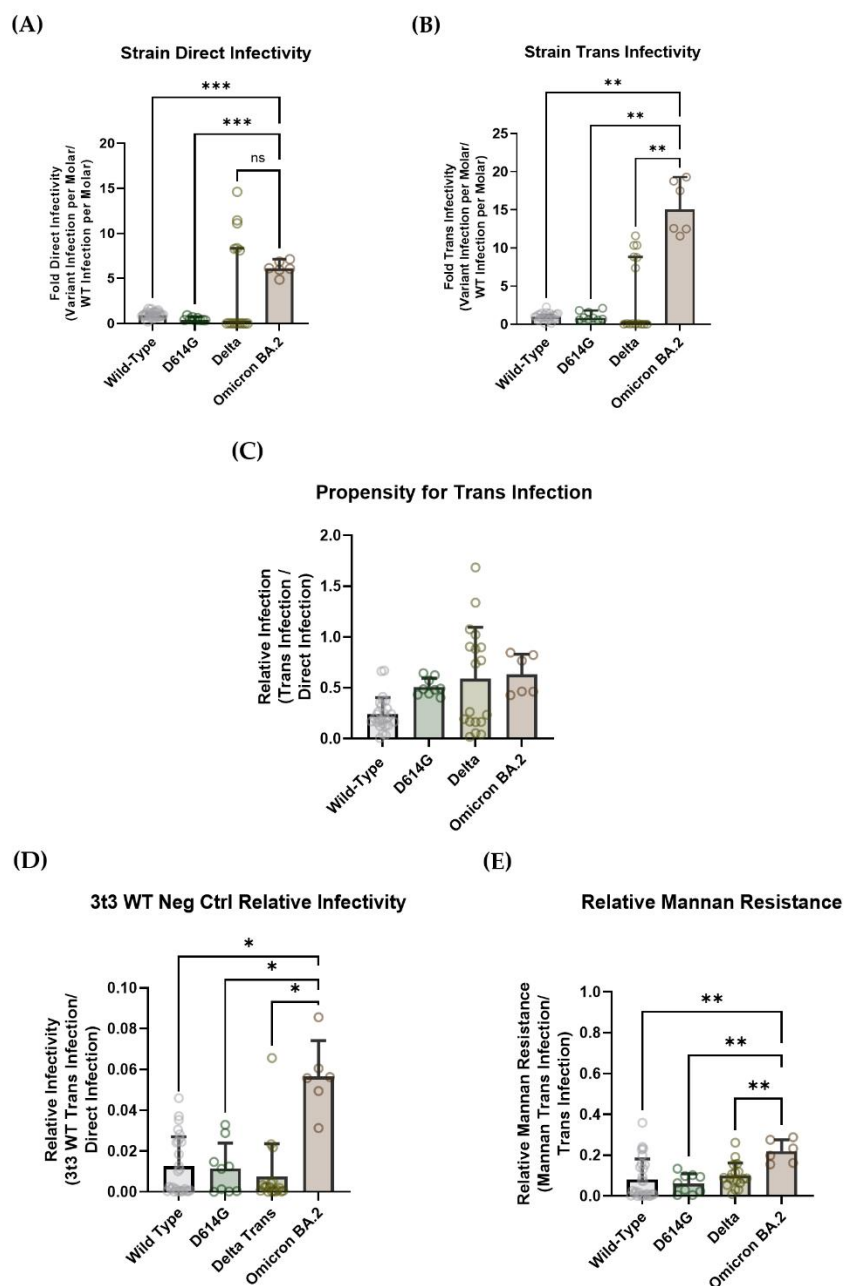


**Figure 7. Assessing if Covid-19 Strains have different infectivity (A)** Direct-infectivity per molar for each strain of virus normalized to Wild-Type/Wuhan strain SARS-CoV-2 Spike pseudovirus. Log-scale graph is depicted on the right. **(B)** Trans-infectivity per molar for each strain of virus normalized to Wild-Type/Wuhan strain SARS-CoV-2 spike pseudovirus. Log-scale graph is depicted on the right. **(C)** Each strains' Trans-infectivity was normalized to Direct-infectivity as described in Figure 5. Data shows that there is no significant difference in DC-SIGN recognition between the strains. **(D)** Each strains' propensity to undergo mannan inhibition of Trans-infection: Trans-infection signal in the presence of mannan is normalized to Trans-infection signal. Data shows that Omicron BA.2 pseudovirus may have some resilience to mannan-based inhibition of Trans-infection. **(E)** Each strains' Trans-infection signal when 3t3 cells that do not express DC-SIGN were used as the capture cell line. Omicron BA.2 pseudotyped virions seem to have some ability to be captured by a DC-SIGN-independent mechanism, yielding a signal that is about 0.06 (or 6%) of the Direct-infectivity signal. **(A), (B), (C), (D), (E)**. Statistical analysis is a Welch ANOVA with an Alpha value of 0.05. \* indicates a P-value < 0.1. \*\* indicates a P-value < 0.01. \*\*\* indicates a P-value < 0.001. \*\*\*\* indicates a P-value < 0.0001.

When the Trans-infectivity signal was parsed from the Direct-infectivity, the Omicron BA.2 strain did not exhibit a significant difference in Trans-infection propensity when compared to Wild-type, D614G, and Delta strains. As mentioned above, the Omicron BA.1 strain virus displayed altered lung infection characteristics *in vivo*, which led us to anticipate that Omicron strains in general might display some variation in DC-SIGN Trans-infection propensity [73]. However, since Omicron BA.2 has mutated to show infection dynamics that are similar to the Wild-Type and Delta strains, it is plausible that Omicron BA.2 has the same propensity to undergo infection-in-trans as the other pseudoviral strains that were tested on our assay [75]. Furthermore, the N-linked glycosylation sites on Omicron BA.2 Spike protein are the same as the Wild-Type and Delta strains, which means that all of the putative epitopes for DC-SIGN binding should be conserved (Figure 7C).

When 20 µg/mL of mannan was added to the DC-SIGN mediated Trans-infection assay to act as a competitive inhibitor, Trans-infection was decreased to about 10% for all non-Omicron strains: Wild-Type = 8.16%, D614G = 6.15%, Delta = 9.96%. Interestingly, Omicron BA.2 retained about twice the Trans-infectivity as the other strains (21.9%) (Figure 7D). Although Omicron BA.2 Spike protein doesn't exhibit any mutations on its glycan sites, Omicron strains in general have about three times the number of Spike mutations as compared to other VOCs, which can cause allosteric changes that alter the conformational dynamics of the Omicron Spike [7, 77-79]. It has been shown that some Omicron-specific S2 domain mutations cause significant distortion of the postfusion structure of the Omicron Spike such that it escapes recognition from a broadly acting peptide inhibitor [75, 80]. Thus, it is conceivable that the mutations in the Omicron BA.2 strain could allow for conformational changes that allow the Spike protein to undergo recognition by other cell surface proteins aside from DC-SIGN, thereby conferring resistance to mannan-mediated inhibition of Trans-infection. Recent evidence shows that SARS-CoV-2 Spike can bind to a variety of host molecules, including neuropilin-1 (NRP1), and leucine-rich repeat containing 15 (LRRC15) [42, 81, 82]. Thus, it could be possible that the mutations in the Omicron BA.2 Spike allow it to exhibit higher affinity for other cell surface molecules and facilitate Trans-infection mediated by other cell surface proteins.

Overall, the observed resistance of Omicron BA.2 pseudovirus to mannan inhibition of DC-SIGN-mediated Trans-infection is likely explained by the interaction of SARS-CoV-2 spike protein with other cell surface proteins. Indeed, performing a Trans-infection assay with 3t3 cells that did not express DC-SIGN displayed a similar trend as

the mannan-exposed 3t3 DC-SIGN+ cells: Omicron BA.2 can be transferred to susceptible cells slightly more than Wild-Type, D614G, or Delta strains (Figure 7E). Admittedly, the differences in Trans-infectivity are mild, so more investigation must be done before making any claim regarding the improved ability of Omicron BA.2 S protein to recognize and bind to alternate host factors. It is also of note that our *in vitro* assays (where a susceptible cell line is added over the top of a ~20% confluent cell monolayer used to capture pseudovirions) do not replicate the environment of lung tissue in the context of true Covid-19 infection.

## 2.4 Discussion

Over the course of the past 3 years, the Covid-19 pandemic has shown that SARS-CoV-2 (and Beta family coronaviruses in general) are incredibly contagious, going from a localized epidemic in Wuhan to a global pandemic in the span of 4 months. The high infectivity of SARS-CoV-2 virus allows it ample opportunity to mutate, as evidenced by the rise of several breakthrough strains that overcame existing therapeutics and vaccines [4, 5, 7, 8, 11, 59]. Coupled with this, the high transmissibility and mutation rate of Covid-19 has allowed it to make multiple zoonotic jumps in its relatively young existence: in addition to its accepted origins as a pangolin coronavirus (originally derived from RatG13, a horseshoe bat coronavirus), SARS-CoV-2 has already jumped from humans to other mammal species like mink and deer, causing concern that the virus could undergo unforeseen mutations in another animal population before jumping back to humans [10, 32, 83]. Hence, there is still a pressing need to identify immutable epitopes on the SARS-CoV-2 virion- also known as “cold spots”- to act as targets for the creation of vaccines and prophylactics that would continue to efficiently inhibit future variants of SARS-CoV-2. Since SARS-CoV-2 establishes initial infection in the host’s respiratory system, this work grants particular focus on identifying epitopes that are involved with the unique process of infecting lung tissue, as opposed to solely focusing on areas of virus that contribute to canonical hACE2-mediated infection (also called “Direct-infection” in this paper’s parlance).

In humans, penetration into the proximal airways of the nasal cavity is the critical step of establishing replicative SARS-CoV-2 infection [84]. Particularly, the ciliated epithelial cells of the nasal and proximal airways express high enough levels of hACE2 to allow for efficient viral entry and SARS-CoV-2 infection [85, 86]. Research has shown that the respiratory airways exhibit a gradient in hACE2 expression, whereby the distal airways deeper in the lungs have much lower hACE2 expression than the proximal and nasal airways [59, 86, 87]. Despite the low hACE2 expression of distal airways, the clinical outcomes of Covid-19 disease have consistently shown that SARS-CoV-2 infection damages the lung tissue, sometimes even in lieu of systemic infection of SARS-CoV-2 [46, 84, 87-92]. Specifically, Covid-19 presents with dysregulation of the surfactant-producing Alveolar Type-2 pneumocyte cells; this results in deteriorated function of the respiratory system as the alveoli collapse and no longer allow for gas exchange [88-90, 93, 94]. Autopsy studies clearly show the cytopathic changes of Alveolar Type-2 cells post-mortem, in spite of the fact that no subset of distal lung cells show over ~6% hACE2 expression within the population [87, 88, 90, 93, 95-97].

At the start of 2021, it was still unknown exactly how SARS-CoV-2 was able to reliably infect the cells of the respiratory tissue [47]. Soon thereafter, researchers

analyzed cell expression databases and found that C-type lectin transmembrane proteins are expressed on the surface of a variety of epithelial, adventitial, and resident immune cells of the lungs [42]. Cell surface lectin receptors have been demonstrated to bind to glycans on the surface of SARS-CoV-2 glycoproteins and facilitate efficient infection-in-trans to distal lung airway cells and cells within the alveoli, effectively enhancing the infectivity of SARS-CoV-2 in the lung airways [39, 40, 42, 44]. This process of viral protein glycosaminoglycan-mediated Trans-infection has been well-characterized for other enveloped viruses, such as HIV, dengue virus, West Nile virus, Ebola virus and more [38, 39, 40]. Ergo, it is accepted that lectin receptors are responsible for facilitating efficient infection of cells in the respiratory system [42-44, 46].

In this study, we assessed the effect of select Spike S1 domain glycans and SARS-CoV-2 Spike proteins from different strains in mediating viral infectivity on in vitro assays that modeled both hACE2-mediated Direct-infection and C-type lectin receptor mediated Trans-infection [10]. Specifically, the C-type lectin DC-SIGN was used as the viral capture receptor, since it has been shown to be capable of binding SARS-CoV-2 Spike proteins in microscopy assays and facilitating virion transfer to cells that modestly express hACE2 [42, 43].

Unlike other viruses that readily shift glycan sites on their spike glycoproteins to assist in evading immune detection, SARS-CoV-2 displays a remarkable degree of immutability regarding its glycan pattern [38-40]. Out of the 101,461 SARS-CoV-2 Spike glycoprotein sequences that were deposited on the NCBI Virus database in the past six months, less than 0.3% show any mutations at any of the 22 Asparagine residues that are consistently shown to be glycosylated [34-37, 98]. Furthermore, even if a strain does exhibit a mutation at a glycan site, evidence suggests that the strain will quickly be outcompeted: in early 2022 some samples of Omicron BA.2 from patients in the UK exhibited an N74K mutation, but a mere month later this mutation was no longer found in the population [53]. In another case, Omicron CM.1 is currently the only VOC strain on the NCBI Virus Database that shows a mutation at any Spike protein glycan site (N17S) [98]. While multiple sequences of Omicron CM.1 were detected in Ireland, Switzerland, California, and Texas, there has only been one recorded case of Omicron CM.1 reported globally in the past 6 months [98]. Although Delta B.1.617.2 and several emerging Omicron XBB strains of SARS-CoV-2 do have mutations at T19 that impede glycosylation at the N17 sequon, it has been known that oligosaccharyltransferases can tolerate some degree of mutation and still attach sugars to Asparagines, suggesting that N17 could still be glycosylated in some strains despite the mutation [99, 100]. Regardless, the maintenance of glycan sites in the vast majority of VOC and VOI strains imply that SARS-CoV-2 virions require their N-linked glycan sites in order to retain infectivity and are thus viable targets for Covid-19 prophylactic development.

Since the majority of prophylactic antibodies and vaccines recognize the S1 domain of the Spike protein, we focused our analysis on uncovering the importance of the glycans proximal to these antibody epitopes [22, 70, 74]. We avoided assessing glycans on the Spike Receptor Binding Domain (such as N331 and N343) because many existing prophylactics already recognize the RBD, and we wished to identify novel epitopes that could act in combination with existing therapeutics. To that end, glycans N17, N61, N74, N122, N149, N165, and N234 were selected for analysis.

Our analysis showed that the removal of N17, N61 and N74 significantly impaired SARS-CoV-2 pseudovirions to undergo hACE2 mediated infection, while the removal of glycans N149 and N165 had no effect (Figure 2D). This is largely in accordance with existing literature, as N17Q, N61Q, N74Q, and N122Q all have been reported to either significantly attenuate infectivity or have no effect [63, 84]. On the other hand, Glycans N149 and N165 have been shown to have unpredictable effects on hACE2-mediated infection of SARS-CoV-2 pseudotyped viruses, ranging from modestly increasing infectivity to significantly decreasing infectivity [63, 84]. Ergo, it is likely that the different effects of N149Q and N165Q are more likely due to the idiosyncrasies of the infectivity assays (e.g. using lentiviral pseudovirions versus VSV pseudovirions, or using different susceptible cell lines) rather than a consistent effect of the glycan mutations on altering SARS-CoV-2 spike dynamics or fusogenic activity.

In our hands, the removal of N234 appeared to increase the ability of pseudovirions to undergo hACE2-mediated Direct-infectivity. While this is unexpected, given the predicted role of N234 in propping up the Spike RBD in the infectious “up” conformation, previous studies have shown that N234 knockout mutations do not affect virion infectivity as much as the purported role of N234 would imply [62, 63]. Indeed, mutating N165- which was hypothesized to perform a similar role as N234- appeared to also boost the infectivity of pseudovirions in previously published literature [61, 63].

Lectin receptor-mediated Trans-infectivity is arguably more important in dictating the initial stages of Covid-19 infection in patients due to the modest hACE2 expression of resident lung cells [42, 47-49]. Our hope was that the selected mutated glycan epitopes could provide the basis for a new class of Covid-19 inhibitors that could work in combinatorial therapies without impeding anti-hACE2 prophylactics. To test this, we developed an in vitro assay that could mimic the process of DC-SIGN-mediated SARS-CoV-2 pseudoviral capture and presentation to a hACE2+ cell line (Figure 4A). After running these assays, each strain’s Trans-infectivity signal was normalized to their Direct-infectivity to obtain the propensity of each glycan mutation in mediating DC-SIGN attachment and transmission to permissive hACE2+ cells (Figure 5B).

After comparing the propensities of glycan mutant pseudovirus strains, glycans N17 and N122 both appeared to be the most integral in enabling DC-SIGN-mediated Trans-infection. The location of N17 and N122 on the Spike protein seems to indicate that DC-SIGN has a preference for binding glycans that are not too close to the RBD, but are also not completely on the periphery of the S1 domain of the Spike (Figure 5C). The importance of N17Q in mediating both Direct- and Trans-infection may have been implied through the course of the Covid-19 pandemic: several strains of SARS-CoV-2 that showed mutations at the N17 sequon have now been quickly outcompeted by other strains [101]. However, this argument is somewhat invalidated by the fact that N17 is also predicted to be predominantly occupied by complex glycans, which should mean that DC-SIGN would not have high binding affinity for the N17 glycans. This may provide some credence to the idea that allosteric and conformational variations make certain Spike glycans particularly vulnerable to DC-SIGN recognition, and that S1 domain glycans that are neither proximal to the RBD nor present on the periphery of the SARS-CoV-2 Spike are uniquely suited to facilitate DC-SIGN mediated infection-in-trans (Figure 5C). Alternatively, virus-expressed spike proteins tend to have less complex glycosylation at each SARS-CoV-2 Spike N-linked glycan site than mammalian-expressed soluble Spike [126]. This may mean that the N17 glycans on virions are high-



mannose and thus truly do serve as viable epitopes for DC-SIGN mediated Trans-infection. Of course, further experimentation is necessary to fully ascertain whether this is true.

Unlike the other glycan mutations, N234Q pseudovirions displayed an increased propensity to be captured by DC-SIGN (Figure 5B). Given that N234 is predicted to aid in keeping the SARS-CoV-2 Spike in the RBD up/open conformation, this leads us to wonder whether the closed conformation of the SARS-CoV-2 Spike has a greater affinity for DC-SIGN than the open conformation [61]. Like N234, N165 is also predicted to assist in propping the RBD of the SARS-CoV-2 Spike in the up position. While we did not observe a similar increase in Trans-infectivity for the N165Q strain, it did not display significantly attenuated Trans-infectivity either. This could be explained by the fact that the N165 glycan is predicted to have less hydrogen bonding to prop the RBD in the up position, which suggests that removal of N165 may not have altered the conformational dynamics of the SARS-CoV-2 Spike enough to alter the ability of DC-SIGN to bind [63]. More work is needed to verify the effect of N234 and N165 on the dynamics of the SARS-CoV-2 Spike, with a possible need to ascertain whether N234Q/N165Q double mutants would no longer have the ability to retain the up/open conformation of the Spike protein. Alternatively, it could be possible that the RBD-down/closed conformation of the SARS-CoV-2 Spike exposes high-mannose glycans to facilitate easier Trans-infection. Thus, another potentially important path of scientific inquiry is to test whether DC-SIGN and other attachment receptors have higher affinity for the RBD-down/closed conformation of the SARS-CoV-2 Spike as opposed to the RBD-up/open conformation.

Interestingly, our results do not seem to agree with FACS-mediated protein-protein binding data from a preprinted article: the authors reported that out of all of the glycans, only the removal of glycosylation at N149 was observed to alter DC-SIGN binding to the SARS-CoV-2 Spike protein, with N149Q decreasing binding by about 2 orders of magnitude [102]. Overall, the lack of consensus in the literature suggests that more work is needed to fully grasp what role individual S1 domain glycans are most important in mediating infection.

Omicron family virus variants have become the dominant circulating strains exhibiting effective breakthrough infection despite displaying lower fusogenic activity than not only Beta and Delta variants of SARS-CoV-2, but also Wild-Type nCov-19 Wuhan virus [6, 73, 103]. What is most concerning regarding the rise of Omicron variants is their immune evasion characteristics, demonstrating that SARS-CoV-2 can mutate relatively quickly and tolerate significant alterations on its Spike protein to regain the ability to efficiently infect humans. Current literature showed that Omicron SARS-CoV-2 was able to establish breakthrough infections when convalescent sera or antibody treatments were diluted 1 to 1.5 orders of magnitude in *in vitro* assays [4, 5, 15, 20, 69, 70, 73, 74]. Therefore, we considered that the threshold for identifying a viable SARS-CoV-2 Spike “cold spot” was an epitope that would lower pseudoviral infectivity by at least two orders of magnitude when compared to Wild-Type nCov-19 Wuhan pseudovirus. This was done so that if escape mutants started to develop to remove the “cold spot” epitope, the resultant strains would lose so much infectious activity that they would be unable to establish persistent infection of a host.

With the advent of combinatorial prophylactic treatments like bispecific antibodies, chimeric viral entry inhibitors, and *de novo in silico* designed inhibitors, it is

relatively easy to develop a prophylactic therapy that targets discrete sites on a target virus. Given the inherent evolutionary pressure for SARS-CoV-2 to avoid mutating its N-linked glycosylation sites, we hoped to identify viable glycan clusters that could serve as highly conserved epitopes that could act as “cold spots” to ensure that SARS-CoV-2 infection did not mutate for further mutant strains. The removal of three glycans in tandem drastically decreased the infectivity of our pseudovirions, with even the strain including N234Q (which consistently appeared to increase infectivity) demonstrating 3 orders of magnitude lower infectivity than unmodified spike virions. There are already prophylactic strategies against other viruses that leverage binding to glycans on the viral spike protein: several anti-HIV antibodies bind to the glycan shield rather than amino acid epitopes, and other globular lectin protein-based inhibitors such as Griffithsin exhibit broad inhibitory activity against a variety of viruses [51, 104-106]. Recent literature has shown considerable success when Griffithsin treatment was combined with a therapeutic that targeted a different epitope on the SARS-CoV-2 Spike- either a designed viral fusion inhibitor called EK1, or with sulfated polysaccharides called carrageenan, or with another glycan-binding inhibitor called Cyanovirin [107-110]. These results hint that if new inhibitors could be designed against unique SARS-CoV-2 epitopes (such as the N17/61/74 or N122/145/234 glycan clusters), they could be combined with other existing Covid-19 therapeutics to create a more potent prophylactic treatment. Furthermore, SARS-CoV-2 virions also contain the M, N, and E structural proteins. It has already been established that the addition of N protein can significantly increase the hACE2-mediated infectivity of SARS-CoV-2 pseudovirions [57]. Since M and E proteins are glycosylated membrane-embedded proteins, and tend to not mutate as frequently as Spike protein, there is a distinct possibility that these proteins could also act as target “cold-spot” epitopes for combinatorial anti-Trans-infection therapy [111]. Current work from our group is ongoing to ascertain whether these structural proteins can potentiate Trans-infectivity and therefore be included [Article in preparation].

By this point, it has been well-characterized that Omicron strains of Covid-19 lead to significantly different infection dynamics in the lungs than previous strains: Omicron strain virus tends to have peak lung tissue infectivity several days post-infection, possibly indicating that Omicron virus has a longer dwell time in the lung airways as mediated by virion capture by attachment receptors before undergoing hACE2-mediated infection [73, 103]. Given that Trans-infection is theorized to be a significant contributor to how SARS-CoV-2 establishes infection in the host respiratory system, it was prudent to assess how Spike proteins from several Variants of Concern could alter the ability of pseudovirions to undergo DC-SIGN-mediated infection. D614G, Delta, and Omicron BA.2 strain Spike proteins were all tested on both Direct- and Trans-infection assays. In our hands, D614G and Delta did not show significantly increased propensity for undergoing DC-SIGN mediated Trans-infection, which was not unexpected when considering the relatively few mutations on the spike protein for these strains. It was surprising that D614G and Delta strain pseudovirus exhibited only slightly higher hACE2-mediated infection compared to Wild-Type Spike pseudotyped lentivirus, considering that existing literature shows Delta strain SARS-CoV-2 causes more severe infection [12].

In our hands, Omicron BA.2 strain pseudovirus showed significantly higher hACE2-mediated infectivity than the other tested strains. Recent literature has shown that Omicron strains range from having comparable infectivity to Wild-Type SARS-CoV-2, to having higher infectivity than D614G and Delta strains [12, 15, 75]. This variation is

likely due to the intricacies of the viral systems and susceptible cell lines that are used for testing the SARS-CoV-2 Spike strains; even different airways in the lungs (i.e. nasal, proximal, distal) have varying susceptibilities to variants of SARS-CoV-2 [12, 75]. Thus, while we observed greater Direct-infectivity for Omicron BA.2 on hACE2-expressing HEK 293t cells, we are cautious in making any claims regarding Omicron BA.2 strain SARS-CoV-2 having higher infectivity in the context of infecting humans, especially considering the complexity of *in vivo* tissues.

There is mounting evidence that the numerous mutations of the Omicron strains cause allosteric changes of the Spike protein [75, 77, 78, 80]. Because the SARS-CoV-2 Spike has been shown to bind to a multitude of cell surface molecules- ranging from sialic acid binding surface receptors, heparan sulfate, glycosphingolipids, and more- it is plausible that the predicted unique structural dynamics of the Omicron BA.2 strain Spike could confer resistance to mannan-mediated inhibition of Trans-infection, as well as some ability to be captured by a fibroblast cell line that did not express DC-SIGN [42, 81, 82]. Most notably, Omicron mutations lead to greater spike processing by furin, which is known to reveal an epitope that is capable of being bound by the cell surface receptors Neuropilin-1 (NRP1) and Neuropilin-2 (NRP2) [112, 113].

Neuropilins are a class of evolutionarily conserved single pass transmembrane proteins that were originally identified by their importance in regulating neurogenesis and angiogenesis in vertebrates [112, 128, 129]. There are two proteins in the neuropilin family, neuropilin-1 (NRP1) and neuropilin-2 (NRP2), each of which can exist as a transmembrane protein or as one of several secreted, truncated isoforms [112, 129]. The transmembrane form of NRP1 and NRP2 are known to bind to and be activated by the C-end rule peptide sequence R/KXXR/KOH where X is any amino acid, and R/K is either an arginine or a lysine [130, 113]. In the case of SARS-CoV-2, the cleavage of the S1/S2 junction RRAR<sup>S</sup> sequence by furin reveals a solvent-accessible peptide sequence can be recognized by Neuropilin (Figure S9) [103]. Hence, it is no surprise that NRP1 has been demonstrated to potentiate SARS-CoV-2 infection both *in vitro* and *in vivo*, but only if the spike undergoes furin cleavage [130, 113].

Several SARS-CoV-2 VOC's have shown mutations close to the furin cleavage site, with H655Y and P681H each individually increasing the propensity of the Spike protein to undergo furin processing [114, 115]. Omicron strains all display both mutations, and they appear to undergo slightly increased spike processing *in vitro* [114]. The 3t3 DC-SIGN cells that act as the capture cell line on our Trans-infection assay are murine fibroblasts, which are known to express high levels of the NRP1 homolog NRP2 [113, 116]. Ergo, it is possible that the Omicron BA.2 pseudovirus's resistance to mannan inhibition of DC-SIGN mediated SARS-CoV-2 Trans-infectivity is due to enhanced furin cleavage, and thus increased attachment to Neuropilin-2.

Another relevant cell surface protein that could contribute to SARS-CoV-2 Trans-infection is Leucine-rich repeat containing 15 (LRRRC15). LRRRC15 is implicated in cell-cell and cell-Extracellular Matrix functions, and while it is not expressed widely, it is found to be localized to tissues that are part of the innate immune system or tissues that are undergoing recovery from the wound process [131]. Notably, LRRRC15 is highly expressed in both lung tissue and fibroblasts, and its expression is shown to increase during Covid-19 infection [131]. The protein exists as two isoforms, LLRC15\_1 and LLRC15\_2, both of which are capable of binding to the SARS-CoV-2 Spike [132].

However, unlike the other attachment receptors we have mentioned so far, a variety of *in vivo* and *in vitro* experiments show LRRC15 impairs SARS-CoV-2 infection, likely because it competes with hACE2 for binding to the Spike RBD [132]. Furthermore, LRRC15 expression is mutually exclusive to hACE2 expression in the lungs, indicating that LRRC15-mediated Spike binding sequesters viruses away from permissive cell types [81].

However, recent studies seem to show that the Spike mutations from Omicron strain viruses are at sites proximal to, if not directly on, epitopes that LRRC15 binds to [81, 82]. Thus, Omicron strains could exhibit greater escape from LRRC15-mediated virus sequestration.

A variety of fibroblasts (such as 3t3 cells) are known to express LRRC15 [132, 133]. Thus, in the context of our *in vitro* Trans-infectivity experiments, Omicron BA.2 could exhibit greater Trans-infectivity than other tested pseudoviral strains because Omicron BA.2 pseudotyped virus can evade 3t3 cell-expressed LRRC15-mediated capture/inhibition.

## 2.5 Conclusions

Overall, this work focused on assessing several S1 domain Spike glycans and 3 VOC strain Spike proteins could affect the ability of SARS-CoV-2 to establish initial infection in the host lung tissue. Since the respiratory tissue only modestly expresses hACE2, it is widely accepted that virion capture and infection-in-trans is the chief process in facilitating infection of the distal airways. Ergo, particular interest was given to testing how the aforementioned characteristics of the SARS-CoV-2 virion can affect DC-SIGN-mediated Trans-infection.

As would be expected from previous literature, the removal of most of the S1 domain glycans (specifically N17, N61, and N74) decreased the hACE2-mediated Direct-infection of the SARS-CoV-2 pseudovirions. The effect of glycan removal on Trans-infectivity was more nuanced, with only the removal of the N-linked glycans at N17 and N122 significantly impairing Trans-infectivity of SARS-CoV-2. Interestingly, the removal of the glycan at N234 increased both the Direct-infectivity and Trans-infectivity of pseudotyped virions, calling into question the hypothesized role of the N234 glycan in ensuring the SARS-CoV-2 Spike stays in the RBD-up infectious conformation.

Given that SARS-CoV-2 Omicron strains mutated significantly to evade immune detection, eventually leading to strains that are capable of establishing breakthrough infection in patients who have received multiple doses of Covid-19 vaccines, we considered whether glycan cluster sites could act as epitopes for the development of prophylactic treatments. The priority was to identify sites that were highly unlikely to mutate due to evolutionary pressure to maintain SARS-CoV-2 virus infectivity. Our work found that both glycan cluster mutations N122/149/234Q and N17/61/74Q significantly impaired SARS-CoV-2 pseudotyped virus, with about 2 orders of magnitude and 5 orders of magnitude lower infectivity, respectively.

Finally, we assessed whether different strains of SARS-CoV-2 could affect how pseudotyped virions could undergo Trans-infection. As expected based off of existing literature, in our hands the Omicron BA.2 strain exhibited increased hACE2 Direct-

infectivity when compared to Wild-Type [117]. While there was no difference in the strains' ability to undergo DC-SIGN mediated Trans-infection, our results hinted that Omicron BA.2 may have a slightly increased propensity to bind to alternative attachment receptors like Neuropilin-2.

Although we found some key facets of the SARS-CoV-2 Spike protein that appeared to affect both hACE2-mediated Direct infectivity and DC-SIGN mediated Trans-infectivity, we finish by emphasizing that our experiments were performed in immortalized lab-adapted cell lines. Optimally, we believe it is important to verify the effects of Spike protein glycan mutations and Omicron BA.2 strain virus on an ex vivo model of human respiratory tissue.

## 2.6 Methods and Materials

### 2.6.1 Cell Lines

All cell lines were maintained in Dulbecco's Modified Eagle Medium (DMEM) (ThermoFisher Cat # 11965-092, Waltham, MA, USA) with specific additives for each cell type. These cells include:

- HEK-293Ft (Homo sapiens, embryonic kidney cells; a generous gift from Dr. David Gravano, University of California, Merced).

- HEK-293t hACE2+ Cells (Homo sapiens, embryonic kidney cells; obtained through BEI Resources, NIAID, NIH: Human Embryonic Kidney Cells [HEK-293T] Expressing Human Angiotensin-Converting Enzyme 2, HEK-293T-hACE2 Cell Line, NR-52511).

- 3t3 Wild-Type Cells (Mus musculus, mouse embryonic fibroblasts; obtained through the NIH HIV Reagent Program, Division of AIDS, NIAID, NIH: NIH-3T3 Cells, ARP-9946, contributed by Drs. Thomas D. Martin and Vineet N. KewalRamani).

- 3t3 DC-SIGN+ Cells (Mus musculus, mouse embryonic fibroblasts; obtained through the NIH HIV Reagent Program, Division of AIDS, NIAID, NIH: NIH 3T3 DC-SIGN+ Cells, ARP-9947, contributed by Drs. Thomas D. Martin and Vineet N. KewalRamani).

Both HEK-293Ft cells and HEK-293t hACE2 cells were maintained in T-75 flasks (Stellar Scientific Cat # SKU:TC30-120, Baltimore, MD, USA) within a 37°C humidified incubator at 4.5% CO<sub>2</sub>. HEK-293Ft cells and HEK-293t hACE2 Cells were cultured in DMEM supplemented with 25 mM HEPES (ThermoFisher Cat # 11344041, Waltham, MA, USA), 2 mM L-glutamine (R&D Systems Cat # R90010, Minneapolis, MN, USA), 250 ug mL<sup>-1</sup> G418 Sulfate (Corning Life Sciences Cat # 30-234-CI, Tewksbury, MA, USA), and 10% Fetal Bovine Serum (R&D Systems Cat # S11150, Minneapolis, MN, USA). This media is heretofore referred to as 293 Media.

3t3 cells were chosen because they have been demonstrated to be deficient in a variety of lectin receptors, including DC-SIGN, Lectin-Like Oxidized Low-Density Lipoprotein Receptor 1 (LOX1), and other C-type lectin (CLEC) family proteins, according to a gene expression database (NIH3t3 cells, Harmonizome.com). Both 3t3 Wild-Type Cells and 3t3 DC-SIGN+ cells were maintained in T-75 flasks within a 37°C humidified incubator at 4.5% CO<sub>2</sub>. 3t3 Wild-Type Cells and 3t3 DC-SIGN+ Cells were cultured in DMEM supplemented with 2 mM GlutaMAX (ThermoFisher Cat # 35050-061,

Waltham, MA, USA), 100 U mL<sup>-1</sup> of Penicillin-Streptomycin solution (Cytiva HyClone Cat # SV30010, Marlborough, MA, USA), and 10% Fetal Bovine Serum (R&D Systems Cat # S11150, Minneapolis, MN, USA). This media is heretofore referred to as 3t3 Media.

When a flask reached 80-95% confluency, cells were passaged 1:10 with 0.05% Trypsin-EDTA (ThermoFisher Cat # 25300-062, Waltham, MA, USA) used to detach cells from surface of plastic flasks. Trypsin was not permitted to exceed a contact time of 5 minutes for any cell line.

### 2.6.2 Pseudovirus Production

Pseudovirus plasmids were obtained through BEI Resources, NIAID, NIH. SARS-CoV-2 spike plasmids were originally purchased from Addgene and were mutated as described above. SARS-CoV-2 Spike pseudotyped HIV virions were produced in a protocol inspired by Crawford et al., 2020 [60]. Briefly, HEK-293Ft cells were maintained in 293 Media and passaged once cells reached 70-100% confluency. The day prior to transfection, HEK-293Ft cells were seeded at a density of approximately  $2.5 \times 10^6$  cells in 8-10 mL of 293 Media into a 100 mm tissue culture petri dish or approximately  $0.2 \times 10^6$  cells in 2-3 mL of 293 Media into a 6-well tissue culture plate (batches of virus were made in either of the two plate types). Cells were allowed to recover for 12-16 hours in a humidified incubator at 37 °C and 5% CO<sub>2</sub>.

Petri dishes/6-well plates were then withdrawn from incubators and cells were assessed for confluency and adhesion. If the cells in petri dishes were 70% confluent and adherent, media was gently replaced with 8 mL of fresh 293 Media. If the cells in 6 well plates were 70% confluent and adherent, media was gently replaced with 3 mL of fresh 293 Media. The petri dish/6-well plate was returned to the incubator for approximately 45 minutes while the plasmids and transfection reagent were prepared. For a 100 mm petri dish, the following plasmids were mixed in 900 µL of serum-free commercial DMEM in a sterile 1.5 mL centrifuge tube: 5 µg of lentiviral backbone Luciferase-IRES-ZsGreen (BEI Resources NR-52516, Manassas, VA, USA) vector, 1.1 µg each of vectors HDM-Hgpm2 (BEI Resources NR-52517, Manassas, VA, USA), pRC-CMV-Rev1b (BEI Resources NR-52519, Manassas, VA, USA) and HDM-tat1b (BEI Resources NR-52518, Manassas, VA, USA), and 1.7 µg of vector pCMV14-3X-Flag-SARS-CoV-2 S (Addgene Cat # 145780, Watertown, MA, USA). For a 6-well tissue culture plate, the same plasmids were mixed in 185 µL of serum-free commercial DMEM in a sterile 1.5 mL centrifuge tube: 1 µg of lentiviral backbone Luciferase-IRES-ZsGreen (BEI Resources NR-52516, Manassas, VA, USA) vector, 0.22 µg each of vectors HDM-Hgpm2 (BEI Resources NR-52517, Manassas, VA, USA), pRC-CMV-Rev1b (BEI Resources NR-52519, Manassas, VA, USA) and HDM-tat1b (BEI Resources NR-52518, Manassas, VA, USA), and 0.34 µg of spike vector pCMV14-3X-Flag-SARS-CoV-2 S (Addgene Cat # 145780).

For the creation of pseudovirus with N-linked glycan spike mutations, we either performed site-directed mutagenesis using PCR or ordered segments of DNA with specified glycan mutations flanked with HindIII and AvrII cut sites (Twist Bioscience, South San Francisco, CA, USA). Segments of DNA were ligated into spike vector pCMV14-3X-Flag-SARS-CoV-2 S that had been digested with HindIII-HF (New England Biolabs Cat # R3104S, Ipswich, MA, USA) and AvrII (New England Biolabs Cat #

R0174S, Ipswich, MA, USA). These mutated pCMV14-3X-Flag-SARS-CoV-2 S Spike vectors were used in the transfection mixture as described above.

For the creation of pseudovirus with one additional structural protein, 1.7 µg of desired M, N, or E protein vector was added to the transfection mixture specified above: pcDNA3.1 SARS-CoV-2 M (Addgene Cat # 158078), pcDNA3.1 SARS-CoV-2 N (Addgene Cat # 158079), pcDNA3.1 SARS-CoV-2 E (Addgene Cat # 158080), respectively. When creating virus with all three structural proteins, 1.7 µg of each additional structural protein vector was added to the transfection mixture as described above.

For the creation of pseudovirus with spike protein with the D614G mutation, PCR was performed as described for the N-linked glycan spike mutations and then used in the same transfection mixture specified above. For the creation of Delta pseudovirus, transfection was performed as described above except pcDNA3.3-SARS2-B.1.617.2 (Addgene Cat # 172320) was used as the Spike protein vector in lieu of pCMV14-3X-Flag-SARS-CoV-2 S. For the creation of Omicron BA.2 pseudovirus, transfection was performed as described above except pcDNA3.3\_SARS2\_omicron BA.2 (Addgene Cat # 183700) was used as the spike vector for transfection in lieu of pCMV14-3X-Flag-SARS-CoV-2 S.

After adding all plasmids, the solution was mixed by pipetting up and down approximately 10 times. For 100 mm petri dish samples, 30 µL of XtremeGENE HP Version 9 (Roche Cat # 06366546001, Mannheim, Germany) was added directly to the solution. For 6-well tissue culture plate samples, 6 µL of XtremeGENE HP Version 9 was added directly to the solution. The viruses with additional structural proteins were exclusively made in 100 mm petri dishes, but instead of using 30 µL of XtremeGENE HP Version 9, 42 µL of XtremeGENE Version 9 was added to the solution to accommodate the increased volume from adding the structural protein vectors. The contents of the tube were again mixed by pipetting up and down approximately 10 times before being allowed to incubate at room temperature for 20-25 minutes. The petri dish/6-well plate was then retrieved from the 37 °C incubator and the DNA + XtremeGENE HP mixture was dripped over the 293Ft cells. The transfected 293Ft cells were then returned to the incubator and allowed to recover for 12-18 hours overnight. After 12-18 hours, petri dishes/6-well plates were again removed from the incubator and the cell media was gently replaced with fresh prewarmed 293 Medium (10 mL for 100 mm petri dishes, 4 mL for 6-well plates). Transfected cells were returned to the incubator. After an additional 48 hours (60-66 hours total post-transfection), petri dishes were removed from the incubator and the medium was gently removed and transferred to a 15 mL tube. This 15 mL tube was then briefly centrifuged at 750 RPM (105 RCF) for 3 minutes to pellet any large cell clumps. The supernatant now containing pseudotyped lentivirus was filtered through a 0.45 µm syringe filter and stored as 450 µL aliquots in low-binding 1.5 mL tubes (ThermoFisher Cat # 90410, Waltham, MA, USA). Aliquots were stored at -75 °C until use in future assays.

### **2.6.3 Pseudovirus Titration**

Each SARS-CoV-2 spike mutant was produced at least twice, yielding at least two batches of pseudovirus for each spike variant. Every batch was titrated using an XpressBio p24 ELISA kit plate carried out according to the manufacturer's instructions (XpressBio Cat # XB-1000, Frederick, MD, USA). The levels of p24 in each well were

measured on a ClarioStar Plus microplate reader set to 450 nm (BMG Labtech, Ortenberg, Germany).

#### 2.6.4 Virus Infectivity Assays

Each well of a clear 96-well cell-culture plate was coated with 25  $\mu$ L of 0.1 mg/mL poly-L-lysine (ScienCell Research Laboratories, Cat # 0413, Carlsbad, CA, USA). The plate was returned to the 37 °C incubator for 1 to 36 hours. After this time, the 96-well plate was removed from the incubator and the poly-L-lysine solution was pipetted out. Wells were then rinsed twice with 40  $\mu$ L of sterile, ultrapure deionized water before being set aside in preparation for seeding.

For Trans-infection experimental samples, 5000-15000 of 3t3 DC-SIGN+ cells were seeded in triplicate into the wells of a pre-prepared poly-L-lysine conditioned 96 well plate as described above. For Trans-infection negative control samples, 3t3 Wild-Type Cells were seeded instead. The 96-well plate was returned to the 37 °C humidified incubator at 4.5% CO<sub>2</sub> in order to allow the 3t3 cells to adhere and recover for 8-12 hours. After recovery, the 96-well plate was retrieved from the incubator and the media was gently pipetted out of wells. Within 1 minute of pipetting out media, 15  $\mu$ L of fresh 3t3 media was added to the wells to prevent the cells from desiccating. Then 25  $\mu$ L of the requisite SARS-CoV-2 pseudovirus variant was added over the to the wells. For negative control samples and Direct-infection samples, 25  $\mu$ L of the requisite SARS-CoV-2 pseudovirus variant was dispensed into empty wells that had been pre-treated with poly-L-lysine. The 96-well plate was returned to the 37°C humidified incubator at 4.5% CO<sub>2</sub> for 2-4 hours to allow for virion capture.

After 2-4 hours had elapsed, the 96-well plate was retrieved from the incubator and the experimental wells were rinsed twice with 40  $\mu$ L of fresh 3t3 media. To do so, the virus media was gently pipetted out of the wells. Within 1 minute of pipetting out media, 40  $\mu$ L of fresh 3t3 media was dispensed into each well to prevent desiccation. Wells were allowed to sit for 1 minute, then media was pipetted out of wells to rinse out unbound virions. 40  $\mu$ L of fresh 3t3 media was once again dispensed into each well, incubated for 1 minute, and once again pipetted out. At this point, 15000-25000 HEK-293t hACE2 cells in 293 media were dispensed into each well. As mentioned above, HEK-293t hACE2 cells were added to wells within 1 minute of media removal to avoid desiccation of 3t3 cells and captured virions. For Direct-infection samples, no rinsing was performed. Instead, HEK-293t hACE2 cells were dispensed directly into the 25  $\mu$ L of SARS-CoV-2 pseudovirus variant in each well. After HEK-293t hACE2 cells were added to wells, the 96-well plate was returned to the incubator.

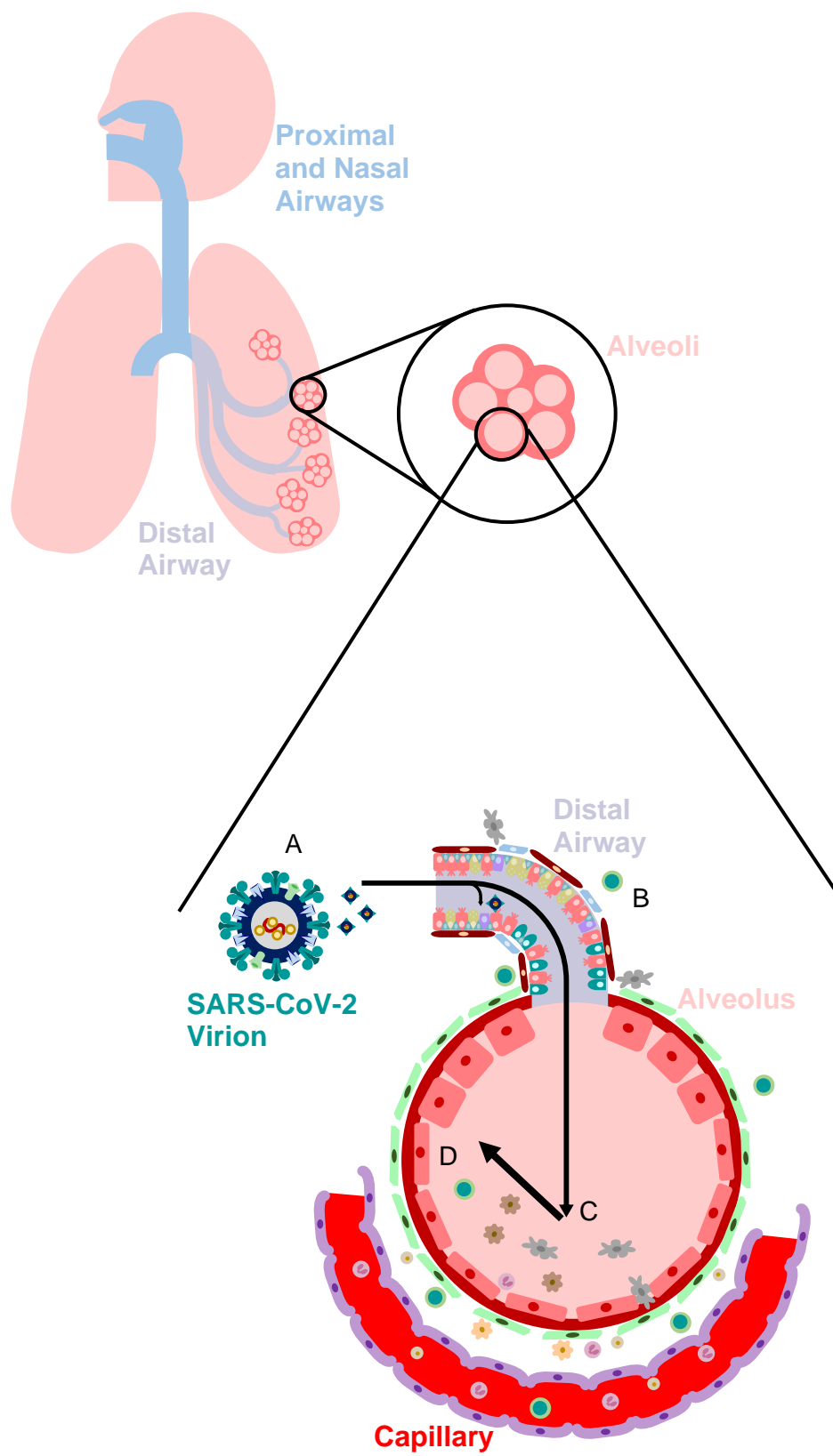
12-16 hours later, the 96-well plate was retrieved from the humidified incubator and 150  $\mu$ L of fresh, pre-warmed 293 Medium was added over the top of each well to ensure that cells remained alive and viable for the duration of the experiment. The 96-well plate was returned to the 37 °C incubator for an additional 36 to 48 hours. After 36-48 hours, the 96-well plate was retrieved from the humidified incubator. Bright-Glo Luciferase Reagent (Promega Corp., Cat # E2610, Madison, WI, USA) was thawed out and protected from light until use. 160-180  $\mu$ L of the medium in each of the infectivity plate wells was pipetted out, leaving about 30  $\mu$ L of the medium in each well after accounting for evaporation during the course of the experiment. 30  $\mu$ L of Bright-Glo reagent was added over the top of the wells and given 2-4 minutes to lyse cells. The contents of each well were then transferred to a white-backed 96-well plate and






















Luciferase signal was read on a CLARIOstar Plus microplate reader (BMG Labtech, Cary, NC, USA) with a 3600 gain and a 1 second normalization time. All samples were run in triplicate with at least two separate biological replicates for each condition. Furthermore, at least two different pseudoviral batches of each SARS-CoV-2 Spike mutation were tested.

For mannan inhibition of DC-SIGN mediated Trans-infection, mannan polymers from *Saccharomyces Cerevisiae* were utilized (Sigma-Aldrich Cat # M7504-100MG, Saint Louis, MO, USA). 100 mg of mannan was dissolved in 40 mL of ultrapure water to create a 2.5 mg/mL stock solution of mannan. When performing a Trans-assay, 64  $\mu$ L of the 2.5 mg/mL mannan stock was diluted to a final volume of 3 mL by adding 2.936 mL of 3t3 media to obtain a final concentration of 0.053 mg/mL (53.3  $\mu$ g/mL) solution of mannan in 3t3 media. 15  $\mu$ L of this 0.053 mg/mL mannan solution was used instead of 15  $\mu$ L of standard 3t3 medium to prevent cells from desiccating just prior to adding 25  $\mu$ L of pseudovirus 3t3 cells. Upon the addition of pseudovirus, the final mannan concentration in wells was at 0.02 mg/mL (20  $\mu$ g/mL).

## 2.7 Supplemental Figures



hACE2-Expressing Cells	DC-SIGN-Expressing Cells	Other Lung Cells
 Goblet Cells	 Goblet Cells	 Neuroendocrine Cells
 Club Cells	 Macrophages	 Type 1 Alveolar Pneumocytes
 Ciliated Cells	 Neutrophils	 Airway Smooth Muscle Cells
 Basal Cells	 Monocytes	
 Adventitial Fibroblasts	 Dendritic Cells	
 Type 2 Alveolar Pneumocytes	 T-Cells	
 Dendritic Cells	 Endothelial Cells	
 Monocytes		
 T-cells		

**Figure S1. Simplified depiction of hACE2 and DC-SIGN expressing cell types in the distal airway and alveolus of the lung, with a particular focus on immune cells.** SARS-CoV-2 virions (A) can infect the squamous epithelial cells of the nasal and upper respiratory airways (not shown), or be conducted to the distal airways, which are comprised of specialized columnar epithelial cells. Some of these cells express enough levels of hACE2 to allow for virion entry (B). But only a small subset of cells in the distal airways express DC-SIGN, meaning that infection of the distal airways isn't very efficient. Most SARS-CoV-2 virions enter into the alveolus and encounter the resident DC-SIGN expressing immune cells (C). These DC-SIGN expressing cells facilitate viral infection-in-trans to hACE2-expressing cells, such as Type 2 Alveolar Pneumocytes (D).

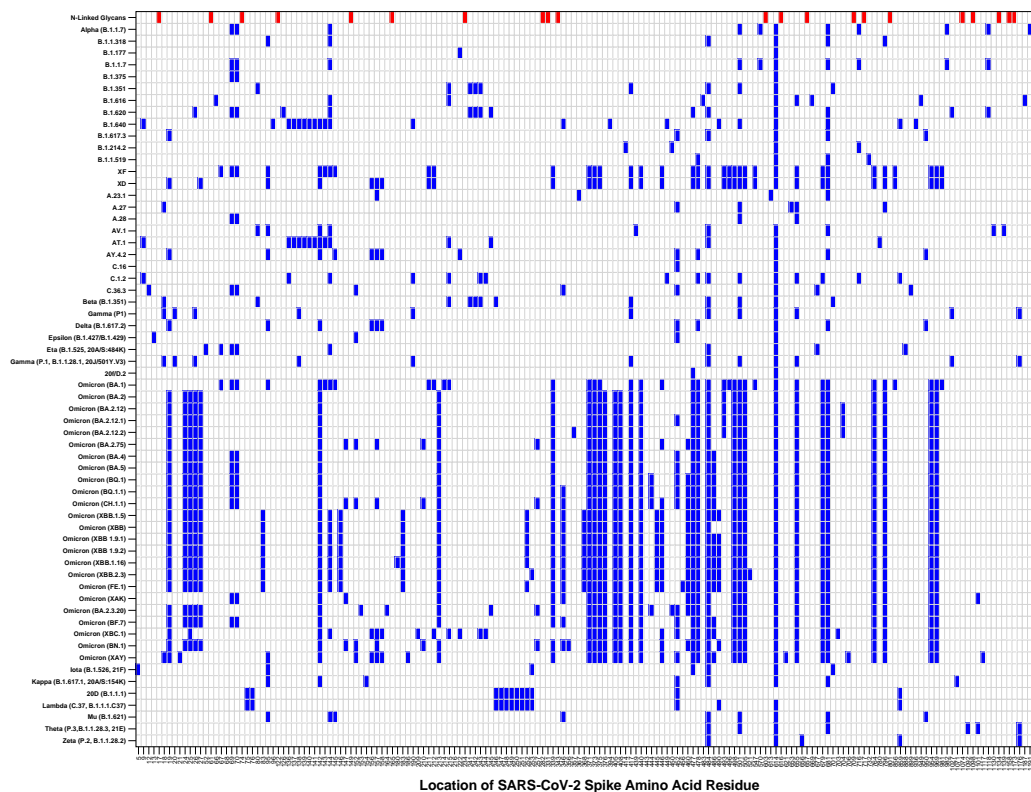


**Figure S2.** Depiction of SARS-CoV-2 Spike gene mutations for key VOC strains, as specified by the European Centre for Disease Prevention and Control (<https://www.ecdc.europa.eu/en/covid-19/variants-concern>), the World Health Organization (<https://www.who.int/activities/tracking-SARS-CoV-2-variants>), and the SIB Swiss Institute of Bioinformatics' ViralZone Website (<https://viralzone.expasy.org/9556>). Glycan sites are depicted at the top row, in red. Location of mutations found in specific Covid-19 viral strains are depicted in blue.

### Average SARS-CoV-2 S Protein N-Linked Glycan Occupancy

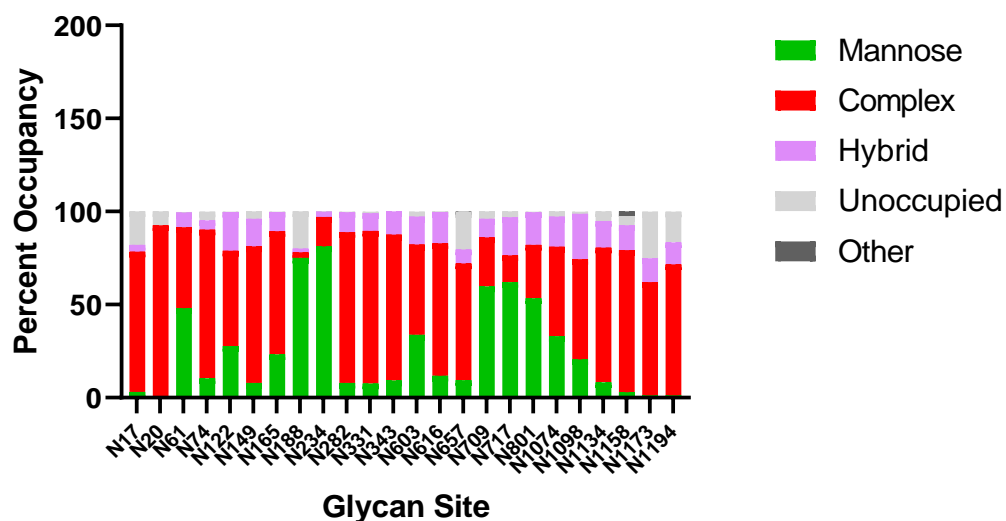


**Figure S3.** The glycan occupancy of the SARS-CoV-2 Spike based on an average of existing literature. For those papers that did not report the exact values, the glycan occupancy was estimated based off of an analysis of the .png figures using the Plotdigitizer application (<https://plotdigitizer.com/>). Note the presence of glycans N20 and N188, both of which are the result of mutations in the Spike protein sequence of the Gamma P.1 strain [122].



**Figure S4.** The glycan occupancy of the SARS-CoV-2 spike that was compiled to make Supplemental Figure 3. These data were published in the following publications listed in our references [34, 35, 36, 37, 63, 118, 119, 120, 121, 122, 123, 124, 125, 126, 127]. For publications that did not explicitly list the glycan occupancy at each site, a best estimate was given based upon their published figures.

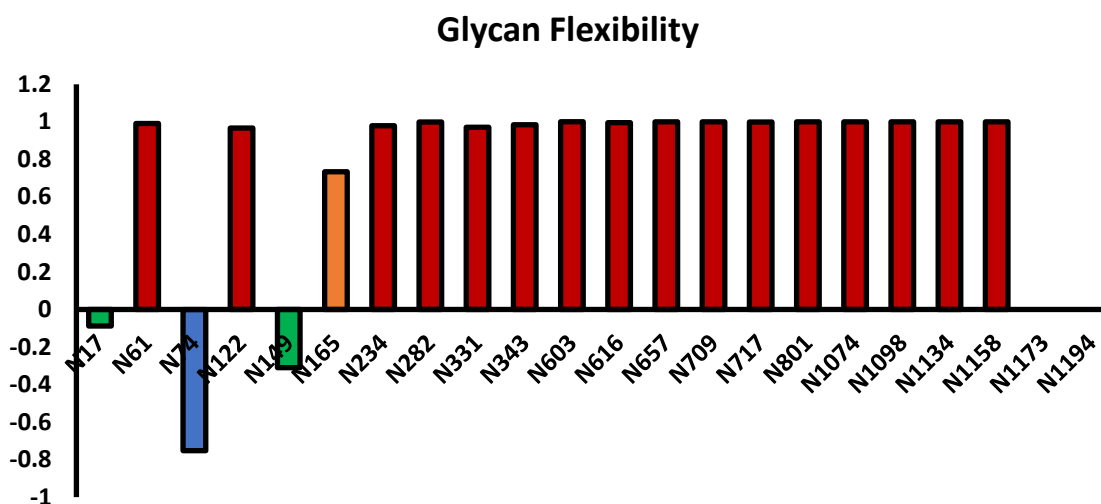


**Figure S5.** Analysis of SARS-CoV-2 Spike flexibility at N-linked glycan residues based on PDB structures as of July 5, 2023. To quantitate the flexibility of each glycan on the SARS-CoV-2 spike, we performed a rough analysis of all full-length SARS-CoV-2 spike cryo-EM structures in the PDB. Since the process of performing Cryo-EM microscopy entails snap-freezing samples and finding concordance between numerous “snapshots” of the protein, areas of high flexibility tend to have low resolution. Thus, we used the resolution of structures on the Protein Data Bank (PDB) as proxies for the degree of flexibility for regions of the SARS-CoV-2 spike. If each glycan residue was on a region that was resolved in the structure, we assigned it a value of 1. If the residue was not resolved, but was next to a well-resolved region, then it was assigned a value of 0. If the residue was not resolved and was not next to a well-resolved region, then it was assigned a value of -1. We averaged all these values for each residue site and then graphed them, above. Therefore, flexible regions are assigned values closer to -1 while rigid regions are assigned a value closer to 1. Bars are color coded such that consistently inflexible regions are colored dark red. Moderately inflexible regions are colored in orange. Moderately flexible regions are colored green. Consistently flexible regions are colored blue.

All spike structures that were analyzed were truncated slightly at the C-terminus, which is why there is no data for residues N1173 and N1194.

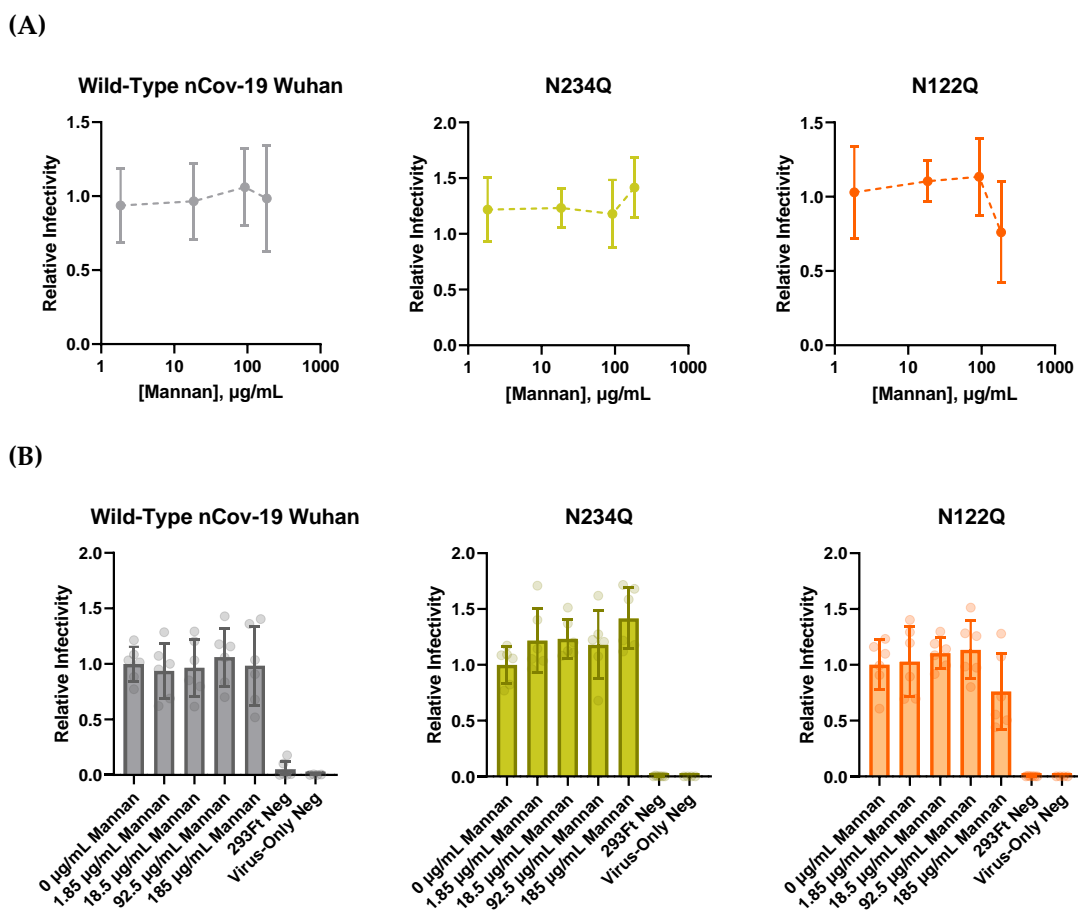


**Figure S6.** To ensure that Mannan had no effect on our SARS-CoV-2 pseudoviral assays beyond DC-SIGN mediated trans-infection, we performed Direct-infectivity assays with three difference strains of pseudovirus in the presence of varying concentrations of mannane. **(A)** Line graphs where each strain's mannane sample infectivity was normalized to the signal from a sample with no mannane. **(B)** Bar graphs showing the same data in addition to the controls. Overall, we found that Mannane had no significant effect on pseudovirus infectivity between 5 to 100  $\mu\text{g/mL}$ . Hence, we opted to use a concentration of 20  $\mu\text{g/mL}$  of mannane to inhibit DC-SIGN infection.



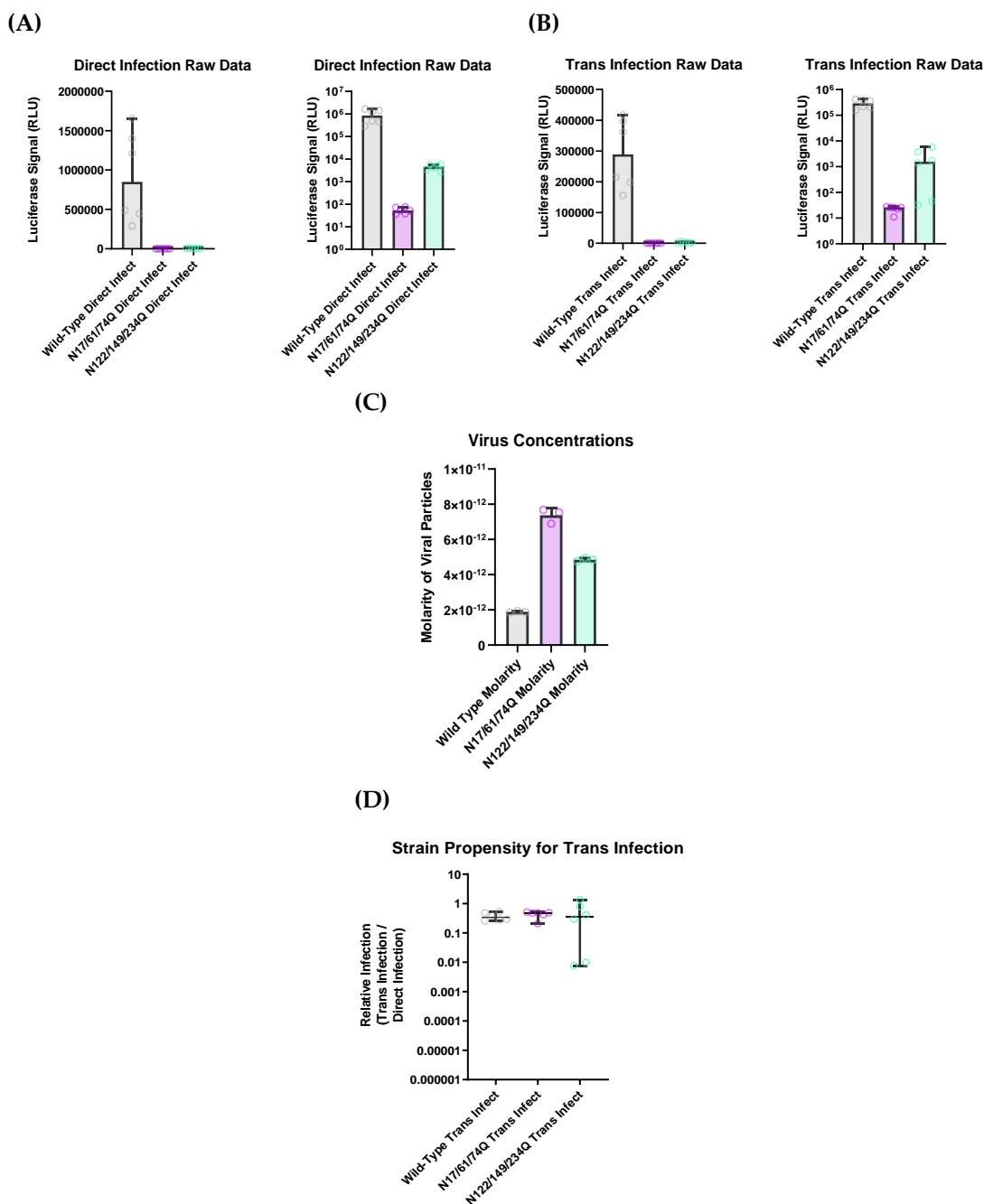


**Figure S7. Cluster mutant strains show significantly lower raw infectivity signal (RLUs) than Wild-Type nCov-19 Wuhan pseudotyped virus despite having higher titers:** (A) Raw Direct-infection signals for Wild-Type nCov-19 Wuhan and cluster strain pseudotyped lentivirions. (B) Raw Trans-infection signals for Wild-Type nCov-19 Wuhan and cluster strain pseudotyped lentivirions. Note that our instrumentation cannot reliably read below 50 RLUs, meaning that the infectivity signals for N1716/174Q virus are too low to conclude that there is any infection compared to both cluster mutant strains. (C) The virus cluster mutant strains were quantified via p24 ELISA assay; the two cluster strains show greater levels of virus than the Wild-type strain, indicating that the lower signal from the cluster mutant strains is not due to low titer. Overall, even though the Wild-Type nCov-19 Wuhan pseudotyped lentivirus had less than half the molarity

of either cluster strain (N17/61/74Q and N122/149/234Q), the raw luciferase reads (in relative light units, or RLU) for both Direct Infection assays and Trans Infection assays displayed at least two orders of magnitude higher RLU than either of the mutants.

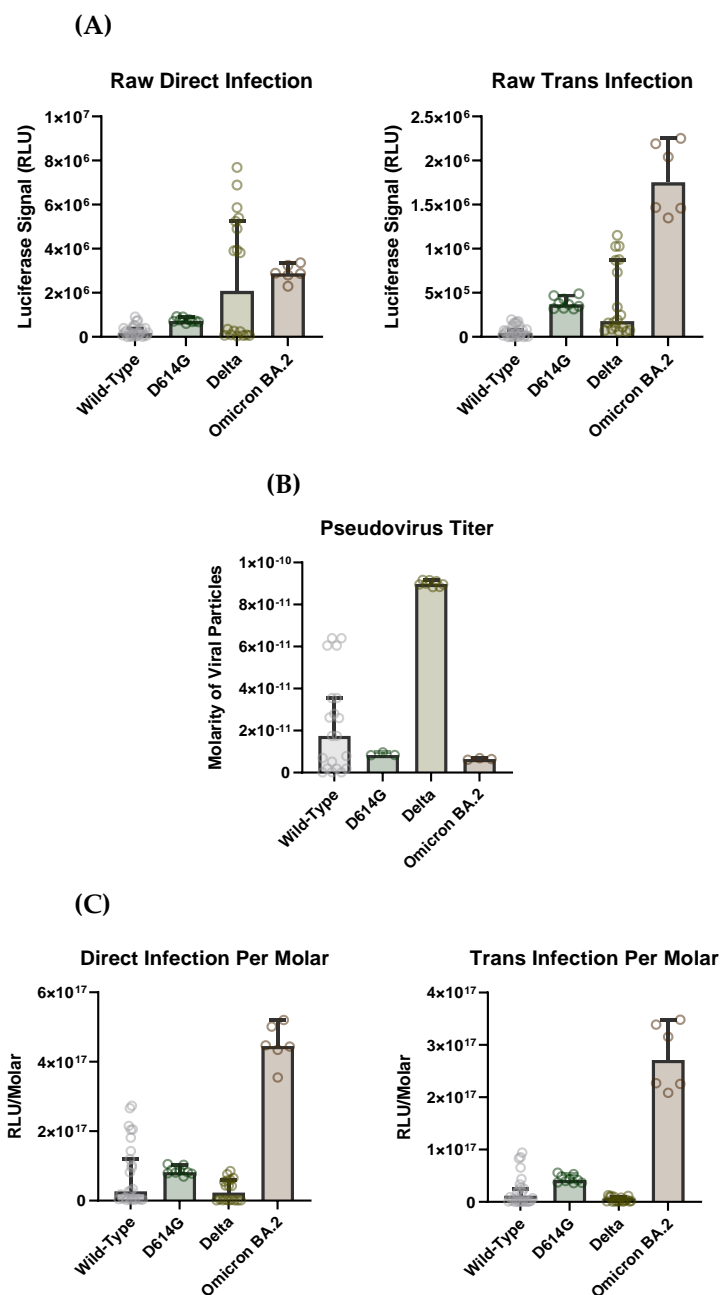
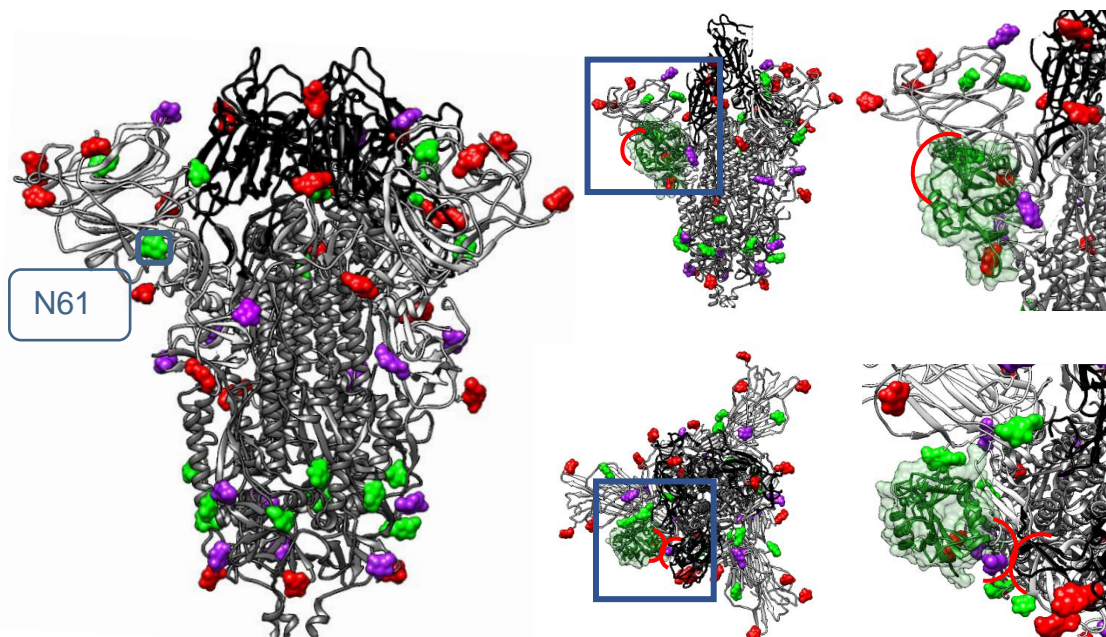


**Figure S8. Demonstration of how Omicron BA.2 had the greatest hACE2-mediated infectivity on *in vitro* assays:** (A) Raw infectivity values for all spike pseudotyped lentivirus. Our titer assays indicate that Delta and Omicron BA.2 strains have similar signal on Direct-infectivity assays. (B) Each lentiviral pseudovirus strain was titered. Even though both Delta and Omicron BA.2 strains had similar infectivity, our Delta strain virus had approximately 10 times more virus detected in the virus sample. (C) Infectivity for each viral strain was normalized to the strain's molarity from the titration assay. The Omicron BA.2 lentivirus pseudovirus strain appeared to have higher infectious capability on our *in vitro* assay than the other strains.

(A)



(B)

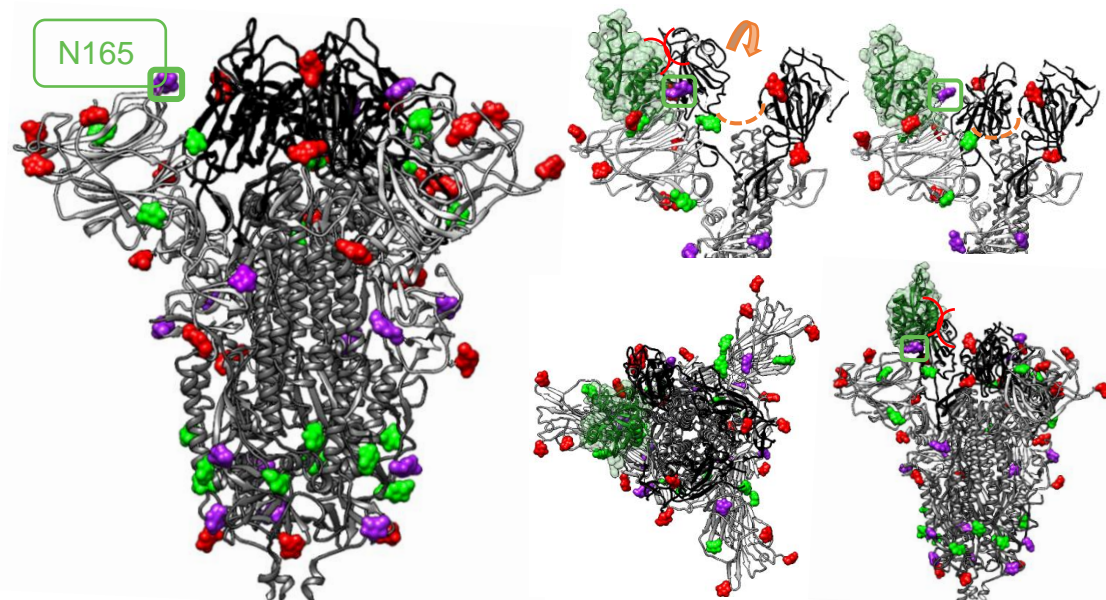


**Figure S9. Depicting the steric clashes when DC-SIGN is overlaid onto SARS-CoV-2 N-linked glycans N61 and N165:** (A) When the DC-SIGN C-terminal CRD is overlaid onto N61, it sterically clashes with the 620-641 loop region of the adjacent Spike monomer, as shown by red curves. There is particularly obvious steric overlap with the glycan at N616, which is the purple glycan close to the red arc. (B) When the DC-SIGN C-terminal CRD is overlaid onto N165, there is a possible clash with the 466-491 loop of the Receptor Binding Motif when the spike is in the up/open conformation. The clashes are shown by red curves. The movement of the RBD from the open conformation to the closed conformation is shown with the orange arrow and dashed curve. SARS-CoV-2 spike is PDB ID: 7NT9 overlaid on 6VYB to obtain glycan sites. The DC-SIGN C-terminal CRD is PDB ID: 1SL4.

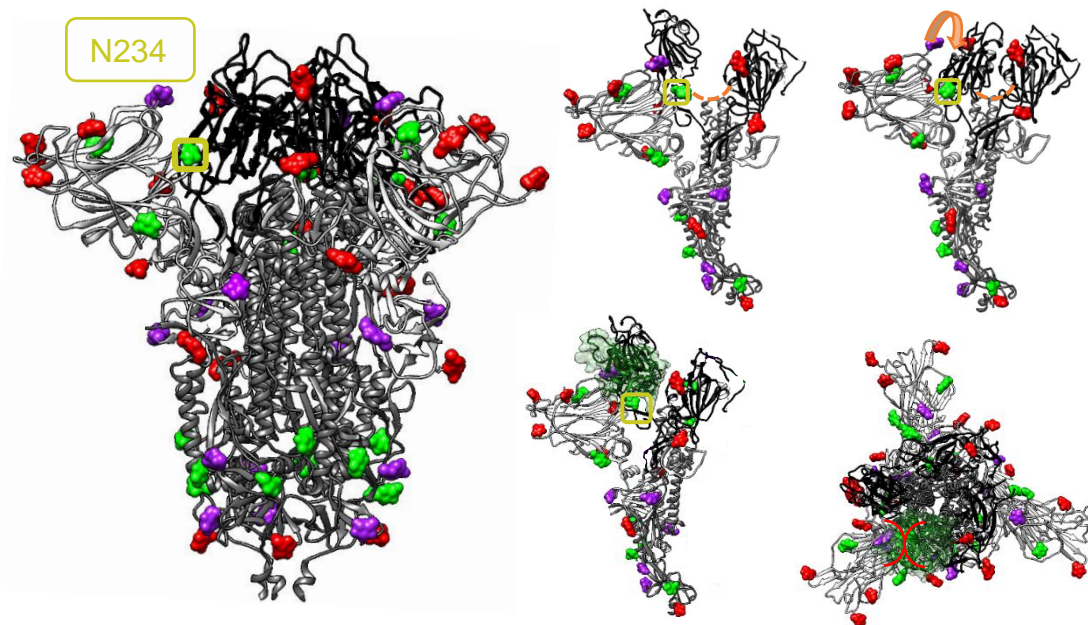


**Figure S10.** Glycan N234 is almost entirely obscured from DC-SIGN recognition, even when the RBD is in the down state. The DC-SIGN CRD seems like it sterically clashes with the 107-116 loop, the 158-169 loop, and glycan N165 on the S1 domain of the Spike protein. As above, the steric clashes are depicted as red curves and the movement of the RBD is shown with the orange arrow and dashed curve.

## 2.8 References

- [1]: Liu, X.; Huang, J.; Li, C.; Zhao, Y.; Wang, D.; Huang, Z.; Yang, K. The role of seasonality in the spread of COVID-19 pandemic. *Environ Res* 2021, 195, 110874, <https://doi.org/10.1016/j.envres.2021.110874>.
- [2]: Klompas, M.; Pandolfi, M.C.; Nisar, A.B.; Baker, M.A.; Rhee, C. Association of Omicron vs Wild-type SARS-CoV-2 Variants With Hospital-Onset SARS-CoV-2 Infections in a US Regional Hospital System. *JAMA* 2022, 328, 296-298, <https://doi.org/10.1001/jama.2022.9609>.
- [3]: Nasimiyu, C.; Matoke-Muhia, D.; Rono, G.K.; Osoro, E.; Ouso, D.O.; Mwangi, J.M.; Mwikwabe, N.; Thiong'o, K.; Dawa, J.; Ngere, I.; Gachohi, J.; Kariuki, S.; Amukoye, E.; Mureithi, M.; Ngere, P.; Amoth, P.; Were, I.; Makayotto, L.; Nene, V.; Abworo, E.O.; Njenga, M.K.; Seifert, S.; Oyola, S.O. Imported SARS-CoV-2 Variants of Concern Drove Spread of Infections across Kenya during the Second Year of the Pandemic. *COVID* 2022, 2, 586-598, <https://doi.org/10.3390/covid2050044>.
- [4]: Yue, C.; Song, W.; Wang, L.; Jian, F.; Chen, X.; Gao, F.; Shen, Z.; Wang, Y.; Wang, X.; Cao, Y. Enhanced transmissibility of XBB.1.5 is contributed by both strong ACE2 binding and antibody evasion. *Lancet Infect Dis* 2023, 23, 278–280, <https://doi.org/10.1101/2023.01.03.522427>.
- [5]: Arora, P.; Cossmann, A.; Schulz, S.R.; Ramos, G.M.; Stankov, M.V.; Jäck, H-M.; Behrens, G.M.N.; Pöhlmann, S.; Hoffman, M. Neutralisation sensitivity of the SARS-CoV-2 XBB.1 lineage. *Lancet Infect Dis* 2023, 23, 147-148, [https://doi.org/10.1016/S1473-3099\(22\)00831-3](https://doi.org/10.1016/S1473-3099(22)00831-3).
- [6]: Our World in Data: SARS-CoV-2 sequences by variant. Available online: <https://ourworldindata.org/grapher/covid-variants-bar> (accessed on 17 July 2023).
- [7]: Altmann, D.M.; Rosemary, J.B. COVID-19 vaccination: The road ahead. *Science* 2022, 375, 1127-1132, <https://doi.org/10.1126/science.abn1755>.
- [8]: Murray, C.J.L.; Piot, P. The Potential Future of the COVID-19 Pandemic: Will SARS-CoV-2 Become a Recurrent Seasonal Infection? *JAMA* 2021, 325, 1249-1250, <https://doi.org/10.1001/jama.2021.2828>.
- [9]: McCormick, K.D.; Mellors, J.W.; Jacobs, J.L. Adaptation of advanced clinical virology assays from HIV-1 to SARS-CoV-2. *Curr Opin HIV AIDS* 2021, 16, 3-10, <https://doi.org/10.1097/COH.0000000000000656>.
- [10]: Carabelli, A.M.; Peacock, T.P.; Thorne, L.G.; Harvey, W.T.; Hughes, J.; COVID-19 Genomics UK Consortium; Peacock, S.J.; Barclay, W.S.; de Silva, T.I.; Towers, G.J.; Robertson, D.L. SARS-CoV-2 variant biology: immune escape, transmission and fitness. *Nat Rev Microbiol* 2023, 21, 162-177, <https://doi.org/10.1038/s41579-022-00841-7>.
- [11]: Zabidi, N.Z.; Liew, H.L.; Farouk, I.A.; Puniyamurti, A.; Yip, A.J.W.; Wijesinghe, V.N.; Low, Z.Y.; Tang, J.W.; Chow, V.T.K.; Lal, S.K. Evolution of SARS-CoV-2 Variants: Implications on Immune Escape, Vaccination, Therapeutic and Diagnostic Strategies. *Viruses* 2023, 15, 944, <https://doi.org/10.3390/v15040944>.

- [12]: Li, L. ; Liao, H. ; Meng, Y.; Li, W.; Han, P.; Liu, K.; Wang, Q.; Li, D.; Zhang, Y.; Wang, L.; Fan, Z.; Zhang, Y.; Wang, Q.; Zhao, X.; Sun, Y.; Huang, N.; Qi, J.; Gao, G.F. Structural basis of human ACE2 higher binding affinity to currently circulating Omicron SARS-CoV-2 sub-variants BA.2 and BA.1.1. *Cell* 2022, 185, 2952-2960.e10, <https://doi.org/10.1016/j.cell.2022.06.023>.
- [13]: Kumar, R.; Murugan, N.A.; Srivastava, V. Improved Binding Affinity of Omicron's Spike Protein for the Human Angiotensin-Converting Enzyme 2 Receptor Is the Key behind Its Increased Virulence. *Int J Mol Sci* 2022, 23, 3409, <https://doi.org/10.3390/ijms23063409>.
- [14]: Kumar, S.; Karuppanan, K.; Subramaniam, G. Omicron (BA.1) and sub-variants (BA.1.1, BA.2, and BA.3) of SARS-CoV-2 spike infectivity and pathogenicity: A comparative sequence and structural-based computational assessment. *J Med Virol* 2022, 94, 4780-4791, <https://doi.org/10.1002/jmv.27927>.
- [15]: Qu, P.; Evans, J.P.; Faraone, J.N.; Zheng, Y.M.; Carlin, C.; Anghelina, M.; Stevens, P.; Fernandez, S.; Jones, D.; Lozanski, G.; Panchal, A.; Saif, L.J.; Oltz, E.M.; Xu, K.; Gumina, R.J.; Liu, S.L. Enhanced neutralization resistance of SARS-CoV-2 Omicron subvariants BQ.1, BQ.1.1, BA.4.6, BF.7, and BA.2.75.2. *Cell Host Microbe* 2023, 31, 9-17.e3, <https://doi.org/10.1016/j.chom.2022.11.012>.
- [16]: Brant, A.C.; Tian, W.; Majerciak, V.; Yang, W.; Zheng, Z-M. SARS-CoV-2: from its discovery to genome structure, transcription, and replication. *Cell Biosci* 2021, 11, 136, <https://doi.org/10.1186/s13578-021-00643-z>.
- [17]: Zandi, M.; Shafaati, M.; Kalantar-Neyestanaki, D.; Pourghadamyari, H.; Fani, M.; Soltani, S.; Kaleji, H.; Abbasi, S. The role of SARS-CoV-2 accessory proteins in immune evasion. *Biomed Pharmacother* 2022, 156, 113889, <https://doi.org/10.1016/j.biopha.2022.113889>.
- [18]: Redondo, N.; Zaldívar-López, S.; Garrido, J.J.; Montoya, M. SARS-CoV-2 Accessory Proteins in Viral Pathogenesis: Knowns and Unknowns. *Front Immunol* 2021, 12, 708264, <https://doi.org/10.3389/fimmu.2021.708264>.
- [19]: Valdez-Cruz, N.A.; García-Hernández, E.; Espitia, C.; Cobos-Marín, L.; Altamirano, C.; Bando-Campos, C.G.; Cofas-Vargas, L.F.; Coronado-Aceves, E.W.; González-Hernández, R.A.; Hernández-Peralta, P.; Juárez-López, D.; Ortega-Portilla, P.A.; Restrepo-Pineda, S.; Zelada-Cordero, P.; Trujillo-Roldán, M.A. Integrative overview of antibodies against SARS-CoV-2 and their possible applications in COVID-19 prophylaxis and treatment. *Microb Cell Fact* 2021, 20, 88, <https://doi.org/10.1186/s12934-021-01576-5>.
- [20]: Hwang, Y.C.; Lu, R.M.; Su, S.C.; Chiang, P-Y.; Ko, S-H.; Ke, F-Y.; Liang, K-H.; Hsieh, T-Y.; Wu, H-C. Monoclonal antibodies for COVID-19 therapy and SARS-CoV-2 detection. *J Biomed Sci* 2022, 29, 1, <https://doi.org/10.1186/s12929-021-00784-w>.
- [21]: Barnes, C.O.; West, A.P.; Huey-Tubman, K.E.; Hoffmann, M.A.G.; Sharaf, N.G.; Hoffman, P.R.; Koranda, N.; Gristick, H.B.; Gaebler, C.; Muecksch, F.; Cetrulo Lorenzi, J.C.; Finkin, S.; Hagglof, T.; Hurley, A.; Millard, K.G.; Weisblum, Y.; Schmidt, F.; Hatziioannou, T.; Bieniasz, P.D.; Caskey, M.; Robbiani, D.F.; Nussenzweig, M.C.; Bjorkman, P.J. Structures of human antibodies bound to SARS-CoV-2 spike reveal

common epitopes and recurrent features of antibodies. *Cell* 2020, 182, 828-842.e16, <https://doi.org/10.1016/j.cell.2020.06.025>.

[22]: Chen, Y.; Zhao, X.; Zhou, H.; Zhu, H.; Jiang, S.; Wang, P. Broadly neutralizing antibodies to SARS-CoV-2 and other human coronaviruses. *Nat Rev Immunol* 2023, 23, 189–199, <https://doi.org/10.1038/s41577-022-00784-3>.

[23]: Jalkanen, P.; Kolehmainen, P.; Häkkinen, H.K.; Huttunen, M.; Tähtinen, P.A.; Lundberg, R.; Maljanen, S.; Reinholm, A.; Tauriainen, S.; Pakkanen, S.H.; Levonen, I.; Nousiainen, A.; Miller, T.; Välimaa, H.; Ivaska, L.; Pasternack, A.; Naves, R.; Ritvos, O.; Österlund, P.; Kuivanen, S.; Smura, T.; Hepojoki, J.; Vapalahti, O.; Lempainen, J.; Kakkola, L.; Kantele, A.; Julkunen, I. COVID-19 mRNA vaccine induced antibody responses against three SARS-CoV-2 variants. *Nat Commun* 2021, 12, 3991, <https://doi.org/10.1038/s41467-021-24285-4>.

[24]: Song, J.Y.; Choi, W.S.; Heo, J.Y.; Lee, J.S.; Jung, D.S.; Kim, S-W.; Park, K-H.; Eom, J.S.; Jeong, S.J.; Lee, J.; Kwon, K.T.; Choi, H.J.; Sohn, J.W.; Kim, Y.K.; Noh, J.Y.; Kim, W.J.; Roman, F.; Ceregido, M.A.; Solmi, F.; Philippot, A.; Walls, A.C.; Carter, L.; Veessler, D.; King, N.P.; Kim, H.; Ryu, J.H.; Lee, S.J.; Park, Y.W.; Park, H.K.; Cheong, H.J. Safety and immunogenicity of a SARS-CoV-2 recombinant protein nanoparticle vaccine (GBP510) adjuvanted with AS03: A randomised, placebo-controlled, observer-blinded phase 1/2 trial. *EBioMedicine* 2022, 51, 101569, <https://doi.org/10.1016/j.eclinm.2022.101569>.

[25]: Zhang, J.; Han, Z.B.; Liang, Y.; Zhang, X.F.; Jin, Y.Q.; Du, L.F.; Shao, S.; Wang, H.; Hou, J.W.; Xu, K.; Lei, W.; Lei, Z.H.; Liu, Z.M.; Zhang, J.; Hou, Y.N.; Liu, N.; Shen, F.J.; Wu, J.J.; Zheng, X.; Li, X.Y.; Li, X.; Huang, W.J.; Wu, G.Z.; Su, J.G.; Li, Q.M. A mosaic-type trimeric RBD-based COVID-19 vaccine candidate induces potent neutralization against Omicron and other SARS-CoV-2 variants. *eLife* 2022, 11, e78633, <https://doi.org/10.7554/eLife.78633>.

[26]: Vu, M.N.; Kelly, H.G.; Kelly, S.J.; Wheatley, A.K. Current and future nanoparticle vaccines for COVID-19. *EBioMedicine* 2021, 74, 103699, <https://doi.org/10.1016/j.ebiom.2021.103699>.

[27]: Cohen, A.A.; Van Doremalen, N.; Greaney, A.J.; Andersen, H.; Sharma, A.; Starr, T.N.; Keeffe, J.R.; Fan, C.; Schulz, J.E.; Gnanapragasam, P.N.P.; Kakutani, L.M.; West Jr., A.P.; Saturday, G.; Lee, Y.E.; Gao, H.; Jette, C.A.; Lewis, M.G.; Tan, T.K.; Townsend, A.R.; Bloom, J.D.; Munster, V.J.; Bjorkman, P.J. Mosaic RBD nanoparticles protect against challenge by diverse sarbecoviruses in animal models. *Science* 2022, 377, eabq0839, <https://doi.org/10.1126/science.abq0839>.

[28]: Bianchini, F.; Crivelli, V.; Abernathy, M.E.; Guerra, C.; Palus, M.; Muri, J.; Marcotte, H.; Piralla, A.; Pedotti, M.; De Gasparo, R.; Simonelli, L.; Matkovic, M.; Toscano, C.; Biggiogero, M.; Calvaruso, V.; Svoboda, P.; Cervantes Rincón, T.; Fava, T.; Podešvová, L.; Shanbhag, A.A.; Celoria, A.; Sgrignani, J.; Stefanik, M.; Hönig, V.; Pranclova, V.; Michalcikova, T.; Prochazka, J.; Guerrini, G.; Mehn, D.; Ciabattini, A.; Abolhassani, H.; Jarrossay, D.; Uguccioni, M.; Medaglini, D.; Pan-Hammarström, Q.; Calzolari, L.; Fernandez, D.; Baldanti, F.; Franzetti-Pellanda, A.; Garzoni, C.; Sedlacek, R.; Ruzek, D.; Varani, L.; Cavalli, A.; Barnes, C.O.; Robbiani, D.F. Human neutralizing antibodies to



- cold linear epitopes and subdomain 1 of the SARS-CoV-2 spike glycoprotein. *Sci Immunol* 2023, 8, eade0958, <https://doi.org/10.1126/sciimmunol.ade0958>.
- [29]: The race to make a variant-proof COVID vaccine. Available online: <https://www.youtube.com/watch?v=ELwYEqzTgSk> (accessed 17 July 2023).
- [30]: Krishnamoorthy, N.; Fakhro, K. Identification of mutation resistance coldspots for targeting the SARS-CoV2 main protease. *IUBMB Life* 2021, 73, 670-675, <https://doi.org/10.1002/iub.2465>.
- [31]: Jackson, C.B.; Farzan, M.; Chen, B.; Choe, H. Mechanisms of SARS-CoV-2 entry into Cells. *Nat Rev Mol Cell Biol* 2022, 23, 3–20, <https://doi.org/10.1038/s41580-021-00418-x>.
- [32]: Shang, J.; Ye, G.; Shi, K.; Wan, Y.; Luo, C.; Aihara, H.; Geng, Q.; Auerbach, A.; Li, F. Structural basis of receptor recognition by SARS-CoV-2. *Nature* 2020, 581, 221–224, <https://doi.org/10.1038/s41586-020-2179-y>.
- [33]: Ge, J.; Yu, J.; Shan, S.; Zhou, H.; Fan, S.; Zhang, Q.; Shi, X.; Wang, Q.; Zhang, L.; Wang, X. Structure of the SARS-CoV-2 spike receptor-binding domain bound to the ACE2 receptor. *Nature* 2020, 581, 215–220. <https://doi.org/10.1038/s41586-020-2180-5>
- [34]: Shajahan, A.; Supekar, N.T.; Gleinich, A.S.; Azadi, P. Deducing the N- and O-glycosylation profile of the spike protein of novel coronavirus SARS-CoV-2. *Glycobiology*. 2020, 30, 981-988, <https://doi.org/10.1093/glycob/cwaa042>.
- [35]: Watanabe, Y.; Allen, J.D.; Wrapp, D.; McLellan, J.S.; Crispin, M. Site-specific glycan analysis of the SARS-CoV-2 spike. *Science* 2020, 369, 330-333, <https://doi.org/10.1126/science.abb9983>.
- [36]: Sanda, M.; Morrison, L.; Goldman, R. N- and O-Glycosylation of the SARS-CoV-2 Spike Protein. *Anal Chem* 2021, 93, 2003–2009, <https://doi.org/10.1021/acs.analchem.0c03173>.
- [37]: Zhao, P.; Praissman, J.; Grant, O.C.; Cai, Y.; Xiao, T.; Rosenbalm, K.; Aoki, K.; Kellman, B.; Bridger, R.; Barouch, D.; Brindley, M.; Lewis, N.; Tiemeyer, M.; Chen, B.; Woods, R.; Wells, L. Virus-Receptor Interactions of Glycosylated SARS-CoV-2 Spike and Human ACE2 Receptor. *Cell Host Microbe* 2020, 28, 586-601.e6, <https://doi.org/10.1016/j.chom.2020.08.004>.
- [38]: Li, Y.; Liu, D.; Wang, Y.; Su, W.; Liu, G.; Dong, W. The Importance of Glycans of Viral and Host Proteins in Enveloped Virus Infection. *Front Immunol* 2021, 12, 638573, <https://doi.org/10.3389/fimmu.2021.638573>.
- [39]: Feng, T.; Zhang, J.; Chen, Z.; Pan, W.; Chen, Z.; Yan, Y.; Dai, J. Glycosylation of viral proteins: Implication in virus-host interaction and virulence. *Virulence* 2022, 13, 670-683, <https://doi.org/10.1080/21505594.2022.2060464>.
- [40]: Raman, R.; Tharakaraman, K.; Sasisekharan, V.; Sasisekharan, R. Glycan–protein interactions in viral pathogenesis. *Curr Opin Struct Biol* 2016, 40, 153–162, <https://doi.org/10.1016/j.sbi.2016.10.003>.
- [41]: Hoffmann, D.; Mereiter, S.; Oh, Y.J.; Monteil, V.; Elder, E.; Zhu, R.; Canena, D.; Hain, L.; Laurent, E.; Grünwald-Gruber, C.; Klausberger, M.; Jonsson, G.; Kellner, M.J.;

Novatchkova, M.; Ticevic, M.; Chabloz, A.; Wirnsberger, G.; Hagelkruys, A.; Altmann, F.; Mach, L.; Stadlmann, J.; Oostenbrink, C.; Mirazimi, A.; Hinterdorfer, P.; Penninger, J.M. Identification of lectin receptors for conserved SARS-CoV-2 glycosylation sites. *EMBO J* 2021, 40, e108375, <https://doi.org/10.15252/embj.2021108375>.

[42]: Lempp, F.A.; Soriaga, L.B.; Montiel-Ruiz, M.; Benigni, F.; Noack, J.; Park, Y.J.; Bianchi, S.; Walls, A.C.; Bowen, J.E.; Zhou, J.; Kaiser, H.; Joshi, A.; Agostini, M.; Meury, M.; Dellota Jr., E.; Jaconi, S.; Cameroni, E.; Martinez-Picado, J.; Vergara-Alert, J.; Izquierdo-Useros, N.; Virgin H.W.; Lanzavecchia, A.; Veessler, D.; Purcell, L.A.; Telenti, A.; Corti, D. Lectins enhance SARS-CoV-2 infection and influence neutralizing antibodies. *Nature* 2021, 598, 342-347, <https://doi.org/10.1038/s41586-021-03925-1>.

[43]: Thépaut, M.; Luczkowiak, J.; Vivès, C.; Labiod, N.; Bally, I.; Lasala, F.; Grimoire, Y.; Fenel, D.; Sattin, S.; Thielens, N.; Schoehn, G.; Bernardi, A.; Delgado, R.; Fieschi, F. DC/L-SIGN recognition of spike glycoprotein promotes SARS-CoV-2 trans-infection and can be inhibited by a glycomimetic antagonist. *PLoS Pathog* 2021, 17, e1009576, <https://doi.org/10.1371/journal.ppat.1009576>.

[44]: Perez-Zsolt, D.; Muñoz-Basagoiti, J.; Rodon, J.; Elosua-Bayes, M.; Raïch-Regué, D.; Risco, C.; Sachse, M.; Pino, M.; Gumber, S.; Paiardini, M.; Chojnacki, J.; Erkizia, I.; Muñoz-Trabudua, X.; Ballana, E.; Riveira-Muñoz, E.; Noguera-Julian, M.; Paredes, R.; Trinité, B.; Tarrés-Freixas, F.; Blanco, I.; Guallar, V.; Carrillo, J.; Blanco, J.; Telenti, A.; Heyn, H.; Segalés, J.; Clotet, B.; Martinez-Picado, J.; Vergara-Alert, J.; Izquierdo-Useros, N. SARS-CoV-2 interaction with Siglec-1 mediates trans-infection by dendritic cells. *Cell Mol Immunol* 2021, 18, 2676–2678, <https://doi.org/10.1038/s41423-021-00794-6>.

[45]: Lim, S.; Zhang, M.; Chang, T.L. ACE2-Independent Alternative Receptors for SARS-CoV-2. *Viruses* 2022, 14, 2535, <https://doi.org/10.3390/v14112535>.

[46]: Mulay, A.; Konda, B.; Garcia Jr., G.; Yao, C.; Beil, S.; Villalba, J.M.; Koziol, C.; Sen, C.; Purkayastha, A.; Kolls, J.K.; Pociask, D.A.; Pessina, P.; de Aja, J.S.; Garcia-de-Alba, C.; Kim, C.F.; Gomperts, B.; Arumugaswami, V.; Stripp, B.R. SARS-CoV-2 infection of primary human lung epithelium for COVID-19 modeling and drug discovery. *Cell Rep* 2021, 35, 109055, <https://doi.org/10.1016/j.celrep.2021.109055>.

[47]: Puray-Chavez, M.; LaPak, K.M.; Schrank, T.P.; Elliott, J.L.; Bhatt, D.P.; Agajanian, M.J.; Jasuja, R.; Lawson, D.Q.; Davis, K.; Rothlauf, P.W.; Liu, Z.; Jo, H.; Lee, N.; Tenneti, K.; Eschbach, J.E.; Shema Mugisha, C.; Cousins, E.M.; Cloer, E.W.; Vuong, H.R.; VanBlargan, L.A.; Bailey, A.L.; Gilchuk, P.; Crowe Jr., J.E.; Diamond, M.S.; Hayes, D.N.; Whelan, S.P.J.; Horani, A.; Brody, S.L.; Goldfarb, D.; Major, M.B.; Kutluay, S.B. Systematic analysis of SARS-CoV-2 infection of an ACE2-negative human airway cell. *Cell Rep* 2021, 36, 109364, <https://doi.org/10.1016/j.celrep.2021.109364>.

[48]: Li, M.Y.; Li, L.; Zhang, Y.; Wang, X-S. Expression of the SARS-CoV-2 cell receptor gene ACE2 in a wide variety of human tissues. *Infect Dis Poverty* 2020, 9, 45, <https://doi.org/10.1186/s40249-020-00662-x>.

[49]: Hikmet, F.; Méar, L.; Edvinsson, Å.; Micke, P.; Uhlén, M.; Lindskog, C. The protein expression profile of ACE2 in human tissues. *Mol Syst Biol* 2020, 16, e9610, <https://doi.org/10.15252/msb.20209610>.

- [50]: Dowling, W.; Thompson, E.; Badger, C.; Mellquist, J.L.; Garrison, A.R.; Smith, J.M.; Paragas, J.; Hogan, R.J.; Schmaljohn, C. Influences of Glycosylation on Antigenicity, Immunogenicity, and Protective Efficacy of Ebola Virus GP DNA Vaccines. *J Virol* 2007, 81, 1821–1837, <https://doi.org/10.1128/JVI.02098-06>.
- [51]: Balzarini, J.; Laethem, K.V.; Hatse, S.; Froeyen, M.; Peumans, W.; Van Damme, E.; Schols, D. Carbohydrate-binding Agents Cause Deletions of Highly Conserved Glycosylation Sites in HIV GP120: A NEW THERAPEUTIC CONCEPT TO HIT THE ACHILLES HEEL OF HIV. *J Biol Chem* 2005, 280, 41005-41014, <https://doi.org/10.1074/jbc.M508801200>.
- [52]: Weng, S.; Shang, J.; Cheng, Y.; Zhou, H.; Ji, C.; Yang, R.; Wu, A. Genetic differentiation and diversity of SARS-CoV-2 Omicron variant in its early outbreak. *Biosaf Health* 2022, 4, 171-178, <https://doi.org/10.1016/j.bsheal.2022.04.004>.
- [53]: Wright, D.W.; Harvey, W.T.; Hughes, J.; Cox, M.; Peacock, T.P.; Colquhoun, R.; Jackson, B.; Orton, R.; Nielsen, M.; Hsu, N.S.; COVID-19 Genomics UK (COG-UK) consortium; Harrison, E.M.; de Silva, T.I.; Rambaut, A.; Peacock, S.J.; Robertson, D.L.; Carabelli, A.M. Tracking SARS-CoV-2 mutations and variants through the COG-UK-Mutation Explorer. *Virus Evol* 2022, 8, veac023, <https://doi.org/10.1093/ve/veac023>.
- [54]: Ko, K.K.K.; Yingtaweessittikul, H.; Tan, T.T.; Wijaya, L.; Cao, D.Y.; Goh, S.S.; Abdul Rahman, N.B.; Chan, K.X.L.; Tay, H.M.; Sim, J.H.C.; Chan, K.S.; Oon, L.L.E.; Nagarajan, N.; Suphavitai, C. Emergence of SARS-CoV-2 Spike Mutations during Prolonged Infection in Immunocompromised Hosts. *Microbiol Spectr* 2022, 10, e0079122, <https://doi.org/10.1128/spectrum.00791-22>.
- [55]: Cobos-Marín, L.; Altamirano, C.; Bando-Campos, C.G.; Cofas-Vargas, L.F.; Coronado-Aceves, E.W.; González-Hernández, R.A.; Hernández-Peralta, P.; Juárez-López, D.; Ortega-Portilla, P.A.; Restrepo-Pineda, S.; Zelada-Cordero, P.; Trujillo-Roldán, M.A. Integrative overview of antibodies against SARS-CoV-2 and their possible applications in COVID-19 prophylaxis and treatment. *Microb Cell Factories* 2021, 20, 88, <https://doi.org/10.1186/s12934-021-01576-5>.
- [56]: Yang, J.; Liu, M.Q.; Liu, L.; Li, X.; Xu, M.; Lin, H.; Liu, S.; Hu, Y.; Li, B.; Liu, B.; Li, M.; Sun, Y.; Chen, Y-Q.; Shi, Z-L.; Yan, H. A triple-RBD-based mucosal vaccine provides broad protection against SARS-CoV-2 variants of concern. *Cell Mol Immunol* 2022, 19, 1279–1289, <https://doi.org/10.1038/s41423-022-00929-3>.
- [57]: Mishra, T.; Sreepadmanabh, M.; Ramdas, P.; Sahu, A.K.; Kumar, A.; Chande A. SARS CoV-2 Nucleoprotein Enhances the Infectivity of Lentiviral Spike Particles. *Front Cell Infect Microbiol* 2021, 11, 663688, <https://doi.org/10.3389/fcimb.2021.663688>.
- [58]: Ozono, S.; Zhang, Y.; Ode, H.; Sano, K.; Tan, T.S.; Imai, K.; Miyoshi, K.; Kishigami, S.; Ueno, T.; Iwatani, Y.; Suzuki, T.; Tokunaga, K. SARS-CoV-2 D614G spike mutation increases entry efficiency with enhanced ACE2-binding affinity. *Nat Commun* 2021, 12, 848, <https://doi.org/10.1038/s41467-021-21118-2>.
- [59]: Meng, B.; Abdullahi, A.; Ferreira, I.A.T.M.; Goonawardane, N.; Saito, A.; Kimura, I.; Yamasoba, D.; Gerber, P.P.; Fatihi, S.; Rathore, S.; Zepeda, S.K.; Papa, G.; Kemp, S.A.; Ikeda, T.; Toyoda, M.; Tan, T.S.; Kuramochi, J.; Mitsunaga, S.; Ueno, T.; Shirakawa, K.; Takaori-Kondo, A.; Brevini, T.; Mallery, D.L.; Charles, O.J.; CITIID-NIHR

BioResource COVID-19 Collaboration; Genotype to Phenotype Japan (G2P-Japan) Consortium; Ecuador-COVID19 Consortium; Bowen, J.E.; Joshi, A.; Walls, A.C.; Jackson, L.; Martin, D.; Smith, K.G.C.; Bradley, J.; Briggs, J.A.G.; Choi, J.; Madissoon, E.; Meyer, K.B.; Mlcochova, P.; Ceron-Gutierrez, L.; Doffinger, R.; Teichmann, S.A.; Fisher, A.J.; Pizzuto, M.S.; de Marco, A.; Corti, D.; Hosmillo, M.; Lee, J.H.; James, L.C.; Thukral, L.; Veessler, D.; Sigal, A.; Sampaziotis, F.; Goodfellow, I.G.; Matheson, N.J.; Sato, K.; Gupta, R.K. Altered TMPRSS2 usage by SARS-CoV-2 Omicron impacts infectivity and fusogenicity. *Nature* 2022, 603, 706-714, <https://doi.org/10.1038/s41586-022-04474-x>.

[60]: Crawford, K.H.D.; Eguia, R.; Dingens, A.S.; Loes, A.N.; Malone, K.D.; Wolf, C.R.; Chu, H.Y.; Tortorici, M.A.; Veessler, D.; Murphy, M.; Pettie, D.; King, N.P.; Balazs, A.B.; Bloom, J.D. Protocol and Reagents for Pseudotyping Lentiviral Particles with SARS-CoV-2 Spike Protein for Neutralization Assays. *Viruses* 2020, 12, 513, <https://doi.org/10.3390/v12050513>.

[61]: Casalino, L.; Gaieb, Z.; Goldsmith, J.A.; Hjorth, C.K.; Dommer, A.C.; Harbison, A.M.; Fogarty, C.A.; Barros, E.P.; Taylor, B.C.; McClellan, J.S.; Fadda, E.; Amaro, R.E. Beyond Shielding: The Roles of Glycans in the SARS-CoV-2 Spike Protein. *ACS Cent Sci* 2020, 6, 1722–1734, <https://doi.org/10.1021/acscentsci.0c01056>.

[62]: Li, Q.; Wu, J.; Nie, J.; Zhang, L.; Hao, H.; Liu, S.; Zhao, C.; Zhang, Q.; Liu, H.; Nie, L.; Qin, H.; Wang, M.; Lu, Q.; Li, X.; Sun, Q.; Liu, J.; Zhang, L.; Li, X.; Huang, W.; Wang, Y. The Impact of Mutations in SARS-CoV-2 Spike on Viral Infectivity and Antigenicity. *Cell* 2020, 182, 1284-1294.e9, <https://doi.org/10.1016/j.cell.2020.07.012>.

[63]: Huang, H.Y.; Liao, H.Y.; Chen, X.; Wang, S.W.; Cheng, C.W.; Shahed-Al-Mahmud, M.; Liu, Y.M.; Mohapatra, A.; Chen, T.H.; Lo, J.M.; Wu, Y.M.; Ma, H.H.; Chang, Y.H.; Tsai, H.Y.; Chou, Y.C.; Hsueh, Y.P.; Tsai, C.Y.; Huang, P.Y.; Chang, S.Y.; Chao, T.L.; Kao, H.C.; Tsai, Y.M.; Chen, Y.H.; Wu, C.Y.; Jan, J.T.; Cheng, T.R.; Lin, K.I.; Ma, C.; Wong, C.H. Vaccination with SARS-CoV-2 spike protein lacking glycan shields elicits enhanced protective responses in animal models. *Sci Transl Med* 2022, 14, eabm0899, <https://doi.org/10.1126/scitranslmed.abm0899>.

[64]: Amraei, R.; Yin, W.; Napoleon, M.A.; Suder, E.L.; Berrigan, J.; Zhao, Q.; Olejnik, J.; Chandler, K.B.; Xia, C.; Feldman, J.; Hauser, B.M.; Caradonna, T.M.; Schmidt, A.G.; Gummuluru, S.; Mühlberger, E.; Chitalia, V.; Costello, C.E.; Rahimi, N. CD209L/L-SIGN and CD209/DC-SIGN Act as Receptors for SARS-CoV-2. *ACS Cent Sci* 2021, 7, 1156-1165, <https://doi.org/10.1021/acscentsci.0c01537>.

[65]: Jumper, J.; Evans, R.; Pritzel, A.; Green, T.; Figurnov, M.; Ronneberger, O.; Tunyasuvunakool, K.; Bates, R.; Židek, A.; Potapenko, A.; Bridgland, A.; Meyer, C.; Kohl, S.A.A.; Ballard, A.J.; Cowie, A.; Romera-Paredes, B.; Nikolov, S.; Jain, R.; Adler, J.; Back, T.; Petersen, S.; Reiman, D.; Clancy, E.; Zielinski, M.; Steinegger, M.; Pacholska, M.; Berghammer, T.; Bodenstein, S.; Silver, D.; Vinyals, O.; Senior, A.W.; Kavukcuoglu, K.; Kohli, P.; Hassabis, D. Highly accurate protein structure prediction with AlphaFold. *Nature* 2021, 596, 583-589, <https://doi.org/10.1038/s41586-021-03819-2>.

[66]: Mirdita, M.; Schütze, K.; Moriwaki, Y.; Heo, L.; Ovchinnikov, S.; Steinegger, M. ColabFold: making protein folding accessible to all. *Nat Methods* 2022, 19, 679-682, <https://doi.org/10.1038/s41592-022-01488-1>.

- [67]: Tabarani, G.; Thépaut, M.; Stroebel, D.; Ebel, C.; Vivès, C.; Vachette, P.; Durand, D.; Fieschi, F. DC-SIGN neck domain is a pH-sensor controlling oligomerization: SAXS and hydrodynamic studies of extracellular domain. *J Biol Chem* 2009, 284, 21229-21240, <https://doi.org/10.1074/jbc.M109.021204>.
- [68]: Gao, M.; Li, H.; Ye, C.; Chen, K.; Jiang, H.; Yu, K. Glycan Epitopes and Potential Glycoside Antagonists of DC-SIGN Involved in COVID-19: In Silico Study. *Biomolecules* 2021, 11, 1586, <https://doi.org/10.3390/biom11111586>.
- [69]: Tada, T.; Zhou, H.; Dcosta, B.M.; Samanovic, M.I.; Chivukula, V.; Herati, R.S.; Hubbard, S.R.; Mulligan, M.J.; Landau, N.R. Increased resistance of SARS-CoV-2 Omicron variant to neutralization by vaccine-elicited and therapeutic antibodies. *EBioMedicine* 2022, 78, 103944, <https://doi.org/10.1016/j.ebiom.2022.103944>.
- [70]: Chen, R.E.; Zhang, X.; Case, J.B.; Winkler, E.S.; Liu, Y.; VanBlargan, L.A.; Liu, J.; Errico, J.M.; Xie, X.; Suryadevara, N.; Gilchuk, P.; Zost, S.J.; Tahan, S.; Droit, L.; Turner, J.S.; Kim, W.; Schmitz, A.J.; Thapa, M.; Wang, D.; Boon, A.C.M.; Presti, R.M.; O'Halloran, J.A.; Kim, A.H.J.; Deepak, P.; Pinto, D.; Fremont, D.H.; Crowe Jr., J.E.; Corti, D.; Virgin, H.W.; Ellebedy, A.H.; Shi, P.Y.; Diamond, M.S. Resistance of SARS-CoV-2 variants to neutralization by monoclonal and serum-derived polyclonal antibodies. *Nat Med* 2021, 27, 717-726, <https://doi.org/10.1038/s41591-021-01294-w>.
- [71]: Jackson, C.B.; Farzan, M.; Chen, B.; Choe, H. Mechanisms of SARS-CoV-2 entry into cells. *Nat Rev Mol Cell Biol* 2022, 23, 3–20, <https://doi.org/10.1038/s41580-021-00418-x>.
- [72]: Khare, S.; Gurry, C.; Freitas, L.; Schultz, M.B.; Bach, G.; Diallo, A.; Akite, N.; Ho, J.; Lee, R.T.C.; Yeo, W.; GISAID Core Curation Team; Maurer-Stroh, S. GISAID's Role in Pandemic Response. *China CDC Weekly* 2021, 3, 1049-1051, <https://doi.org/10.46234/ccdcw2021.255>.
- [73]: Suzuki, R.; Yamasoba, D.; Kimura, I.; Wang, L.; Kishimoto, M.; Ito, J.; Morioka, Y.; Nao, N.; Nasser, H.; Uriu, K.; Kosugi, Y.; Tsuda, M.; Orba, Y.; Sasaki, M.; Shimizu, R.; Kawabata, R.; Yoshimatsu, K.; Asakura, H.; Nagashima, M.; Sadamasu, K.; Yoshimura, K.; The Genotype to Phenotype Japan (G2P-Japan) Consortium; Sawa, H.; Ikeda, T.; Irie, T.; Matsuno, K.; Tanaka, S.; Fukuhara, T.; S, Kei. Attenuated fusogenicity and pathogenicity of SARS-CoV-2 Omicron variant. *Nature* 2022, 603, 700–705, <https://doi.org/10.1038/s41586-022-04462-1>.
- [74]: VanBlargan, L.A.; Errico, J.M.; Halfmann, P.J.; Zost, S.J.; Crowe Jr, J.E.; Purcell, L.A.; Kawaoka, Y.; Corti, D.; Fremont, D.H.; Diamond, M.S. An infectious SARS-CoV-2 B.1.1.529 Omicron virus escapes neutralization by therapeutic monoclonal antibodies. *Nat Med* 2022, 28, 490–495, <https://doi.org/10.1038/s41591-021-01678-y>.
- [75]: Hui K.P.Y.; Ng, K-C.; Ho, J.C.W.; Yeung, H-Y.; Ching, R.H.H.; Gu, H.; Chung, J.C.K.; Chow, V.L.Y.; Sit, K-Y.; Hsin, M.K.Y.; Au, T.W.K.; Poon, L.L.M.; Peiris, M.; Nicholls, J.M.; Chan, M.C.W. Replication of SARS-CoV-2 Omicron BA.2 variant in ex vivo cultures of the human upper and lower respiratory tract. *eBioMedicine* 2022, 83, 104232, <https://doi.org/10.1016/j.ebiom.2022.104232>.
- [76]: Korber, B.; Fischer, W.M.; Gnanakaran, S.; Yoon, H.; Theiler, J.; Abfalterer, W.; Hengartner, N.; Giorgi, E.E.; Bhattacharya, T.; Foley, B.; Hastie, K.M.; Parker, M.D.;

Partridge, D.G.; Evans, C.M.; Freeman, T.M.; de Silva, T.I.; Sheffield COVID-19 Genomics Group; McDanal, C.; Perez, L.G.; Tang, H.; Moon-Walker, A.; Whelan, S.P.; LaBranche, C.C.; Saphire, E.O.; Montefiori, D.C. Tracking Changes in SARS-CoV-2 Spike: Evidence that D614G Increases Infectivity of the COVID-19 Virus. *Cell* 2020, 182, 812-827.e19, <https://doi.org/10.1016/j.cell.2020.06.043>.

[77]: Willett, B.J.; Grove, J.; MacLean, O.A.; Wilkie, C.; De Lorenzo, G.; Furnon, W.; Cantoni, D.; Scott, S.; Logan, N.; Ashraf, S.; Manali, M.; Szemiel, A.; Cowton, V.; Vink, E.; Harvey, W.T.; Davis, C.; Asamaphan, P.; Smollett, K.; Tong, L.; Orton, R.; Hughes, J.; Holland, P.; Silva, V.; Pascall, D.J.; Puxty, K.; da Silva Filipe, A.; Yebra, G.; Shaaban, S.; Holden, M.T.G.; Pinto, R.M.; Gunson, R.; Templeton, K.; Murcia, P.R.; Patel, A.H.; Klenerman, P.; Dunachie, S.; PITCH Consortium; COVID-19 Genomics UK (COG-UK) Consortium; Haughney, J.; Robertson, D.L.; Palmarini, M.; Ray, S.; Thomson, E.C. SARS-CoV-2 Omicron is an immune escape variant with an altered cell entry pathway. *Nat Microbiol* 2022, 7, 1161-1179, <https://doi.org/10.1038/s41564-022-01143-7>.

[78]: Gobeil, S.M.; Henderson, R.; Stalls, V.; Janowska, K.; Huang, X.; May, A.; Speakman, M.; Beaudoin, E.; Manne, K.; Li, D.; Parks, R.; Barr, M.; Deyton, M.; Martin, M.; Mansouri, K.; Edwards, R.J.; Sempowski, G.D.; Saunders, K.O.; Wiehe, K.; Williams, W.; Korber, B.; Haynes, B.F.; Acharya, P. Structural diversity of the SARS-CoV-2 Omicron spike. *Mol Cell* 2022, 82, 2050-2068.e6, <https://doi.org/10.1101/2022.01.25.477784>.

[79]: Tian, D.; Sun, Y.; Xu, H.; Ye, Q. The emergence and epidemic characteristics of the highly mutated SARS-CoV-2 Omicron variant. *J Med Virol* 2022, 94, 2376-2383, <https://doi.org/10.1002/jmv.27643>.

[80]: Yang, K.; Wang, C.; Kreuzberger, A.J.B.; White, K.I.; Pfuetzner, R.A.; Esquivies, L.; Kirchhausen, T.; Brunger, A.T. Structure-based design of a SARS-CoV-2 Omicron-specific inhibitor. *PNAS* 2023, 120, e2300360120, <https://doi.org/10.1073/pnas.2300360120>.

[81]: Berkowitz, R.L.; Ostrov, D.A. The Elusive Coreceptors for the SARS-CoV-2 Spike Protein. *Viruses* 2022, 15, 67, <https://doi.org/10.3390/v15010067>.

[82]: Kuhaudomlarp, S.; Imberty, A. Involvement of sialoglycans in SARS-COV-2 infection: Opportunities and challenges for glyco-based inhibitors. *IUBMB Life* 2022, 74, 1253-1263, <https://doi.org/10.1002/iub.2692>.

[83]: Porter, A.F.; Purcell, D.F.J.; Howden, B.P.; Duchene, S. Evolutionary rate of SARS-CoV-2 increases during zoonotic infection of farmed mink. *Virus Evol* 2023, 9, vead002, <https://doi.org/10.1093/ve/vead002>.

[84]: Gallo, O.; Locatello, L.G.; Mazzoni, A.; Novelli, L.; Annunziato, F. The central role of the nasal microenvironment in the transmission, modulation, and clinical progression of SARS-CoV-2 infection. *Mucosal Immunol* 2021, 14, 305-316, <https://doi.org/10.1038/s41385-020-00359-2>.

[85]: Wu, C.T.; Lidsky, P.V.; Xiao, Y.; Cheng, R.; Lee, I.T.; Nakayama, T.; Jiang, S.; He, W.; Demeter, J.; Knight, M.G.; Turn, R.E.; Rojas-Hernandez, L.S.; Ye, C.; Chiem, K.; Shon, J.; Martinez-Sobrido, L.; Bertozzi, C.R.; Nolan, G.P.; Nayak, J.V.; Milla, C.; Andino, R.; Jackson, P.K. SARS-CoV-2 replication in airway epithelia requires motile

cilia and microvillar reprogramming. *Cell* 2023, 186, 112-130.e20, <https://doi.org/10.1016/j.cell.2022.11.030>.

[86]: Sungnak, W.; Huang, N.; Bécavin, C.; Berg, M.; Queen, R.; Litvinukova, M.; Talavera-López, C.; Maatz, H.; Reichart, D.; Sampaziotis, F.; Worlock, K.B.; Yoshida, M.; Barnes, J.L.; HCA Lung Biological Network. SARS-CoV-2 entry factors are highly expressed in nasal epithelial cells together with innate immune genes. *Nat Med* 2020, 26, 681–687, <https://doi.org/10.1038/s41591-020-0868-6>.

[87]: Hou, Y.J.; Okuda, K.; Edwards, C.E.; Martinez, D.R.; Asakura, T.; Dinnon, K.H. 3rd; Kato, T.; Lee, R.E.; Yount, B.L.; Mascenik, T.M.; Chen, G.; Olivier, K.N.; Ghio, A.; Tse, L.V.; Leist, S.R.; Gralinski, L.E.; Schäfer, A.; Dang, H.; Gilmore, R.; Nakano, S.; Sun, L.; Fulcher, M.L.; Livraghi-Butrico, A.; Nicely, N.I.; Cameron, M.; Cameron, C.; Kelvin, D.J.; de Silva, A.; Margolis, D.M.; Markmann, A.; Bartelt, L.; Zumwalt, R.; Martinez, F.J.; Salvatore, S.P.; Borczuk, A.; Tata, P.R.; Sontake, V.; Kimple, A.; Jaspers, I.; O’Neal, W.K.; Randell, S.H.; Boucher, R.C.; Baric, R.S. SARS-CoV-2 Reverse Genetics Reveals a Variable Infection Gradient in the Respiratory Tract. *Cell* 2020, 182, 429-446.e14, <https://doi.org/10.1016/j.cell.2020.05.042>.

[88]: Mason, R.J. Thoughts on the alveolar phase of COVID-19. *Am J Physiol* 2020, 319, L115-L120, <https://doi.org/10.1152/ajplung.00126.2020>.

[89]: Calkovska, A.; Kolomaznik, M.; Calkovsky, V. Alveolar type II cells and pulmonary surfactant in COVID-19 era. *Physiol Res* 2021, 70, S195-S208, <https://doi.org/10.33549/physiolres.934763>.

[90]: Singh, A.; Zaheer, S.; Kumar, N.; Singla, T.; Ranga, S. Covid19, beyond just the lungs: A review of multisystemic involvement by Covid19. *Pathol Res Pract* 2021, 224, 153384, <https://doi.org/10.1016/j.prp.2021.153384>.

[91]: Francistiová, L.; Klepe, A.; Curley, G.; Gulya, K.; Dinnyés, A.; Filkor, K. Cellular and Molecular Effects of SARS-CoV-2 Linking Lung Infection to the Brain. *Front Immunol* 2021, 12, 730088, <https://doi.org/10.3389/fimmu.2021.730088>.

[92]: Polidoro, R.B.; Hagan, R.S.; de Santis Santiago, R.; Schmidt, N.W. Overview: Systemic Inflammatory Response Derived From Lung Injury Caused by SARS-CoV-2 Infection Explains Severe Outcomes in COVID-19. *Front Immunol* 2020, 11, 1626, <https://doi.org/10.3389/fimmu.2020.01626>.

[93]: Lukassen, S.; Chua, R.L.; Trefzer, T.; Kahn, N.C.; Schneider, M.A.; Muley, T.; Winter, H.; Meister, M.; Veith, C.; Boots, A.W.; Hennig, B.P.; Kreuter, M.; Conrad, C.; Eils, R. SARS-CoV-2 receptor ACE2 and TMPRSS2 are primarily expressed in bronchial transient secretory cells. *EMBO J* 2020, 39, e105114, <https://doi.org/10.15252/embj.20105114>.

[94]: Zhang, Y.; Geng, X.; Tan, Y.; Li, Q.; Xu, C.; Xu, J.; Hao, L.; Zeng, Z.; Luo, X.; Liu, F.; Wang, H. New understanding of the damage of SARS-CoV-2 infection outside the respiratory system. *Biomed Pharmacother* 2020, 127, 110195, <https://doi.org/10.1016/j.biopha.2020.110195>.

[95]: Oprinca, G.C.; Muja, L.A. Postmortem examination of three SARS-CoV-2-positive autopsies including histopathologic and immunohistochemical analysis. *Int J Legal Med* 2021, 135, 329–339, <https://doi.org/10.1007/s00414-020-02406-w>.

- [96]: Ruaro, B.; Salton, F.; Braga, L.; Wade, B.; Confalonieri, P.; Volpe, M.C.; Baratella, E.; Maiocchi, S.; Confalonieri, M. The history and mystery of alveolar epithelial type II cells: Focus on their physiologic and pathologic role in lung. *Int J Mol Sci* 2021, 22, 2566, <https://doi.org/10.3390/ijms22052566>.
- [97]: Sajuthi, S.P.; DeFord, P.; Li, Y.; Jackson, N.D.; Montgomery, M.T.; Everman, J.L.; Rios, C.L.; Pruesse, E.; Nolin, J.D.; Plender, E.G.; Wechsler, M.E.; Mak, A.C.Y.; Eng, C.; Salazar, S.; Medina, V.; Wohlford, E.M.; Huntsman, S.; Nickerson, D.A.; Germer, S.; Zody, M.C.; Abecasis, G.; Kang, H.M.; Rice, K.M.; Kumar, R.; Oh, S.; Rodriguez-Santana, J.; Burchard, E.G.; Seibold, M.A. Type 2 and interferon inflammation regulate SARS-CoV-2 entry factor expression in the airway epithelium. *Nat Commun* 2020, 11, 5139, <https://doi.org/10.1038/s41467-020-18781-2>.
- [98]: SARS-CoV-2 Variants Overview. Available online: <https://www.ncbi.nlm.nih.gov/activ> (accessed 15 July 2023).
- [99]: Shajahan, A.; Pepi, L.E.; Rouhani, D.S.; Heiss, C.; Azadi, P. Glycosylation of SARS-CoV-2: structural and functional insights. *Anal Bioanal Chem* 2021, 413, 7179-7193, <https://doi.org/10.1007/s00216-021-03499-x>.
- [100]: Dutta, D.; Mandal, C.; Mandal, C. Unusual glycosylation of proteins: Beyond the universal sequon and other amino acids. *Biochimica et Biophysica Acta* 2017, 1861, 3096-3108, <https://doi.org/10.1016/j.bbagen.2017.08.025>.
- [101]: Shajahan, A.; Pepi, L.; Kumar, B.; Murray, N.; Azadi, P. Site Specific N- and O-glycosylation mapping of the Spike Proteins of SARS-CoV-2 Variants of Concern. *Sci Rep* 2022, 13, 10053, <https://doi.org/10.21203/rs.3.rs-2188138/v1>.
- [102]: Soh, W.T.; Liu, Y.; Nakayama, E.E.; Ono, C.; Torii, S.; Nakagami, H.; Matsuura, Y.; Shioda, T.; Arase, H. The N-terminal domain of spike glycoprotein mediates SARS-CoV-2 infection by associating with L-SIGN and DC-SIGN. *bioRxiv* 2020, <https://doi.org/10.1101/2020.11.05.369264>.
- [103]: Zhang, J.; Cai, Y.; Lavine, C.L.; Peng, H.; Zhu, H.; Anand, K.; Tong, P.; Gautam, A.; Mayer, M.L.; Rits-Volloch, S.; Wang, S.; Sliz, P.; Wesemann, D.R.; Yang, W.; Seaman, M.S.; Lu, J.; Xiao, T.; Chen, B. Structural and functional impact by SARS-CoV-2 Omicron spike mutations. *Cell Rep* 2022, 39, 110729, <https://doi.org/10.1016/j.celrep.2022.110729>.
- [104]: Kwong, P.D.; Mascola, J.R.; Nabel, G.J. Broadly neutralizing antibodies and the search for an HIV-1 vaccine: the end of the beginning. *Nat Rev Immunol* 2013, 13, 693-701. doi: 10.1038/nri3516
- [105]: Doores, K.J. The HIV glycan shield as a target for broadly neutralizing antibodies. *FASEB J* 2015, 29, 4679-4691, <https://doi.org/10.1111/febs.13530>.
- [106]: Fischer, K.; Nguyen, K.; LiWang, P.J. Griffithsin Retains Anti-HIV-1 Potency with Changes in gp120 Glycosylation and Complements Broadly Neutralizing Antibodies PGT121 and PGT126. *Antimicrob Agents Chemother* 2019, 64, e01084-19, <https://doi.org/10.1128/AAC.01084-19>.
- [107]: Cai, Y.; Xu, W.; Tang, J.; Cao, N.; Lan, Q.; Lu, L.; Jiang, S. A bivalent protein targeting glycans and HR1 domain in spike protein potently inhibited infection of SARS-



CoV-2 and other human coronaviruses. *Cell Biosci* 2021, 11, 128, <https://doi.org/10.1186/s13578-021-00638-w>.

[108]: Nangarlia, A.; Hassen, F.F.; Canziani, G.; Bandi, P.; Talukder, C.; Zhang, F.; Krauth, D.; Gary, E.N.; Weiner, D.B.; Bieniasz, P.; Navas-Martin, S.; O'Keefe, B.R.; Ang, C.G.; Chaiken, I. Irreversible Inactivation of SARS-CoV-2 by Lectin Engagement with Two Glycan Clusters on the Spike Protein. *Biochemistry* 2023, 62, 2115–2127, <https://doi.org/10.1021/acs.biochem.3c00109>.

[109]: Guo, L.; Lin, S.; Chen, Z.; Cao, Y.; He, B.; Lu, G. Targetable elements in SARS-CoV-2 S2 subunit for the design of pan-coronavirus fusion inhibitors and vaccines. *Signal Transduct Target Ther* 2023, 8, 197, <https://doi.org/10.1038/s41392-023-01472-x>.

[110]: Alsaidi, S.; Cornejal, N.; Mahoney, O.; Melo, C.; Verma, N.; Bonnaire, T.; Chang, T.; O'Keefe, B.R.; Sailer, J.; Zydowsky, T.M.; Teleshova, N.; Romero, J.A.F. Griffithsin and Carrageenan Combination Results in Antiviral Synergy against SARS-CoV-1 and 2 in a Pseudoviral Model. *Mar Drugs* 2021, 19, 418, <https://doi.org/10.3390/md19080418>.

[111]: Abavisani, M.; Rahimian, K.; Mahdavi, B.; Tokhanbigli, S.; Siasakht, M.M.; Farhadi, A.; Kodori, M.; Mahmanzar, M.; Meshkat, Z. Mutations in SARS-CoV-2 structural proteins: a global analysis. *Virol J* 2022, 19, 220, <https://doi.org/10.1186/s12985-022-01951-7>.

[112]: Mayi, B.S.; Leibowitz, J.A.; Woods, A.T.; Ammon, K.A.; Liu, A.E.; Raja, A. The role of Neuropilin-1 in COVID-19. *PLoS Pathog* 2021, 17, e1009153, <https://doi.org/10.1371/journal.ppat.1009153>.

[113]: Cantuti-Castelvetri, L.; Ojha, R.; Pedro, L.D.; Djannatian, M.; Franz, J.; Kuivanen, S.; van der Meer, F.; Kallio, K.; Kaya, T.; Anastasina, M.; Smura, T.; Levantov, L.; Szirovicza, L.; Tobi, A.; Kallio-Kokko, H.; Österlund, P.; Joensuu, M.; Meunier, F.A.; Butcher, S.J.; Winkler, M.S.; Mollenhauer, B.; Helenius, A.; Gokce, O.; Teesalu, T.; Hepojoki, J.; Vapalahti, O.; Stadelmann, C.; Balistreri, G.; Simons, M. Neuropilin-1 facilitates SARS-CoV-2 cell entry and infectivity. *Science* 2020, 370, 856-860, <https://doi.org/doi:10.1126/science.abd2985>.

[114]: Vu, M.N.; Morris, D.R.; Alvarado, R.E.; Lokugamage, K.G.; Zhou, Y.; Estes, L.K.; McLeland, A.M.; Schindewolf, C.; Plante, J.A.; Ahearn, Y.P.; Morgan, A.L.; Meyers, W.M.; Murray, J.T.; Weaver, S.C.; Walker, D.H.; Russell, W.K.; Routh, A.L.; Plante, K.S.; Menachery, V. Loss-of-function mutation in Omicron variants reduces spike protein expression and attenuates SARS-CoV-2 infection. *bioRxiv* 2023, <https://doi.org/10.1101/2023.04.17.536926>.

[115]: Shrestha, L.B.; Foster, C.; Rawlinson, W.; Tedla, N.; Bull, R.A. Evolution of the SARS-CoV-2 omicron variants BA.1 to BA.5: Implications for immune escape and transmission. *Rev Med Virol* 2022, 32, e2381, <https://doi.org/10.1002/rmv.2381>.

[116]: Barthe, M.; Hertereau, L.; Lamghari, N.; Osman-Ponchet, H.; Braud, V.M. Receptors and Cofactors That Contribute to SARS-CoV-2 Entry: Can Skin Be an Alternative Route of Entry? *Int J Mol Sci* 2023, 24, 6253, <https://doi.org/10.3390/ijms24076253>.

- [117]: Fan, Y.; Li, X.; Zhang, L.; Wan, S.; Zhou, F. SARS-CoV-2 Omicron variant: recent progress and future perspectives. *Sig Transduct Target Ther* 2022, 7, 141, <https://doi.org/10.1038/s41392-022-00997-x>.
- [118]: Wang, D.; Baudys, J.; Bundy, J.L.; Solano, M.; Keppel, T.; Barr, J.R. Comprehensive Analysis of the Glycan Complement of SARS-CoV-2 Spike Proteins Using Signature Ions-Triggered Electron-Transfer/Higher-Energy Collisional Dissociation (ETHcD) Mass Spectrometry. *Anal Chem* 2020, 92, 14730-14739, <https://doi.org/10.1021/acs.analchem.0c03301>.
- [119]: Zhang, S.; Go, E.P.; Ding, H.; Anang, S.; Kappes, J.C.; Desaire, H.; Sodroski, J.G. Analysis of Glycosylation and Disulfide Bonding of Wild-Type SARS-CoV-2 Spike Glycoprotein. *J Virol* 2022, 96, e0162621, <https://doi.org/10.1128/JVI.01626-21>.
- [120]: Yao, H.; Song, Y.; Chen, Y.; Wu, N.; Xu, J.; Sun, C.; Zhang, J.; Weng, T.; Zhang, Z.; Wu, Z.; Cheng, L.; Shi, D.; Lu, X.; Lei, J.; Crispin, M.; Shi, Y.; Li, L.; Li, S. Molecular Architecture of the SARS-CoV-2 Virus. *Cell* 2020, 183, 730-738.e13, <https://doi.org/10.1016/j.cell.2020.09.018>.
- [121]: Brun, J.; Vasiljevic, S.; Gangadharan, B.; Hensen, M.; Chandran, A.V.; Hill, M.L.; Kiappes, J.L.; Dwek, R.A.; Alonzi, D.S.; Struwe, W.B.; Zitzmann, N. Assessing Antigen Structural Integrity through Glycosylation Analysis of the SARS-CoV-2 Viral Spike. *ACS Cent Sci* 2021, 7, 586-593, <https://doi.org/10.1021/acscentsci.1c00058>.
- [122]: Newby, M.L.; Fogarty, C.A.; Allen, J.D.; Butler, J.; Fadda, E.; Crispin, M. Variations within the Glycan Shield of SARS-CoV-2 Impact Viral Spike Dynamics. *J Mol Biol* 2023, 435, 167928, <https://doi.org/10.1016/j.jmb.2022.167928>.
- [123]: Kuo, C.W.; Yang, T.J.; Chien, Y.C.; Yu, P.Y.; Hsu, S.D.; Khoo, K.H. Distinct shifts in site-specific glycosylation pattern of SARS-CoV-2 spike proteins associated with arising mutations in the D614G and Alpha variants. *Glycobiology* 2022, 32, 60-72, <https://doi.org/10.1093/glycob/cwab102>.
- [124]: Shajahan, A.; Pepi, L.; Kumar, B.; Murray, N.; Azadi, P. Site Specific N- and O-glycosylation mapping of the Spike Proteins of SARS-CoV-2 Variants of Concern. *Sci Rep* 2023, 13, 10053, <https://doi.org/10.1038/s41598-023-33088-0>.
- [125]: Zhang, Y.; Zhao, W.; Mao, Y.; Chen, Y.; Wang, S.; Zhong, Y.; Su, T.; Gong, M.; Du, D.; Lu, X.; Cheng, J.; Yang, H. Site-specific N-glycosylation Characterization of Recombinant SARS-CoV-2 Spike Proteins. *Mol Cell Proteomics* 2021, 13, 10058, <https://doi.org/10.1074/mcp.RA120.002295>.
- [126]: Tian, Y.; Parsons, L.M.; Jankowska, E.; Cipollo, J.F. Site-Specific Glycosylation Patterns of the SARS-CoV-2 Spike Protein Derived From Recombinant Protein and Viral WA1 and D614G Strains. *Front Chem* 2021, 9, 767448, <https://doi.org/10.3389/fchem.2021.767448>.
- [127]: Allen, J.D.; Chawla, H.; Samsudin, F.; Zuzic, L.; Shivgan, A.T.; Watanabe, Y.; He, W.T.; Callaghan, S.; Song, G.; Yong, P.; Brouwer, P.J.M.; Song, Y.; Cai, Y.; Duyvesteyn, H.M.E.; Malinauskas, T.; Kint, J.; Pino, P.; Wurm, M.J.; Frank, M.; Chen, B.; Stuart, D.I.; Sanders, R.W.; Andrabi, R.; Burton, D.R.; Li, S.; Bond, P.J.; Crispin, M. Site-Specific Steric Control of SARS-CoV-2 Spike Glycosylation. *Biochemistry* 2021, 60, 2153-2169, <https://doi.org/10.1021/acs.biochem.1c00279>.

- [128]: Geretti E, Klagsbrun M. Neuropilins: novel targets for anti-angiogenesis therapies. *Cell Adh Migr.* 2007 Apr-Jun;1(2):56-61. doi: 10.4161/cam.1.2.4490. Epub 2007 Apr 25. PMID: 19329879; PMCID: PMC2633972.
- [129]: Dhupar R, Jones KE, Powers AA, Eisenberg SH, Ding K, Chen F, Nasarre C, Cen Z, Gong YN, LaRue AC, Yeh ES, Luketich JD, Lee AV, Oesterreich S, Lotze MT, Gemmill RM, Soloff AC. Isoforms of Neuropilin-2 Denote Unique Tumor-Associated Macrophages in Breast Cancer. *Front Immunol.* 2022 Apr 27;13:830169. Doi: 10.3389/fimmu.2022.830169. PMID: 35651620; PMCID: PMC9149656.
- [130]: Teesalu T, Sugahara KN, Kotamraju VR, Ruoslahti E. C-end rule peptides mediate neuropilin-1-dependent cell, vascular, and tissue penetration. *PNAS.* 2009 Sep 22; 106(38): 16157-16162. <https://doi.org/10.1073/pnas.0908201106>
- [131]: Ray U, Pathoulas CL, Thirusangu P, Purcell JW, Kannan N, Shridhar V. Exploiting LRRC15 as a Novel Therapeutic Target in Cancer. *Cancer Research.* 2022 May 03; 82(9): 1675–1681. <https://doi.org/10.1158/0008-5472.CAN-21-3734>
- [132]: Loo L, Waller MA, Moreno CL, Cole AJ, Stella AO, Pop OT, Jochum AK, Ali OH, Denes CE, Hamoudi Z, Chung F, Aggarwal A, Low JKK, Patel K, Siddiquee R, Kang T, Mathivanan S, Mackay JP, Jochum W, Flatz L, Hesselton D, Turville S, Neely GG. Fibroblast-expressed LRRC15 is a receptor for SARS-CoV-2 spike and controls antiviral and antifibrotic transcriptional programs. *PLoS Biol.* 2023 Feb 9;21(2):e3001967. doi: 10.1371/journal.pbio.3001967. PMID: 36757924; PMCID: PMC9910744.
- [133]: Gene: *Lrrc15* (leucine rich repeat containing 15) *Mus musculus*. Rat Genome Database. <https://rgd.mcw.edu/rgdweb/report/gene/main.html?id=733251>

## Chapter 3

### The Antiviral Activity of Lectin Griffithsin Against SARS-CoV-2 Appears to be Enhanced By Interactions With Structural Proteins

This work is under preparation for submission to *Viruses* with slight modifications.

#### 3.1 Abstract

While SARS-CoV-2 vaccines have curtailed the fatalities associated with Covid-19, the newer strains of SARS-CoV-2 are mutating to evade immune detection and breakthrough vaccine-induced immunity. Although these new strains of SARS-CoV-2 virus cause milder symptoms, at-risk persons are still not guaranteed to recover from infection. Furthermore, the history of the pandemic showed us that novel Covid-19 strains that exhibit higher mortality and pathogenicity can arise quickly: the Delta strain was initially detected during a time where Covid-19 infection rates were declining. Thus, there is still pressing need to develop a potent, broad-acting antiviral agent to prevent infection of newer SARS-CoV-2 breakthrough strains.

The Red algae-derived protein Griffithsin is a potent, dimeric, broad-acting inhibitor of various viruses ranging from HIV, HPV, SARS-CoV-1, and more. Griffithsin is stable, relatively easy to produce in large quantities, and well-tolerated by the human body, making it an attractive starting point for a robust anti-Covid-19 prophylactic agent. At the current time, several papers have found that Griffithsin is a moderate inhibitor of SARS-CoV-2 hACE2-mediated infection, displaying IC<sub>50</sub> values ranging from the tens of nM to almost 10  $\mu$ M. We noticed that Griffithsin seemed to display better inhibition capabilities against genuine SARS-CoV-2 coronavirus particles as opposed to SARS-CoV-2 pseudotyped lentivirions. Thus, we wanted to explore what traits of the SARS-CoV-2 coronavirus rendered it more susceptible to Griffithsin inhibition. To do so, we reasoned that the causative factor enhancing SARS-CoV-2 coronaviral particle susceptibility was a structural feature on the exterior of the virus. Genuine coronaviral particles only incorporate 4 proteins in their architecture: the Spike protein, and the three additional structural proteins M (Membrane), N (Nucleocapsid) and E (Envelope). We created coronaviral particles with the additional structural proteins and assessed their susceptibility to Griffithsin-mediated inhibition of SARS-CoV-2 infection.

We also took the opportunity to assess whether several other mutations of Griffithsin- namely, a version of Griffithsin that was resistant to post-translational oxidation, and another that exhibited monovalent binding as opposed to bivalent binding- were capable of retaining antiviral potency.

Finally, we also tested whether Griffithsin could inhibit SARS-CoV-2 capture and infection-in-trans as mediated by the lectin receptor DC-SIGN. This Trans-infection process is thought to be particularly important in mediating initial SARS-CoV-2 infection in the host respiratory system, as discussed in Chapter 2 of this dissertation.

Our results suggest that the SARS-CoV-2 M protein increases viral susceptibility to Griffithsin inhibition. In addition, our data showed that neither the Griffithsin variant that was resistant to post-translational oxidation nor the variant with monovalent binding exhibited much difference in inhibiting SARS-CoV-2 Direct-infection or Trans-infection.

Finally, our Trans-infectivity assays showed that the additional SARS-CoV-2 structural proteins M, N, and E did not affect the ability of DC-SIGN to mediate Trans-infectivity.

### 3.2 Introduction

The COVID-19 pandemic remains a significant challenge for society, with over 760 million cases and about 6.95 million deaths globally as of August 2023 [1]. While the development of several COVID-19 vaccines has alleviated the severity of the pandemic, COVID-19 cases still persist, with about 10,000 COVID-19 hospitalizations occurring weekly nationwide in the United States throughout the months of May to July of 2023 [1-4]. This is in part due to the ease of transmissibility of SARS-CoV-2, with the ability to be transmitted via airborne respiratory droplets and fomites [2]. But in addition to the ease of transmission of the coronaviral virion, the SARS-CoV-2 Spike protein undergoes immune escape quite readily, with studies demonstrating that the neutralizing activity of plasma samples taken from individuals who received either the Pfizer or Moderna vaccinations were significantly less effective against several mutant strains of the SARS-CoV-2, including the UK (B.1.1.7/501Y.V1), South Africa (B.1.351/501Y.V2) and Brazil (P.1) strains [2,3,5]. More concerning, the most recent Omicron XBB.1.5 strain has numerous mutations in its spike sequence that have established breakthrough infections in patients who have received multiple booster doses of COVID-19 vaccines [6, 7]. Coupled with the advent of new viral strains, vaccination also is not always 100% protective or suitable for all patients: some immunodeficient individuals appear to show a drastically reduced capability to produce antibodies against Omicron strains, even with multiple vaccinations [8, 9]. Complicating this, there is still robust global vaccine hesitancy, with reluctance growing amongst new parents and younger age groups in several countries around the world [10]. Taken together, all of this indicates it is still valuable to explore preventative treatments to curtail the spread of SARS-CoV-2. Indeed, vaccine companies like AstraZeneca and Merck are currently developing prophylactic treatments for SARS-CoV-2 such as Evusheld and LAGEVRIO/molnupiravir, respectively [11, 12].

Griffithsin is a small (~12.8 kilodalton), dimeric, Red algae-derived lectin that displays inhibitory activity against a wide variety of viruses, ranging from Human Immunodeficiency Virus (Retroviridae family), Herpes Simplex Virus (Herpesviridae family), Japanese Encephalitis Virus (Flaviviridae family), Human Papillomavirus (Papillomaviridae family), and other Coronaviridae family viruses including MERS-CoV and SARS-CoV [13, 14, 15]. Each Griffithsin monomer contains three sugar-binding sites which each have a high affinity for mannose glycans [16]. Viral glycoproteins typically are highly glycosylated, presenting ample mannose sugars that can act as binding sites for Griffithsin, thereby impeding viral entry and infectivity [13]. This protein can be synthesized economically either in plants or bacterial expression systems, has been shown to have low toxicity in mammals, can withstand temperatures up to 78 deg C, maintains inhibitory capability after several weeks of exposure to 50 deg C, can withstand at least five freeze-thaw cycles, and survives exposure to a variety of pH and concentrated acid and base solutions for at least 24 hours [17-20]. Although Wild-Type Griffithsin (WT-Grft) has been shown to undergo oxidation at residue M78 in cervicovaginal environments, mutating M78 to Glutamine yields a variant of Griffithsin called M78Q-

Griffithsin (Q-Grft), which exhibits many of the same chemical and inhibitory properties as Wild-Type Griffithsin while resolving the complications that could arise from oxidation [17, 21]. Due to Griffithsin's favorable pharmacokinetic properties, it is currently in clinical trials as a treatment for HIV and Q-Grft is also currently undergoing trials as a nasal spray for prophylaxis against SARS-CoV-2 [18, 22, 23].

Another facet of Griffithsin's use as a prophylactic agent is the theorized importance of Griffithsin's ability to cross-link target proteins together. As a bivalent sugar-binding protein, evidence from several studies strongly suggests that Griffithsin is capable of binding to epitopes from two separate HIV-1 gp120 proteins at the same time, causing aggregation of the gp120 proteins on the surface of the viral particle and possibly also aggregation of HIV-1 viruses [19, 24]. Removing the sugar-binding moieties to prevent bi-valent binding significantly impairs WT-Grft's ability to inhibit HIV pseudovirus, despite only mildly diminishing the affinity of Griffithsin for HIV-1 gp120 [24]. Other studies show Wild-Type Griffithsin causes aggregation of flagellated unicellular pathogens [25]. Dimeric Griffithsin and other dimeric lectins such as Cyanovirin-N are also shown to cause yeast cells to agglutinate, thereby lending further credence to the idea that the inhibitory capabilities of these lectins are tied to their ability to cross-link target proteins [26, 27].

From what we gathered from a search in the current literature, all other existing *in vitro* assessments of Griffithsin's activity against SARS-CoV-2 have not assessed whether retaining Griffithsin's ability to cross-link proteins is important in maintaining its potency against SARS-CoV-2 [28-31]. In this study, we first aimed to assess whether the M78Q mutation could affect Griffithsin's ability to act as an anti-SARS-CoV-2 entry inhibitor. We then endeavored to ascertain whether Griffithsin needed to have bivalent binding capability in order to retain the same ability to prevent SARS-CoV-2 entry. We attempted to work with a constitutive monomer of Griffithsin, but it has been well known that the constitutive monomeric forms of Griffithsin display severely decreased stability; we found that this was also the case for our monomeric Griffithsin [19]. To work around this, we adopted a strategy published in previous work from our group and produced a heterodimeric variant of Griffithsin whereby one subunit had its three mannose-binding sites re-moved [19]. This ensured that we could obtain a variant of Griffithsin that did not weaken the stability of the protein by abolishing the ability of the protein to dimerize, but also did not have the ability to engage in bivalent binding.

In the several studies have come out assessing WT-Grft's potential use as an anti-SARS-CoV-2 prophylactic, Griffithsin tends to show a half-maximal inhibitory concentration against SARS-CoV-2 pseudotyped lentivirus in the ~300 nM to ~2000 nM range (which is about an order of magnitude less potent than Griffithsin's inhibitory capabilities against other viruses like HIV, SIV, Hepatitis C, or Japanese Encephalitis Virus) [28-31]. Despite this diminished antiviral capability, the aforementioned favorable pharmacokinetic properties, ease of production, and high stability of Griffithsin means that the consensus in the literature is WT-Grft is still a viable prophylactic agent to combat COVID-19 [28-32]. However, in some of the same studies that assessed WT-Grft's antiviral activity against SARS-CoV-2 pseudotyped lentivirus, it was also tested on replication competent SARS-CoV-2 coronaviral particles [29-31]. Interestingly, WT-Grft seemed to

consistently exhibit more efficient inhibition of authentic SARS-CoV-2 coronavirus, with a half-maximal inhibitory concentration ranging from 33.2 nM to 100.1 nM (Table 1) [29-31]. To our knowledge, no group has yet explored potential reasons why Griffithsin appears to exhibit higher antiviral potency against genuine replication-competent SARS-CoV-2 virus when compared to SARS-CoV-2 pseudotyped lentivirus.

Article	Reference Number	Source of Griffithsin	Viral Strain	Inhibitory Capabilities Against SARS-CoV-2 Pseudotyped Lentivirus or other <i>in vitro</i> model assessing Spike alone	Inhibitory Capabilities Against SARS-CoV-2 Coronaviral Particles
Alsaïdi S, et. al. Griffithsin and Carrageenan Combination Results in Antiviral Synergy against SARS-CoV-1 and 2 in a Pseudoviral Model. <i>Mar Drugs</i> . 2021 Jul 26;19(8):418. doi: 10.3390/md19080418.	27	Expressed in <i>Nicotiana benthamiana</i> plants transduced with a tobacco mosaic virus vector expressing GRFT	Wild-Type:	Inhibition of pseudoviral infection <i>in vitro</i> on HeLa cells expressing hACE2: EC50 = 20.6 µg/mL (1610 nM)	Not Reported
			D641G:	Inhibition of pseudoviral infection <i>in vitro</i> on HeLa cells expressing hACE2: EC50 = 37.6 µg/mL (2940 nM)	
			K417N /E484K/ N501Y*:	Inhibition of pseudoviral infection <i>in vitro</i> on HeLa cells expressing hACE2: EC50 = 31.6 µg/mL (2750 nM)	
Cai Y, et. al. Griffithsin with A Broad-Spectrum Antiviral Activity by Binding Glycans in Viral Glycoprotein Exhibits Strong Synergistic Effect in Combination with A Pan-Coronavirus Fusion Inhibitor Targeting SARS-CoV-2 Spike S2 Subunit. <i>Virol Sin</i> . 2020	28	Expressed in <i>Escherichia coli</i> BL21 (DE3) via pET expression vector	Wild-Type:	Inhibition of pseudoviral infection <i>in vitro</i> on HuH-7 cells: IC50 = 292.5 nM to 447.3 nM	Inhibition of coronaviral particle infection <i>in vitro</i> on VeroE6 cells: IC50 = 63 nM

Dec;35(6):857-860. doi: 10.1007/s12250-020-00305-3.			Wild-Type:	Inhibition of SARS-CoV-2 Spike mediated HuH-7 cell-cell fusion: IC50 = 322.9 nM	
Cai Y, et. al. A bivalent protein targeting glycans and HR1 domain in spike protein potently inhibited infection of SARS-CoV-2 and other human coronaviruses. Cell Biosci. 2021 Jul 8;11(1):128. doi: 10.1186/s13578-021-00638-w.	29	Expressed in <i>Escherichia coli</i> BL21 (DE3) via pET expression vector	Wild-Type:	Inhibition of HuH-7 cell pseudoviral infection <i>in vitro</i> : IC50 = 510.8 nM	Inhibition of coronaviral particle infection on <i>in vivo</i> mice models: IC50 = 100.1 nM
			Wild-Type:	Inhibition of Caco-2 cell pseudoviral infection <i>in vitro</i> : IC50 = 885.7 nM	
			Wild-Type:	Inhibition of SARS-CoV-2 Spike mediated cell-cell fusion: IC50 = 322.9 nM	
Ahan RE, et. al. A Highly Potent SARS-CoV-2 Blocking Lectin Protein. ACS Infect Dis. 2022 Jul 8;8(7):1253-1264. doi: 10.1021/acscinfecdis.2c00006.	30	Expressed in <i>Escherichia coli</i> BL21 (DE3) via pET expression vector	Wild-Type:	Binding affinity of Spike to Grft protein determined by Isothermal Titration Calorimetry (ITC): Kd = 9900 nM	



			Wild-Type:	Binding affinity of Spike to Grft protein determined by Quartz Crystal Microbalance with Dissipation monitoring (QCM-D): Kd = 1600 nM	Inhibition of coronaviral particle infection <i>in vitro</i> on VeroE6 cells: IC50 = 33.2 nM
			Delta:		Inhibition of coronaviral particle infection <i>in vitro</i> on VeroE6 cells: IC50 = 34.0 nM
			Omicron:		Inhibition of coronaviral particle infection <i>in vitro</i> on VeroE6 cells: IC50 = 5.4 nM

\*The authors report K1417N but we believe this is a typo of K417N

**Table 1:** A summary of Wild-Type Griffithsin's antiviral capabilities against SARS-CoV-2 pseudotyped lentivirus versus coronaviral particles, as published in the literature.

A possible explanation for the disparity in WT-Grft inhibition between lentiviral pseudovirus and genuine SARS-CoV-2 coronaviral particles could be due the differences in the viral architecture. HIV and other lentiviruses express approximately 7-14 spike glycoproteins that dictate viral tropism on the surface of a 100 nm diameter membrane-encapsulated virus [33, 34]. Other than these proteins, the surface of lentiviruses are essentially bare of other virus-specific structural features. SARS-CoV-2 coronaviral virions share several features with lentivirus, also being ~100 nm membrane-encapsulated viruses that express 11-41 Spike proteins (S) that dictate viral tropism and mediate the infection process [35]. But the novel coronavirus nCoV-19 genome expresses several other structural proteins that are packaged with the SARS-CoV-2 virion. These include: 1) the Nucleocapsid protein, N, which interacts with the viral genome, 2) the Envelope protein, E, which is expressed on the surface of the virions and is important for maintaining viral pathogenesis, and 3) the Membrane protein, M, which is also expressed on the virus surface [36, 37]. As in other coronaviruses, all three structural proteins interact with each other and the spike to facilitate viral budding, protein transport through the Endoplasmic Reticulum, and viral attachment [38-42].

We wished to ascertain whether the additional SARS-CoV-2 structural proteins M, N, and E could be responsible for the apparent increased susceptibility of the coronaviral virions to Wild-Type Griffithsin-based inhibition.

Finally, although the human Angiotensin Converting Enzyme 2 (hACE2) has been solidified as the required receptor to facilitate SARS-CoV-2 viral entry, the SARS-CoV-2 virion is known to be able to infect cells that only modestly express the hACE2 receptor [43, 44]. This is perhaps best exemplified by how although COVID-19 presents as a respiratory illness, the human respiratory system only modestly expresses the SARS-CoV-2 entry receptor hACE2 [40, 43, 45-47]. While this initially perplexed researchers, it has now been widely accepted that cell surface attachment receptors are capable of binding to the SARS-CoV-2 virion and facilitate efficient viral infection of cells that have poor hACE2 expression [46, 48-50]. Among these attachment receptors, lectin receptors such as DC-SIGN have been known to enhance the infectivity of a variety of viruses, including human T-cell lymphotropic virus type 1, Enterovirus 71, Dengue Virus, and HIV-1 [26, 27, 51, 52, 53, 54]. The consensus is that DC-SIGN receptor-mediated Trans-infection is crucial in facilitating the initial infection respiratory tissue in the context of COVID-19 [46, 48].

Since DC-SIGN preferentially binds to the same high-mannose glycans that Griffithsin binds to, it seemed likely that Griffithsin could act as a competitive inhibitor against DC-SIGN-mediated Trans-infection [13, 14, 18, 19, 56]. To test this, we performed two assays that modeled the process of DC-SIGN-mediated Trans-infection *in vitro*.

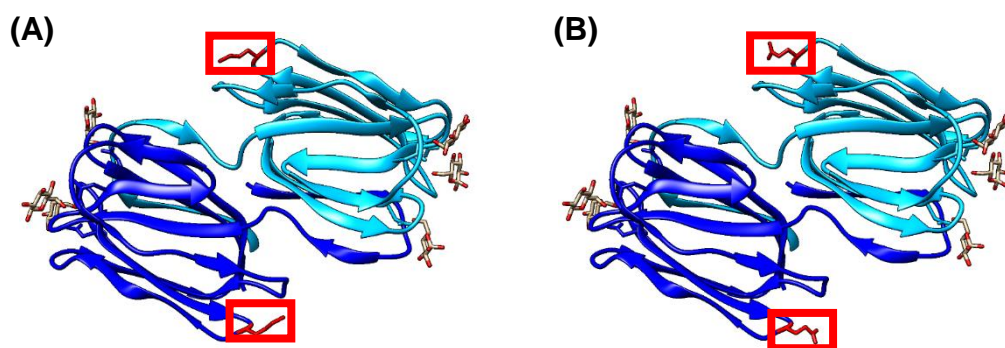
Overall, our results suggest that both WT-Grft and Q-Grft inhibit SARS-CoV-2 spike mediated pseudovirus infection, but are more potent against the virions that also expressed the additional structural proteins. We further found that the cross-linking capabilities of Griffithsin are not nearly as important in retaining its antiviral activity against SARS-CoV-2 pseudotyped virions as compared to HIV-1 virions. For DC-SIGN mediated Trans-infection assays, we performed two different assays to test the effect that Griffithsin had on inhibiting SARS-Cov-2 pseudoviral infection. In the course of our experiments, we found that none of the Griffithsin variants were effective inhibitors on either Trans-infection assay model. Similarly, the addition of the M, N, and E structural proteins did not seem to affect the DC-SIGN mediated Trans-infection capability of SARS-CoV-2 pseudotyped lentivirions. However, we did find that the addition of the M structural protein increased WT-Grft's potency as an inhibitor on *in vitro* hACE2-mediated Direct assays. This may provide an explanation for why Wild-Type Griffithsin appears to display greater prophylactic/inhibitory activity against genuine nCoV-19 coronavirus infection versus SARS-CoV-2 spike pseudotyped particles, thereby providing more support to the idea that Griffithsin could be leveraged as an effective nasal spray or other antiviral formulation for use against COVID-19.

### 3.3 Results

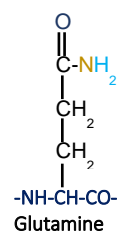
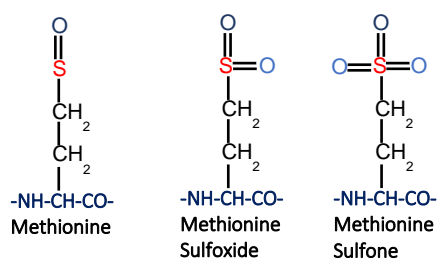
#### 3.3.1 Wild-Type Griffithsin and M78Q Griffithsin Both Display Moderate Anti-SARS-CoV-2 Inhibitory Capabilities

The FDA guidelines for potential protein-based therapeutics is unambiguous in dictating that health science researchers must carefully assess therapeutic candidates for post-translational modification [55]. If a therapeutic undergoes post-translational modification, much quality control assessment must be performed, including testing the physical and pharmacokinetic properties of the post-translationally modified derivatives, quantifying the rate at which the protein undergoes modification, and providing an estimate for the proportion of modified derivatives in the final product [60]. This sort of quality control assessment, while important, might be less expeditious than simply mutating the protein therapeutic to avoid such arbitrary post-translational modifications. In the case of Griffithsin, oxidation has been found to occur at Methionine 78 (Figure 1A, 1B, 1C) [17, 21]. Thankfully, researchers have already found that mutating M78 to a Glutamine alleviates the issues of post-translational modification, making M78Q Griffithsin an easier candidate to use for clinical trials [65].

Before embarking on assessing whether Griffithsin could act as a suitable inhibitor of SARS-CoV-2 viral infection, we first verified that the M78Q mutation did not disrupt the native fold of WT-Grft. This was important because although the antiviral/prophylactic capability of recombinant Q-Grft has been verified to match WT-Grft in the literature, there does not yet appear to published verification that recombinant production of M78Q Griffithsin in *E. coli* does indeed produce a protein that exhibits structural similarity to WT-Grft [21, 65, 66]. To do so, we produced <sup>15</sup>N labeled WT-Grft and Q-Grft (as described in Methods Section 2.2, above) and then assessed both proteins by NMR HSQC (Figure 1A, 1B). Our spectra show that not only did Q-Grft retain the same overall fold of WT-Grft, but also that the Q78 amino acid was clearly discernable on the NMR, as evidenced by the presence of its twin side chain hydrogens at the same <sup>15</sup>N ppm value (Figure 1D) [67].



(C)



(D)

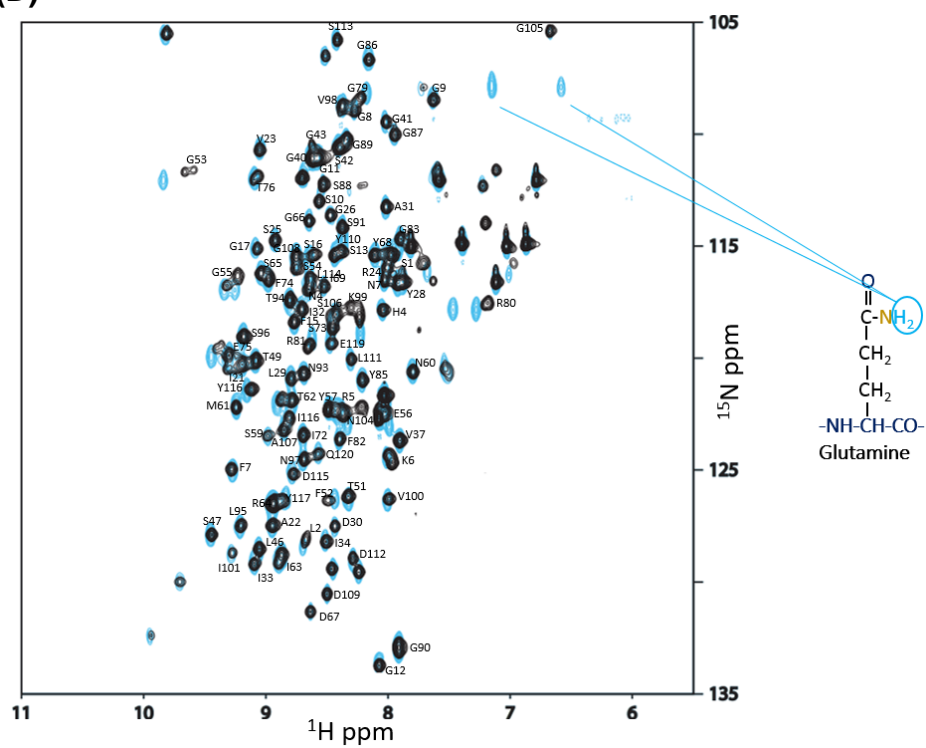


**Figure 1: (A), (B)** The schematic diagram of Wild-Type Griffithsin compared to M78Q Griffithsin. The location of Methionine 78 is highlighted in red. On the left, **(A)**, is a depiction of WT-Grft while on the right, **(B)**, is a depiction of Methionine 78 mutated to Glutamine (a.k.a. Q-Grft). **(C)** Depiction of post-translational oxidation that occurs on Methionine. **(D)** NMR spectrum overlay of Q-Griffithsin (teal blue) underneath WT-Griffithsin (black). The overlay shows peaks have a high degree of concordance, indicating that the fold of Q-Grft matches the fold of WT-Grft. The spectrum of WT-Grft was compared to previous spectra of functional Griffithsin produced previously [16, 24]. The expected peaks of the sidechain Q78 Glutamine are pointed out in teal.

After performing this quality control check, we then sought to test the antiviral capabilities of both the WT-Grft and Q-Grft proteins on pseudoviral infectivity assays. The SARS-CoV-2 Spike protein is known to have 22 highly-conserved N-linked glycan sites; analysis of existing literature reveals that N61, N234, N709, N717, and N801 are all typically occupied by high-mannose glycans, with N122, N165, N603, N1074, and N1098 also showing a >25% propensity to be occupied by high-mannose or complex glycans (see Chapter 2, Figure S3). Since Griffithsin has a sub-nanomolar affinity to high-mannose sugars, it is likely that the aforementioned glycan sites act as epitopes that allow Griffithsin to bind to the Spike protein and prevent viral infection (Figure 2A) [3, 15, 44]. The inhibitory capabilities of the WT-Grft and Q-Grft proteins were tested on a SARS-CoV-2 hACE2-mediated pseudoviral assay, heretofore referred to as a “Direct Infectivity” assay (Figure 2B). In our hands, WT-Grft and Q-Grft showed a moderate ability to impede pseudoviral infection, with IC<sub>50</sub> values of 2.74  $\mu$ M and 3.53  $\mu$ M, respectively (Figure 2C). While these values are not as potent as the inhibitory capabilities of Griffithsin against other viruses, these values are largely within the range of values expected for SARS-CoV-2 pseudoviral inhibition (Table 1) and is still considered to be potent enough for Griffithsin to be considered a viable agent for prophylactic treatments [27].

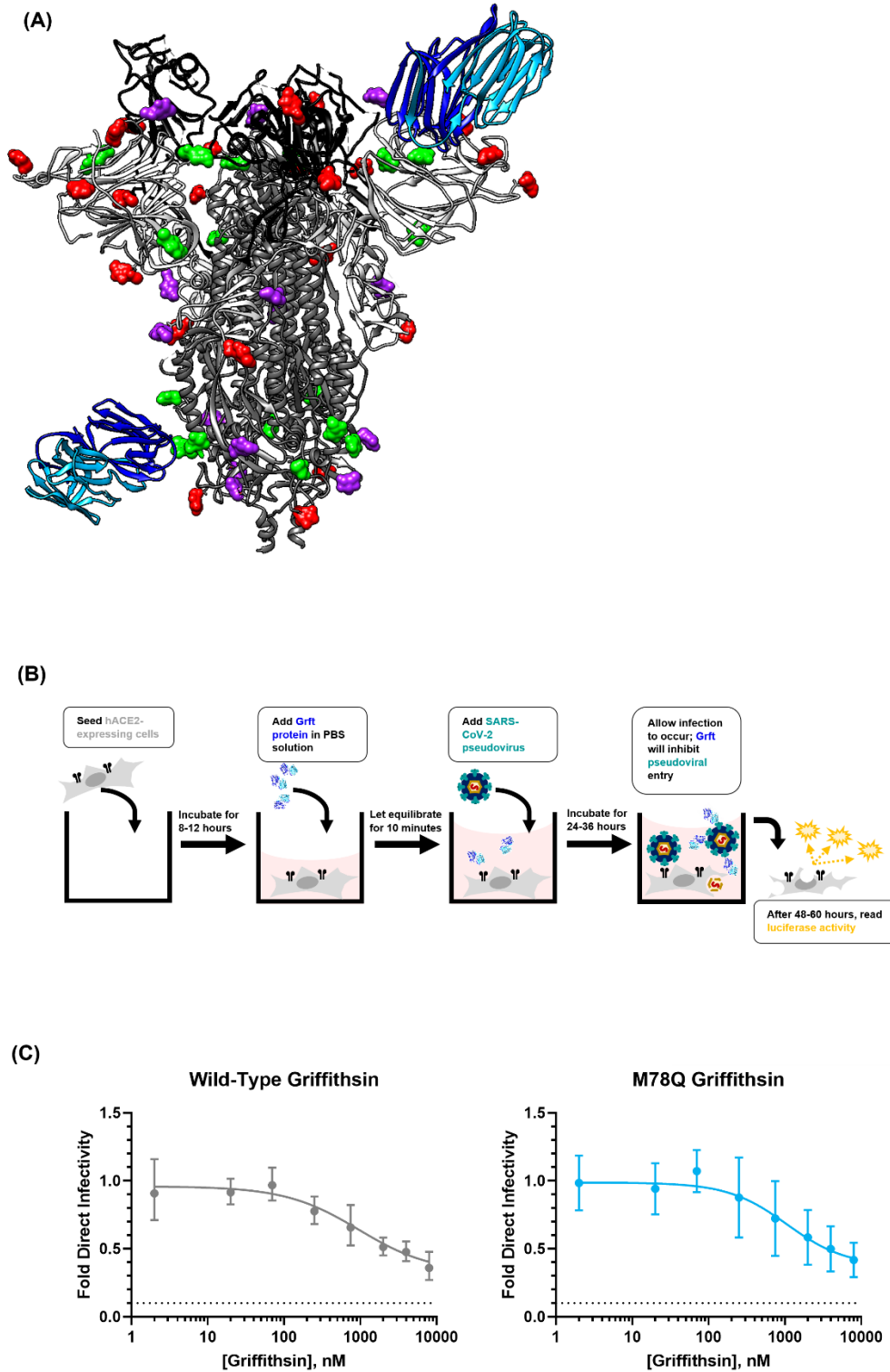


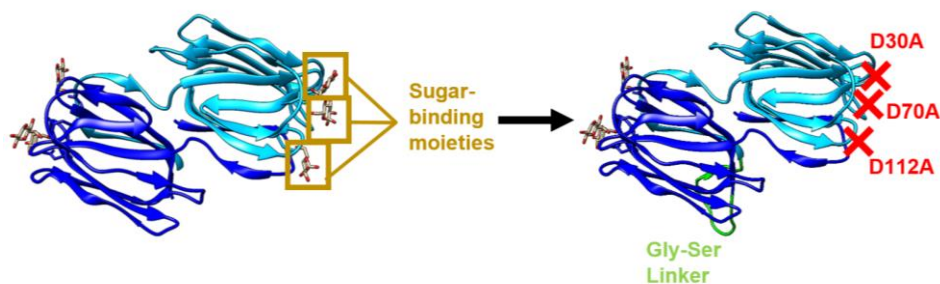
**Figure 2: Depiction of how Grft may impede SARS-CoV-2 Spike mediated infectivity. A.)** Representation of Griffithsin (PDB: 2NUO) on the SARS-CoV-2 Spike. To get high resolution of the loop

regions where N-linked glycans are present, two Spike PDB structures were overlaid on each other (PDB ID: 7NT9 and 6VYB). The glycans are color coded to match the type of glycan that is present on the Spike protein (high mannose, complex, and hybrid/no consensus between high mannose and complex). **B.)** Schematic depiction of Griffithsin inhibition of hACE2-mediated SARS-CoV-2 viral Direct infection. **C.)** Inhibition of SARS-CoV-2 pseudoviral infection by Wild-Type Griffithsin (gray) and M78Q Griffithsin (teal blue). Dashed line indicates one order of magnitude lower infectivity. Data were fit with a Four parameter variable slope curve (Graphpad Prism).

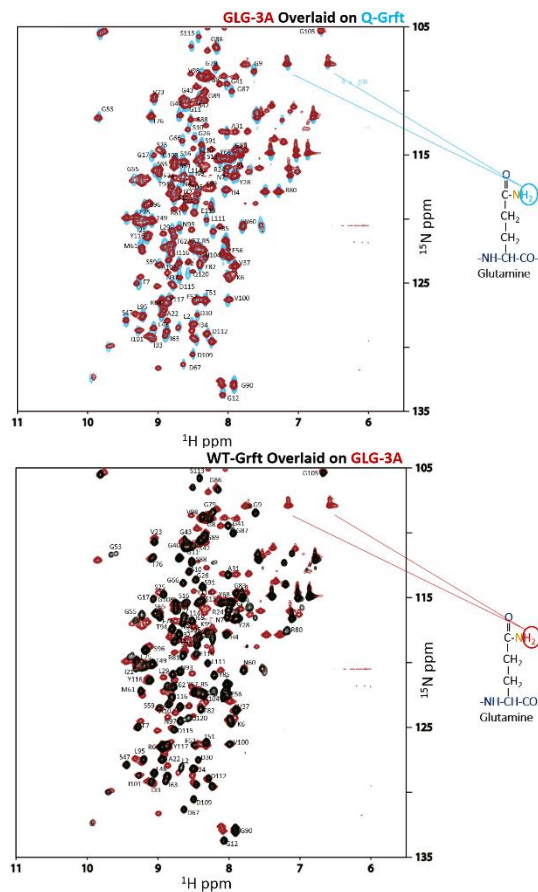
### 3.3.2 Removing the Cross-Linking Capability of Griffithsin Does Not Appear to Affect the Inhibitory Capability of Griffithsin

A key trait of the Griffithsin protein is that it is a domain-swapped dimer with each monomer's three sugar-binding moieties oriented in opposite directions relative to each other (Figure 3A). This allows for Griffithsin to not only exhibit bivalent binding to a target epitope, but also endows Griffithsin with the ability to cross-link target proteins together. This cross-linking capability allows for Griffithsin to aggregate Spike proteins into bunches or clusters, which is crucial in maintaining Griffithsin's inhibitory capabilities against viruses such as HIV-1 and Hantaan virus [19, 24, 68]. Despite how both WT-Grft and Q-Grft did not show particularly potent antiviral activity on our Direct Assays, we still wished to investigate whether this cross-linking capability of Griffithsin was important in the context of inhibiting SARS-CoV-2 Spike-mediated infection. Griffithsin is currently in clinical trials, meaning that even if it does not have exceptional inhibitory capabilities against SARS-CoV-2, it still may be a pharmacologically favorable, non-immunogenic starting point for either a combinatorial prophylactic treatment or for the creation of a better SARS-CoV-2 viral entry inhibitor [22, 23]. Hence, uncovering the key structural and functional features governing the inhibitory capabilities of the Griffithsin would assist in altering the protein to produce a better prophylactic against SARS-CoV-2.

**A.)**



**B.)**



C.)

## Grft-L-Grft 3A Onearmed

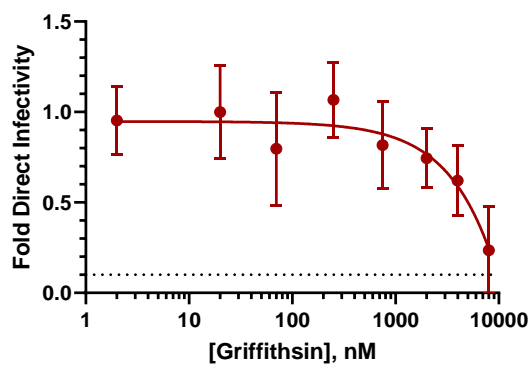


**Figure 3: A)** Depiction of how the obligate dimer GLG-3A was produced. M78Q Griffithsin monomers were linked with a 16-amino acid Glycine and Serine linker (depicted in green). The sugar-binding Aspartates on one of the monomers were mutated to Alanines to eliminate the ability of Griffithsin to cross-link proteins. **B)** The NMR overlay of GLG-3A shows high degree of overlap with both M78Q Griffithsin (left, dark red GLG-3A overlaid onto teal Q-Grft) and Wild-Type Griffithsin (right, black WT-Grft overlaid onto dark red GLG-3A), indicating the protein is folded and functional. GLG-3A has M78Q mutations, which are indicated on the spectra. **C)** Inhibition of SARS-CoV-2 pseudotyped lentivirus with GLG-3A on the same assay as depicted in Fig. 2B.



Dashed line indicates one order of magnitude lower infectivity. Data were fit with a Four parameter variable slope curve (Graphpad Prism).

In order to remove Griffithsin's bivalent binding, we attempted to create a monomeric form of Griffithsin. Although existing literature has shown that it is possible to create Monomeric Griffithsin (Mono-Grft) by inserting a Gly-Ser in the domain-swapped beta sheet of Griffithsin (1GS 17-18) and mutating Leucine 2 to a Serine (L2S), when we produced this variant of Griffithsin, the lyophilized protein appeared to be insoluble at pH 6.5-7.5 [19]. We did find that we could resuspend sufficient amounts of Mono-Grft at pH 2.5 to run on NMR HSQC, but the resultant spectrum indicated that the Mono-Grft was not well-folded (Figure S1A). When the pH of the Mono-Grft sample was raised from pH 2.5 to above 6, the protein did appear to adopt a fold that had some similarity with WT-Grft, but the sample aggregated over the course of an hour (Figure S1B). The poor solubility of Mono-Grft made it unsuitable for further testing as a potential antiviral therapeutic.

Our group has previously reported workaround to produce a Griffithsin variant with monovalent binding capabilities, whereby the Griffithsin dimer is expressed as a single polypeptide chain with a 16-amino acid long Glycine-Serine linker between the two Griffithsin monomers [16, 24]. The three sugar binding moieties on one of the Griffithsin monomer domains are removed via mutagenesis, yielding a constitutively dimeric form of Griffithsin with only one half of the protein being able to bind to sugars (Figure 3A). This "Onearmed" variant of Griffithsin retains the overall structure of the Wild-Type Griffithsin dimer, but is only capable of monovalent binding to sugar epitopes. This variant- heretofore referred to as GLG-3A- was produced with M78Q mutations on both monomeric domains of the Griffithsin dimer and its structure was verified to be similar to both WT-Grft and Q-Grft by NMR HSQC (Figure 3B).

When GLG-3A was tested on our Direct Infectivity assay as depicted in Figure 2B, it appeared to behave similarly to both WT-Grft and Q-Grft, albeit with an approximately 2- to 4-fold diminished antiviral capability ( $IC_{50} = 5.03 \mu M$ ) (Figure 3C). This is in contrast to GLG-3A inhibition tests with HIV-1 pseudovirus, whereby removing the crosslinking ability of Griffithsin diminished its antiviral activity by approximately 100- to 1000- fold [24]. Ergo, while it appears as though the cross-linking and Spike aggregation is crucial in mediating the antiviral capability of Griffithsin in the context of HIV, it does not appear to greatly contribute to etiology of Griffithsin-based SARS-CoV-2 pseudoviral inhibition.

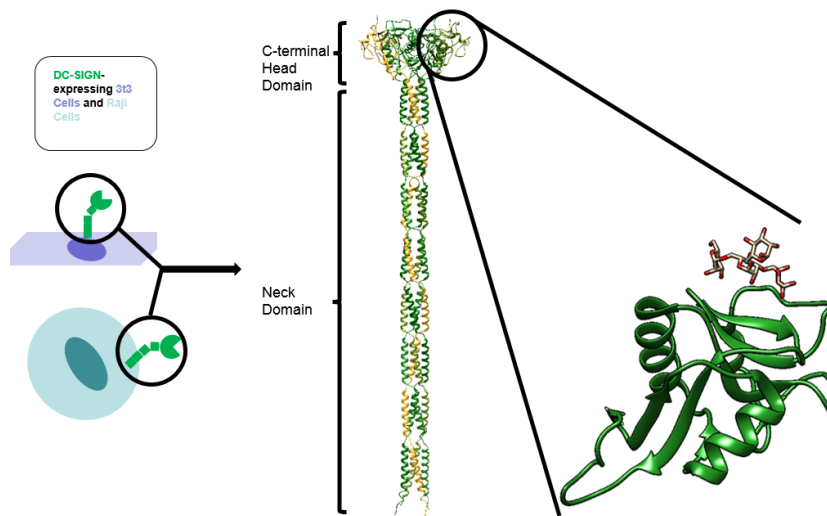
### 3.3.3 Grft is a Moderate Inhibitor of Direct Infection, and Does Not Prevent DC-SIGN Facilitated Trans-infection

Recent evidence has shown that although COVID-19 presents as a respiratory disease, the cells in the lung tissue only moderately express the hACE2 receptor [47, 49, 50]. While this initially puzzled scientists, the widely accepted theory now is that other cell-surface proteins are able to act as attachment receptors that capture and present the SARS-CoV-2 virus, thereby to enhancing the infectivity of SARS-CoV-2 and allowing for efficient infection of lung cells that modestly express hACE2 [43, 44, 46, 48].

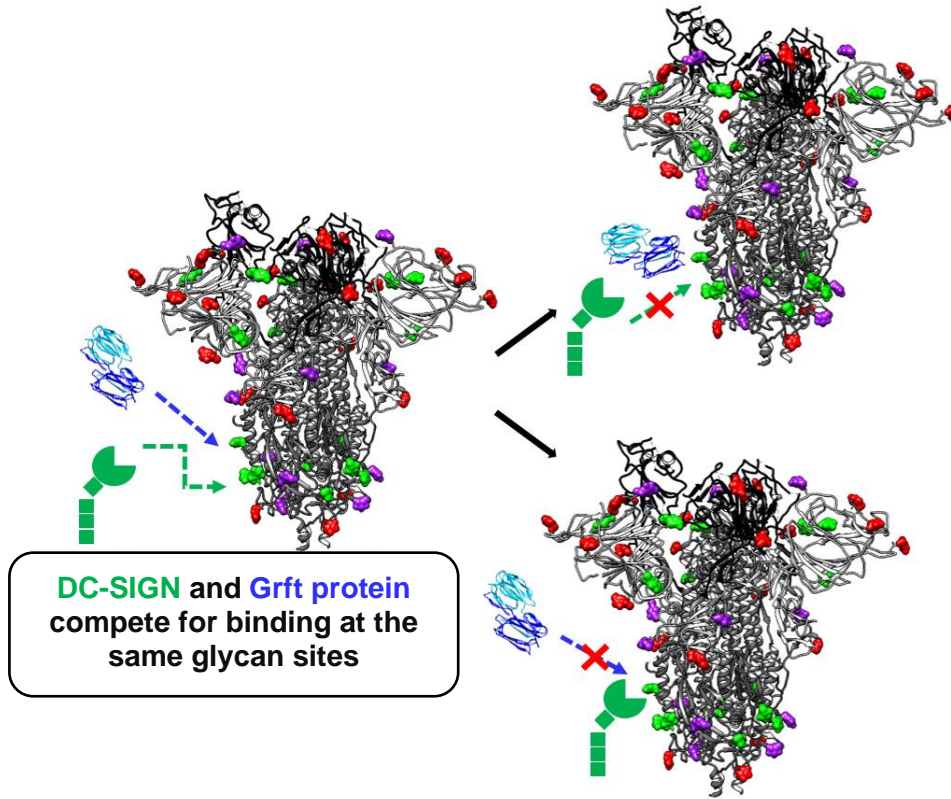
One of these attachment receptors that has been able to show a consistent ability to facilitate trans-infection of SARS-CoV-2 pseudovirions on *in vitro* assays is called

Dendritic Cell-Specific Intercellular adhesion molecule-3-Grabbing Non-integrin (DC-SIGN) [46, 59]. DC-SIGN is a tetrameric, 46 kDa cell surface protein that is comprised of an N-terminal transmembrane domain, a relatively long Neck domain, and a C-terminal Head Domain (Figure 4A). The C-terminal Head Domain encompasses the Carbohydrate Recognition Domain (CRD) and is known to have a high affinity for high-mannose sugars, thereby allowing DC-SIGN to capture a variety of membrane-encapsulated viruses- ranging from human T-cell lymphotropic virus type 1, Enterovirus 71, Dengue Virus, and HIV-1- and potentiate efficient viral infection into susceptible cells [26, 27, 48, 51-54, 56]. In recent literature, it has been demonstrated that DC-SIGN is capable of recognizing N-linked glycans on the SARS-CoV-2 Spike protein to mediate viral presentation and infection of cells [48].

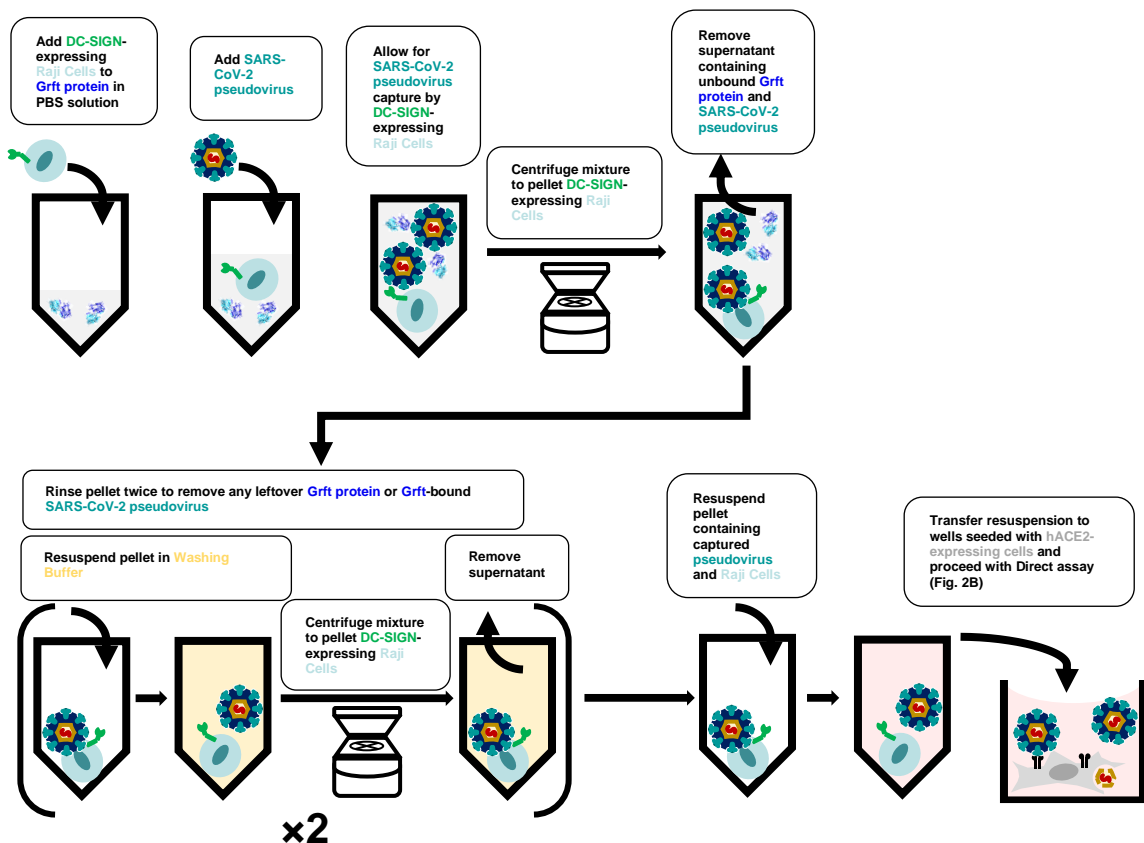
A.)



B.)



C.)



D.)

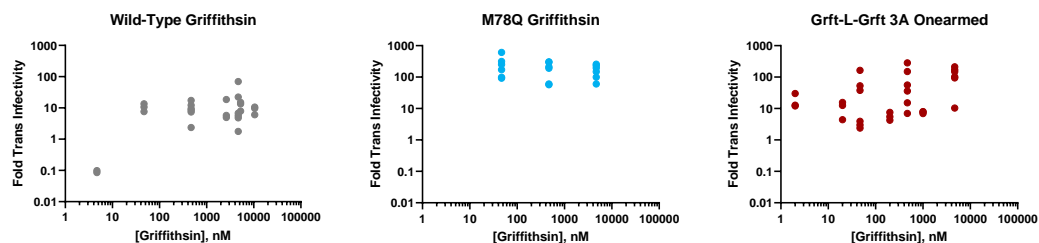


#### Figure 4: Griffithsin Appears to Enhance DC-SIGN Mediated Trans Infection via Raji cells.

(A) Simplified depiction of the DC-SIGN lectin receptor on the surface of 3t3 and Raji cells. The DC-SIGN extracellular domain ribbon structure is an AlphaFold prediction of the DC-SIGN protein's extracellular domain [69, 70]. The structure was chosen by selecting the closest prediction to a previously constructed structure from Tabarani, G. et. al. [71]. We further zoom in on the C-terminal Carbohydrate Recognition Domain (CRD) of DC-SIGN bound to mannan (PDB ID: 1SL4).

(B) Depiction of DC-SIGN CRD bound to high-mannose N-linked glycans on the SARS-CoV-2 Spike protein. In theory, Griffithsin should compete with DC-SIGN for binding to the same high-mannose glycans.

(C) Diagram depicting the process of Raji DC-SIGN+ cell mediated SARS-CoV-2 pseudovirus Trans-infection.

(D) Results of Griffithsin inhibition of Raji DC-SIGN+ cell mediated Trans-infection. WT-Grft was tested first and was found to consistently enhance Trans-infectivity. Q-Grft appeared to behave similarly, although it enhanced Trans-infectivity to a greater extent than WT-Grft. We then tested GLG-3A to observe whether Griffithsin-mediated cross-linking could explain the enhanced infectivity of WT-Grft and Q-Grft. Oddly, all Griffithsin variants seemed to enhance Trans-infectivity on our assay.

Because Griffithsin is also able to bind to high-mannose glycans on viral Spike proteins, we theorized that Griffithsin could act as a potent competitive inhibitor of DC-SIGN mediated Trans-infection (Figure 4B) [16]. To test this, we designed an assay that made use of the paired B-cell Burkitt lymphoma derived cell lines Raji/Raji DC-SIGN+ that had been used to model HIV-1 DC-SIGN mediated Trans-infection (Figure 4C) [61-63]. Raji cells have already been used as a workhorse strain for Trans-infection experiments with other viruses, notably with HIV-1 and Ebola Virus [60-63]. Briefly, the assay was run as follows: the B-cell Burkitt lymphoma derived Raji cell line that was transfected to constitutively express DC-SIGN (Raji DC-SIGN+) and its nontransfected control (Raji Wild-Type) was incubated with SARS-CoV-2 pseudotyped lentivirions. After allowing the DC-SIGN-expressing cells to capture the virus, the cells were washed twice and then added to wells containing hACE2+ HEK-293T cells. The virions that had been captured by the DC-SIGN+ Raji cells were allowed to infect the hACE2+ HEK-293T cells and the infectivity was measured by luciferase activity as described in the Direct infectivity assay in Figure 2B.

After verifying that the Raji cells and Raji DC-SIGN+ cells were not themselves permissible to SARS-CoV-2 infection (Figure S2A, S2B), we verified that DC-SIGN-mediated Trans-infection could be inhibited with a competitive inhibitor of the DC-SIGN mannose-binding site (Figure S3A, S3B). Coupled with how Raji Wild-Type cells did not facilitate Trans-infection, this provided strong evidence that Raji DC-SIGN+ cells were indeed capable of capturing SARS-CoV-2 pseudotyped virions and facilitating Trans-infection on our in vitro assay (Figure S4).

We then used this Raji Cell Mediated Trans-infectivity assay system to test whether WT-Grft could act as an inhibitor of DC-SIGN mediated viral capture and transfer to susceptible cells. We performed this assay in the presence of different concentrations of WT-Grft (Figure 4D). Oddly, 4.7 nM of WT-Grft appeared to inhibit Raji DC-SIGN+ cell mediated Trans-infection. But, when the concentration of WT-Grft was increased to 47 nM, the SARS-CoV-2 pseudovirus appeared to display greatly enhanced infectivity, reaching infectivity values that were 1 order of magnitude higher than samples without any Griffithsin present.

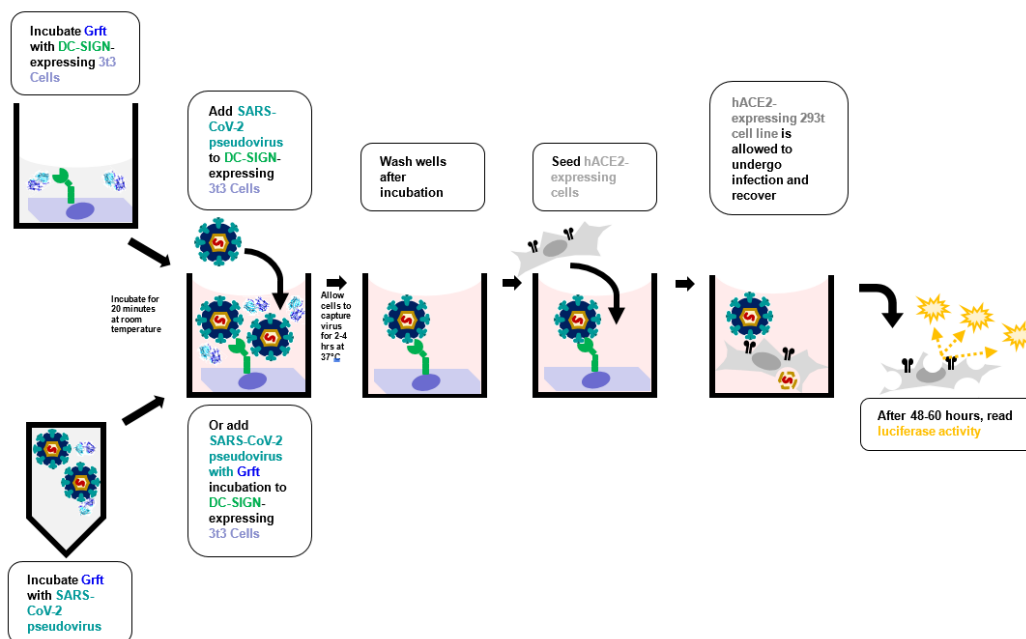
Our initial hypothesis to explain this phenomenon was that the aforementioned cross-linking capabilities of Griffithsin could tether multiple viruses together, thereby allowing a single DC-SIGN CRD to capture more than one virion. Because the SARS-CoV-2 Spike protein had numerous high-mannose glycosylation sites, there conceivably could be enough epitopes on the virion to allow for both Griffithsin and DC-SIGN to bind to the same Spike protein. This Griffithsin-mediated cross-linking would in turn allow a single DC-SIGN receptor to capture and deliver clusters of multiple SARS-CoV-2 virions provided to susceptible cells. Alternatively, we thought that WT-Grft could be cross-linking viral particles to such an extent that the particles were able to be pelleted by centrifugation without the need to be captured by DC-SIGN-expressing cells. But, when we performed our experiments with the monovalent variant of Griffithsin that was incapable of cross-linking proteins together (GLG-3A), we observed a similar phenomenon as described for WT-Grft: GLG-3A consistently appeared to enhance Raji DC-SIGN+ SARS-CoV-2 pseudoviral infectivity by at least 1 order of magnitude (Figure 4D).

For the purposes of completion, we performed a less intensive screen of Q-Grft to verify that the M78Q mutation did not alter the trend of increased Raji DC-SIGN+ infectivity. As shown in Figure 4D, 47 nM of Q-Grft was also sufficient to enhance infectivity on our Raji Trans infectivity assay by at least 1 order of magnitude, indicating that Q-Grft, much like WT-Grft and GLG-3A, enhanced Raji cell-mediated Trans-infection.

As a B cell line, Raji cells express a variety of Complement receptors, some of which can serve as attachment receptors for other viruses like Epstein Barr Virus (EBV), Hantavirus, and HIV-1 [72]. B cells can also directly recognize antigens from pathogenic molecules (such as viruses) either via their Toll-like Receptors or B Cell Receptors [73, 74]. This recognition can lead to B cell activation and differentiation, even in the absence of T-cells, potentially leading to the secretion of a variety of cytokines and cytotoxic molecules [73-77]. All of this means that the process of SARS-CoV-2 pseudoviral exposure or Griffithsin incubation with Raji cells could possibly induce signaling cascades or alterations in cell surface protein expression, thereby causing the observed increase in Raji DC-SIGN+ cell mediated pseudoviral Trans-infectivity to susceptible hACE2+ HEK-293T cells [73, 74]. Even though Raji cells have been reported to be suitable *in vitro* Trans-infection models for other viruses- like HIV-1, Human T-Cell Lymphotropic Virus Type 1, and Enterovirus 71- we believed that it was prudent to assess Griffithsin inhibition of Trans-infection on another paired DC-SIGN+/DC-SIGN- cell system to verify whether the enhanced Trans-infectivity we were observing on the Raji cell assay was consistent [51, 52, 61-63].

To verify whether Griffithsin was indeed truly capable of enhancing SARS-CoV-2 pseudoviral Trans-infectivity, we performed a Trans-infectivity assay that made use of a DC-SIGN+ cell line that was dissimilar to Raji cells. The 3t3 cell line is an adherent murine fibroblast cell line that has low innate expression of lectin receptors and Complement receptors [58]. We were able to obtain a paired 3t3 and DC-SIGN+ 3t3 cell line from NIH AIDS reagent, which allowed us to develop an alternative *in vitro* DC-SIGN mediated Trans-assay [59]. Briefly, 3t3 cells were seeded in the wells of a 96-well plate and allowed to recover overnight. To test whether Griffithsin interaction with virions or Griffithsin interaction with DC-SIGN was responsible for increasing the Trans-infectivity of SARS-CoV-2 pseudovirions, we performed two different procedures: we either 1) pre-incubated of SARS-CoV-2 pseudotyped lentivirus with Griffithsin proteins before adding to 3t3 cells, or 2) Griffithsin was first added to 3t3 cells before SARS-CoV-2 pseudotyped virions were added over the top (Figure 5A). Wells were then washed twice and susceptible hACE2+ HEK-293T cells were added to wells to allow for infection. After 48-60 hours, viral infectivity was measured by luciferase activity assay as described in Figure 2B, above.

A.)



B.)

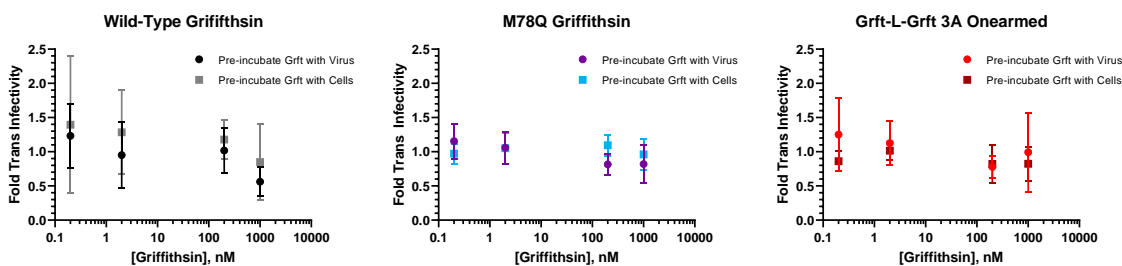


**Figure 5:** Griffithsin doesn't affect Trans-Infection in 3t3 Cells. **(A)** Diagram depicting the process of 3t3 DC-SIGN+ cell mediated SARS-CoV-2 pseudovirus Trans-infection. **(B)** Depiction of Griffithsin inhibition of 3t3 DC-SIGN+ cell mediated Trans-infection. Circular data points indicate protocol where Griffithsin was pre-incubated with SARS-CoV-2 pseudovirus before adding to 3t3 DC-SIGN+ cells. Rectangular data points indicate protocol where Griffithsin was pre-incubated with 3t3 cells before SARS-CoV-2 pseudovirus was added to well. For both infectivity protocols, all Griffithsin variants did not appear to have any significant effect on enhancing or inhibiting 3t3 DC-SIGN+ cell-mediated Trans-infectivity.

The results of the DC-SIGN+ 3t3 cell-mediated assay showed that all three Griffithsin variants (WT-Grft, Q-Grft, and GLG-3A) appeared to have no effect on DC-SIGN-mediated Trans-infection of SARS-CoV-2 pseudovirus. Furthermore, neither pre-incubation of Griffithsin with DC-SIGN-expressing cells and pre-incubation of Griffithsin with SARS-CoV-2 pseudovirus led to a significant difference in viral infectivity. The lack of Griffithsin-mediated enhancement of Trans-infectivity on 3t3 cells led us to believe

that the enhanced Trans-infectivity observed in Figure 4 with Raji Cells was likely due to unforeseen signaling changes or interactions in the Raji cell line.

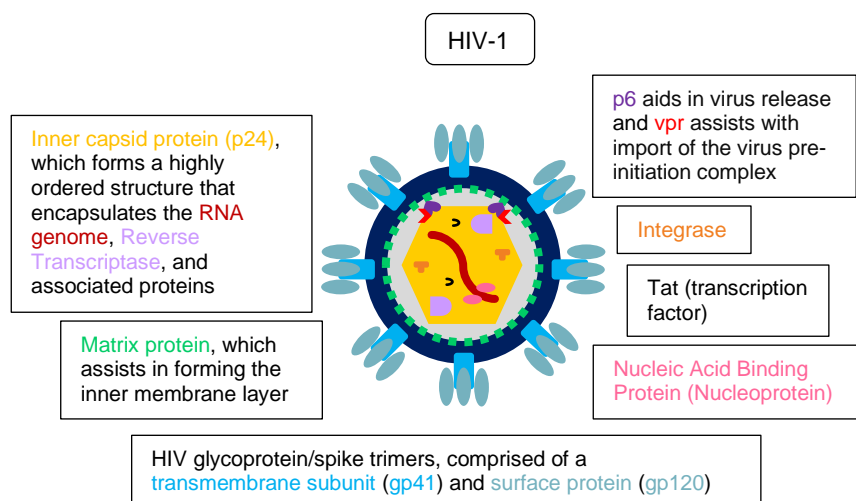
Given the results from the Raji cell and 3t3 cell Trans infectivity assays, we were left to conclude that, at the very least, no variant of Griffithsin (WT-Grft, Q-Grft, and GLG-3A) exhibited any appreciable ability to act as an inhibitor of DC-SIGN-mediated capture of SARS-CoV-2 pseudotyped lentivirions.

### 3.3.4 Additional SARS-CoV-2 structural proteins do not significantly contribute to Trans-Infection

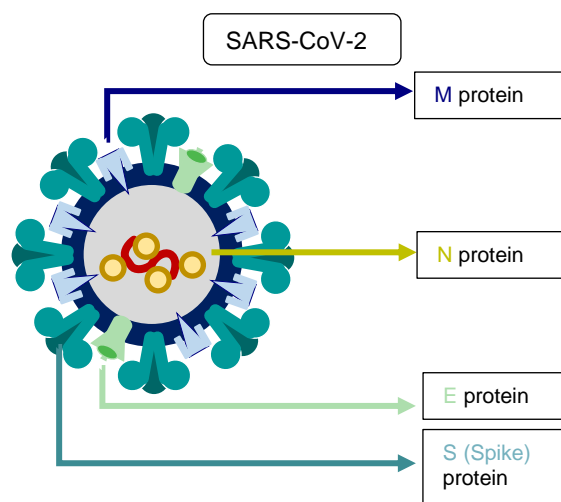
Although HIV lentivirions and SARS-CoV-2 virions share many similar features- both are membrane enveloped virions about 100 nm in diameter with approximately the same number of spike proteins on their surface- they do differ in the number and type of proteins that are incorporated into the final virion [33, 34]. HIV lentivirions only express the gp120/41 Spike Glycoprotein trimers on their surface, with numerous other proteins sequestered inside of the viral particle (Figure 6A).

While the SARS-CoV-2 Spike protein is necessary to dictate the tropism of the virus and mediate the infection process, the nCoV-19 genome also expresses several other structural proteins that are packaged with the SARS-CoV-2 virion. These include: 1) the nucleocapsid protein, N, which interacts with the viral genome, 2) the envelope protein, E, which is expressed on the surface of the virions and is important for maintaining viral pathogenesis, and 3) the membrane protein, M, which is also expressed on the virus surface and can potentially act as an ion channel or a sugar transporter (Figure 6B, 6C, 6D) [78, 89]. As in other coronaviruses, all three structural proteins interact with each other and the spike to facilitate viral budding, protein transport through the Endoplasmic Reticulum, and viral attachment. [38-42]

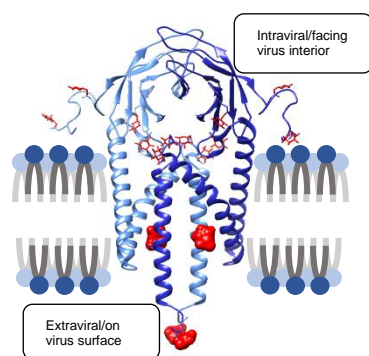
A.)







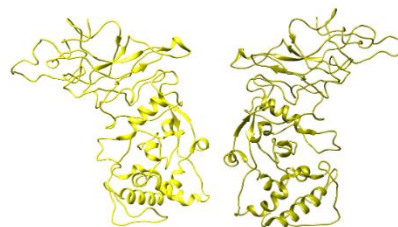
B.)



M protein Sequence

```
MADSNNGTITVEELKKLLEQWNLNLNVIGFLF
LTWICLLQFAYANRNRFLYIIIKLIFLWLL
WPVTLACFVLAAYRINWITGGIAIAMA
CLVGLMWLSYFIASFRLFARTRSMWSF
NPETNILLNVPLHGTILTRPLLESELVIG
AVILRGHLRIAGHHLGRCDIKDLPKEITV
ATSRTLSYYKLGASQRVAGDSGFAAYS
RYRIGNNYKLNTDHSSSSNIALLVQ
```

C.)



N protein Sequence

```
MSDNGPQNQRNAPRITFGGSPDSTGNSQNG
ERSGARSKQRRPQGLPNNTASWFTALTQHG
KEDLKFPRGQGVPINTNSSPDDQIGYRRAT
RRIRGGDGKMKDLSRWYFYLLTGPEAGL
PYGANKDGIIWVATEGALNTPKDHIGTRNPA
NNAAIVLQLPQGTTLPKGFYAEGSRGGSQAS
SRSSSRSRNSSRNSTPGSSRGTSPARMAGN
GGDAALALLLLDRLNQLESKMSGKGQQQQG
QTVTKSAEASKKPRQRTATKAYNVTQAF
GRRGPEQTQGNFGDQELIRQGTDYKHWPQI
AQFAPSASAFFGMSRIGMEVTPSGTWLTYTG
AIKLDDKDPNFKDQVILLNKHIDAYKTFPPTEP
KKDKKKKADETQALPQRQKKQTVTLLPAAD
LDDFSKQLQSSMSSADSTQA
```

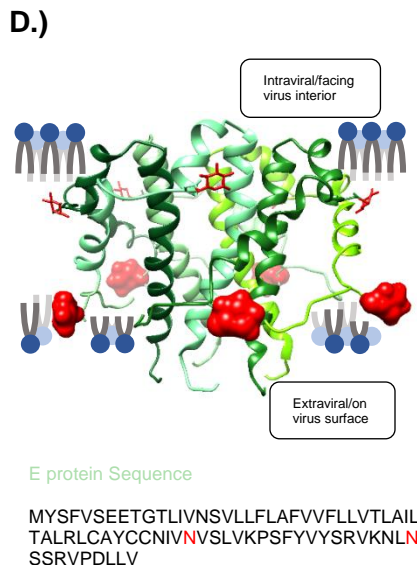


**Figure 6: Structure and glycosylation of the three SARS-CoV-2 structural proteins. (A)** Simplified depiction of SARS-CoV-2 lentiviral pseudovirions (left) versus SARS-CoV-2 coronavirus virions. HIV lentivirions incorporate numerous features into their viral particles, as they must carry the machinery necessary to reverse transcribe the lentiviral RNA genome and incorporate it into the host DNA genome [33]. In contrast, coronavirus particles only incorporate the structural proteins M, N and E in addition to the Spike protein. However, both M and E proteins are present on the surface of coronavirus virions, while the surface of lentiviral pseudovirions are essentially bare of any protein aside from Spike glycoprotein. **(B)** M protein sequence and dimeric structure, with 8 potential N-linked glycosylation sites shown in red. The M protein is the most highly expressed protein on the surface of the SARS-CoV-2 virion and exists as a homodimer. The 2 glycans that are on the extraviral side of the virion and are potentially accessible for DC-SIGN lectin receptor recognition are depicted as space-filling models [78]. The glycan at N216 is on an engineered loop because there was no resolution for the glycan on the PDB structure. PDB ID: 7VGR by Zhang, Z. et. al., unpublished data. **(C)** The N protein exists as a homodimer and is localized to the interior of the virion. It is not anticipated to undergo glycosylation. Rather, it is expected to mediate viral RNA genome packaging and regulating host immune responses [57]. PDB ID: 8FG2 by Casasanta, M. et. al. *Microsc Microanal*, 2022. **(D)** SWISS-Model predicted structure of the SARS-CoV-2 E-protein [79-87]. The E protein exists as a homopentamer on the viral surface and has two expected glycan sites, depicted in red. Glycan N66 is closer to the extraviral side of the viral membrane and is thus depicted as a space filling model in the figure [24, 88].

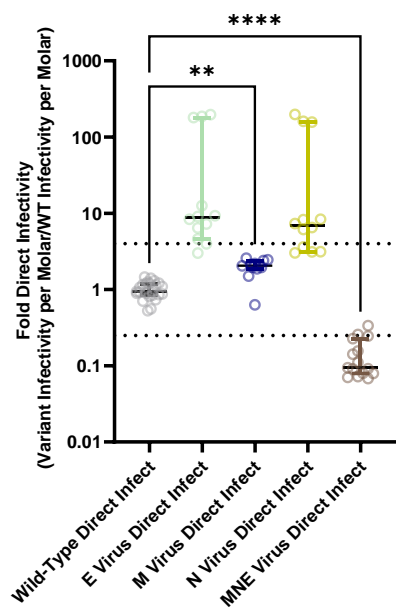
To our knowledge, there is currently no research that has assessed whether the SARS-CoV-2 structural proteins alter DC-SIGN mediated Trans-infection [38, 39]. This is particularly important for adequately modeling the initiation of COVID-19 infection, since SARS-CoV-2 is theorized to rely on attachment and presentation by surface proteins like C-type lectin receptors in order to efficiently infect the low-hACE2-expressing cells of the oral epithelium and respiratory airways [44, 48]. Specific focus is given to the SARS-CoV-2 M and E proteins, as they are both glycosylated proteins on the viral surface and can therefore potentially contribute significantly to SARS-CoV-2 recognition by lectin receptors [40]. The M and E proteins are predicted to have 8 glycosites and 2 glycosites, respectively, although only a subset of these glycans are oriented towards the exterior of the viral particle (Figure 6B, 6D). Regardless, the presence of both the M and E proteins on the surface of the coronaviral virion could

provide significant number of accessible high-mannose glycans for virus recognition, capture, and trans-infection [78].

To ascertain the effect of the M, N, and E proteins on DC-SIGN mediated Trans-infection, four viral strains were produced: three had one additional structural protein incorporated in the SARS-CoV-2 nCoV-19 Wuhan Wild-Type strain lentiviral particle (either M, N, or E protein) (Figure S5A, S5B), and a final strain was produced with all three structural proteins included with the lentiviral system (Figure S5C). To do this, we followed a procedure inspired from recent literature where the additional structural proteins were co-transfected with the vectors necessary for SARS-CoV-2 pseudotyped lentiviral production [39]. As would be expected from previous literature, the addition of these proteins individually appeared to increase hACE2-mediated Direct-infectivity for the pseudovirus (although the wide distribution of infectivity for M and E protein strains meant that we couldn't state that the increased infectivity was statistically significant) (Figure 7A) [39]. On a per molar basis, however, the per molar infectivity of the MNE strain was actually lower than the Wild-Type spike-only strain despite having a much higher raw luciferase signal than the Wild-Type, E, and M strains (Figure 7A, Figure S6A, Figure S6C). This could be explained by how the MNE pseudoviral solution likely also contains a high number of SARS-CoV-2 coronavirus-like particles (cVLPs). The expression of all of the SARS-CoV-2 structural genes is sufficient to generate cVLPs, and even though these cVLPs should not have the ability to package the luciferase transfer sequence, a significant number of the viral particles likely incorporated some p24 protein because its expression was under the strong, constitutively active CMV promoter on the lentiviral backbone vector [38]. This thereby likely artificially increased the estimated molarity of our titered MNE virions (Figure S5A, S5B, Figure S6C).

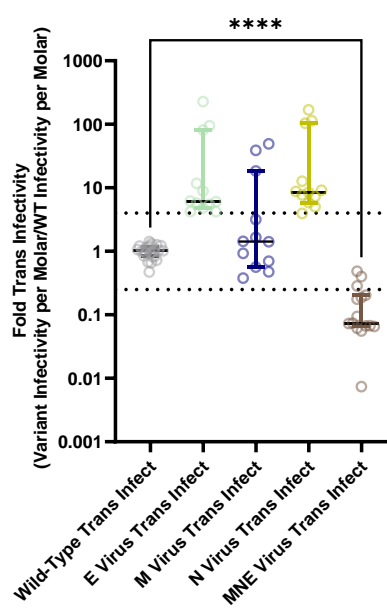
A.)

Accessory Protein Effect on Direct Infectivity



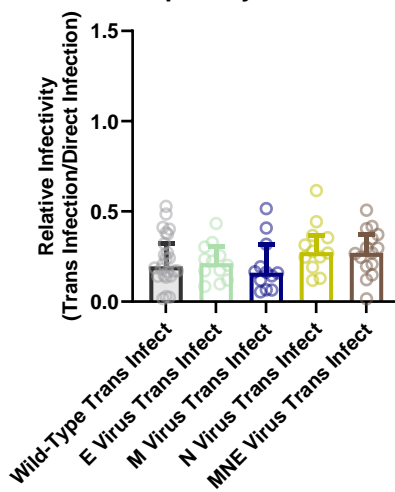
B.)

Accessory Protein Effect on Trans Infectivity



C.)

Strain Propensity for Trans Infection



D.)

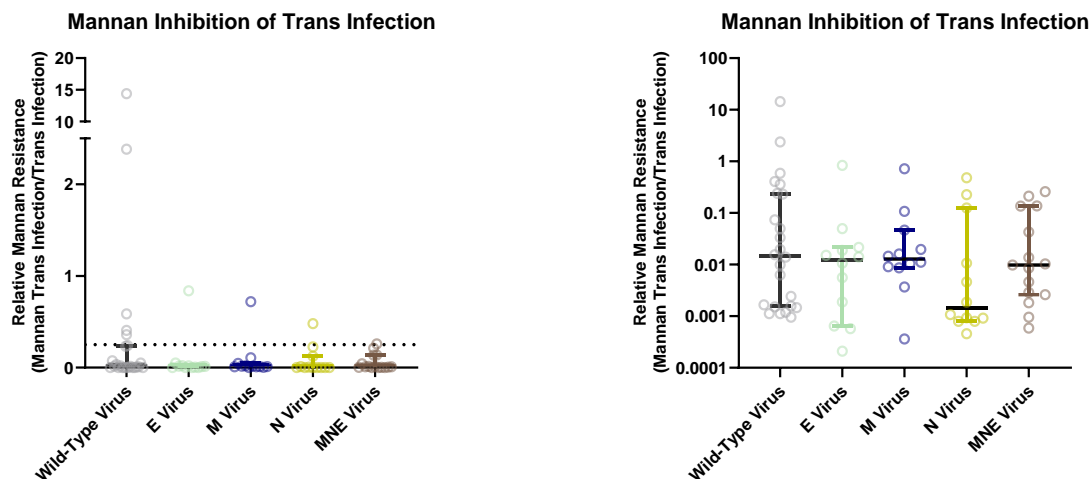


**Figure 7. Structural proteins enhance the ability of SARS-CoV-2 pseudovirus to undergo direct-infection but have no effect on Trans-infection. A.)** Direct-infectivity per mole for each SARS-CoV-2 pseudovirus strain. **B.)** Trans-infectivity per molar for each SARS-CoV-2 pseudoviral strain. **C.)** Each strain's Trans-infectivity signal is normalized to their Direct-infectivity to obtain the strain propensity to undergo Trans-infection. **D.)** To verify that the viral strains were indeed undergoing DC-SIGN mediated trans-infection, experiments were performed in the presence of 20  $\mu\text{g}/\text{mL}$  of mannan. Mannan decreased Trans-infectivity by the same extent for all strains (about 93% inhibition), indicating that the additional SARS-CoV-2 structural proteins do not significantly contribute to DC-SIGN mediated Trans-infection. As above, dashed line indicates 4-fold decrease in infectivity as inspired by previous literature [85]. **A, B, C, D.** Statistical analysis is a Welch ANOVA with an Alpha value of 0.05. \* indicates a P-value < 0.1. \*\* indicates a P-value < 0.01. \*\*\* indicates a P-value < 0.001. \*\*\*\* indicates a P-value < 0.0001.

Running these Structural protein viral strains on the 3t3 DC-SIGN+ cell-mediated Trans-infection assay and normalizing each strain's per Molar luciferase signal (Figure 7B) to their respective hACE2-mediated Direct-infectivity per Molar luciferase signal (Figure 7A) revealed no significant difference between the strains' propensity to undergo Trans-infection (Figure 7C, Figure S7), indicating that there is relatively little interaction between DC-SIGN and the other SARS-CoV-2 surface glycoproteins. This was further supported by the fact that all strains exhibited the same mannann susceptibility, suggesting DC-SIGN-mediated virus binding is not affected by the other structural proteins present (Figure 7D, Figure S8).

### 3.3.5 Additional SARS-CoV-2 structural proteins modulate viral susceptibility to Griffithsin inhibition of hACE2 Direct Infection

At this time, several research articles have been published reporting the antiviral capabilities of Griffithsin against hACE2-mediated direct infectivity of SARS-CoV-2 virions [28-31]. However, a consistent pattern in the literature is that Griffithsin exhibits more potent inhibitory capabilities against SARS-CoV-2 coronaviral virions than SARS-CoV-2 pseudotyped lentiviral virions (Table 1) [28-31]. To our knowledge, there has

been no published work exploring what is responsible for the increased potency of Griffithsin against coronaviral SARS-CoV-2 particles as opposed to SARS-CoV-2 pseudotyped lentiviral particles.

Since Griffithsin inhibition is typically mediated via its binding to glycan sites on viral surface proteins, and since SARS-CoV-2 coronaviral particles express more glycoproteins on the surface than lentiviral virions (including M and E structural proteins in addition to viral Spike protein), we believed that the additional structural proteins could be responsible for the increased vulnerability of the genuine SARS-CoV-2 coronaviral virion to Griffithsin-mediated inhibition. To test this, we utilized the strains of SARS-CoV-2 pseudotyped lentiviral virions that incorporated M, N, E, or MNE proteins as described in section 3.4 (Figure S5). Because previous literature used exclusively WT-Grft, and because WT-Grft gave less variability on our Direct-infectivity assays (see Figure 2C), we exclusively used WT-Grft to assess the effect the additional structural proteins had on the SARS-CoV-2 hACE2-mediated Direct infectivity assay as described in Figure 2B.

Our results indicated that SARS-CoV-2 pseudovirus incorporating the N and E proteins did not display an increased susceptibility to WT-Grft; rather, it seemed as though the N and E proteins increased viral resistance to Griffithsin, with IC<sub>50</sub> values of 5.79  $\mu$ M and 7.96  $\mu$ M, respectively (Figure 8B, 8C). This is not unexpected, as it has been previously shown that the N protein is capable of increasing the infectivity of SARS-CoV-2 pseudotyped lentivirions [39]. Meanwhile, both pseudovirus variants that incorporated M protein in the virion (i.e. pseudovirus with only M protein as the additional structural protein as well as pseudovirus with all three M, N, and E structural proteins incorporated into the pseudovirus) displayed significantly greater susceptibility to WT-Grft inhibition, with IC<sub>50</sub> values of 0.24  $\mu$ M (240.2 nM) and 0.41  $\mu$ M (412.4 nM), respectively (Figure 8A, 8D). These results seem indicate that the M protein is capable of being recognized by Griffithsin, thereby increasing the number of Griffithsin on the surface of the virion and allowing for more potent inhibition. These results largely followed our hypothesis and expectations: given that M protein is the most numerous protein on the surface of the SARS-CoV-2 virion, and it contains multiple accessible putative glycan sites, it is not unexpected that the inclusion of M protein on pseudoviral particles provide multiple epitopes that allow for Griffithsin-based recognition and inhibition [78].

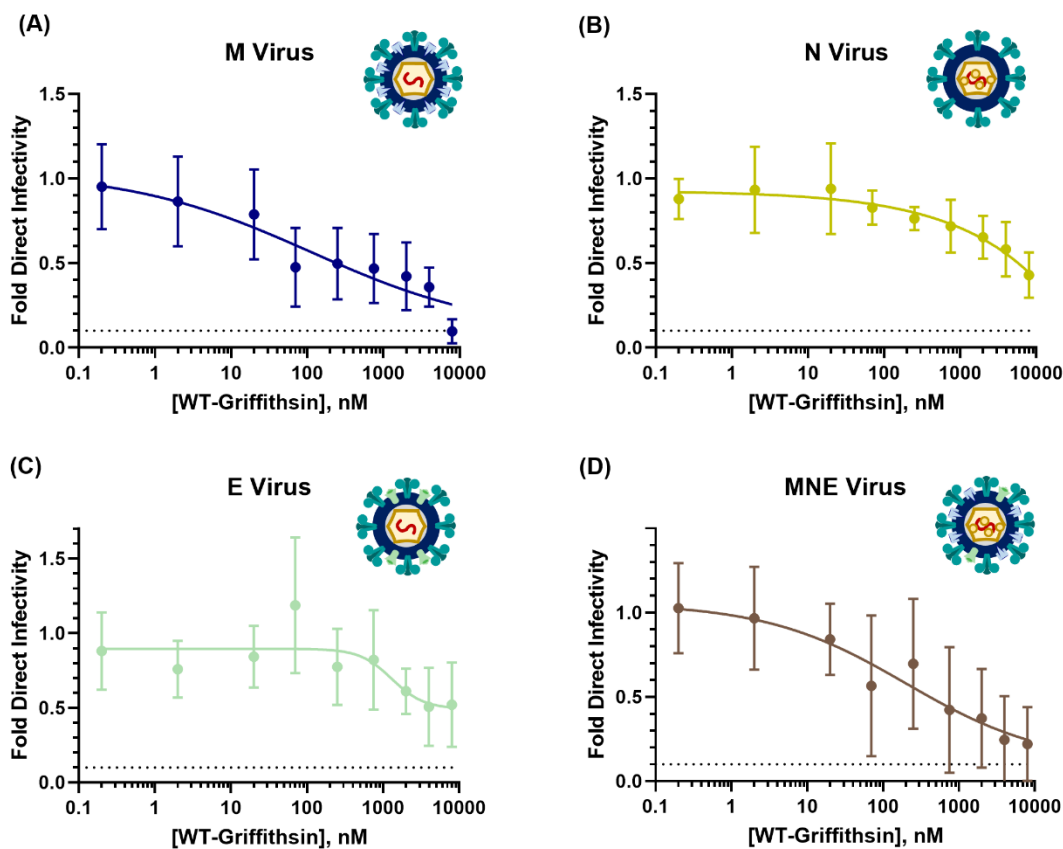


**Figure 8. Structural proteins perform variable roles in enhancing and diminishing the ability of SARS-CoV-2 pseudovirus to be inhibited by Wild-Type Griffithsin.** (A) Inhibition of Direct-infectivity of SARS-CoV-2 pseudovirus strain expressing M protein shows enhanced susceptibility to WT-Grft; IC<sub>50</sub> = 0.24  $\mu$ M. (B) Inhibition of Direct-infectivity of SARS-CoV-2 pseudovirus strain expressing N protein shows diminished susceptibility to WT-Grft; IC<sub>50</sub> = 5.79  $\mu$ M. (C) Inhibition of Direct-infectivity of SARS-CoV-2 pseudovirus strain expressing E protein shows diminished susceptibility to WT-Grft; IC<sub>50</sub> = 7.96  $\mu$ M. (D) Inhibition of Direct-infectivity of SARS-CoV-2 pseudovirus strain expressing all three additional structural proteins M, N, E shows enhanced susceptibility to WT-Grft; IC<sub>50</sub> = 0.41  $\mu$ M. Data were fit with a Four parameter variable slope curve (Graphpad Prism).

### 3.4 Discussion

The rollout of COVID-19 vaccines has led to the abatement of SARS-CoV-2 associated mortality [1, 2]. However, recent strains of the SARS-CoV-2 virus show a remarkable ability to evade immune detection and breakthrough vaccine inhibition; Omicron sublineages have been shown to engender symptomatic infection in patients who had received up to 4 vaccine doses [2]. Thus, it is estimated that COVID-19 will persist as an annual disease, much like the common cold or the seasonal flu [2, 3]. In fact, the Summer of 2023 heralded a surge in COVID-19 infections, coupled with a steady increase in SARS-CoV-2 samples in wastewater [91]. Due to the threat of even mild forms of COVID-19 to lead to breakthrough infections that could eventually yield

fatal respiratory dysfunction, there is still a need to explore broad-spectrum prophylactic options to combat SARS-CoV-2 entry and infection [2, 3, 91].

The Red-algae *Griffithsia* sp.-derived lectin Griffithsin is well-suited to act as a viral inhibitor: Griffithsin is remarkably stable, easy to produce in large quantities, able to be formulated in various materials ranging from liquids to hydrogels to lyophilized powder, is nonimmunogenic, and displays broad antiviral activity [17-20, 92, 93]. Because of these favorable characteristics, Griffithsin is currently in clinical trials as both an anti-HIV-1 and anti- COVID-19 prophylactic treatment [13, 14, 18, 19, 22, 23]. However, because it can undergo spontaneous oxidation at Methionine 78, a variant of Griffithsin with an M78Q mutation was created in order to fulfill the necessary requirement to create a shelf-stable drug that is compliant with approval guidelines for FDA drugs [17, 94]. While the efficacy of M78Q Griffithsin as an antiviral agent was verified in 2019, implying that Q-Grft is an effective therapeutic, we provide proof in this paper that recombinant Q-Grft can be cheaply produced in *E. coli* and does indeed adopt the same overall fold as WT-Grft, as assessed by NMR HSQC. We further found that WT-Grft and Q-Grft displayed similar IC<sub>50</sub> values to each other when tested on an in vitro assay that modeled hACE2-mediated Direct infection, at 2.74  $\mu\text{M}$  and 3.53  $\mu\text{M}$ , respectively.

Another key feature of Griffithsin is that it is a domain-swapped dimer with three carbohydrate binding sites on each monomer, which grants Griffithsin the ability to cross-link viral spike proteins. This cross-linking activity is thought to be crucial in mediating Griffithsin's antiviral potency against HIV-1 pseudovirus infection in vitro [19, 24, 25]. To test whether this phenomenon held true for SARS-CoV-2 pseudovirus inhibition, we produced a constitutive dimer of Griffithsin that had its sugar-binding moieties removed on one of its monomeric domains, thereby preventing this variant from being able to cross-link viral proteins (GLG-3A). In our hands, GLG-3A displayed an IC<sub>50</sub> of 5.03  $\mu\text{M}$ , which is only approximately 1.86-fold higher than WT-Grft's IC<sub>50</sub> and 1.42  $\mu\text{M}$ . Considering how GLG-3A shows 84- to 178-fold higher IC<sub>50</sub> when it was tested on HIV-1 pseudotyped lentiviral Direct inhibition assays, we feel confident in concluding that the cross-linking capability of Griffithsin does not greatly contribute to its inhibitory activity against SARS-CoV-2 pseudotyped lentivirus' hACE2-mediated Direct infection.

During the course of the COVID-19 pandemic, it became apparent that C-type lectin receptors such as DC-SIGN were crucial in mediating SARS-CoV-2 viral infection of cells in the respiratory airways that only modestly express hACE2 [45-49]. Since DC-SIGN exhibits high affinity for binding to the same high-mannose glycans that Griffithsin binds to, we hypothesized that Griffithsin could be a viable inhibitor of DC-SIGN-mediated Trans-infection. To test this, we developed two different Trans-infectivity procedures inspired by previous assessments [59, 62, 63]. When the B-cell lymphoma-derived DC-SIGN+ Raji cell line was used as the virus capture cell line, we found that all three variants of Griffithsin significantly increased DC-SIGN-mediated Trans-infectivity. In contrast, when the murine embryonic fibroblast-derived DC-SIGN+ 3t3 cell line was used as the virus capture cell line, we found that all three variants of Griffithsin did not appreciably enhance or inhibit DC-SIGN-mediated SARS-CoV-2 pseudoviral Trans-infectivity.

A possible explanation for why Griffithsin seems to enhance DC-SIGN+ Raji cell-mediated Trans-infectivity could be that Griffithsin could cross-link SARS-CoV-2 virions



together to such an extent that the clustered virus particles are able to be pelleted during the centrifugation steps of the Raji Trans-infection assay. However, this would not explain how the GLG-3A variant of Griffithsin (which is incapable of cross linking) is able to also enhance viral infectivity. Since Raji cells are derived from B cells, which are active immune cells, they could be capable of binding to viral pathogen epitopes via Toll-like Receptors, B cell Receptors, or Complement Receptors and undergoing activation [73, 74, 95]. Raji cells specifically express an excess of cell surface receptors when compared to standard B cells, indicating that there is a distinct possibility that they express enough surface receptors to enable T-cell independent antigen responses [73, 75, 76]. B cells are also activated by lectins that bind to fucose, leading to cell differentiation and the secretion of both pro- and anti-inflammatory molecules [96]. Unfortunately, DC-SIGN is a lectin that is capable of binding to fucose, further complicating the possible processes that might be affecting the Raji cells in our assay [97]. Activated B cells express and secrete antiviral molecules such as Granzyme B, which could in turn impede SARS-CoV-2 pseudoviral entry of hACE2+ HEK-293T cells on the Trans-assay [73, 74]. Alternatively, Griffithsin could protect virions from these proteases, making it appear as though the SARS-CoV-2 pseudovirus infectivity is enhanced by the presence of Griffithsin. Finally, Raji cells have recently been discovered to undergo phagocytosis of pathogens, a function that flies in the face of previously-established convention regarding the role of B cells [98]. Thus, Griffithsin could enhance infectivity by preventing SARS-CoV-2 pseudoviruses from being recognized and phagocytosed by Raji cells. In short, B cells engage in numerous different functions and roles within the mammalian body, and so there are many confounding variables that could explain why Raji cells- as a B cell derived cell line- could undergo Griffithsin-enhanced Trans-infectivity of SARS-CoV-2 pseudotyped virions [99]. All of this served as strong justification for us to move from performing the Raji cell Trans assay to the 3t3 cell Trans assay.

We performed the 3t3 cell Trans assay in a manner inspired by recently-published work in our lab [59]. However, to ascertain whether Griffithsin interaction with SARS-CoV-2 pseudotyped virions or Griffithsin interaction with DC-SIGN was responsible for enhancing Trans-infection, we performed the assays pre-incubating the Griffithsin variants with either the 3t3 DC-SIGN+ cells or with virus samples. In the end, it appeared that pre-incubating all variants of Griffithsin (WT-Grft, Q-Grft, and GLG-3A) with virus or with DC-SIGN+ cells had no affect the ability of SARS-CoV-2 pseudotyped virions to undergo Trans-infection.

When the data from both kinds of Trans-assay were taken together, the evidence seems to suggest that at the very least, Griffithsin does not act as a viable inhibitor of SARS-CoV-2 DC-SIGN-mediated Trans-infection. Since there are 22 putative glycan sites on each monomer of the SARS-CoV-2 Spike protein, it highly likely that even if Griffithsin blocks DC-SIGN from binding a particular glycan, DC-SIGN can easily shift from binding one glycan to binding to another [48]. Also, Griffithsin does not have high affinity for fucose, meaning that DC-SIGN could still facilitate Trans-infection via binding to fucosylated glycans [57, 96, 97].

We also noticed a consistent trend in the literature whereby Griffithsin seemed to exhibit better inhibitory capabilities against genuine SARS-CoV-2 coronaviral particles than SARS-CoV-2 pseudotyped lentivirions (Table 1). When tested against SARS-CoV-2 pseudotyped lentiviral virions, these studies found that WT-Grft displayed a half-

maximal inhibitory concentration of 1.61  $\mu\text{M}$ , 293 nM and 511 nM, respectively [28-30]. These values are at least one order of magnitude poorer than WT-Grft's ability to inhibit other viruses such as HIV, SIV, Hepatitis C, or Japanese Encephalitis Virus [32]. In addition, the researchers who found the half-maximal inhibitory concentration of WT-Grft against authentic SARS-CoV-2 coronavirus to be 33.2 nM calculated the dissociation constant between WT-Grft and SARS-CoV-2 Spike protein to be 1.6-9.9  $\mu\text{M}$ , indicating Griffithsin did not have strong binding affinity for the SARS-CoV-2 Spike protein. For the two papers where SARS-CoV-2 pseudotyped lentivirus and authentic SARS-CoV-2 virions were assessed on comparable in vitro assays, it was reported that Wild Type-Griffithsin had a 4.65-fold to 5.10-fold better inhibitory capability against SARS-CoV-2 coronavirus verses SARS-CoV-2 lentiviral particles [29, 30].

Unlike lentiviral pseudovirions- which only express the SARS-CoV-2 Spike protein on their surface- SARS-CoV-2 coronaviral particles also express the M and E structural proteins on their surface. It has already been established that the addition of N protein can significantly increase the hACE2 mediated infectivity of SARS-CoV-2 pseudovirions, while the M and E proteins appeared to have no significant impact on pseudoviral Direct-infectivity [39]. However, because M and E are glycosylated membrane-embedded proteins, we theorized they could act as targets for Griffithsin-mediated viral inhibition. Notably, M is the most abundant protein on the surface of the SARS-CoV-2 virion, meaning it theoretically provides the majority of N-linked glycan epitopes on the surface of the virion [78]. Using data from three other coronaviruses (SARS-CoV-1, Mouse Hepatitis virus, and Feline coronavirus), it is estimated that the SARS-CoV-2 particle expresses  $\sim 1100$  M protein dimers on its surface [100]. Based off of our understanding of the accessible glycans on the M protein dimer, we therefore estimate that there are about 4400 N-linked glycan epitopes on the SARS-CoV-2 virus surface due to the M protein (Figure 6B). For comparison, there are about 1716 N-linked glycans from the  $\sim 26$  Spike trimers predicted to be on the surface of the SARS-CoV-2 virion [35]. Ergo, there are about 2.56-fold more N-linked glycans from the M protein than from the Spike protein, meaning that the presence of the M protein could significantly increase the ability of Griffithsin to bind to the virus particle. Indeed, we found that when the M protein was expressed and likely incorporated into the SARS-CoV-2 pseudoviral virion, the IC<sub>50</sub> of WT-Grft on our Direct-infectivity assays decreased by about an order of magnitude, strongly suggesting that Griffithsin inhibits genuine SARS-CoV-2 coronaviral infection by binding to the M structural proteins on the virion in addition to the Spike protein (Figure 8A, 8D).

We also found that the addition N and E proteins decreased the susceptibility of SARS-CoV-2 pseudotyped lentivirions to Griffithsin-mediated inhibition of Direct-infectivity (Figure 8B, 8C). This was somewhat expected for the N protein strain pseudovirus: previous literature reported that the inclusion of N protein in SARS-CoV-2 pseudotyped lentivirions significantly increased the infectivity of pseudotyped lentivirus [39]. We saw a similar phenomenon in our Direct-infectivity assays, although the change in infectivity was not drastic enough to constitute a significantly higher infectivity (Figure 7A).

On the other hand, the E protein has the lowest amount of integration into the genuine SARS-CoV-2 coronaviral particle [101]. In existing literature, the E protein did not appear to substantially increase pseudotyped lentivirus Direct-infectivity; however, in our hands, the E protein appeared to induce a similar increase in Direct Infectivity as the

N protein when incorporated into SARS-CoV-2 pseudotyped lentivirus [39]. Hence, it stands to reason that the E protein's ability to enhance viral infectivity could allow SARS-CoV-2 pseudotyped virions to efficiently infect cells despite the presence of Griffithsin.

Finally, we assessed whether the additional structural proteins could enhance the Trans-infectivity of SARS-CoV-2 pseudovirions. Again, since both the M and E proteins are membrane-embedded glycoproteins, we initially hypothesized that DC-SIGN could recognize epitopes on these structural proteins in addition to the Spike protein, thereby contributing to greater Trans-infection capability. While incorporation of the N and E protein into the SARS-CoV-2 pseudovirion appeared to marginally increase Direct-infectivity, the propensity for the virus to undergo Trans-infection remained largely unchanged (Figure 7C). This was not surprising, since the N protein is localized to the interior of the virion, it is thus unable to be recognized by cell surface receptors; similarly, E protein is poorly expressed and incorporated on the surface of viral particles, meaning that it wouldn't provide that drastic of an increase in epitopes on the surface of the virion [101].

Unexpectedly, the presence of M protein did not appear to enhance the propensity of pseudotyped virions to undergo DC-SIGN mediated Trans infection at all (Figure 7C). Even when all three additional structural proteins were expressed together, the MNE strain pseudotyped virus displayed no difference in its propensity to undergo DC-SIGN mediated Trans infection. Taken together, we posit that while Griffithsin favors binding to the M protein, DC-SIGN instead primarily interacts with the glycans on the Spike protein. Thus, this would explain why the addition of M protein does not enhance Trans-infectivity and why Griffithsin is not an effective inhibitor of DC-SIGN mediated Trans-infection.

For future studies, we aim to assess whether Griffithsin has any ability to prevent viral Trans-infectivity by other attachment receptors that bind to sugar moieties (such as SIGLEC1 and L-SIGN) [46]. Furthermore, it is important to perform more biophysical assessments to verify whether Griffithsin truly has high affinity for the additional SARS-CoV-2 structural proteins, especially the M protein.

### **3.5 Methods and Materials**

#### **3.5.1 DNA Construction**

The gene encoding the Wild-Type Griffithsin (WT-Grft) protein (with an Alanine at position 31 to substitute a non-standard amino acid and an N-terminal 6xHis tag) was cloned into the pET15-b expression vector (Novagen, Madison, WI, USA) between the NcoI and BamHI restriction sites as described previously [16, 57].

The gene sequence for M78Q Griffithsin (Q-Grft) with an N-terminal 6xHis tag and a Methionine to Glutamine substitution at position 78 was ordered from Twist Biosciences already inserted into the pET28b vector between the NcoI and XhoI restriction sites.

The gene sequence for Griffithsin – linker – Griffithsin One armed (GLG-3A) was created by first ordering the gene sequence for M78Q Griffithsin with an N-terminal

6xHis tag and a C-terminal linker with a BamHI site inserted into the pET28b vector between the NcoI and XhoI restriction sites (Twist Bioscience, South San Francisco, CA, USA). Then the gene sequence for M78Q Griffithsin with an N-terminal BamHI site and Aspartate to Alanine mutations at positions 30, 70, and 112 inserted into the pET28b vector between the NcoI and XhoI restriction sites (again from Twist Bioscience). Both vectors were then digested with BamHI and XhoI. The M78Q Griffithsin sequence with D30A/D70A/D112A mutations was then inserted into the vector with the N-terminal 6xHis tagged M78Q Griffithsin sequence to yield a pET28b vector with N-terminal 6xHis tagged M78Q Griffithsin – linker – M78Q Griffithsin D30A/D70A/D112A. The linker sequence is as follows: SSSGGGGSGGGSSSGS.

The gene encoding for Monomeric Griffithsin protein (with a 1GS insertion at positions 18 and 19, and the Leucine at position 2 substituted for a Serine) with an N-terminal 6xHis tag was inserted into the pET28b vector between the NcoI and XhoI restriction sites [58].

### 3.5.2 Protein Production and Purification

All proteins were produced as described previously [16]. Briefly, plasmids of Griffithsin variants described above were transformed into BL21-Gold (DE3) Competent Cells (Agilent Technologies Catalog # 200131, Santa Clara, CA, USA). Once flasks reached an optical density at 600 nm (OD600) of 0.50 to 0.75, protein production was induced with 0.6 mM of isopropyl  $\beta$ -d-1-thiogalactopyranoside (IPTG, Millipore Sigma OmniPur–Calbiochem, Catalog # 5820, Burlington, MA, USA) and allowed to further incubate at 37 °C for 6 to 10 hours.

After incubation, cells were harvested at 6000  $\times$  g for 10 min, and the pellet was re-suspended in Resuspension Buffer (6 M Guanidine hydrochloride, 200 mM NaCl, 10 mM Benzamidine, and 50 mM Tris, pH 8). The solution was French pressed two to three times at 16,000 lb/in<sup>2</sup>, and then centrifuged at 13500  $\times$  g for 1 hour. The soluble portion was loaded onto a Ni chelating column (Qiagen Catalog # 30210, Germantown, MD, USA) equilibrated with the same Resuspension Buffer. The Nickel columns were washed with Washing Buffer (6 M Guanidine hydrochloride, 200 mM NaCl, and 50 mM Sodium Phosphate, pH 7) to remove nonspecifically bound proteins. Bound Griffithsin was eluted from columns with Elution Buffer (6 M Guanidine hydrochloride, 200 mM NaCl, and 50 mM Sodium Acetate, pH 3). Griffithsin proteins were refolded by dropwise addition into 10x greater volume of chilled Refold buffer (550 mM L-Arginine, 200 mM NaCl, 50 mM Tris, 1 mM EDTA, pH 8). The protein was allowed to refold for 12 hours at 4 °C before the solution was dialyzed twice in 4 Liters of 150 mM NaCl, 20 mM Tris, pH 8 at 4 °C for 6-12 hours each. The protein solution was then dialyzed four times against 4 Li-ters of 50 mM NaCl, 10 mM Tris, pH 8 at 4 °C for 6-12 hours each.

The protein was purified on a C4 reversed-phase chromatography column (Vydac, Hesperia, CA, USA). The Griffithsin constructs were purified on a gradient of Water with 0.1% Trifluoroacetic Acid as the counterion (Buffer A) to Acetonitrile with 0.1% Trifluoro-acetic Acid as the counterion (Buffer B). The loading solution for the C4 column was 92% Buffer A, 8% Buffer B. Griffithsin constructs tended to elute at approximately 70% Buffer A, 30% Buffer B. After C4 reversed-phase chromatography, elution fractions containing Griffithsin were pooled and lyophilized in a Labconco freeze-dry system for long-term storage. All samples were analyzed by sodium dodecyl sulfate-

polyacrylamide gel electrophoresis (SDS-PAGE) at each step of purification to confirm the proper size of the specific Griffithsin construct.

### 3.5.3 Nuclear Magnetic Resonance (NMR) Spectroscopy

Griffithsin variants were expressed in M9 minimal media with  $15\text{NH}_4\text{Cl}$  as the sole nitrogen source following the protocol described above. After proteins were lyophilized, the Wild-Type Griffithsin, M78Q Griffithsin, and Griffithsin-Linker-Griffithsin One Armed were resuspended in 20 mM Sodium phosphate, pH 7 buffer. Monomeric Griffithsin did not efficiently dissolve in pH 7 buffer, so it was initially resuspended in 20 mM Sodium Phosphate, pH 2.5 buffer. This was then diluted with an equal volume of 20 mM Sodium Phosphate, pH 9 buffer to obtain a final pH that varied between 6.62 to 6.96.

The sample of protein was then taken to 5% D<sub>2</sub>O and 2,2-dimethyl-2-silapentane-5-sulfonic acid (DSS, Cambridge Isotope Laboratories Inc., Catalog # DLM-32-10, Tewksbury, MA, USA) was added for calibration. Spectra were collected at 25°C on a four-channel 600-MHz Bruker Avance III spectrometer. Data were processed using NMRPipe as described previously [24].

### 3.5.4 Cell Lines

All cell lines were maintained in T-75 flasks (Stellar Scientific Cat # SKU:TC30-120, Baltimore, MD, USA) placed in a 37°C humidified incubator (ThermoFisher NAPCO Series 8000DH CO<sub>2</sub> Incubator, Catalog # 7003584, Waltham, MA, USA) with 4.5% CO<sub>2</sub>. These cells include:

- HEK-293FT (Homo sapiens, embryonic kidney cells; a generous gift from Dr. David Gravano, University of California, Merced).
- HEK-293T cells expressing Human Angiotensin-Converting Enzyme 2/hACE2 (Homo sapiens, embryonic kidney cells; obtained through BEI Re-sources, NIAID, NIH: Human Embryonic Kidney Cells [HEK-293T] Express-ing Human Angiotensin-Converting Enzyme 2, HEK-293T-hACE2 Cell Line, NR-52511).
- 3t3 Wild-Type Cells (Mus musculus, mouse embryonic fibroblasts; obtained through the NIH HIV Reagent Program, Division of AIDS, NIAID, NIH: NIH-3T3 Cells, ARP-9946, contributed by Drs. Thomas D. Martin and Vineet N. KewalRamani).
- 3t3 DC-SIGN+ Cells (Mus musculus, mouse embryonic fibroblasts; obtained through the NIH HIV Reagent Program, Division of AIDS, NIAID, NIH: NIH 3T3 DC-SIGN+ Cells, ARP-9947, contributed by Drs. Thomas D. Martin and Vineet N. KewalRamani).
- Raji Wild-Type Cells (Homo sapiens, Epstein Barr Virus (EBV)-positive Bur-kitt lymphoma line originally obtained from the American Type Culture Collection (ATCC); obtained through the NIH HIV Reagent Program, Division of AIDS, NIAID, NIH: Raji Cells, ARP-9944, contributed by Drs. Li Wu and Vineet N. KewalRamani).

- Raji DC-SIGN+ Cells (Homo sapiens, Epstein Barr Virus (EBV)-positive Burkitt lymphoma line originally obtained from the American Type Culture Collection (ATCC); obtained through the NIH HIV Reagent Program, Division of AIDS, NIAID, NIH: Raji Cells, ARP-9945, contributed by Drs. Li Wu and Vineet N. KewalRamani).

HEK-293FT Cells and HEK-293T hACE2+ Cells were cultured in Dulbecco's Modified Eagle Medium (DMEM) (ThermoFisher Catalog # 11965-092, Waltham, MA, USA) supplemented with 25 mM HEPES (ThermoFisher Catalog # 11344041, Waltham, MA, USA), 2 mM L-glutamine (R&D Systems Catalog # R90010, Minneapolis, MN, USA), 250 µg mL<sup>-1</sup> G418 Sulfate (Corning Life Sciences Catalog # 30-234-CI, Tewksbury, MA, USA), and 10% Fetal Bovine Serum (R&D Systems Catalog # S11150, Minneapolis, MN, USA). This media is heretofore referred to as 293 Media. Both HEK-293FT Cells and HEK-293T hACE2+ Cells were cultured as adherent monolayers in T-75 flasks.

3t3 cells were chosen because they have been demonstrated to be deficient in a variety of lectin receptors, including DC-SIGN (CD209), LOX1 (OLR1), and CLEC family proteins, as according to a gene expression database (NIH3t3 cells, Harmonizome.com, [https://maayanlab.cloud/Harmonizome/gene\\_set/nih+3T3/BioGPS+Mouse+Cell+Type+and+Tissue+Gene+Expression+Profiles](https://maayanlab.cloud/Harmonizome/gene_set/nih+3T3/BioGPS+Mouse+Cell+Type+and+Tissue+Gene+Expression+Profiles)) [58]. Furthermore, they have been shown to not be permissive to SARS-CoV-2 pseudoviral infection [59]. 3t3 Wild-Type Cells and 3t3 DC-SIGN+ Cells were cultured in DMEM supplemented with 2 mM GlutaMAX (ThermoFisher Cat # 35050-061, Waltham, MA, USA), 100 U mL<sup>-1</sup> of Penicillin-Streptomycin solution (Cytiva HyClone Cat # SV30010, Marlborough, MA, USA), and 10% Fetal Bovine Serum (R&D Systems Cat # S11150, Minneapolis, MN, USA). This media is heretofore referred to as 3t3 Media. Both 3t3 Wild-Type Cells and 3t3 DC-SIGN+ Cells were cultured as adherent monolayers in T-75 flasks.

Raji cells were chosen because the paired Raji Wild-Type and Raji DC-SIGN+ cell lines have been a workhorse strain in viral Trans infection assays [60-63]. Both Raji Wild-Type Cells and Raji DC-SIGN+ Cells were maintained in T-75 flasks within a 37°C humidified incubator at 4.5% CO<sub>2</sub>. Raji Wild-Type Cells and Raji DC-SIGN+ Cells were cultured in Roswell Park Memorial Institute 1640 Medium (RPMI) (ThermoFisher Cat # 11875-085, Waltham, MA, USA) supplemented with 100 U mL<sup>-1</sup> of Penicillin-Streptomycin solution (Cytiva HyClone Cat # SV30010, Marlborough, MA, USA), and 10% Fetal Bovine Serum (R&D Systems Cat # S11150, Minneapolis, MN, USA). This media is heretofore referred to as Raji Media. Both Raji cell lines were cultured as suspension cells in upright T-75 flasks.

When a flask reached 80-95% confluency, adherent cells (HEK-293FT, HEK-293T hACE2, 3t3 Wild-Type, and 3t3 DC-SIGN+ Cells) were passaged 1:10 with 0.05% Tryp-sin-EDTA (ThermoFisher Cat # 25300-062, Waltham, MA, USA) used to detach cells from surface of flasks. Trypsin was not permitted to exceed a contact time of 5 minutes for any cell line.

When Raji Wild-Type Cells or Raji DC-SIGN+ Cells reached a density of 5 × 10<sup>6</sup> cells per mL, cells were split by diluting 10-fold in fresh Raji medium.

All cell lines were used within 1.5 months from being revived to minimize the likelihood that cell protein expression changed.

### 3.5.5 Pseudovirus Production

Pseudovirus plasmids were obtained through BEI Resources, NIAID, NIH. SARS-CoV-2 spike plasmids were originally purchased from Addgene and were mutated as described above. SARS-CoV-2 spike pseudotyped HIV virions were produced in a protocol inspired by Crawford et al., 2020 [64]. Briefly, HEK-293FT cells were maintained in 293 Media and passaged once cells reached 70-100% confluency. The day prior to transfection, HEK-293FT cells were seeded at a density of approximately  $2.5 \times 10^6$  cells in 8-10 mL of 293 Media into a 100 mm tissue culture petri dish or approximately  $0.2 \times 10^6$  cells in 2-3 mL of 293 Media into a 6-well tissue culture plate (batches of virus were made in either of the two plate types). Cells were allowed to recover for 12-16 hours in a humidified incubator at 37 °C and 5% CO<sub>2</sub>.

Petri dishes/6-well plates were then withdrawn from incubators and cells were assessed for confluency and adhesion. If the cells in petri dishes were 70% confluent and adherent, media was gently replaced with 8 mL of fresh 293 Media. If the cells in 6 well plates were 70% confluent and adherent, media was gently replaced with 3 mL of fresh 293 Media. The petri dish/6-well plate was returned to the incubator for approximately 45 minutes while the plasmids and transfection reagent were prepared. For a 100 mm petri dish, the following plasmids were mixed in 900  $\mu$ L of serum-free commercial DMEM in a sterile 1.5 mL centrifuge tube: 5  $\mu$ g of lentiviral backbone Luciferase-IRES-ZsGreen (BEI Resources NR-52516, Manassas, VA, USA) vector, 1.1  $\mu$ g each of vectors HDM-Hgpm2 (BEI Resources NR-52517, Manassas, VA, USA), pRC-CMV-Rev1b (BEI Resources NR-52519, Manassas, VA, USA) and HDM-tat1b (BEI Resources NR-52518, Manassas, VA, USA), and 1.7  $\mu$ g of vector pCMV14-3X-Flag-SARS-CoV-2 S (Addgene Cat # 145780, Watertown, MA, USA). For a 6-well tissue culture plate, the same plasmids were mixed in 185  $\mu$ L of serum-free commercial Dulbecco's Modified Eagle Medium in a sterile 1.5 mL centrifuge tube: 1  $\mu$ g of lentiviral backbone Luciferase-IRES-ZsGreen (BEI Resources NR-52516, Manassas, VA, USA) vector, 0.22  $\mu$ g each of vectors HDM-Hgpm2 (BEI Resources NR-52517, Manassas, VA, USA), pRC-CMV-Rev1b (BEI Resources NR-52519, Manassas, VA, USA) and HDM-tat1b (BEI Resources NR-52518, Manassas, VA, USA), and 0.34  $\mu$ g of spike vector pCMV14-3X-Flag-SARS-CoV-2 S (Addgene Cat # 145780).

Pseudovirus with additional structural proteins were exclusively produced in 100 mm petri dishes. To do so, 1.7  $\mu$ g of desired M, N, or E protein vector was added to the transfection mixture specified above: pcDNA3.1 SARS-CoV-2 M (Addgene Cat # 158078), pcDNA3.1 SARS-CoV-2 N (Addgene Cat # 158079), pcDNA3.1 SARS-CoV-2 E (Addgene Cat # 158080), respectively.

When creating MNE virus/pseudovirus with all three structural proteins incorporated in the virion, 1.7  $\mu$ g of each additional structural protein vector described above was added to the transfection mixture.

After adding all plasmids, the solution was mixed by pipetting up and down approximately 10 times. For 100 mm petri dish samples, 30  $\mu$ L of XtremeGENE HP Version 9 (Roche Cat # 06366546001, Mannheim, Germany) was then added directly to the solution. When making MNE virus/pseudovirus with all three additional structural

proteins, 40  $\mu$ L of XtremeGENE HP Version 9 was added to the solution instead. For 6-well tissue culture plate samples, 8  $\mu$ L of XtremeGENE HP Version 9 was added directly to the solution. The contents of the tube were again mixed by gently tapping approximately 10 times before being allowed to incubate at room temperature for 20-25 minutes. The petri dish/6-well plate was then retrieved from the 37 °C incubator and the DNA + Xtreme-GENE HP mixture was dripped over the HEK 293FT cells. The transfected HEK 293FT cells were then returned to the incubator and allowed to recover for 12-18 hours overnight. After 12-18 hours, petri dishes/6-well plates were again removed from the incubator and the cell media was gently replaced with fresh prewarmed 293 Medium (10 mL for 100 mm petri dishes, 4 mL for 6-well plates). Transfected cells were returned to the incubator. After an additional 48 hours (60-66 hours total post-transfection), petri dishes were re-moved from the incubator and the medium was gently removed and transferred to a 15 mL tube. This 15 mL tube was then briefly centrifuged at 105  $\times$  g for 3 minutes to pellet any large cell clumps. The supernatant was filtered through a 0.45  $\mu$ m syringe filter and stored as 450  $\mu$ L aliquots in low-binding 1.5 mL tubes (ThermoFisher Cat # 90410, Waltham, MA, USA). Aliquots were stored at -75 °C until use in future assays.

### 3.5.6 Pseudovirus Titration

SARS-CoV-2 pseudovirus pseudotyped with Wild-Type SARS-CoV-2 3xFlag Spike protein was produced multiple times to ensure results were not due to batch-to-batch variation. Similarly, SARS-CoV-2 pseudovirions with additional structural proteins were produced at least twice, yielding at least two batches of pseudovirus to ensure results were not due to batch-to-batch variation. Every batch of virus was titrated using an XpressBio p24 ELISA kit plate carried out according to the manufacturer's instructions (XpressBio Cat # XB-1000, Frederick, MD, USA). The levels of p24 in each well were measured on a ClarioStar Plus microplate reader set to 450 nm (BMG Labtech, Ortenberg, Germany).

### 3.5.7 Virus Direct-Infectivity Assays

On day 1, each well of a clear 96-well cell-culture plate was coated with 25  $\mu$ L of 0.1 mg/mL poly-L-lysine (ScienCell Research Laboratories, Cat # 0413, Carlsbad, CA, USA). The plate was returned to the 37 °C incubator for 1 to 36 hours. After this time, the 96-well plate was removed from the incubator and the poly-L-lysine solution was pipetted out. Wells were then rinsed twice with 40  $\mu$ L of sterile, ultrapure deionized water before being set aside in preparation for seeding.

After wells were prepped, 15000-25000 of HEK 293T-hACE2+ cells were seeded in triplicate into the wells of a pre-prepared poly-L-lysine conditioned 96 well plate. As a control, at least three wells were seeded with 15000-25000 HEK-293FT cells. The 96-well plate was returned to the 37 °C humidified incubator at 4.5% CO<sub>2</sub> in order to allow the HEK-293 cells to adhere and recover for 8-12 hours.

While cells recovered, Griffithsin proteins were resuspended in sterile commercial Phosphate-Buffered Saline (PBS) (ThermoFisher Cat # 14190-136,



Waltham, MA, USA) to create a stock solution. Griffithsin protein was serially diluted in PBS for inhibition assay.

After cells had recovered, the 96-well plate was retrieved from the incubator and the media was gently pipetted out of wells. Within 1 minute of pipetting out media, 20  $\mu$ L of fresh 293 media was added to the wells to prevent the cells from desiccating. Then 20  $\mu$ L of the requisite Griffithsin protein dilution in PBS was added in triplicate to wells. Wells were allowed to equilibrate for 10 minutes, then 20  $\mu$ L of the requisite SARS-CoV-2 pseudo-virus variant was added to the wells. Then the 96-well plate was returned to the 37 °C humidified incubator at 4.5% CO<sub>2</sub> in order to allow the HEK-293 cells to adhere and re-cover.

12-16 hours later, the 96-well plate was retrieved from the humidified incubator and 150  $\mu$ L of fresh, pre-warmed 293 Medium was added over the top of each well to ensure that cells remained alive and viable for the duration of the experiment. The 96-well plate was returned to the 37 °C incubator for an additional 36 to 48 hours.

After 36-48 hours, the 96-well plate was retrieved from the humidified incubator. Bright-Glo Luciferase Reagent (Promega Corp., Cat # E2610, Madison, WI, USA) was thawed out and kept wrapped in foil until use. 160-180  $\mu$ L of the medium in each of the infectivity plate wells was pipetted out, leaving about 30  $\mu$ L of the medium in each well after accounting for evaporation during the course of the experiment. 30  $\mu$ L of Bright-Glo reagent was added over the top of the wells and given 2-4 minutes to lyse cells. The contents of each well were then transferred to a white-backed 96-well plate and luciferase signal was again read on a ClarioStar Plus microplate reader with a 3600 gain and a 1 second normalization time. All samples were run in triplicate with at least two separate biological replicates for each condition.

### **3.5.8 Virus Direct-Infectivity Control Assays of Raji Cells**

For Direct-infectivity controls for Raji cells, 96-well plates were prepped with poly-L-lysine as described above. Then 15000-25000 cells of HEK 293T-hACE2+ cells in 100  $\mu$ L and 15000-25000 cells of either Raji DC-SIGN+ cells or Raji Wild-Type cells in 100  $\mu$ L were seeded in triplicate into the wells of a pre-prepared poly-L-lysine conditioned 96 well plate and allowed to recover for 8-12 hours in a 37 °C humidified incubator at 4.5% CO<sub>2</sub>. This allowed for HEK 293T-hACE2+ cells to adhere to wells and Raji cells to fall to bottom of wells. Then 50  $\mu$ L of media was gently removed from wells. From our observations, although the Raji cells did not appear to adhere to wells, they did not move from the bottom of the wells when we removed media. Then 50  $\mu$ L of SARS-CoV-2 pseudo-virus solution was added over the top of the wells. Then the 96-well plate was returned to the 37 °C humidified incubator at 4.5% CO<sub>2</sub> in order to allow the HEK-293 cells and Raji cells to undergo infection.

12-16 hours later, the 96-well plate was retrieved from the humidified incubator and 150  $\mu$ L of fresh, pre-warmed 293 Medium was added over the top of each 293T-hACE2+ well. 150  $\mu$ L of fresh, pre-warmed Raji Medium was added over the top of each Raji DC-SIGN+/Raji Wild-Type well. This was to ensure that cells remained alive and viable for the duration of the experiment. The 96-well plate was returned to the 37 °C humidified incubator for an additional 36 to 48 hours.

After 36-48 hours, the 96-well plate was retrieved from the humidified incubator. Bright-Glo Luciferase Reagent (Promega Corp., Cat # E2610, Madison, WI, USA) was thawed out and kept wrapped in foil until use. 160-180  $\mu\text{L}$  of the medium in each of the infectivity plate wells was pipetted out, leaving about 30  $\mu\text{L}$  of the medium in each well after accounting for evaporation during the course of the experiment. Empirically, Raji cells did not appear to move when we gently removed media from wells. 30  $\mu\text{L}$  of Bright-Glo reagent was then added over the top of the wells and given 2-4 minutes to lyse cells. The contents of each well were then transferred to a white-backed 96-well plate and luciferase signal was again read on a ClarioStar Plus microplate reader with a 3600 gain and a 1 second normalization time.

### 3.5.9 Virus Raji Cell Mediated Trans-Infectivity Assays

Raji cell Trans-infection assays were inspired by protocols described previously with some modifications [60, 61-63]. For Trans-infection experimental samples, 10000-20000 HEK-293T hACE2+ cells were seeded in triplicate into the wells of a pre-prepared poly-L-lysine conditioned 96-well plate as described above. For negative control samples, HEK-293FT cells were seeded in triplicate as well. The 96-well plate was returned to the 37 °C humidified incubator at 4.5% CO<sub>2</sub> in order to allow the HEK-293 cells to adhere and recover for 8-16 hours overnight.

The next day, Griffithsin protein sample was then resuspended in commercial PBS as described above, and was serially diluted with PBS so that at least 500  $\mu\text{L}$  of Griffithsin protein was present for each dilution concentration. 400  $\mu\text{L}$  of each Griffithsin dilution was aliquoted into a 1.5 mL low-protein binding microcentrifuge tube (ThermoFisher Cat # 90410, Waltham, MA, USA). For positive controls, a sample of 400  $\mu\text{L}$  PBS was pre-pared in one of the 1.5 mL low-protein binding microcentrifuge tubes.

Next, the Raji DC-SIGN+ cell flask and Raji Wild-Type cell flask were retrieved from the 37 °C humidified incubator. About half of the cell media was collected in a 50 mL centrifuge tube and pelleted by centrifugation at 200  $\times$  g for 3 minutes. Supernatant was carefully removed with a serological pipet and each Raji cell type was taken to 5-10 mL of 200000-400000 cells per mL with fresh Raji media. Then, 250  $\mu\text{L}$  of this cell suspension was added to a 1.5 mL low-protein binding microcentrifuge tube containing a serial Grif-fithsin dilution in PBS as described above.

Finally, 55  $\mu\text{L}$  of SARS-CoV-2 pseudoviral solution was added to each tube and allowed to incubate at room temperature for 2 hours. After incubation, the cells were centrifuged for 15 minutes at 100  $\times$  g to gently collect the cells. Supernatant was gently removed and pellets were resuspended with 200  $\mu\text{L}$  of 2% Fetal Bovine Serum in PBS (here-tofore referred to as Washing Buffer). Cells were centrifuged again for 15 minutes at 100  $\times$  g and the supernatant was gently removed. Pellets were once again resuspended with 200  $\mu\text{L}$  of Washing Buffer. Samples of cells were collected by centrifuging for 15 minutes at 100  $\times$  g and the supernatant was gently removed for a total of two washes. Pellets containing Raji cells with captured pseudovirus were then resuspended in 90  $\mu\text{L}$  of DMEM supplemented with 10% Fetal Bovine Serum (heretofore referred to as Final Infec-tivity Media).

Then the 96-well plate with seeded HEK-293 cells was retrieved from the humidified incubator and media within wells was gently replaced with 30  $\mu\text{L}$  of fresh 293 media. 30  $\mu\text{L}$  of Raji cells with captured pseudovirus in Final Infectivity Media as

described above was added to requisite wells. The 96-well plate was then returned to the 37 °C humidified incubator at 4.5% CO<sub>2</sub> in order to allow the captured pseudovirions to infect the adhered 293 cells.

12-16 hours later, the 96-well plate was retrieved from the humidified incubator and 90 µL of fresh, pre-warmed 293 Medium was added over the top of each well to ensure that cells remained alive and viable for the duration of the experiment. The 96-well plate was returned to the 37 °C incubator for an additional 36 to 48 hours. After 36-48 hours, the 96-well plate was retrieved from the humidified incubator and the luminescence assay was performed as described in the Direct-infectivity assay as described above.

When doing mannan inhibition of Raji cell capture, a dilution series of mannan in PBS was created instead of a serial Griffithsin dilution. The Raji cells were pipetted into the mannan dilutions and the protocol was continued with no additional changes. Details on the mannan used are in the Methods section on 3t3 cells, below.

### **3.5.10 Virus 3t3 Cell Mediated Trans-Infectivity Assays**

Trans-infection assays were performed as described in previous literature [59]. Briefly, for Trans-infection experimental samples, 5000-15000 of 3t3 DC-SIGN+ cells were seeded in triplicate into the wells of a pre-prepared poly-L-lysine conditioned 96-well plate as described above. For Trans-infection negative control samples, 3t3 Wild-Type Cells were seeded instead. The 96-well plate was returned to the 37 °C humidified incubator at 4.5% CO<sub>2</sub> in order to allow the 3t3 cells to adhere and recover for 8-12 hours.

For Trans-infectivity tests with Griffithsin inhibitors, two different protocols were tested: Griffithsin pre-incubated with virus, and Griffithsin pre-incubated with 3t3 cells.

For the Griffithsin pre-incubated with virus protocol, 10 µL of the desired dilution of the requisite Griffithsin variant (WT-Grft, Q-Grft, GLG-3A) was added to 30 µL of SARS-CoV-2 pseudotyped lentivirus solution and left at room temperature to incubate. After 20 minutes of Griffithsin incubation with virus, the 96-well plate was retrieved from the humidified incubator and the media was gently pipetted out of wells. Within 1 minute of pipetting out the media, the 40 µL Griffithsin-pseudovirus mixture was added to the well. We ran each Griffithsin dilution in triplicate.

For the Griffithsin pre-incubated with 3t3 cells protocol, 50 µL stock dilution ladder of each requisite Griffithsin variant (WT-Grft, Q-Grft, GLG-3A) was prepared in PBS. The 96-well plate was then retrieved from the humidified incubator and the media was gently pipetted out of wells. Within 1 minute of pipetting out media, the 10 µL of Griffithsin variant in PBS was added to the requisite well and the 96-well plate was left at room temperature to incubate for 20 minutes. We found that 10 µL of PBS was a sufficient volume to ensure enough moisture remained in the wells to prevent 3t3 cells from desiccating during the 20 minute incubation time period. After 20 minutes had elapsed, 30 µL of SARS-CoV-2 pseudotyped lentivirus was added to the wells.

For Trans-infectivity tests with SARS-CoV-2 pseudotyped lentiviral variants (M, N, E, and MNE Trans-infectivity tests), the 96-well plate was retrieved from the incubator after cells had recovered for the allotted 8-12 hours. The media was gently pipetted out of wells. Within 1 minute of pipetting out media, 15 µL of fresh 3t3 media was added to

the wells to prevent the cells from desiccating. Then 25  $\mu\text{L}$  of the requisite SARS-CoV-2 pseudovirus variant was added over the top of the wells.

After the pseudovirus was added to the wells of the 96-well plate, the plate was returned to the 37°C humidified incubator at 4.5% CO<sub>2</sub> for 2-4 hours to allow for virion capture.

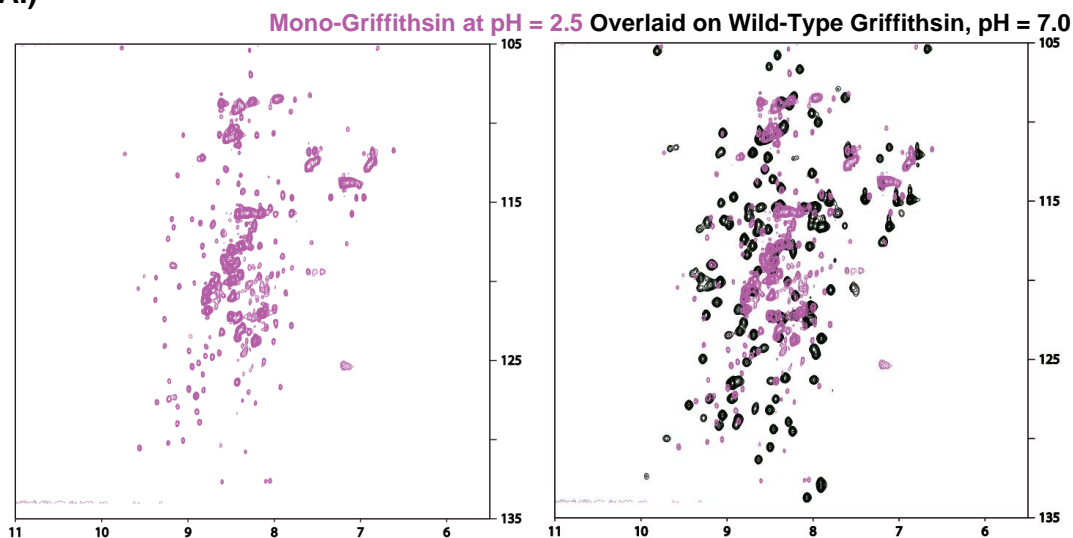
After 2-4 hours had elapsed, the 96-well plate was retrieved from the humidified incubator and the experimental wells were rinsed twice with 40  $\mu\text{L}$  of fresh 3t3 media. To do so, the virus-containing media was gently pipetted out of the wells. Within 1 minute of pipetting out media, 40  $\mu\text{L}$  of fresh 3t3 media was dispensed into each well to prevent desiccation. Wells were allowed to sit for 1 minute, then media was pipetted out of wells to rinse out unbound virions. 40  $\mu\text{L}$  of fresh 3t3 media was once again dispensed into each well, incubated for 1 minute, and once again pipetted out. At this point, 15000-25000 HEK-293T hACE2 cells in 293 media were dispensed into each well. As mentioned above, HEK-293T hACE2 cells were added to wells within 1 minute of media removal to avoid desiccation of 3t3 cells and captured virions. After HEK-293T hACE2 cells were added to wells, the 96-well plate was returned to the incubator.

12-16 hours later, the 96-well plate was retrieved from the humidified incubator and 150  $\mu\text{L}$  of fresh, pre-warmed 293 Medium was added over the top of each well to ensure that cells remained alive and viable for the duration of the experiment. The 96-well plate was returned to the 37 °C incubator for an additional 36-48 hours. After 36-48 hours, the 96-well plate was retrieved from the humidified incubator. Bright-Glo Luciferase Reagent (Promega Corp., Cat # E2610, Madison, WI, USA) was thawed out and protected from light until use. 160-180  $\mu\text{L}$  of the medium in each of the infectivity plate wells was pipetted out, leaving about 30  $\mu\text{L}$  of the medium in each well after accounting for evaporation during the course of the experiment. 30  $\mu\text{L}$  of Bright-Glo reagent was added over the top of the wells and given 2-4 minutes to lyse cells. The contents of each well were then transferred to a white-backed 96-well plate and luciferase signal was read on a CLAR-IO-star Plus microplate reader (BMG Labtech, Cary, NC, USA) with a 3600 gain and a 1 second normalization time.

For mannan inhibition of 3t3 cell DC-SIGN mediated trans-infection, mannan polymers from *Saccharomyces Cerevisiae* were utilized (Sigma-Aldrich Cat # M7504-100MG, Saint Louis, MO, USA). 100 mg of mannan was dissolved in 40 mL of ultrapure water to create a 2.5 mg/mL stock solution of mannan. When performing trans-assay, 64  $\mu\text{L}$  of the 2.5 mg/mL mannan stock was diluted to a final volume of 3 mL by adding 2.936 mL of 3t3 media to obtain a final concentration of 0.053 mg/mL (53.3  $\mu\text{g}/\text{mL}$ ) solution of mannan in 3t3 media. 15  $\mu\text{L}$  of this 0.053 mg/mL mannan solution was used instead of 15  $\mu\text{L}$  of standard 3t3 medium to prevent cells from desiccating just prior to adding 25  $\mu\text{L}$  of pseudo-virus 3t3 cells. Upon the addition of pseudovirus, the final mannan concentration in wells was at 0.02 mg/mL (20  $\mu\text{g}/\text{mL}$ ). This 20  $\mu\text{g}/\text{mL}$  concentration of mannan was used because it had previously been shown to be sufficient to consistently inhibit 3t3 DC-SIGN+ cell mediated Trans-infection of SARS-CoV-2 pseudovirus without appreciably affecting hACE2+ mediated Direct-infection [59].

### 3.6 Supplemental Figures

A.)



B.)

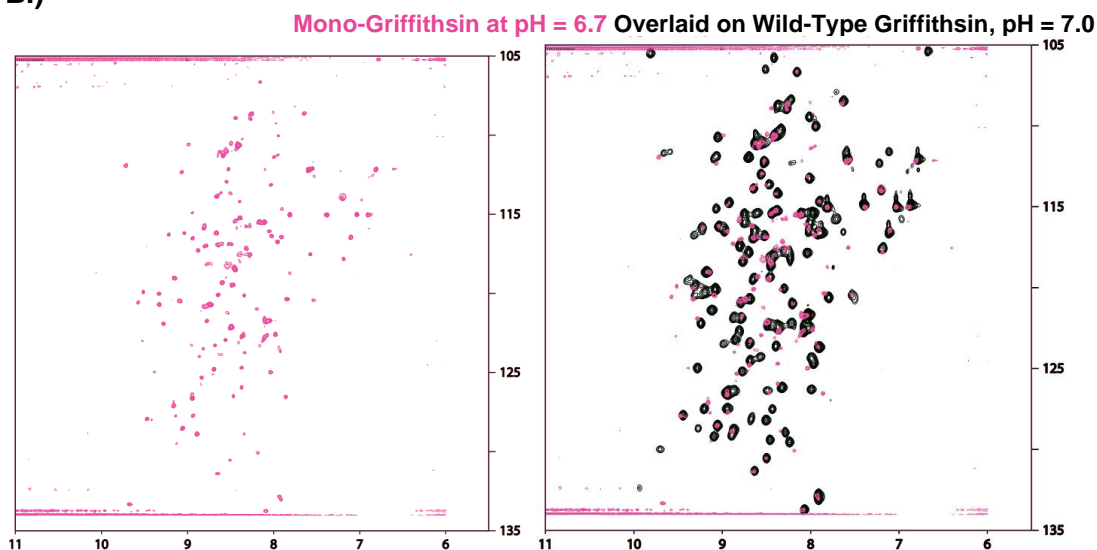
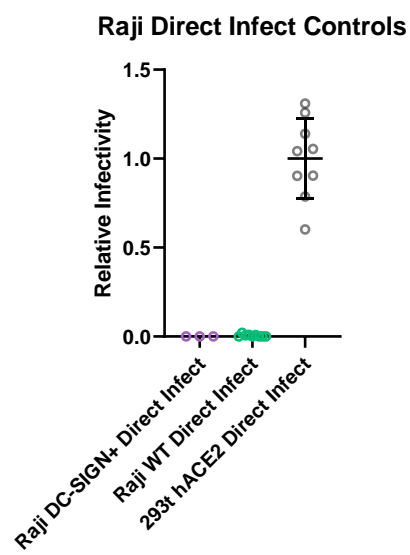


**Figure S1: A.)** The NMR HSQC spectrum of Mono-Griffithsin at pH 2.5 (purple). The variation in peak intensity indicates that the protein is not stable and is likely forming aggregates. When the spectrum is overlaid on WT-Grft taken at pH 7.0, several peaks look shifted (as would be expected due to changes in pH between the two spectra). **B.)** The NMR HSQC spectrum of Mono-Griffithsin at pH 6.7 (pink). The protein precipitated during this run, as hinted at by the greatly reduced peak intensity on the spectrum. However, the majority of the peaks overlay with Wild-Type Griffithsin, indicating that the subset of Mono-Griffithsin that remains in solution is likely well-folded and functional. However, Mono-Griffithsin appeared to have a saturation limit beneath 1  $\mu\text{M}$  in this solution, making it unsuitable for further assessment.

A.)



B.)

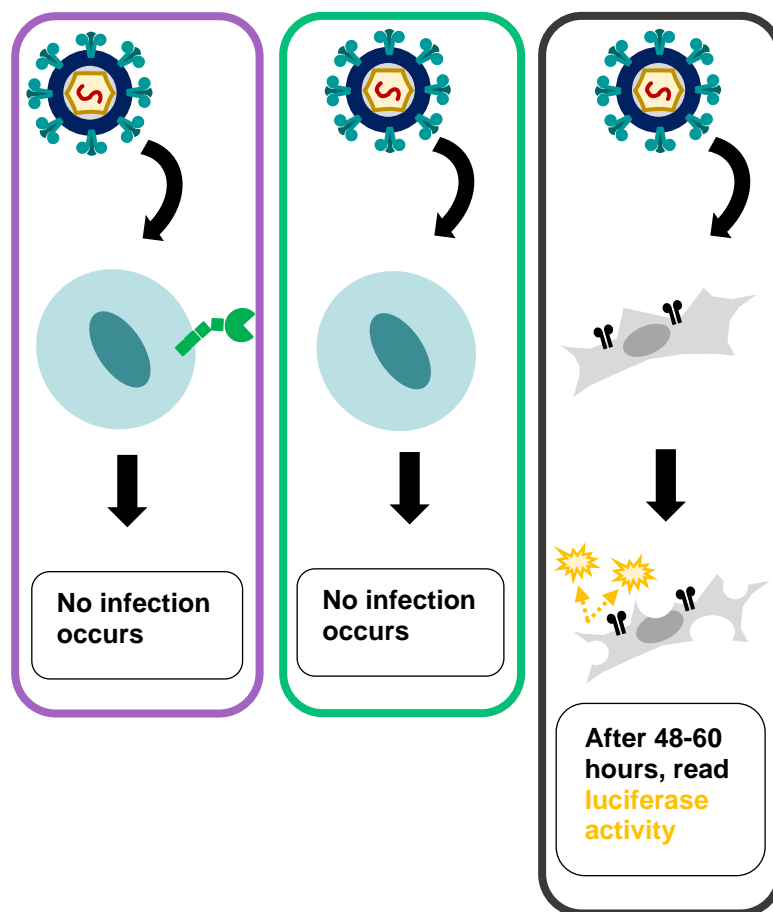
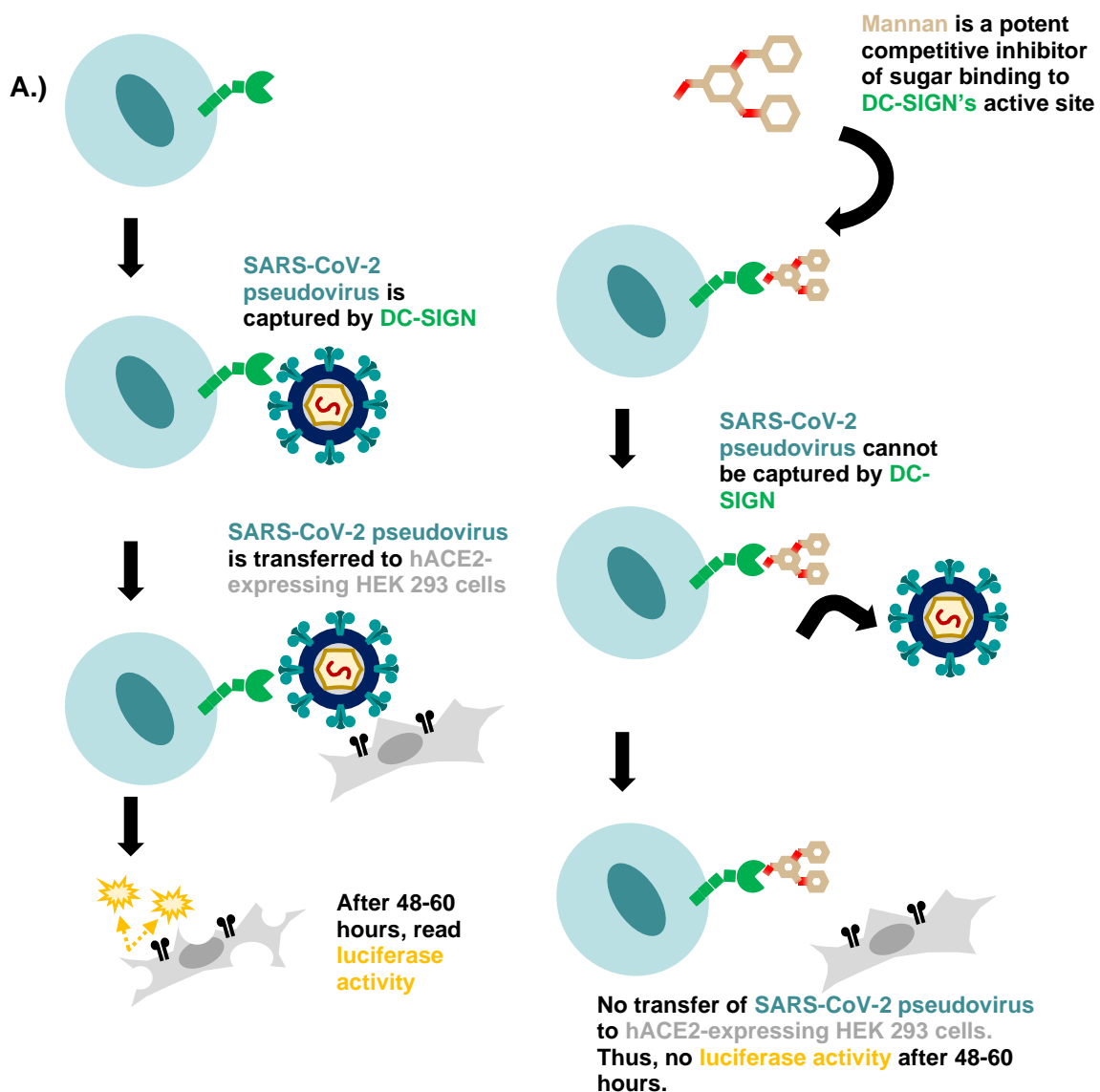


**Figure S2: Verification that Raji WT and Raji DC-SIGN+ cells were not permissible to SARS-CoV-2 pseudoviral infection. A.)** The comparison of Direct infection signal of

Raji DC-SIGN+ Cells and Raji WT Cells exposed to SARS-CoV-2 pseudotyped virions to the Direct infection signal of 293T hACE2+ cells shows that they did not allow for infection. **B.)** Schematic depictions of Direct infection assay.



B.)  
Mannan Inhibition of Trans Infection

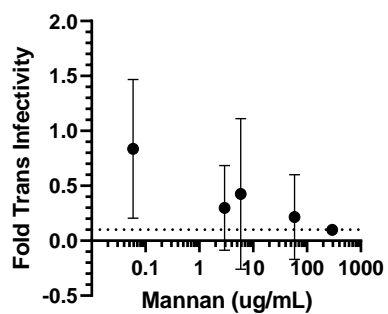
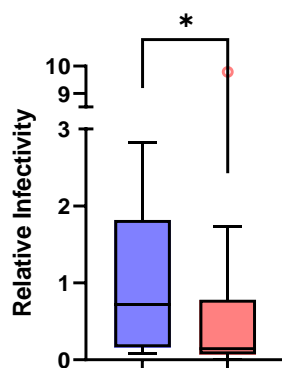




**Figure S3: Verification that mannan acts as an inhibitor of Raji DC-SIGN+ Cell-mediated Trans-infection. A.)** Schematic diagram of how mannan inhibits Raji DC-SIGN+ mediated Trans-infection. **B.)** Results of Mannan inhibition of a Raji DC-SIGN+ mediated Trans-infection assay. This was performed to verify that DC-SIGN was indeed the cell surface protein that was responsible for capturing virions during Trans-infection.

## Raji Trans Assay Controls



■ Positive Control Trans Infection Raji DC-SIGN

■ Negative Control Trans-Infection Raji WT Cells

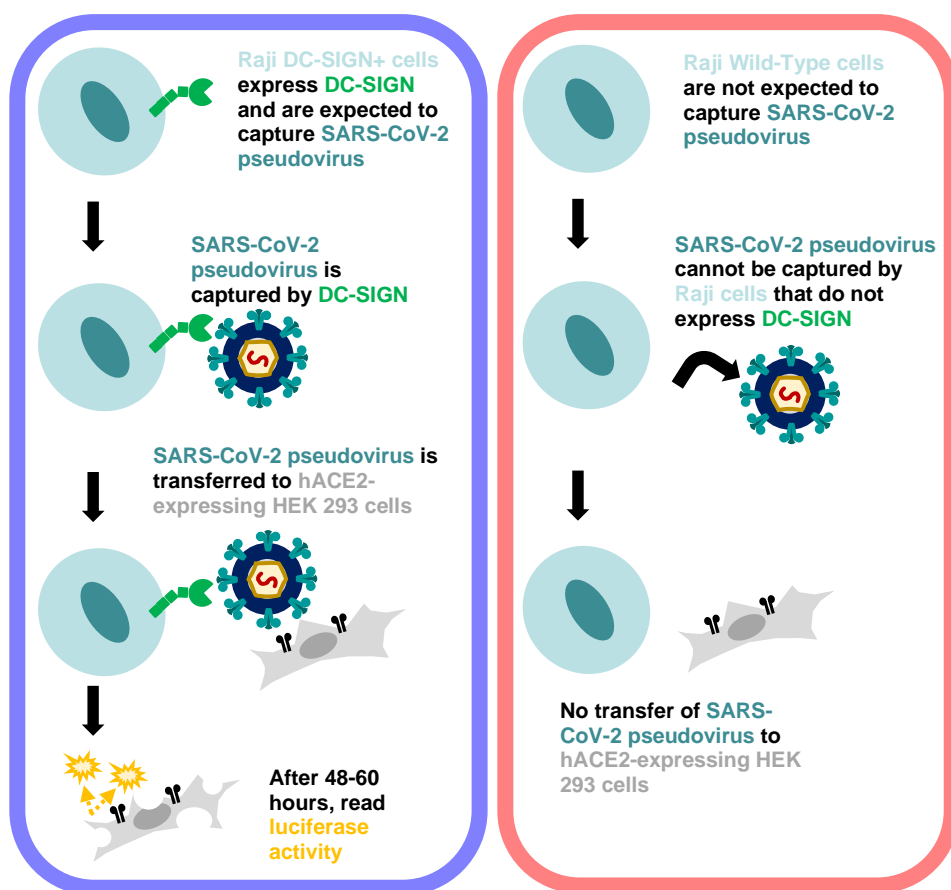


**Figure S4:** Raji assay controls were summarized to see the difference between viral capture for Raji WT cells versus Raji DC-SIGN+ cells. Plot depicts medians with values between the 10<sup>th</sup> to 90<sup>th</sup> percentile. Despite the wide range of Relative Infectivity values for both Positive Control and Negative Control samples, comparing the median and 10<sup>th</sup>-90<sup>th</sup> percentile values for both groups shows that Raji DC-SIGN+ cells appear to facilitate more Trans-infectivity than Raji WT cells. The high variability in data values was endemic to nearly all of our assays we performed with Raji cells, which was another key driving factor that led us to want to verify our results with 3t3 cells. \* indicates a  $p$ -value < 0.1 on a Mann-Whitney T-test.

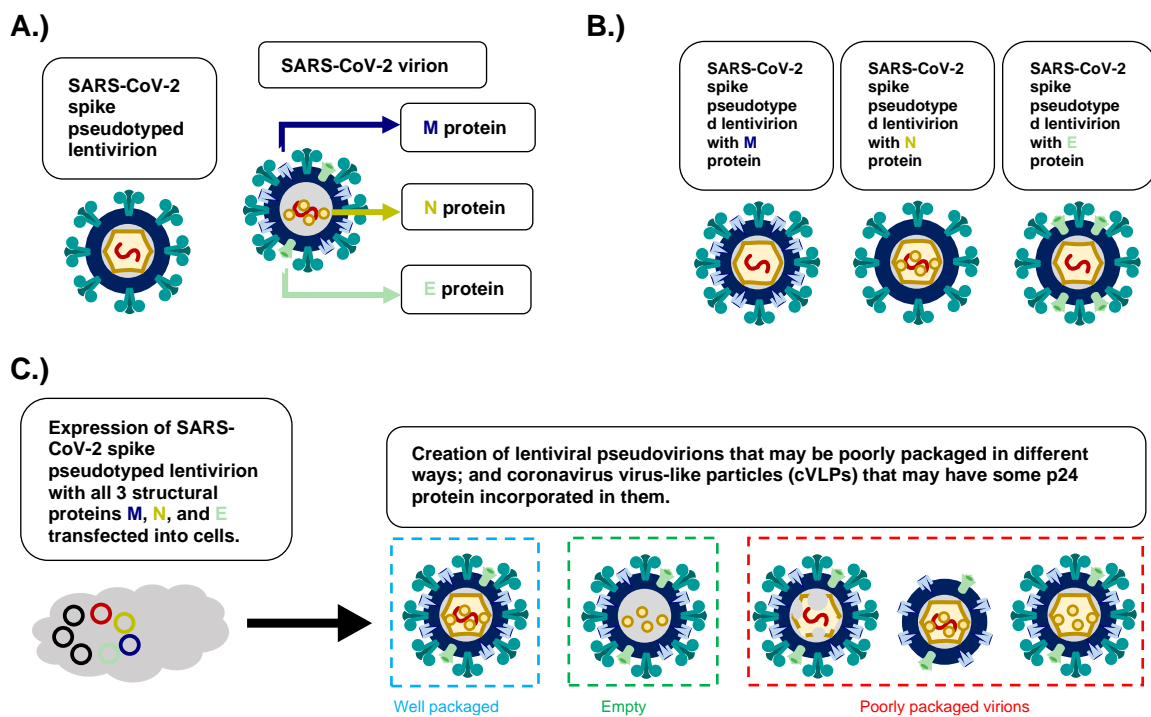


**Figure S5. Representative diagrams of virions described in this chapter. A.)** Comparison of the exterior of SARS-CoV-2 Spike pseudotyped lentivirions to SARS-CoV-2 coronaviral particles. **B.)** Also depicted are representations of the three coronavirus strains where each of the 3 structural proteins were added in turn. The N protein stays on the interior of the virion while M and E are expressed on the surface. **C.)** Simplified depiction of the transfection process to create pseudovirions; structural protein vectors are depicted in blue, yellow and mint green while the transfer vector is shown in red. Other lentiviral packaging vectors are depicted in black. Transfected cells can produce well-packaged MNE lentiviral pseudovirions (in teal blue box). In addition, expression of M, N, and E proteins can form coronaviral Virus-Like Particles (cVLPs, in green box). These cVLPs and other noninfectious poorly-packaged viral particles (in red box) may incorporate some p24, which can increase the apparent viral titer on p24 ELISA assays.

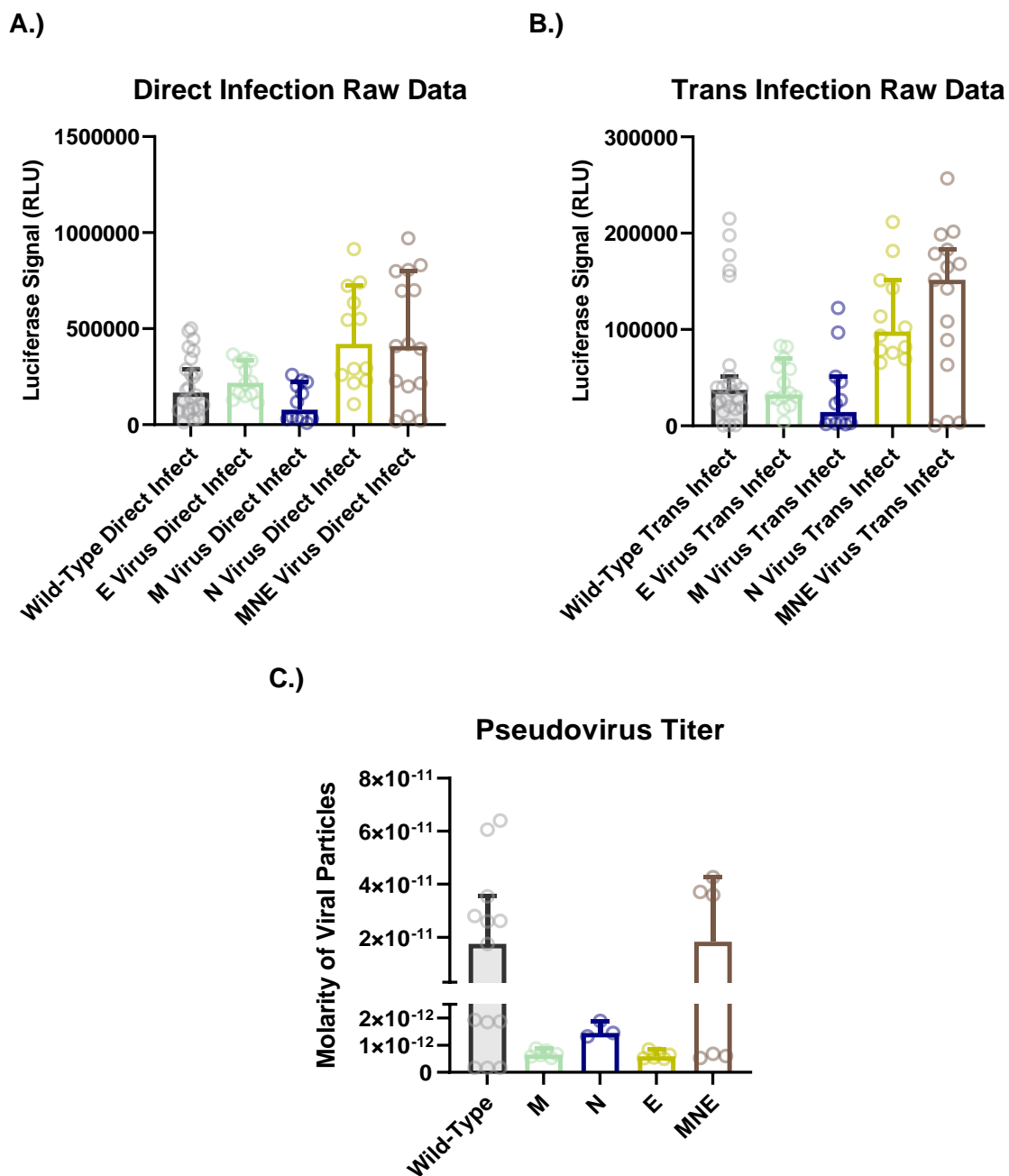


**Figure S6. A.)** Depiction of the raw hACE2-mediated Direct Infection Luciferase signal for all SARS-CoV-2 pseudoviral strains. **B.)** Depiction of the raw 3t3 DC-SIGN+ cell-mediated Direct Infection Luciferase signal for all SARS-CoV-2 pseudoviral strains. **C.)** Pseudoviral titer as measured by p24 ELISA assay. At least two different batches of virus were made for each variant. Plots depict medians with 95% Confidence Interval.

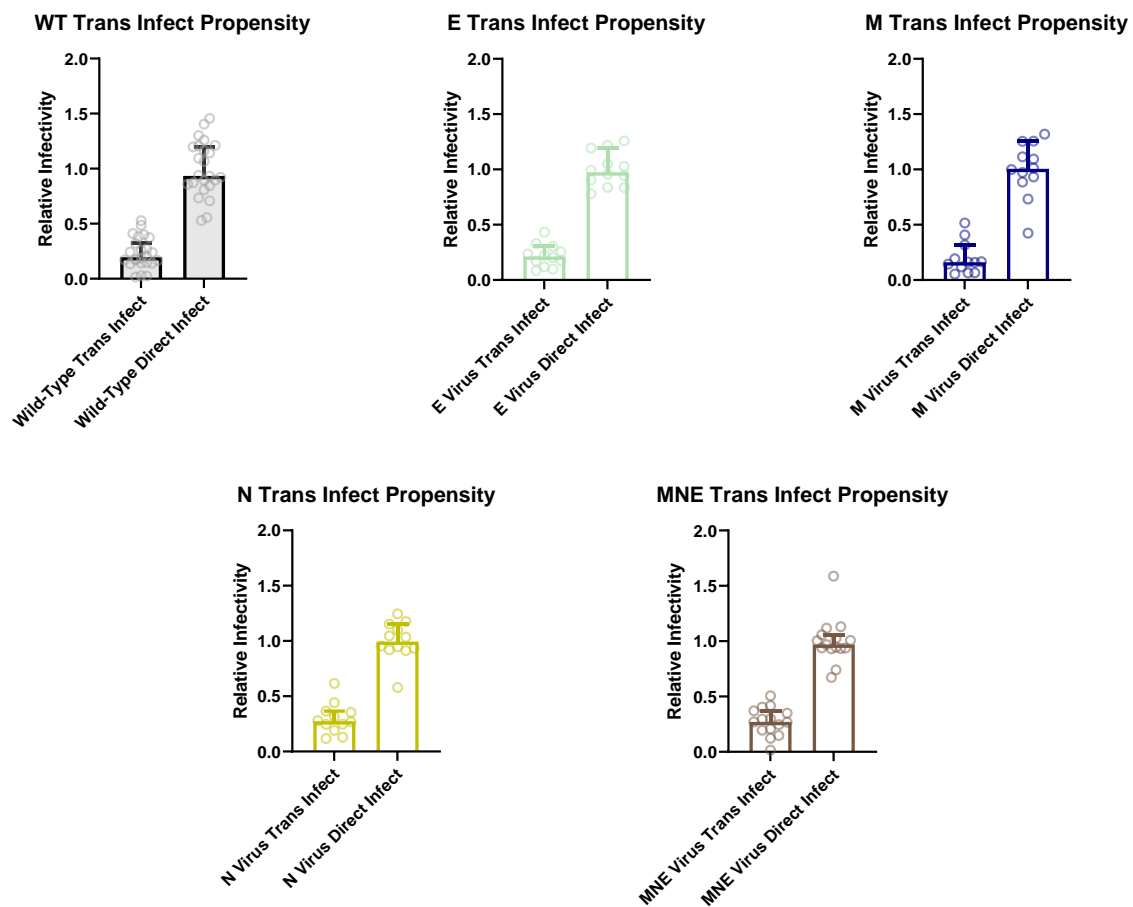


**Figure S7:** Comparisons depicting additional structural protein pseudoviral strains' propensity to undergo 3t3 DC-SIGN+ cell mediated Trans Infectivity as normalized to Direct Infection.

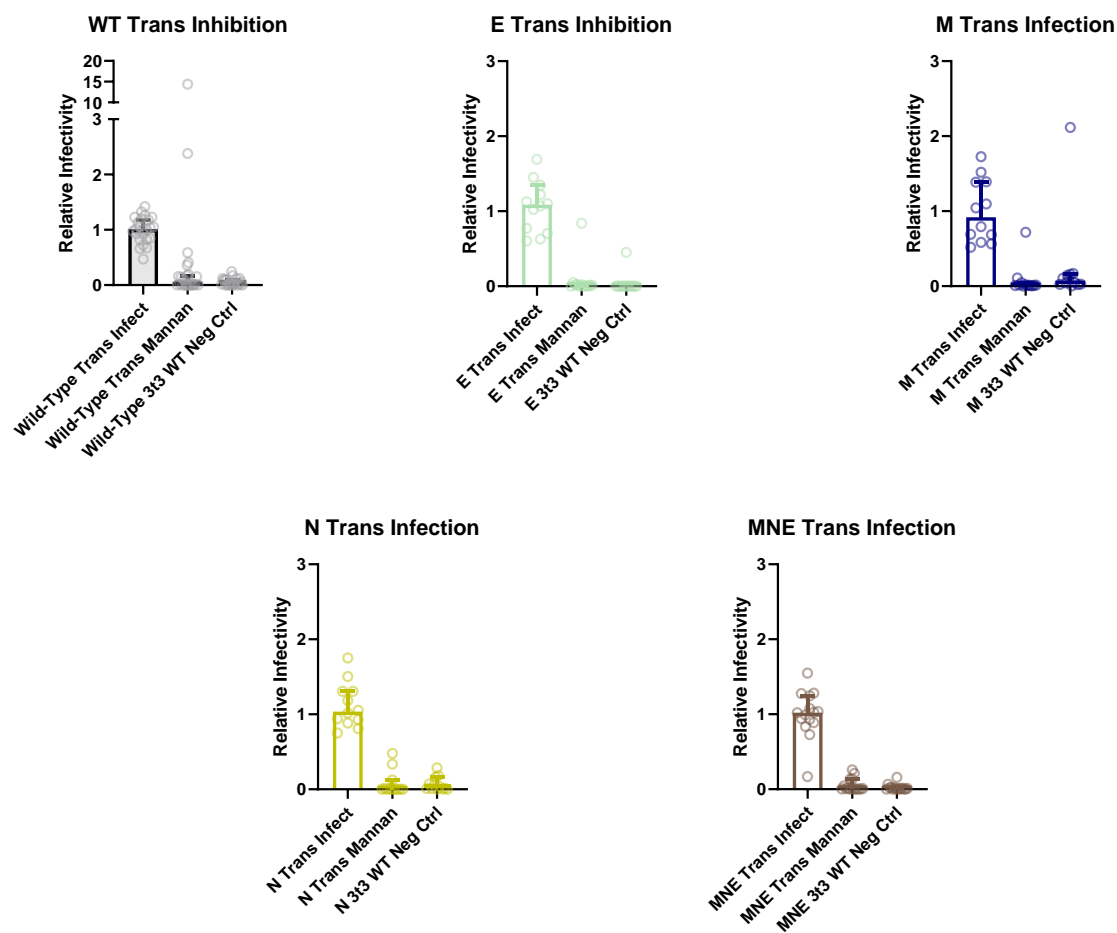


**Figure S8:** Comparisons depicting additional structural protein pseudoviral strains' susceptibility to mannan on 3t3 cell assay. For each sample, virus infectivity per molar was normalized to each strain's Trans-infection signal.

### 3.7 References

- [1]: WHO Coronavirus (COVID-19) Dashboard. Available online: <https://covid19.who.int/> (accessed on 25 August 2023).
- [2]: Zabidi, N.Z.; Liew, H.L.; Farouk, I.A.; Puniyamurti, A.; Yip, A.J.W.; Wijesinghe, V.N.; Low, Z.Y.; Tang, J.W.; Chow, V.T.K.; Lal, S.K. Evolution of SARS-CoV-2 Variants: Implications on Immune Escape, Vaccination, Therapeutic and Diagnostic Strategies. *Viruses*. 2023 Apr 10;15(4):944. <https://doi.org/10.3390/v15040944>.
- [3]: Chen, X.; Huang, H.; Ju, J.; Sun, R.; Zhang, J. Impact of vaccination on the COVID-19 pandemic in U.S. states. *Sci Rep*. 2022;12(1554). <https://doi.org/10.1038/s41598-022-05498-z>.
- [4]: CDC Covid Data tracker. Available online: <https://covid.cdc.gov/covid-data-tracker/#datatracker-home> (accessed on 29 July 2023).
- [5]: Wang, Z.; Schmidt, F.; Weisblum, Y.; Muecksch, F.; Barnes, C.O.; Finkin, S.; Schaefer-Babajew, D.; Cipolla, M.; Gaebler, C.; Lieberman, J.A.; et al. mRNA vaccine-elicited antibodies to SARS-CoV-2 and circulating variants. *Nature*. 2021;592: 616-622. <https://doi.org/10.1038/s41586-021-03324-6>.
- [6]: Yue, C.; Song, W.; Wang, L.; Jian, F.; Chen, X.; Gao, F.; Shen, Z.; Wang, Y.; Wang, X.; Cao, Y. Enhanced transmissibility of XBB.1.5 is contributed by both strong ACE2 binding and antibody evasion. *Lancet Infect. Dis*. 2023, 23, 278–280. [https://doi.org/10.1016/S1473-3099\(23\)00010-5](https://doi.org/10.1016/S1473-3099(23)00010-5).
- [7]: Arora, P.; Cossmann, A.; Schulz, S.R.; Ramos, G.M.; Stankov, M.V.; Jäck, H-M.; Behrens, G.M.N.; Pöhlmann, S.; Hoffman, M. Neutralisation sensitivity of the SARS-CoV-2 XBB.1 lineage. *Lancet Infect. Dis*. 2023;23(2):147-148. [https://doi.org/10.1016/S1473-3099\(22\)00831-3](https://doi.org/10.1016/S1473-3099(22)00831-3).
- [8]: Nadesalingam, A.; Cantoni, D.; Aguinam, E.T.; Chan, A.C.; Paloniemi, M.; Ohlendorf, L.; George, C.; Carnell, G.; Lyall, J.; Ferrari, M.; et. al. Vaccination and protective immunity to SARS-CoV-2 omicron variants in people with immunodeficiencies. *Lancet Microbe*. 2023 Feb;4(2):e58-e59. [https://doi.org/10.1016/S2666-5247\(22\)00297-X](https://doi.org/10.1016/S2666-5247(22)00297-X).
- [9]: Frasca, L.; Ocone, G.; Palazzo, R. Safety of COVID-19 Vaccines in Patients with Autoimmune Diseases, in Patients with Cardiac Issues, and in the Healthy Population. *Pathogens*. 2023;12(2): 233. <https://doi.org/10.3390/pathogens12020233>
- [10]: Lazarus, J.V.; Wyka, K.; White, T.M.; Picchio, C.A.; Gostin, L.O.; Larson, H.J.; Rabin, K.; Ratzan, S.C.; Kamarulzaman, A.; El-Mohandes, A. A survey of COVID-19 vaccine acceptance across 23 countries in 2022. *Nat. Med*. 2023;29: 366–375. <https://doi.org/10.1038/s41591-022-02185-4>
- [11]: Kemp, A. Update on US Food and Drug Administration Emergency Use Authorisation of Evusheld. AstraZeneca. 2023 Jan 26. Available online: <https://www.astrazeneca.com/media-centre/press-releases/2023/update-on-evusheld-us-eua.html> (accessed on 31 July 2023).



- [12]: Moody, M.; Ryan, P.; Dannenbaum, P.; Kruper R.; Carvalho, C. Merck and Ridgeback's Investigational Oral Anti-viral Molnupiravir Reduced the Risk of Hospitalization or Death by Approximately 50 Percent Compared to Placebo for Patients with Mild or Moderate COVID-19 in Positive Interim Analysis of Phase 3 Study. Merck & Co., Inc. 2021 Oct 1. Available online: <https://www.merck.com/news/merck-and-ridgebacks-investigational-oral-antiviral-molnupiravir-reduced-the-risk-of-hospitalization-or-death-by-approximately-50-percent-compared-to-placebo-for-patients-with-mild-or-moderat/> (ac-cessed on 31 July 2023).
- [13]: Lee, C. Griffithsin, a Highly Potent Broad-Spectrum Antiviral Lectin from Red Algae: From Discovery to Clinical Application. *Mar. Drugs* 2019, 17, 567. <https://doi.org/10.3390/md17100567>.
- [14]: O'Keefe, B.R.; Giomarelli, B.; Barnard, D.L.; Shenoy, S.R.; Chan, P.K.; McMahon, J.B.; Palmer, K.E.; Barnett, B.W.; Meyerholz, D.K.; Wohlford-Lenane, C.L.; McCray, P.B. Jr. Broad-spectrum in vitro activity and in vivo efficacy of the antiviral protein griffithsin against emerging viruses of the family Coronaviridae. *J Virol.* 2010 Mar;84(5):2511-21. <https://doi.org/10.1128/JVI.02322-09>.
- [15]: Fischer, K.; Nguyen, K.; LiWang, P.J. Griffithsin Retains Anti-HIV-1 Potency with Changes in gp120 Glycosylation and Complements Broadly Neutralizing Antibodies PGT121 and PGT126. *Antimicrob. Agents Chemother.* 2019, 64, e01084-e19. <https://doi.org/10.1128/AAC.01084-19>.
- [16]: Xue, J.; Gao, Y.; Hoorelbeke, B.; Kagiampakis, I.; Zhao, B.; Demeler, B.; Balzarini, J.; LiWang, P.J. The role of individual carbohydrate-binding sites in the function of the potent anti-HIV lectin griffithsin. *Mol Pharm.* 2012 Sep 4;9(9):2613-25. <https://doi.org/10.1021/mp300194b>.
- [17]: Kramzer, L.F.; Hamorsky, K.T.; Graebing, P.W.; Wang, L.; Fuqua, J.L.; Matoba, N.; Lasnik, A.B.; Moncla, B.J.; Zhang, J.; Palmer, K.E.; et al. Preformulation Characterization of Griffithsin, a Biopharmaceutical Candidate for HIV Prevention. *AAPS PharmSciTech.* 2021 Feb 24;22(3): 83. <https://doi.org/10.1208/s12249-021-01931-0>
- [18]: Siddiqui, S.; Ahmed, A. Griffithsin; A Potential Therapeutic Agent for SARS-CoV-2. *Acta sci. microbiol.* 2022 Jan 27;5(2):82-87.
- [19]: Moulaei, T.; Shenoy, S.R.; Giomarelli, B.; Thomas, C.; McMahon, J.B.; Dauter, Z.; O'Keefe, B.R.; Wlodawer, A. Monomerization of viral entry inhibitor griffithsin elucidates the relationship between multivalent binding to carbo-hydrates and anti-HIV activity. *Structure.* 2010 Sep 8;18(9):1104-15. <https://doi.org/10.1016/j.str.2010.05.016>.
- [20]: Kouokam, J.C.; Huskens, D.; Schols, D.; Johannemann, A.; Riedell, S.K.; Walter, W.; Walker, J.M.; Matoba, N.; O'Keefe, B.R.; Palmer, K.E. Investigation of griffithsin's interactions with human cells confirms its outstanding safety and efficacy profile as a microbicide candidate. *PLoS One.* 2011;6(8):e22635. <https://doi.org/10.1371/journal.pone.0022635>.
- [21]: Nabeta, H.W.; Kouokam, J.C.; Lasnik, A.B.; Fuqua, J.L.; Palmer, K.E. Novel Antifungal Activity of Q-Griffithsin, a Broad-Spectrum Antiviral Lectin. *Microbiol Spectr.* 2021 Oct 31;9(2):e0095721. <https://doi.org/10.1128/Spectrum.00957-21>.

- [22]: Teleshova, N.; Keller, M.J.; Fernández Romero, J.A.; Friedland, B.A.; Creasy, G.W.; Plagianos, M.G.; Ray, L.; Barnable, P.; Kizima, L.; Rodriguez, A.; et al. Results of a phase 1, randomized, placebo-controlled first-in-human trial of griffithsin formulated in a carrageenan vaginal gel. *PLoS One*. 2022 Jan 20;17(1):e0261775. <https://doi.org/10.1371/journal.pone.0261775>.
- [23]: Brand, R. Griffithsin-based Rectal Microbicide for PREvention of Viral ENtry (PREVENT) (PREVENT). Clinical-Trials.gov identifier: NCT04032717. Updated July 6, 2023. <https://clinicaltrials.gov/ct2/show/NCT04032717> (accessed on 18 August 2023).
- [24]: Xue, J.; Hoorelbeke, B.; Kagiampakis, I.; Demeler, B.; Balzarini, J.; LiWang, P.J. The griffithsin dimer is required for high-potency inhibition of HIV-1: evidence for manipulation of the structure of gp120 as part of the griffithsin dimer mechanism. *Antimicrob Agents Chemother*. 2013 Aug;57(8):3976-89. <https://doi.org/10.1128/AAC.00332-13>.
- [25]: Moulaei, T.; Alexandre, K.B.; Shenoy, S.R.; Meyerson, J.R.; Krumpke, L.R.; Constantine, B. Wilson, J.; Buckheit, R.W. Jr; McMahon, J.B.; Subramaniam, S.; Wlodawer, A.; O'Keefe, B.R. Griffithsin tandemers: flexible and potent lectin inhibitors of the human immunodeficiency virus. *Retrovirology*. 2015 Jan 23;12:6. <https://doi.org/10.1186/s12977-014-0127-3>.
- [26]: Chatterjee, A.; Ratner, D.M.; Ryan, C.M.; Johnson, P.J.; O'Keefe, B.R.; Secor, W.E.; Anderson, D.J.; Robbins, P.W.; Samuelson, J. Anti-Retroviral Lectins Have Modest Effects on Adherence of *Trichomonas vaginalis* to Epithelial Cells In Vitro and on Recovery of *Tritrichomonas foetus* in a Mouse Vaginal Model. *PLoS One*. 2015 Aug 7;10(8):e0135340. <https://doi.org/10.1371/journal.pone.0135340>.
- [27]: Matej, E.; Zheng, A.; Furey, W.; Rose, J.; Aiken, C.; Gronenborn, A.M. Anti-HIV activity of defective cyanovirin-N mutants is restored by dimerization. *J Biol Chem*. 2010 Apr 23;285(17):13057-65. <https://doi.org/10.1074/jbc.M109.094938>.
- [28]: Alsaidi, S.; Cornejal, N.; Mahoney, O.; Melo, C.; Verma, N.; Bonnaire, T.; Chang, T.; O'Keefe, B.R.; Sailer, J.; Zydowsky, T.M.; et al. Griffithsin and Carrageenan Combination Results in Antiviral Synergy against SARS-CoV-1 and 2 in a Pseudoviral Model. *Mar. Drugs* 2021, 19, 418. <https://doi.org/10.3390/md19080418>
- [29]: Cai, Y.; Xu, W.; Gu, C.; Cai, X.; Qu, D.; Lu, L.; Xie, Y.; Jiang, S. Griffithsin with A Broad-Spectrum Antiviral Activity by Binding Glycans in Viral Glycoprotein Exhibits Strong Synergistic Effect in Combination with A Pan-Coronavirus Fusion Inhibitor Targeting SARS-CoV-2 Spike S2 Subunit. *Virol Sin*. 2020 Dec;35(6):857-860. <https://doi.org/10.1007/s12250-020-00305-3>.
- [30]: Cai, Y.; Xu, W.; Tang, J.; Cao, N.; Lan, Q.; Lu, L.; Jiang, S. A bivalent protein targeting glycans and HR1 domain in spike protein potently inhibited infection of SARS-CoV-2 and other human coronaviruses. *Cell Biosci*. 2021 Jul 8;11(1):128. <https://doi.org/10.1186/s13578-021-00638-w>.
- [31]: Ahan, R.E.; Hanifnezhad, A.; Kehribar, E.Ş.; Oguzoglu, T.C.; Földes, K.; Özçelik, C.E.; Filazi, N.; Öztop, S.; Palaz, F.; Önder, S.; et al. A Highly Potent SARS-CoV-2 Blocking Lectin Protein. *ACS Infect Dis*. 2022 Jul 8;8(7):1253-1264. <https://doi.org/10.1021/acscinfecdis.2c00006>.

- [32]: Lusvarghi, S.; Bewley, C.A. Griffithsin: An Antiviral Lectin with Outstanding Therapeutic Potential. *Viruses* 2016, 8, 296. <https://doi.org/10.3390/v8100296>
- [33]: German Advisory Committee Blood (Arbeitskreis Blut), Subgroup 'Assessment of Pathogens Transmissible by Blood'. *Human Immunodeficiency Virus (HIV). Transfus Med Hemother.* 2016 May;43(3):203-22. <https://doi.org/10.1159/000445852>.
- [34]: Stano, A.; Leaman, D.P.; Kim, A.S.; Zhang, L.; Autin, L.; Ingale, J.; Gift, S.K.; Truong, J.; Wyatt, R.T.; Olson, A.J.; et al. Dense Array of Spikes on HIV-1 Virion Particles. *J Virol.* 2017 Jun 26;91(14):e00415-17. <https://doi.org/10.1128/JVI.00415-17>.
- [35]: Yao, H.; Song, Y.; Chen, Y.; Wu, N.; Xu, J.; Sun, C.; Zhang, J.; Weng, T.; Zhang, Z.; Wu, Z.; et al. Molecular Architecture of the SARS-CoV-2 Virus. *Cell* 2020, 183, 730–738.e13 <https://doi.org/10.1016/j.cell.2020.09.018>.
- [36]: Li, L.; Liao, H.; Meng, Y.; Li, W.; Han, P.; Liu, K.; Wang, Q.; Li, D.; Zhang, Y.; Wang, L.; et al. Structural basis of human ACE2 higher binding affinity to currently circulating Omicron SARS-CoV-2 sub-variants BA.2 and BA.1.1. *Cell* 2022, 185, 2952–2960.e10. <https://doi.org/10.1016/j.cell.2022.06.023>.
- [37]: Jackson, C.B.; Farzan, M.; Chen, B.; Choe, H. Mechanisms of SARS-CoV-2 entry into Cells. *Nat. Rev. Mol. Cell Bi-ol.* 2022, 23, 3–20. <https://doi.org/10.1038/s41580-021-00418-x>
- [38]: Syed, A.M.; Taha, T.Y.; Tabata, T.; Chen, I.P.; Ciling, A.; Khalid, M.M.; Sreekumar, B.; Chen, P.Y.; Hayashi, J.M.; Soczek, K.M.; et al. Rapid assessment of SARS-CoV-2-evolved variants using virus-like particles. *Science.* 2021 Dec 24;374(6575):1626-1632. <https://doi.org/10.1126/science.abl6184>.
- [39]: Mishra, T.; Sreepadmanabh, M.; Ramdas, P.; Sahu, A.K.; Kumar, A.; Chande, A. SARS CoV-2 Nucleoprotein Enhances the Infectivity of Lentiviral Spike Particles. *Front Cell Infect Microbiol.* 2021 Apr 23;11:663688. <https://doi.org/10.3389/fcimb.2021.663688>.
- [40]: Shajahan, A.; Pepi, L.E.; Rouhani, D.S.; Heiss, C.; Azadi, P. Glycosylation of SARS-CoV-2: structural and functional insights. *Anal Bioanal Chem.* 2021 Dec;413(29):7179-7193. <https://doi.org/10.1007/s00216-021-03499-x>.
- [41]: Monje-Galvan, V.; Voth, G.A. Molecular interactions of the M and E integral membrane proteins of SARS-CoV-2. *Faraday Discuss.* 2021 Sep 20;232. <https://doi.org/10.1101/2021.04.29.442018>.
- [42]: Zhang, J.; Kennedy, A.; Xing, L.; Bui, S.; Reid, W.; Joppich, J.; Ahat, E.; Rose, M.; Tang, Q.; Tai, A.W.; et al. SARS-CoV-2 triggers Golgi fragmentation via down-regulation of GRASP55 to facilitate viral trafficking. *bioRxiv.* 2022 Mar 4. <https://doi.org/10.1101/2022.03.04.483074>
- [43]: Lim, S.; Zhang, M.; Chang, T.L. ACE2-Independent Alternative Receptors for SARS-CoV-2. *Viruses* 2022, 14, 2535. <https://doi.org/10.3390/v14112535>
- [44]: Ebrahim, L.; Xu, C.; Wang, A.; Hernandez, C.; Siclari, N.; Rajah, D.; Walter, L.; Marras, S.A.E.; Tyagi, S.; Fine, D.H.; et al. Oral Epithelial Cells Expressing Low or Undetectable Levels of Human Angiotensin-Converting Enzyme 2 Are Susceptible to

SARS-CoV-2 Virus Infection In Vitro. *Pathogens* 2023, 12, 843.

<https://doi.org/10.3390/pathogens12060843>

[45]: Puray-Chavez, M.; LaPak, K.M.; Schrank, T.P.; Elliott, J.L.; Bhatt, D.P.; Agajanian, M.J.; Jasuja, R.; Lawson, D.Q.; Davis, K.; Rothlauf, P.W.; et al. Systematic analysis of SARS-CoV-2 infection of an ACE2-negative human airway cell. *Cell Rep.* 2021, 36, 109364. <https://doi.org/10.1016/j.celrep.2021.109364>.

[46]: Lempp, F.A.; Soriaga, L.B.; Montiel-Ruiz, M.; Benigni, F.; Noack, J.; Park, Y.J.; Bianchi, S.; Walls, A.C.; Bowen, J.E.; Zhou, J.; et al. Lectins enhance SARS-CoV-2 infection and influence neutralizing antibodies. *Nature* 2021, 598, 342–347. <https://doi.org/10.1038/s41586-021-03925-1>.

[47]: Hikmet, F.; Méar, L.; Edvinsson, Å.; Micke, P.; Uhlén, M.; Lindskog, C. The protein expression profile of ACE2 in human tissues. *Mol Syst Biol.* 2020 Jul;16(7):e9610. <https://doi.org/10.15252/msb.20209610>.

[48]: Thépaut, M.; Luczkowiak, J.; Vivès, C.; Labiod, N.; Bally, I.; Lasala, F.; Grimoire, Y.; Fenel, D.; Sattin, S.; Thielens, N.; et al. DC/L-SIGN recognition of spike glycoprotein promotes SARS-CoV-2 trans-infection and can be inhibited by a glycomimetic antagonist. *PLoS Pathog.* 2021, 17, e1009576. <https://doi.org/10.1371/journal.ppat.1009576>.

[49]: Hoffmann, D.; Mereiter, S.; Oh, Y.J.; Monteil, V.; Elder, E.; Zhu, R.; Canena, D.; Hain, L.; Laurent, E.; Grünwald-Gruber, C.; et al. Identification of lectin receptors for conserved SARS-CoV-2 glycosylation sites. *EMBO J.* 2021, 40, e108375. <https://doi.org/10.15252/embj.2021108375>.

[50]: Li, M.Y.; Li, L.; Zhang, Y.; Wang, X.-S. Expression of the SARS-CoV-2 cell receptor gene ACE2 in a wide variety of human tissues. *Infect. Dis. Poverty* 2020, 9, 45. <https://doi.org/10.1186/s40249-020-00662-x>.

[51]: Jain, P.; Manuel, S.L.; Khan, Z.K.; Ahuja, J.; Quann, K.; Wigdahl, B. DC-SIGN mediates cell-free infection and transmission of human T-cell lymphotropic virus type 1 by dendritic cells. *J Virol.* 2009 Nov;83(21):10908-21. <https://doi.org/10.1128/JVI.01054-09>.

[52]: Ren, X.X.; Ma, L.; Liu, Q.W.; Li, C.; Huang, Z.; Wu, L.; Xiong, S-D.; Wang, J-H.; Wang, H-B. The molecule of DC-SIGN captures enterovirus 71 and confers dendritic cell-mediated viral trans-infection. *Virol J.* 2014, 11, 47. <https://doi.org/10.1186/1743-422X-11-47>.

[53]: Tassaneetrithep, B.; Burgess, T.H.; Granelli-Piperno, A.; Trumfheller, C.; Finke, J.; Sun, W.; Eller, M.A.; Pattana-panyasat, K.; Sarasombath, S.; Birx, D.L.; et al. DC-SIGN (CD209) mediates dengue virus infection of human dendritic cells. *J Exp Med.* 2003 Apr 7;197(7):823-9. <https://doi.org/10.1084/jem.20021840>.

[54]: Geijtenbeek, T.B.; Kwon, D.S.; Torensma, R.; van Vliet, S.J.; van Duijnhoven, G.C.; Middel, J.; Cornelissen, I.L.; Nottet, H.S.; KewalRamani, V.N.; Littman, D.R.; et al. DC-SIGN, a dendritic cell-specific HIV-1-binding protein that enhances trans-infection of T cells. *Cell.* 2000 Mar 3;100(5):587-97. [https://doi.org/10.1016/s0092-8674\(00\)80694-7](https://doi.org/10.1016/s0092-8674(00)80694-7).

- [55]: Drug-Drug Interaction Assessment for Therapeutic Proteins: Guidance for Industry. <https://www.fda.gov/media/140909/download> (accessed on 10 September 2023)
- [56]: Feinberg, H.; Castelli, R.; Drickamer, K.; Seeberger, P.H.; Weis, W.I. Multiple modes of binding enhance the affinity of DC-SIGN for high mannose N-linked glycans found on viral glycoproteins. *J Biol Chem.* 2007 Feb 9;282(6):4202-9. <https://doi.org/10.1074/jbc.M609689200>.
- [57]: Mori, T.; O'Keefe, B.R.; Sowder, R.C. 2nd; Bringans, S.; Gardella, R.; Berg, S.; Cochran, P.; Turpin, J.A.; Buckheit, R.W. Jr; McMahan, J.B.; Boyd, M.R. Isolation and characterization of griffithsin, a novel HIV-inactivating protein, from the red alga *Griffithsia* sp. *J Biol Chem.* 2005 Mar 11;280(10):9345-53. <https://doi.org/10.1074/jbc.M411122200>.
- [58]: Rouillard, A.D.; Gundersen, G.W.; Fernandez, N.F.; Wang, Z.; Monteiro, C.D.; McDermott, M.G.; Ma'ayan, A. The harmonizome: a collection of processed datasets gathered to serve and mine knowledge about genes and proteins. *Da-tabase (Oxford).* 2016 Jul 3;2016. pii: baw100. <https://doi.org/10.1093/database/baw100>.
- [59]: Bains, A.; Guan, W.; LiWang, P.J. The Effect of Select SARS-CoV-2 N-Linked Glycan and Variant of Concern Spike Protein Mutations on C-Type Lectin-Receptor-Mediated Infection. *Viruses* 2023, 15, 1901. <https://doi.org/10.3390/v15091901>
- [60]: McKay, L. G. A. The Effects of HIV-1, HCV and Ebola Virus Envelope Proteins on Modulating Viral Phenotypes and Activity. Dissertation. University of Liverpool, Liverpool, England, United Kingdom, 2018 Jul. The University of Liverpool Repository. Available online: [https://livrepository.liverpool.ac.uk/3031002/1/201064897\\_Jul2018.pdf](https://livrepository.liverpool.ac.uk/3031002/1/201064897_Jul2018.pdf) (ac-cessed on 27 August 2023).
- [61]: Chung, N.P.; Breun, S.K.; Bashirova, A.; Baumann, J.G.; Martin, T.D.; Karamchandani, J.M.; Rausch, J.W.; Le Grice, S.F.; Wu, L.; Carrington, M.; et al. HIV-1 transmission by dendritic cell-specific ICAM-3-grabbing nonintegrin (DC-SIGN) is regulated by determinants in the carbohydrate recognition domain that are absent in liver/lymph node-SIGN (L-SIGN). *J Biol Chem.* 2010 Jan 15;285(3):2100-12. <https://doi.org/10.1074/jbc.M109.030619>.
- [62]: Wu, L.; Martin, T.D.; Carrington, M.; KewalRamani, V.N. Raji B cells, misidentified as THP-1 cells, stimulate DC-SIGN-mediated HIV transmission. *Virology.* 2004 Jan 5;318(1):17-23. <https://doi.org/10.1016/j.virol.2003.09.028>.
- [63]: Di Gianvincenzo, P.; Chiodo, F.; Marradi, M.; Penadés, S. Chapter two - Gold manno-Glyconanoparticles for In-tervening in HIV gp120 Carbohydrate-Mediated Processes. In *Methods in Enzymology*; Editor: Düzgüneş, N.; Academic Press: Cambridge, MA, USA, 2012; Volume 509, pp. 21-40. <https://doi.org/10.1016/B978-0-12-391858-1.00002-2>.
- [64]: Crawford, K.H.D.; Eguia, R.; Dingens, A.S.; Loes, A.N.; Malone, K.D.; Wolf, C.R.; Chu, H.Y.; Tortorici, M.A.; Velesler, D.; Murphy, M.; et al. Protocol and Reagents for Pseudotyping Lentiviral Particles with SARS-CoV-2 Spike Protein for Neutralization Assays. *Viruses* 2020, 12, 513. <https://doi.org/10.3390/v12050513>.
- [65]: Nabeta, H.W.; Zahin, M.; Fuqua, J.L.; Cash, E.D.; Leth, I.; Strauss, M.; Novak, J.; Wang, L.; Siegwald, A.; Sheppard, R.A., et al. A Phase 1a/1b Clinical Trial Design to

Assess Safety, Acceptability, Pharmacokinetics and Tolerability of Intranasal Q-Griffithsin for COVID-19 Prophylaxis. *University of Louisville Journal of Respiratory Infections*. 2022 Nov, 6(1), a22. <https://doi.org/10.55504/2473-2869.1250>.

[66]: Nabeta, H.W.; Lasnik, A.B.; Fuqua, J.L.; Wang, L.; Rohan, L.C.; Palmer, K.E. Antiviral lectin Q-Griffithsin suppresses fungal infection in murine models of vaginal candidiasis. *Front Cell Infect Microbiol*. 2022 Oct 18, 12, 976033. <https://doi.org/10.3389/fcimb.2022.976033>.

[67]: Cavanagh, J.; Fairbrother, W.J.; Palmer III, A.G.; Skleton, N.J. Chapter 9 – Larger Proteins and Molecular Interactions. In *Protein NMR Spectroscopy – Principles and Practice*, 2nd Edition; Editors: Cavanagh, J.; Fairbrother, W.J.; Palmer, A.G.; Rance, M.; Skleton, N.J.; Academic Press: Cambridge, MA, USA, 2007; pp. 725-780. <https://doi.org/10.1016/B978-012164491-8/50011-7>.

[68]: Zhao, Y.; Zhao, N.; Cai, Y.; Zhang, H.; Li, J.; Liu, J.; Ye, C.; Wang, Y.; Dang, Y.; Li, W.; et al. An algal lectin griffithsin inhibits Hantaan virus infection in vitro and in vivo. *Front Cell Infect Microbiol*. 2022 Dec 12, 12, 881083. <https://doi.com/10.3389/fcimb.2022.881083>.

[69]: Jumper, J.; Evans, R.; Pritzel, A.; Green, T.; Figurnov, M.; Ronneberger, O.; Tunyasuvunakool, K.; Bates, R.; Žídek, A.; Potapenko, A.; et al. Highly accurate protein structure prediction with AlphaFold. *Nature* 2021, 596, 583–589. <https://doi.org/10.1038/s41586-021-03819-2>

[70]: Varadi, M.; Anyango, S.; Deshpande, M.; Nair, S.; Natassia, C.; Yordanova, G.; Yuan, D.; Stroe, O. Wood, G. Laydon, A.; et al. AlphaFold Protein Structure Database: massively expanding the structural coverage of protein-sequence space with high-accuracy models. *Nucleic Acids Res*. 2022 Jan 7, 50(D1), D439-D444. <https://doi.org/10.1093/nar/gkab1061>.

[71]: Tabarani, G.; Thépaut, M.; Stroebel, D.; Ebel, C.; Vivès, C.; Vachette, P.; Durand, D.; Fieschi, F. DC-SIGN neck domain is a pH-sensor controlling oligomerization: SAXS and hydrodynamic studies of extracellular domain. *J. Biol. Chem*. 2009, 284, 21229–21240. <https://doi.org/10.1074/jbc.M109.021204>.

[72]: Lukácsi, S.; Mácsik-Valent, B.; Nagy-Baló, Z.; Kovács, K.G.; Kliment, K.; Bajtay, Z.; Erdei, A. Utilization of complement receptors in immune cell-microbe interaction. *FEBS Lett*. 2020 Aug, 594(16), 2695-2713. <https://doi.com/10.1002/1873-3468.13743>.

[73]: Marquart, H.V.; Olesen, E.H.; Johnson, A.A.; Damgaard, G.; Leslie, R.G. A comparative study of normal B cells and the EBV-positive Burkitt's lymphoma cell line, Raji, as activators of the complement system. *Scand J Immunol*. 1997 Sep, 46(3), 246-53. <https://doi.org/10.1046/j.1365-3083.1997.d01-122.x>.

[74]: Upasani, V.; Rodenhuis-Zybert, I.; Cantaert, T. Antibody-independent functions of B cells during viral infections. *PLoS Pathog*. 2021 Jul 22, 17(7), e1009708. <https://doi.org/10.1371/journal.ppat.1009708>.

[75]: Obukhanych, T.V.; Nussenzweig, M.C. T-independent type II immune responses generate memory B cells. *J Exp Med*. 2006 Feb 20, 203(2), 305-10. <https://doi.org/10.1084/jem.20052036>.

- [76]: Mond, J.J.; Lees, A.; Snapper, C.M. T cell-independent antigens type 2. *Annu Rev Immunol.* 1995, 13, 655-692. <https://doi.org/10.1146/annurev.iy.13.040195.003255>.
- [77]: Lewis, R.; Wang, H.; Schreuder, G.; Marsh, S.; Kennedy, L. Chapter 2 - Antigens, Immunogens, Vaccines, and Immunization. In *Immunology Guidebook*; Editors: Cruse, J.M.; Lewis, R. E.; Wang, H. Academic Press: Cambridge, MA, USA, 2004; pp. 17-45. <https://doi.org/10.1016/B978-012198382-6/50026-1>.
- [78]: Zhang, Z.; Nomura, N.; Muramoto, Y.; Ekimoto, T.; Uemura, T.; Liu, K. Yui, M.; Kono, N.; Aoki, J.; Ikeguchi, M.; et al. Structure of SARS-CoV-2 membrane protein essential for virus assembly. *Nat Commun.* 2022 Aug 5, 13, 4399. <https://doi.org/10.1038/s41467-022-32019-3>.
- [79]: Waterhouse, A.; Bertoni, M.; Bienert, S.; Studer, G.; Tauriello, G.; Gumienny, R.; Heer, F.T.; de Beer, T.A.P.; Rempfer, C.; Bordoli, L.; et al. SWISS-MODEL: homology modelling of protein structures and complexes. *Nucleic Acids Res.* 2018, 46(W1), W296-W303. <https://doi.org/10.1093/nar/gky427>.
- [80]: Bienert, S.; Waterhouse, A.; de Beer, T.A.P.; Tauriello, G.; Studer, G.; Bordoli, L.; Schwede, T. The SWISS-MODEL Repository - new features and functionality. *Nucleic Acids Res.* 2017 Jan 4;45(D1), D313-D319. <https://doi.org/10.1093/nar/gkw1132>.
- [81]: Guex, N.; Peitsch, M.C.; Schwede, T. Automated comparative protein structure modeling with SWISS-MODEL and Swiss-PdbViewer: A historical perspective. *Electrophoresis.* 2009 Jun;30 Suppl 1, S162-S173. <https://doi.org/10.1002/elps.200900140>.
- [82]: Studer, G.; Tauriello, G.; Bienert, S.; Biasini, M.; Johner, N.; Schwede, T. ProMod3 - A versatile homology modelling toolbox. *PLoS Comput Biol.* 2021 Jan 28;17(1):e1008667. <https://doi.org/10.1371/journal.pcbi.1008667>.
- [83]: Studer, G.; Rempfer, C.; Waterhouse, A.M.; Gumienny, R.; Haas, J.; Schwede, T. QMEANDisCo - distance constraints applied on model quality estimation. *Bioinformatics.* 2020 Mar 1;36(6), 1765-1771. <https://doi.org/10.1093/bioinformatics/btz828>.
- [84]: Studer, G.; Biasini, M.; Schwede, T. Assessing the local structural quality of transmembrane protein models using statistical potentials (QMEANBrane). *Bioinformatics.* 2014 Sep 1;30(17), i505-11. <https://doi.org/10.1093/bioinformatics/btu457>.
- [85]: Benkert, P.; Biasini, M.; Schwede, T. Toward the estimation of the absolute quality of individual protein structure models. *Bioinformatics.* 2011 Feb 1;27(3), 343-350. <https://doi.org/10.1093/bioinformatics/btq662>.
- [86]: Bertoni, M.; Kiefer, F.; Biasini, M.; Bordoli, L.; Schwede, T. Modeling protein quaternary structure of homo- and hetero-oligomers beyond binary interactions by homology. *Sci Rep.* 2017 Sep 5, 7(1), 10480. <https://doi.org/10.1038/s41598-017-09654-8>.
- [87]: Mariani, V.; Biasini, M.; Barbato, A.; Schwede, T. IDDT: a local superposition-free score for comparing protein structures and models using distance difference tests. *Bioinformatics.* 2013 Nov 1, 29(21), 2722-2728. <https://doi.org/10.1093/bioinformatics/btt473>.

- [88]: Antonides, L.H.; Hurst, Q.W.; Ives, C.M.; Ramberg, K.; Ostrovitsa, N.; Scanlan, E.; Caffrey, M.; Pitt, S.J.; Zachariae, U. The SARS-CoV-2 envelope (E) protein forms a calcium- and voltage-activated calcium channel. *bioRxiv*. 2022, <https://doi.org/10.1101/2022.10.11.511775>.
- [89]: Thomas, S. The Structure of the Membrane Protein of SARS-CoV-2 Resembles the Sugar Transporter SemiSWEET. *Pathog Immun*. 2020 Oct 19, 5(1), 342-363. <https://doi.org/10.20411/pai.v5i1.377>.
- [90]: Li Q, Wu J, Nie J, Zhang L, Hao H, Liu S, Zhao C, Zhang Q, Liu H, Nie L, Qin H, Wang M, Lu Q, Li X, Sun Q, Liu J, Zhang L, Li X, Huang W, Wang Y. The Impact of Mutations in SARS-CoV-2 Spike on Viral Infectivity and Antigenicity. *Cell*. 2020 Sep 3, 182(5), 1284-1294.e9. <https://doi.org/10.1016/j.cell.2020.07.012>.
- [91]: del Rio, C.; Malani, P.N. COVID-19 in the Fall of 2023—Forgotten but Not Gone. *JAMA*. 2023 Sep 12. <https://doi.org/10.1001/jama.2023.19049>.
- [92]: Zhang, L.; Herrera, C.; Coburn, J.; Olejniczak, N.; Ziprin, P.; Kaplan, D.; LiWang P.J. Sustained release and stability to high temperatures of HIV inhibitors by encapsulation in silk fibroin disks. *ACS Biomater Sci Eng*. 2017, 3(8), 1654-1665. <https://doi.org/10.1021/acsbiomaterials.7b00167>.
- [93]: Yavuz, B.; Morgan, J.L.; Herrera, C.; Harrington, K.; Perez-Ramirez, B.; LiWang, P.J.; Kaplan, D.L. Sustained Release Silk Fibroin Discs: Antibody and Protein Delivery for HIV Prevention. *J Control Release*. 2019 May 10, 301, 1-12. <https://doi.org/10.1016/j.jconrel.2019.03.001>.
- [94]: Fuqua, J.L.; Hamorsky, K.; Khalsa, G.; Matoba, N.; Palmer, K.E. Bulk production of the antiviral lectin griffithsin. *Plant Biotechnol J*. 2015 Oct, 13(8), 1160-1168. <https://doi.org/10.1111/pbi.12433>.
- [95]: Kremlitzka, M.; Mácsik-Valent, B.; Erdei, A. Regulation of B cell functions by Toll-like receptors and complement. *Immunol Lett*. 2016 Oct, 178, 37-44. <https://doi.org/10.1016/j.imlet.2016.07.015>.
- [96]: Wilhelm, I.; Levit-Zerdoun, E.; Jakob, J.; Villringer, S.; Frensch, M.; Übelhart, R.; Landi, A.; Müller, P.; Imberty, A.; Thuenauer, R.; et al. Carbohydrate-dependent B cell activation by fucose-binding bacterial lectins. *Sci Signal*. 2019 Mar 5, 12(571), eaao7194. <https://doi.org/10.1126/scisignal.aao7194>.
- [97]: Geurtsen, J.; Driessen, N.N.; Appelmelk, B.J. Mannose–fucose recognition by DC-SIGN. *Microbial Glycobiology*. 2010, 673–695. <https://doi.org/10.1016/B978-0-12-374546-0.00034-1>.
- [98]: García-Pérez, B.E.; De la Cruz-López, J.J.; Castañeda-Sánchez, J.I.; Muñoz-Duarte, A.R.; Hernández-Pérez, A.D.; Vil-legas-Castrejón, H.; García-Latorre, E.; Caamal-Ley, A.; Luna-Herrera, J. Macropinocytosis is responsible for the uptake of pathogenic and non-pathogenic mycobacteria by B lymphocytes (Raji cells). *BMC Microbiol*. 2012 Oct 31, 12, 246. <https://doi.org/10.1186/1471-2180-12-246>.
- [99]: Hoffman, W.; Lakkis, F.G.; Chalasani, G. B Cells, Antibodies, and More. *Clin J Am Soc Nephrol*. 2016 Jan 7, 11(1), 137-54. <https://doi.org/10.2215/CJN.09430915>.



[100]: Neuman, B.W.; Kiss, G.; Kunding, A.H.; Bhella, D.; Baksh, M.F.; Connelly, S.; Droese, B.; Klaus, J.P.; Makino, S.; Sawicki, S.G.; et al. A structural analysis of M protein in coronavirus assembly and morphology. *J Struct Biol.* 2011 Apr, 174(1), 11-22. <https://doi.org/10.1016/j.jsb.2010.11.021>.

[101]: Cao, Y.; Yang, R.; Lee, I.; Zhang, W.; Sun, J.; Wang, W.; Meng, X. Characterization of the SARS-CoV-2 E Protein: Sequence, Structure, Viroporin, and Inhibitors. *Protein Sci.* 2021 Jun, 30(6), 1114-1130. <https://doi.org/10.1002/pro.4075>.

## Chapter 4

### **An Investigation into SARS-CoV-2 Pseudotyped Virus Stability and the Development of Assays to Evaluate the Physical Properties of Virions**

This chapter makes use of work that has been published as a part of: Mortazavi M\*, Bains A\*, Afsah-Hejri L, Ehsani R, LiWang PJ. SARS-CoV-2 pseudotyped virus persists on the surface of multiple produce but can be inactivated with gaseous ozone. *Heliyon*. 2022 Aug;8(8):e10280. doi: 10.1016/j.heliyon.2022.e10280. Epub 2022 Aug 15. doi: 10.1016/j.heliyon.2022.e10280. [1]

\* Both authors contributed equally to the publication

#### **4.1 Abstract**

Due to the immense societal and economic impact that the COVID-19 pandemic has caused, limiting the spread of SARS-CoV-2 is one of the most important priorities at this time. The global interconnectedness of the food industry makes it one of the biggest concerns for SARS-CoV-2 outbreaks. Although fomites are currently considered a low-risk route of transmission for SARS-CoV-2, new variants of the virus can potentially alter the transmission dynamics. In this study, we compared the survival rate of pseudotyped SARS-CoV-2 on plastic with some commonly used food samples (i.e., apple, strawberry, grapes, tomato, cucumber, lettuce, parsley, Brazil nut, almond, cashew, and hazelnut). The porosity level and the chemical composition of different food products affect the virus's stability and infectivity. Our results showed that tomato, cucumber, and apple offer a higher survival rate for the pseudotyped viruses. Next, we explored the effectiveness of ozone in deactivating the SARS-CoV-2 pseudotyped virus on the surface of tomato, cucumber, and apple. We found that the virus was effectively inactivated after being exposed to 15 ppm of ozone for one hour under ambient conditions. The results of our study indicate that ozonated air can likely provide a convenient method of effectively disinfecting bulk food shipments that may harbor the SARS-CoV-2 virus.

Bains A then reports on some work he has done independently to assess the physical properties of the SARS-CoV-2 pseudovirus.

#### **4.2 Introduction**

As new prevention protocols and tools are developed, the emergence of new variants makes the fight against the COVID-19 pandemic more challenging [2]. New variants are likely harbingers for future SARS-CoV-2 mutants that will display increased transmissibility and contagiousness. Due to this risk, it is important to revisit preventative measures against COVID-19. While there are several studies that investigate the transmission of the virus through aerosol droplets and physical objects, less attention has been paid to contaminated food products as potential carriers of SARS-CoV-2 [3, 4].

Viruses have recently been recognized as a significant cause of foodborne diseases in the world [5]. In the 2002-2003 coronavirus outbreak, there was significant concern over whether SARS-CoV-1 was transmitted through the fecal-oral route in addition to respiratory transmission [6, 57, 58]. While this was not a major concern for SARS coronaviruses, numerous other coronaviruses are spread via the fecal-oral route.

Upon infecting humans, the virus spreads through respiratory droplets and contaminated surfaces [7]. The principal mode of SARS-CoV-2 transmission is through exposure to respiratory particles carrying the infectious viruses. However, a lower risk of transmission occurs through contacting contaminated fomites [8]. Research shows that the coronavirus particles can remain active in the air for up to 3 hours and on non-organic surfaces such as plastic for up to 72 hours [9, 10, 11].

In the food supply chain, contamination by foodborne viruses can occur at any step, starting from pre-harvest, during the post-harvest process, throughout product transportation or distribution, and even before consumption [3, 12]. Indeed, food-derived fomites are a major route of transmission for at least two hepatitis viruses: Hepatitis A virus, which is responsible for the most foodborne viral infections per year, and Hepatitis E virus, which is known to be a zoonotic virus [13]. So far, food consumption has not been recognized as a route for SARS-CoV-2 transmission [14]. But there are several members of the Coronaviridae family viruses that are enteric viruses, such as Bovine coronavirus and Feline coronavirus [60, 61]. Ergo, there is still ambiguity about the foodborne transmission of SARS-CoV-2, and a potential worry that the virion itself could mutate to acquire enteric transmission capabilities that are common in other coronaviruses. Furthermore, the SARS-CoV-2 virion is quite stable, with evidence showing that it can be detected in stool samples from infected individuals [59]. Unlike bacteria, mold, and yeast, viruses (including coronaviruses) are not capable of replication and growth on food surfaces [15, 16]. However, they can survive on food surfaces or packages depending on the virus stability. Other environmental factors such as temperature, pH, relative humidity, and the presence of nearby oxidizing agents affect the virus half-life [5, 17]. Potentially, foods can act as a vehicle to facilitate the virus's transmission either locally or at the global level. The issue of food cross-contamination puts agricultural workers in general and food handlers in particular at higher risk of viral infections. Evidence shows that workers who come into close contact with animals that are carriers of species-specific coronaviruses or food products from organisms that carry coronaviruses exhibit levels of circulating anti-coronavirus antibodies, despite not reporting having fallen sick [61, 62]. This suggests the possibility that regular contact with food products that carry viruses can eventually lead to enough exposure to viral antigens to elicit an immune response [62]. Applying standard disinfection procedures on food products can prevent the potential transmission of SARS-CoV-2 and other foodborne diseases.

SARS-CoV-2 belongs to the betacoronavirus ( $\beta$ CoV) genus from the Coronaviridae family [18]. SARS-CoV-2 is an enveloped virus, meaning that the genomic RNA is packaged within a fatty or lipid membrane [19]. There are four proteins that form the main structure of the virus; Spike (S), Membrane (M), Envelope (E), and Nucleocapsid (N) proteins [20] (Figure 1a). The lipid membrane or envelope contains the virus proteins such as spike (S) which promotes the viral attachment to the host cell [21] and acts as a natural shield that protects the RNA genetic material. The trade-off between the stability of the outer membrane and the ability to release the RNA after entry into the host cell constrains the virus to be susceptible to oxidation and disinfection.

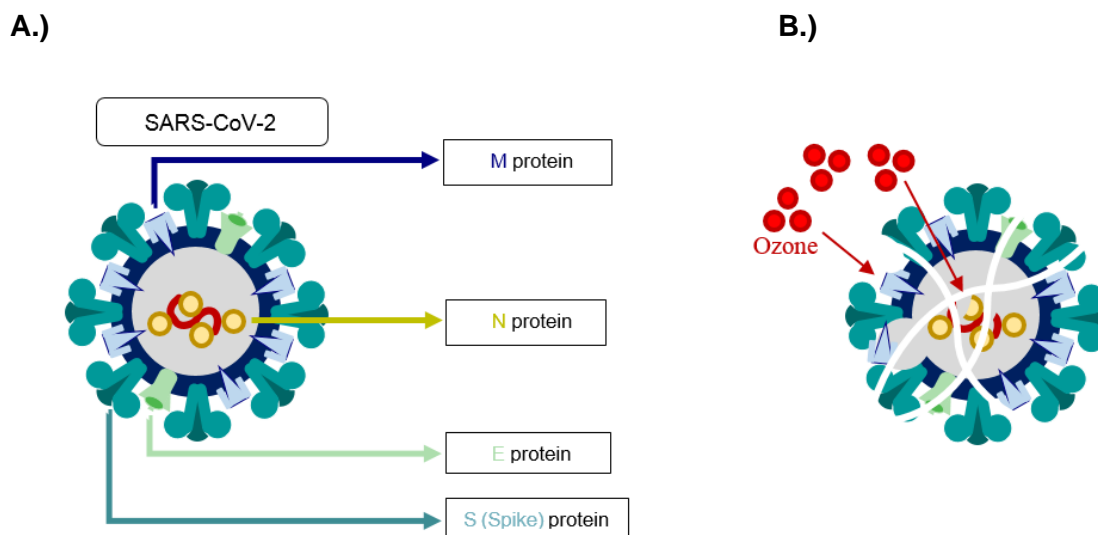


**Figure 1. A.)** Cartoon rendition of the SARS-CoV-2 structure. **B.)** SARS-CoV-2 oxidized and inactivated by ozone. While the exact etiology behind ozone-based neutralization of SARS-CoV-2 and similarly structured viruses is unresolved, gaseous ozone is known to damage viral proteins, RNA, and lipids [29, 36, 37]. We aimed to depict how it is likely that ozone damages these different molecules of the virus concertedly, which leads to inactivation.

Ozone, the triatomic form of oxygen, is a natural gas with a high oxidation/reduction potential [22]. It is a suitable alternative for chemical disinfectants in the food industry, and a residue-free fumigant for microbial control and shelf-life extension of fresh produce [23, 24].

Several studies have proved the efficacy of ozone in viral inactivation [11, 25, 26, 27, 28, 29, 30, 31]. For example, application of 6.25 ppm ozone for 5 min resulted in a 1.6 log<sub>10</sub> reduction in Murine norovirus MNV-1 on the surface of green onions, and a 2.91 log<sub>10</sub> reduction on the surface of lettuce samples [32]. Brié et al. 2018 showed that a low concentration of ozone (3 ppm for 1 min) inactivated Murine norovirus on the surface of raspberries (> 3.3 log<sub>10</sub> reduction) while Hepatitis A virus (HAV) on raspberries was inactivated after 3 min exposure to 5 ppm ozone [29].

Ozonation is also an ideal method for disinfection of packaging materials and preservation of heat-sensitive foods [33]. Both gaseous and aqueous forms of ozonation can effectively inactivate SARS-CoV-2 [34, 35]. Ozone attacks the lipid envelope and spike proteins of SARS-CoV-2 (Figure 1B), disrupts the viral attachment process, and inhibits replication [36, 38] showed that ozone can successfully eliminate SARS-CoV-2 from the surface of personal protective equipment (PPE). In another recent study, 95% inactivity was reported after SARS-CoV-2 was exposed to 0.1 mg L<sup>-1</sup> ozone gas for 10 hours [39]. Murata et al., 2021 showed a 3-log reduction for SARS-CoV-2 after 10 seconds of exposure to 2 mg L<sup>-1</sup> aqueous ozone, meaning that a low concentration of

ozone can be used as an alternative to chemical disinfectants in the handwashing process [39].

Through the food supply chain, fresh produce such as fruits and vegetables and bulk nuts can be contaminated with viral particles and potentially transmit viral contamination to individuals. Given the credible possibility that the virus survives on a variety of surfaces, this study aims to assess the propensity of different food products acting as vehicles to spread SARS-CoV-2. Next, we investigate the effectiveness of ozonated air (OA) on the deactivation of SARS-CoV-2 pseudovirus present on the surface of selected fresh produce. We assess how OA may damage SARS-CoV-2 Spike proteins on the surface of viral particles by performing a capture Enzyme-Linked Immunosorbent Assay (ELISA).

## 4.3 Results

### 4.3.1 Virus Survival on Various Produce Surfaces

To evaluate the virus survival on different produce surfaces without any eradication measures, single-round lentivirus pseudotyped with the SARS-CoV-2 Spike protein was spotted on a variety of food items: dry rosids (almond, cashew, Brazil nut, hazelnut), asterid leaves (parsley, lettuce), cruciferous vegetables (broccoli), rosid fruits (cucumber, tomato, apple, grape), and an aggregate accessory fruit (strawberry). 75  $\mu$ L of the single-round virus was spotted onto the surface of these foods and incubated for 1 hour. In general, this led to the evaporation of the liquid. The spot was then rehydrated with 90  $\mu$ L of 293 media and the rehydrated virus was used to infect hACE2-bearing 293t cells to determine viral vitality. We also included an assessment of the survival of this pseudovirus on an inert, non-biological surface (plastic) to compare the degree to which the virus is damaged solely by evaporation on different surfaces. As a positive control, the virus was added directly to the susceptible hACE2 transfected 293t cells from frozen aliquots without being spotted or dried.

The recovery of viral infectivity after incubation on the surface of the fruit was found to be highest on tomato, at 59.4% relative to the positive control (Figure 2). High rates of retention of viral infectivity were also observed with cucumber, apple, and cashew at 40.9%, 28.7%, and 18.3% infectivity respectively. Retention of viral infectivity of pseudovirus above 1% (the ISO-inspired recommended standard) was also found for cashews, Brazil nuts, hazel nuts, parsley, lettuce, and broccoli. As expected, the plastic surface also showed high retention of infectivity at 58.2% after 1 hour of drying [10, 29]. Meanwhile, the recovery rate of the virus on the surface of almond, grape, and strawberry was under 1% (determined by a bootstrapped One-tailed t-test). The significant differences in pseudovirus survival on different produce surfaces (determined by a One-Way ANOVA) indicate that the food matrix itself affects the infectivity of pseudovirus.

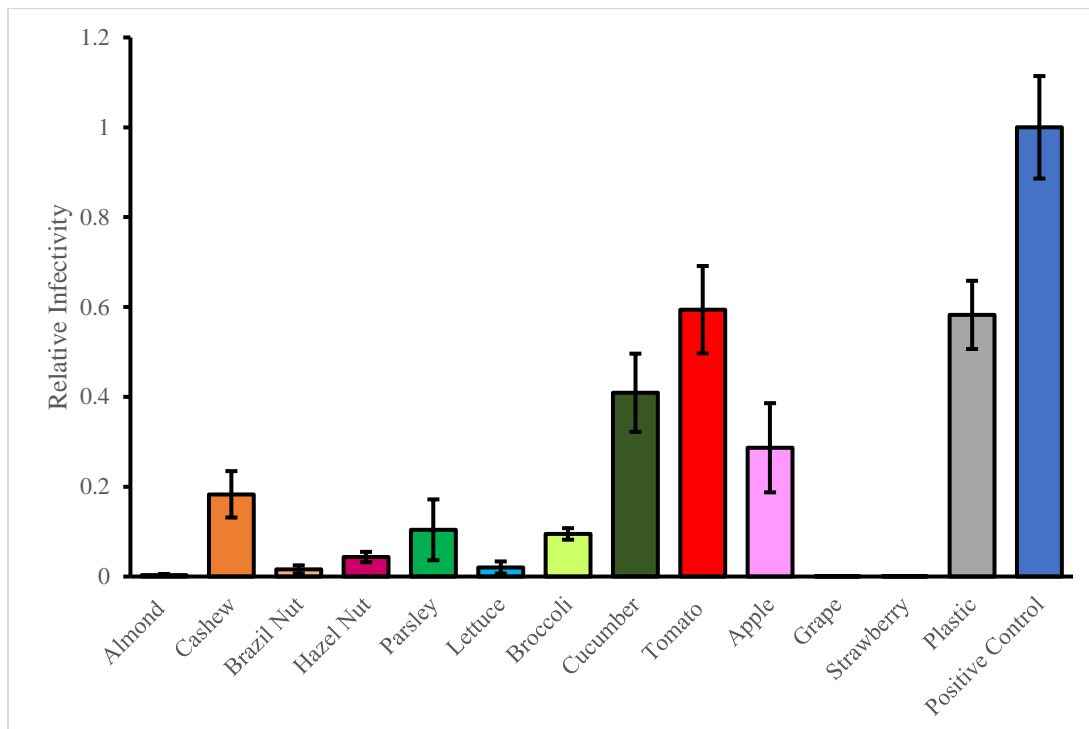


**Figure 2.** The relative retention of infectivity of SARS-CoV-2 pseudotyped virus after being spotted onto the surface of food samples without further eradication measures. Here, the results are normalized based on the positive control. The positive control was 25  $\mu$ L of single-round virus directly added to infect susceptible cells without spotting or drying on a surface. Tomato, cucumber, and apple showed a higher rate of infectivity compared to other samples.

Based on our results from a Tukey-Kramer Multiple Comparison Test, we found that cucumber, tomato, and apple were the food samples with the greatest similarity in signal to the Positive Control. They had the highest retention of viral infectivity after spotting on the surface (more than 20%), and also share the trait of having a very high moisture content (96%, 94.78%, and 83.6%, respectively) [40, 41, 42]. The high retention of infectivity in cucumber, tomato, and apple could also be explained by the presence of the wax layer that is added to these items for retail sale. Among all produce samples, only cucumber, tomato, and apple are normally covered with a thick layer of wax to increase their shelf life. This wax, much like plastic, may hinder viral droplet adsorption into the matrix beneath the protein surface, which may help retain the integrity of the virion.

#### 4.3.2 Effect of Gaseous Ozone on the Surface Survival of SARS-CoV-2

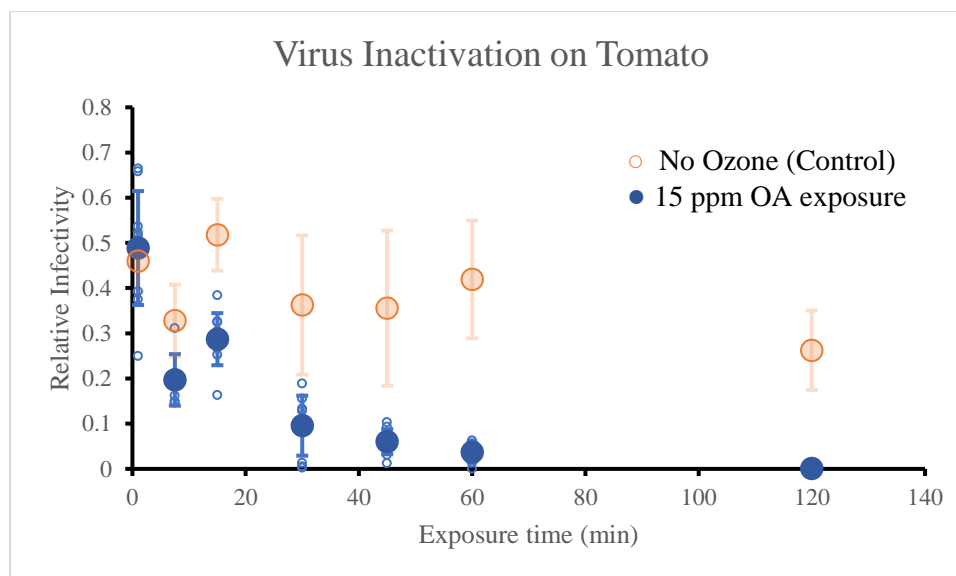
As mentioned before, it is important to develop an environmentally friendly and residue-free method virus sterilization so as to eliminate the concern for potential Covid-19 transmission via contact with contaminated foods. Unlike sterilization procedures that make use of chemicals such as chlorine or physical processes such as heat, ozone minimizes damage to foodstuffs and can easily be produced on-site at a low cost at

almost any point in the food production process. It is easily dissipated and rapidly rendered non-toxic when left in the open air. Also, a comparative study indicates that ozone inactivates viruses faster than chlorine [56].

To test the viability of ozone in sterilizing SARS-CoV-2 pseudovirus-contaminated foodstuffs, we first looked for produce that would have the highest likelihood of retaining active virus on their surface. In our experiment with food samples (Figure 2), cucumber, tomato, and apple provided high pseudoviral survival after 1 hour of incubation on their surface. We thus chose these items of produce to use as fomites for our ozone inactivation study.

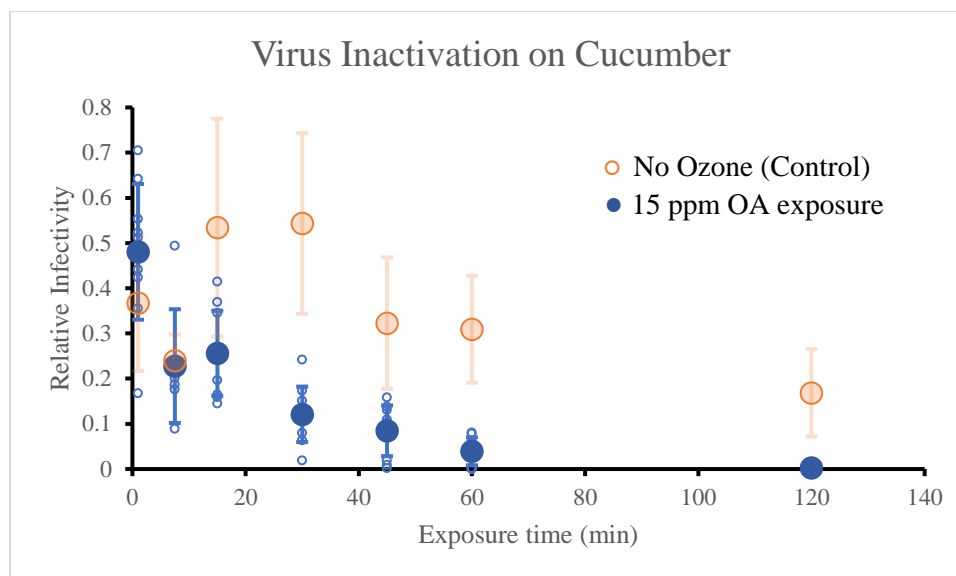
In these experiments, 75  $\mu\text{L}$  of pseudovirus was spotted onto the surface of the sample and then exposed to ozone. Figure 3 shows the relative infectivity of the SARS-CoV-2 pseudotyped virus on the surface of the three products with and without 15 ppm of ozonated air over the course of two hours of exposure. The control group (orange) was kept in containment, while the experimental groups (blue) were exposed to 15 ppm of ozone for the time depicted on the x-axis of each graph. The experiments were conducted under ambient conditions with the relative humidity of  $50\% \pm 10\%$  and a temperature of  $22\text{ }^\circ\text{C} \pm 2\text{ }^\circ\text{C}$ . To collect the virus from the surface of both the controlled and the ozone-treated samples, viral spots were resuspended with 90  $\mu\text{L}$  of 293 Media. As shown in Figure 3, for all produce samples, the ozone exposure significantly reduced the SARS-CoV-2 infectivity, with relatively no retention of infectivity after 60 minutes.

A.)





B.)



C.)

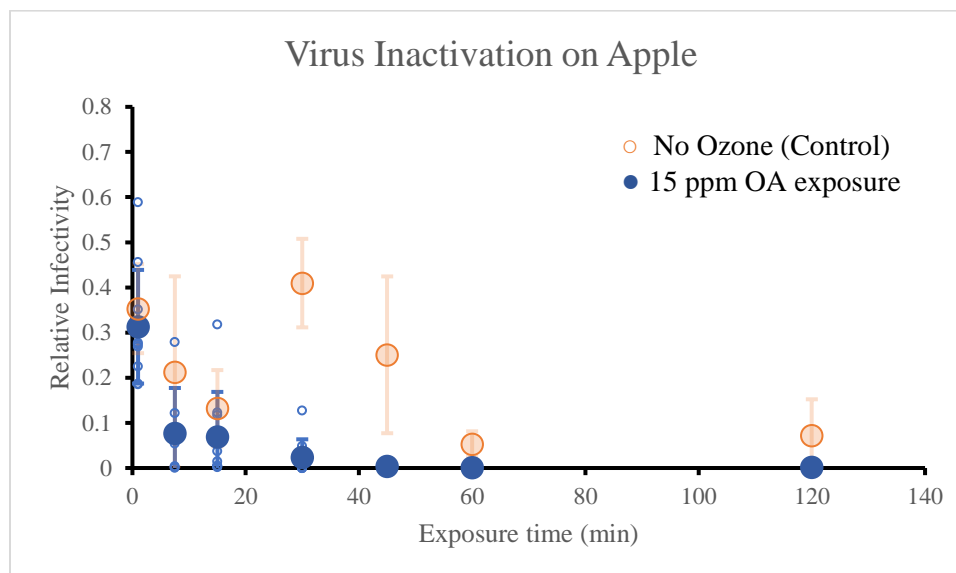


**Figure 3.** The relative infectivity of SARS-CoV-2 pseudotyped virus on the surface of **A)** tomato, **B)** cucumber, and **C)** apple, in the presence (blue) and the absence (red) of 15 ppm of ozonated air (OA). Relative infectivity was obtained by normalizing values with the positive control. The positive control was 25  $\mu$ L of virus from a frozen aliquot directly onto susceptible cells (i.e., virus was not spotted onto any surfaces). Samples consistently show inhibition of virus infectivity after 60 minutes of OA exposure.

As shown in Figure 3, the viral infectivity tended to drop with prolonged exposure to ozone. While there was some fluctuation in the trend at ~7.5 minutes to 30 minutes, the observed data variability is within the expectations for biological model systems: the

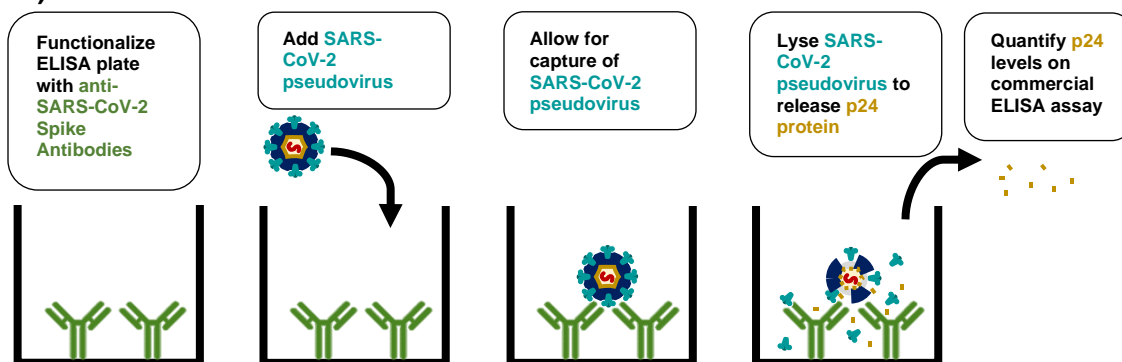
expression of large mammalian proteins and the efficient packaging of viruses are known to fluctuate, even when cell lines and culture conditions are kept constant [43, 44, 45]. Furthermore, proteins have fluctuating lifespans within cells, which may further explain some of the observed variability in the signals for replicates of our luciferase-based assays [46]. However, even with these caveats, the variability for our ozone inactivation results fall inside of the twofold range of data that is considered acceptable for serological assays, providing strong evidence that ozone did indeed efficiently decontaminate our samples [47, 48].

Gaseous ozone dosages of 3-300 ppm\*min have been found to be effective in neutralizing several families of viruses from sterile surfaces [29, 49, 50]. But other viruses exhibit resistance to gaseous ozone treatment, with some retaining up to 80% infectivity after over 400 ppm\*min of ozone [51]. In comparison, we found SARS-CoV-2 pseudovirus was moderately susceptible to ozone treatment, with 225 ppm\*min leading to 48-74% inactivation. Furthermore, doses of 675 ppm\*min ozone led to at least 85% viral inactivation and 1800 ppm\*min guaranteed 100% inactivation of our pseudovirus. While this is a higher dose than several other viruses, it is not a prohibitively large amount of ozone, as we could reliably obtain 15 ppm of ozone within three minutes of turning on our commercial ozone generator.

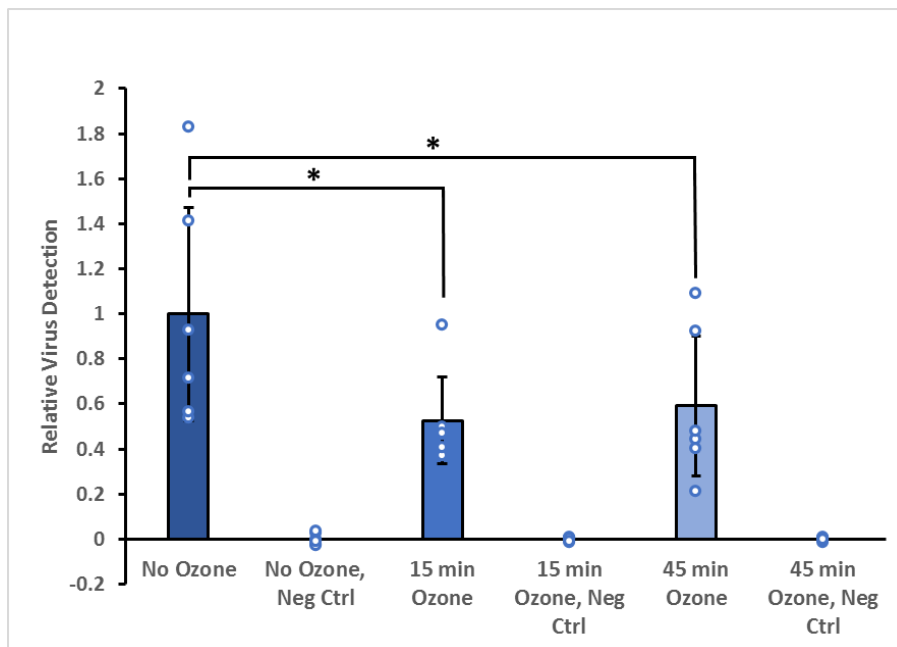
#### 4.3.3 The Effect of Gaseous Ozone on Viral SARS-CoV-2 Spike

We further investigated how ozone reduces virus load by inquiring whether ozone significantly damaged the structure of virus-associated SARS-CoV-2 Spikes. To do so, we performed a viral capture ELISA assay by coating a plate with an anti-SARS-CoV-2 Spike antibody to capture virions before then washing sample wells to remove uncaptured virus. Viral samples that appear to be captured by the antibody coated on plate wells were then lysed and viral concentration was determined by measuring p24 on a commercial ELISA assay (Figure 4A).

A.)



B.)



C.)

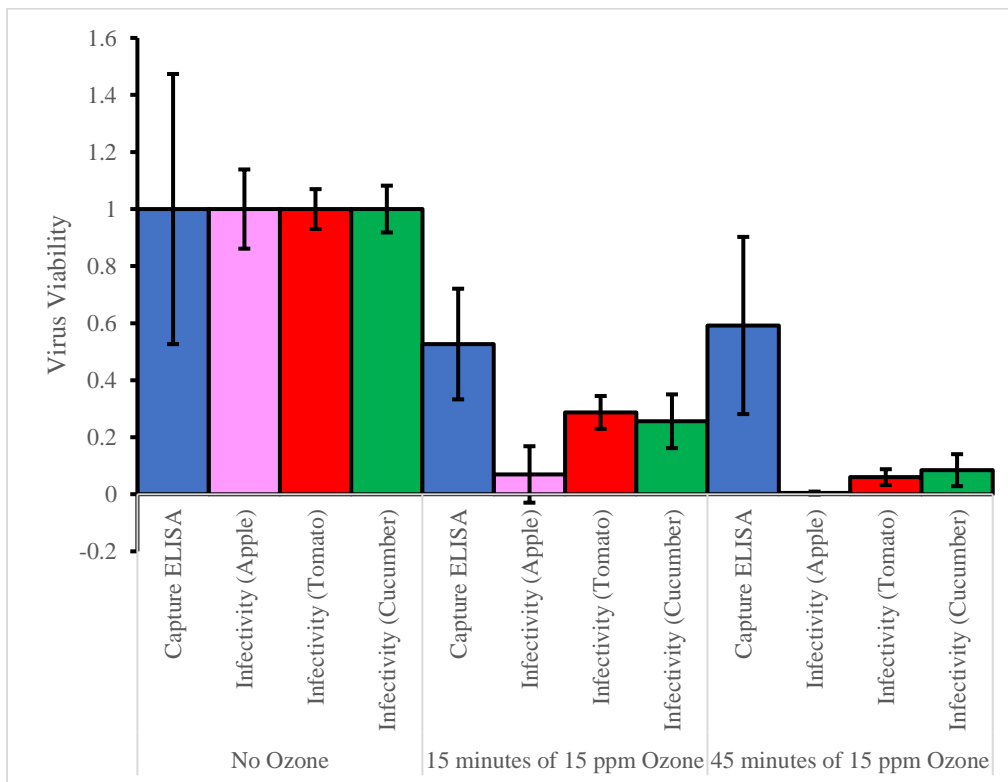


**Figure 4. A.)** Simplified schematic representation of the capture ELISA assay **B.)** SARS-CoV-2 spike damage as quantified by capture ELISA. Negative control wells were not coated with anti-SARS-CoV-2 spike antibody. This was done to ensure that the ozone exposure did not lead to virus samples

nonspecifically interacting with plate wells or BSA. Significant differences in infectivity are shown as asterisks. We performed a One-Way ANOVA test comparing ozone-exposed samples to each other with an  $\alpha = 0.10$  followed by a Tukey-Kramer Multiple Comparison Test. **C.)** SARS-CoV-2 spike damage (blue) versus infectivity on produce: apple (pink), tomato (red), and cucumber (green). Data show infectivity decreases to a greater extent than SARS-CoV-2 spike protein degrades during 15 ppm of OA exposure, implying that ozone sterilized surfaces by damaging more than just the SARS-CoV-2 Spike protein.

It was found that the ozone treatment had a moderate decrease in the ability of the antibody to bind the ozone-treated pseudovirus (Figure 4). After 15 minutes of ozone treatment, the assay shows a decrease of about 47.3% of binding by anti-spike antibody. However, continued ozone exposure doesn't appear to accumulate significantly more damage to the virus spike protein: at 45 minutes of ozone treatment, a time frame that almost wholly inactivates the virus on the surface of produce, the antibody is still able to successfully bind the spike protein at a level of about 40.8%. While the decrease in virus detection was statistically significant with an  $\alpha = 0.10$ , the rate and extent of SARS-CoV-2 spike protein inactivation were not commensurate with the ability of ozone to neutralize the virus on the surface of produce. Therefore, while the data indicate that ozone causes some damage to the viral spike or its presentation on the surface of the virus, this does not entirely explain the ability of ozone to completely inactivate the virus. This result is not unexpected, as previous studies on the effects of ozone on the RNA of virus found that viral inactivation did not necessarily correlate with damage to the virus genome [29]. It is entirely possible that ozone damage to the SARS-CoV-2 Spike did not entirely destroy the epitope detected by the antibody but rather resulted in a combination of effects that overall render the virus noninfectious.

#### 4.4 Discussion

Our results showed that several different kinds of produce could be effective media for SARS-CoV-2 pseudovirus transmission. While we tested only a few representative pieces of produce, it is likely that other popular foodstuffs could maintain significant survival of SARS-CoV-2 virions. Due to the potential connection between SARS-CoV-2 infection and food safety, it is crucial to impose specific disinfection and food handling strategies to reduce the risk of contamination. Ozone generators are relatively compact and can be easily reused, thereby providing an economical and time-efficient disinfection method suitable for large amounts of produce [52].

We tested this by selecting the three foods with the highest virus retention on our produce test (apples, tomatoes, and cucumbers) and subjecting them to neutralization tests with aerosolized ozone (OA). Our results suggest that 60 minutes of ozone exposure (15 ppm OA) inactivated SARS-CoV-2 on the surface of all selected food samples and did not damage cuticle cells nor affect cell membrane integrity. Virus-associated SARS-CoV-2 spike ELISA capture assays did not display ozone damage concomitant to the loss of infectivity as expected from ozone exposure infectivity assays. This was likely because ozone-mediated viral neutralization occurs by damaging a variety of biomolecules in the virions, including membrane lipids, RNA within the capsid, and other surface or capsid proteins. The accumulation of this damage to various aspects of the virus is likely what is responsible for successful disinfection and virus load reduction.

Gaseous ozone is diffusive in air and can penetrate through the underside of surfaces or areas that are obscured from direct light emission [55]. Ozone also rapidly decomposes into oxygen and leaves no toxic by-product, thereby making it a viable alternative to liquid and light-based disinfection methods [36, 52]. These properties make ozone a particularly useful disinfectant for food shipments, where bulk crates of produce can be disinfected collectively with minimal need for follow-up washing or processing. Ozonation of produce could take place at the packaging plants, during storage, or transportation. We hope that the results of our study can provide some direction into developing safe food shipping and handling strategies in the context of the global SARS-CoV-2 pandemic.

## 4.5 Future Experiments and Preliminary Testing

### 4.5.1 Bio-Layer Interferometry as a Means to Measure Structural Features of Membrane-Bound Viruses- Screening for Solvents

Building upon our success with performing a virus capture ELISA assay, we wished to utilize rapid protein-protein interaction techniques to produce an assay to quickly and quantitatively assess whether virus-embedded proteins can interact with a binding partner. Bio-Layer Interferometry (BLI) is a sensitive and high-throughput technique that can measure protein-protein interactions without relying on fluorescent labels or other labeling of analyte proteins.

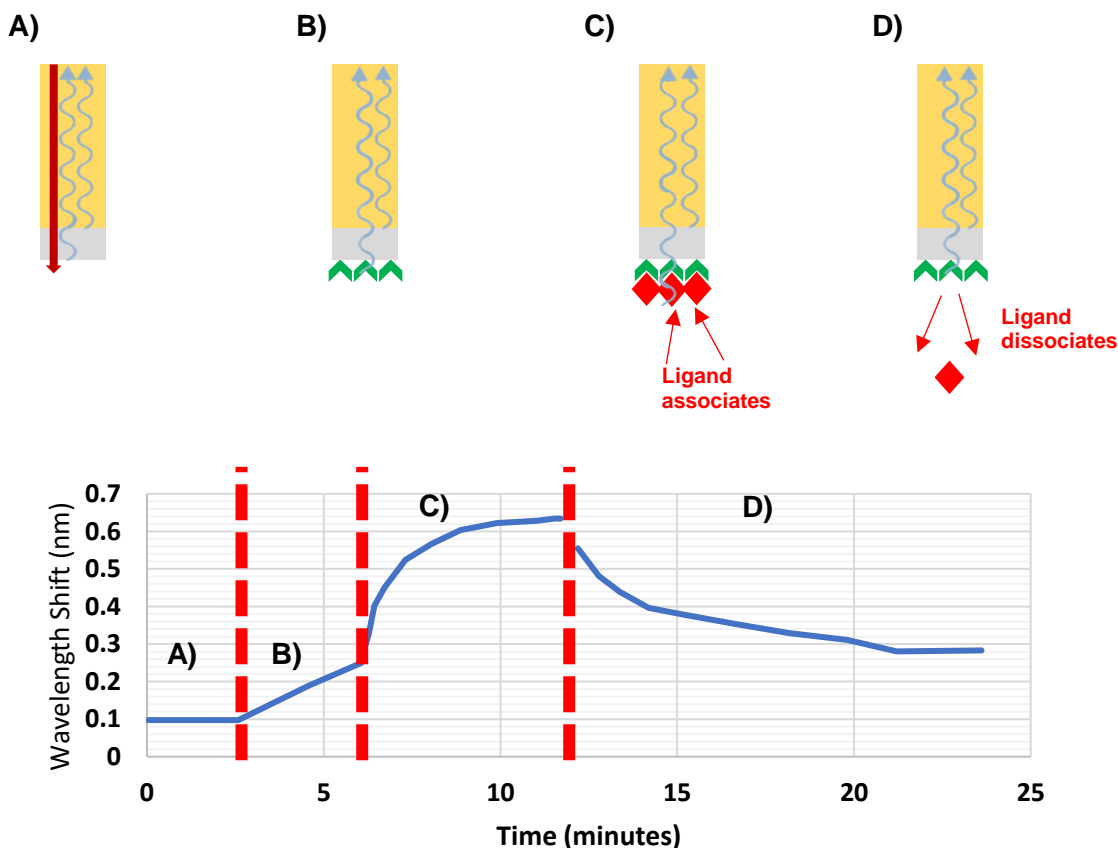


**Figure 5:** Schematic representation of BLI and the data curves that we expect to see on the instrument. **A.)** At the start, light is shone directly down the probe (dark red arrow), with the interference pattern showing light has a unique interference pattern when it reflects off the surface at the end of the probe tip versus when it reflects off of the surface comprised of the interface of proteins that are synthetically attached to the end of the probe and water (grey layer). Usually these proteins at the end of the probe tip recognize common tags used in protein engineering, such as biotin, anti-His or anti-Flag antibodies, or protein A. **B.)** Then, the user is able to functionalize the probe with a desired “capture protein” (green chevrons). The effective length between the surface at the end of the probe tip and the surface comprised of the protein-water interface is extended to include these green proteins, slightly altering the interference frequency between the two reflected lights. **C.)** Then the functionalized probe tip is placed into a third solution containing a ligand (red diamonds) that can bind to the capture protein. The surface comprised of the protein-water interface lengthens again, further altering the interference frequency between the reflected light in the probe. **D.)** Finally, the probe is dipped into a solution to allow for the ligand to dissociate from the capture protein. If the experiment works as expected, the interference wavelength should once again match what was observed in **B.)**. Along the bottom is a schematic diagram of a BLI curve that matches the steps described above [63].

BLI works by measuring the change in wavelength interference upon the binding of an analyte at the end of a probe tip (Figure 5). In brief, light is shone down a probe tip that is functionalized with protein. Each new protein layer effectively acts like a new material with a different refractive index for light. Thus, light will reflect off of each surface, displaying a thin-film interference pattern that can then be interpreted to be related to the amount of mass at the end of a probe tip.

Since pseudoviral samples are harvested from supernatant after transfecting HEK-293Ft cells with the requisite vectors, our virus is typically in a solvent that has numerous additives in it so that cells can survive the process of virus production. The solvent is typically the medium that the cells are cultured in; for HEK 293Ft cells, this is 293 media (described in section 4.6.1) supplemented with 10% Fetal Bovine Serum. At times, we can lower the Fetal Bovine Serum concentration, but typically cell viability and pseudoviral titer drops significantly if we entirely eliminate the additives.

To test which solvent is suitable for use in BLI, we performed a test to see if solvents would lead to any unexpected noise on our BLI system. We first used Griffithsin used as the capture protein on BLI probes; Grft was dissolved in Q buffer and loaded onto tips as per manufacturer’s protocols. Then functionalized tips were dipped into the specified cell culture media and related solvents to assess if there was any unexpected fluctuations in signal (Figure 6A, 6B). Q buffer is the manufacturer suggested solution for the ligand capture/dissociation steps; thus it was used as a control in these experiments (Figure 6A, grey curve). Based on our results, the 0% FBS in OptiMEM and DPBS by itself were the only two solvents that exhibited no unwanted effects on the probe tip. The sample with DPBS + 0.05% NP-40 showed some unwanted variations in wavelength shift, but the changes were small enough to where we considered this a viable backup buffer to continue testing as well.

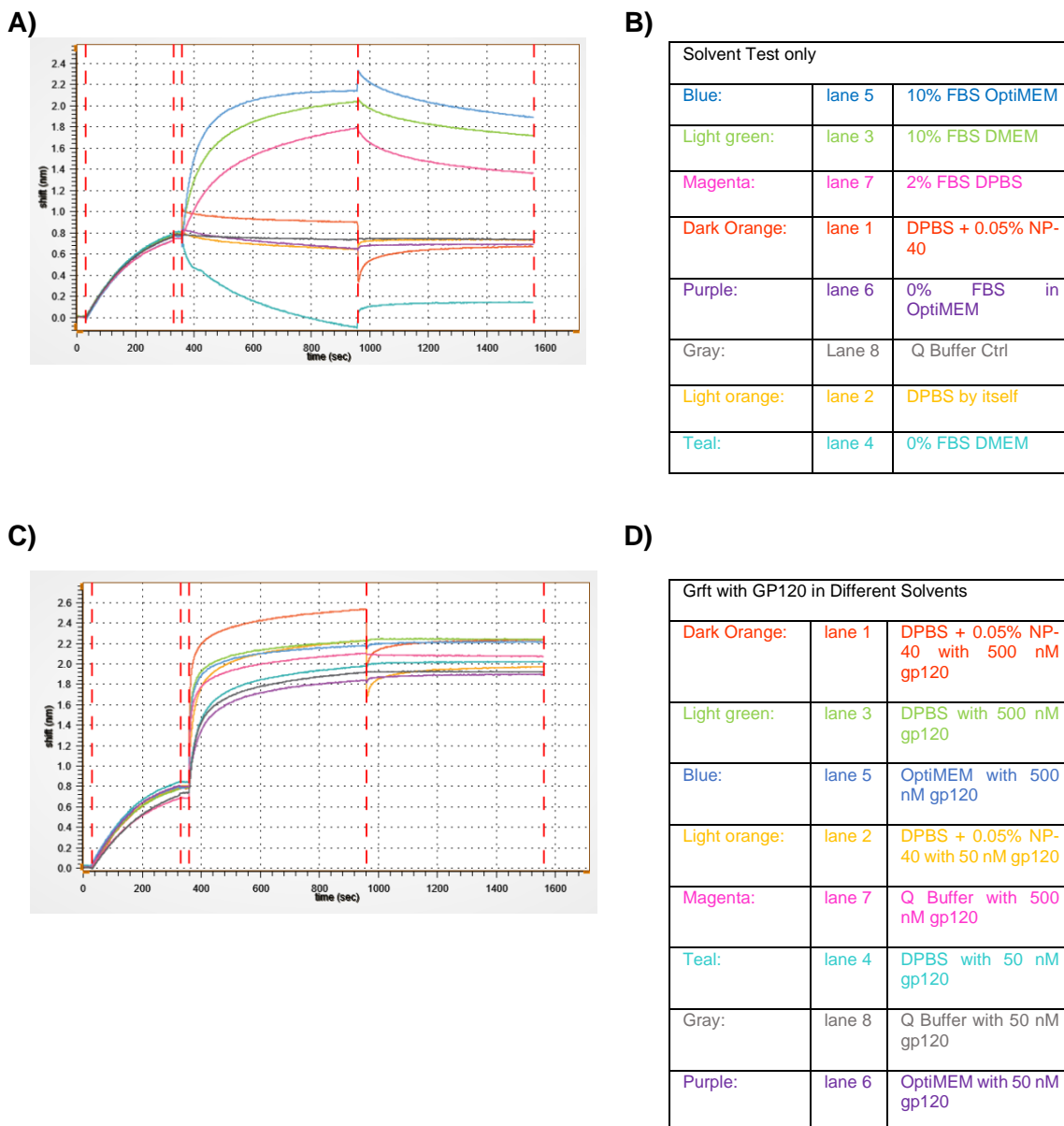


**Figure 6:** BLI tests of Griffithsin-mediated capture of HIV-1 gp120. **A, B.)** We first tested whether Grft-functionalized probes had any unintended wavelength fluctuations if they were placed into solvent without any ligand for the association and dissociation steps. Since no ligand was in these solutions, we expected to see no wavelength change in the final two steps of our BLI run. While the grey, light orange, and purple curves (referring to the Q Buffer control, DPBS by itself, and 0% FBS in OptiMEM samples, respectively) behaved well, all the other solvents displayed unexpected wavelength variations. Of note, all solvents with FBS showed significant binding of protein onto the probe tip. **C, D.)** The most well-behaved buffers were then used to dissolve the HIV-1 gp120 protein and the Griffithsin-mediated capture of GP120 was measured by BLI. Griffithsin captured gp120 in all samples, although the Dark Orange and Light Orange samples had unexpected fluctuations in their wavelength shifts when the probe was moved from the association step to the dissociation step. Given that these two buffers both contained the mild detergent 0.05% NP-40, we attributed this fluctuation to the presence of NP-40.

After performing a screen with only solvents, we then repeated the Grft screening experiment, except we added a ligand to the solvents. Since Griffithsin was our capture protein, we used HIV-1 gp120 as the ligand. Griffithsin has been shown to have 1.5-12 nanomolar binding affinity for gp120 when the two proteins were assessed on a similar assay in the past [64]. Ergo, we used this protein pair as a control to screen for solvent effects, since the binding affinity between Griffithsin and gp120 should be so strong that they should exhibit some binding even in solutions that are not optimal for binding. We ran experiments with gp120 dissolved in PBS, gp120 dissolved in Opti-MEM, and gp120 dissolved in PBS + 0.05% NP-40. As a control, we again used the manufacturer's recommendation of gp120 dissolved in Q buffer. Furthermore, we tested two difference concentrations of gp120 for each solvent: 50 nM and 500 nM. This was to ensure Griffithsin-mediated capture of gp120 even in solvents that were not ideal. Given that we functionalized probe tips with 50 nM Griffithsin solution, there should have been an excess of gp120 ligand even in the 50 nM gp120 samples.

Our results indicated that the Griffithsin-gp120 interaction was clearly strong enough to be maintained in all of the tested solvents. We did observe some unexpected fluctuations in their wavelength shifts when the probe was moved from the association step to the dissociation step. Given that these two buffers both contained the mild detergent 0.05% NP-40, we attributed this fluctuation the presence of NP-40 (Figure 6C, Dark Orange and Light Orange curves). In all cases, the Grft-gp120 interaction was so strong we did not see any appreciable dissociation in the final step.

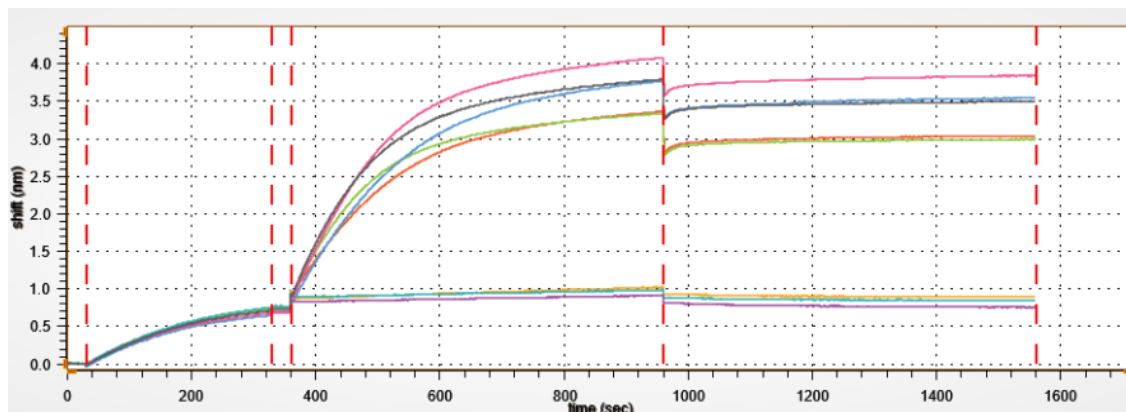
#### **4.5.2 Bio-Layer Interferometry as a Means to Measure Structural Features of Membrane-Bound Viruses- Screening for Virus Detection**

After testing Griffithsin-gp120 binding interaction using proteins, we then moved into trying to see whether we could detect proteins if they were on the surface of a virus. However, we wanted to ensure that our virus samples were not expressed in one of the solutions that we had ruled out in our initial test; thus, most of our existing pseudoviral stocks were not viable for assessment, as the virus was expressed in a DMEM solvent with 10% FBS. To work around this, we freshly transfected cells in a 96 well plate with the vectors necessary to produce pseudovirus with the desired spike on them. We ensured that the virus was expressed into solvent that was compatible with our BLI assays, and then tested the ability of Griffithsin functionalized BLI probes to capture virions. We decided to test pseudovirions functionalized with Wild-Type SARS-CoV-2 Spike, Wild-Type PVO.4 HIV-1 gp120, and then a variant of HIV-1 PVO.4 gp120 with a N295/332/448Q knockout mutation to remove glycosylation. The N295/332/448Q knockout mutation was referred to as 3°. The vectors of HIV-1 PVO.4 protein was originally made by Dr. Kathryn E. Fischer.

We also decided to try transfecting only the viral Spike proteins in eukaryotic cells in the 96 well plate and then lysing the cells in DPBS + 0.05% NP-40 to release Spike proteins into the supernatant. As negative controls, we had a well of untransfected cells and a well of cells transfected with a vector that expressed only luciferase and ZsGreen. Our hope was that the NP-40 did not lyse HEK-293Ft cells to such an extent that other cell glycoproteins could bind to the Griffithsin-functionalized BLI probe.



A)



B)

Transfection run 05132022		
Magenta:	lane 7	Transfect ZsGreen in DPBS with 0.05% NP-40
Gray:	lane 8	Non transfected cells in DPBS with 0.05% NP-40
Blue:	lane 5	SARS-CoV-2 spike in DPBS with 0.05% NP-40
Light green:	lane 3	PVO.4 3° GP120 in DPBS with 0.05% NP-40
Dark Orange:	lane 1	PVO.4 GP120 in DPBS with 0.05% NP-40
Light orange:	lane 2	Virus PVO.4 GP120 express in OptiMEM
Teal:	lane 4	Virus PVO.4 3° GP120 express in Opti-MEM
Purple:	lane 6	Virus SARS CoV-2 express in OptiMEM

↑ Gives strong binding signal  
↓ Gives low or no binding signal

**Figure 7: A.)** Raw BLI reads for the transfected cells specified in **B.)**. We see that the virus-transfected wells provide no appreciable binding signal. Meanwhile, all the wells that consisted of Spike proteins expressed on the surface of cells and lysed with NP-40 showed binding by BLI. Unfortunately, our controls with NP-40 lysed HEK-293Ft cells that were not transfected to express Spike protein (magenta and grey wells) showed the same amount of binding by BLI. This implies to us that some component of the HEK-293 cell lysate is efficiently captured by Griffithsin functionalized probes.

Our results from the BLI transfection tests indicated that pseudovirions are not efficiently detected by Griffithsin-functionalized probes (Figure 7A). Furthermore, our test with transfected cell lysates seem like they have strong binding to Griffithsin functionalized BLI probes regardless of whether the cells express a viral Spike protein. In fact, the negative control samples of HEK-293Ft cells that were either not transfected, or HEK-293Ft cells that were transfected to express luciferase and ZsGreen (magenta and grey, Figure 7B), have slightly higher BLI binding than the virus-transfected HEK-

293Ft cells with GP120. Ergo, we believe that the NP-40 detergent might be releasing many eukaryotic glycoproteins in addition to the Spike protein on the surface of the cells.

In conclusion, we still need to perform more tests to develop the best conditions for Eukaryotic cell-expressed Spike protein. Perhaps we need to find a low enough concentration of NP-40 detergent to release proteins expressed on the surface of the HEK-293Ft cell but not fully solubilize all of the additional proteins. However, when it comes to capturing pseudotyped virions, we at the very least must compare viral binding to BLI probes with viral particles that do not express any spike proteins (“Bald Virus”). Experiments are currently underway to perform these controls. Thus far, we cannot obtain consistent results.

## 4.6 Methods and Materials

### 4.6.1 Pseudovirus and Plasmids Creation

In this study, virus-associated experiments are performed in a biosafety level 2 (BSL-2) laboratory which only allows for pseudotyped SARS-CoV-2 research. Pseudovirus plasmids were obtained through BEI Resources, NIAID, NIH. SARS-CoV-2 spike pseudotyped HIV virions were produced in a protocol inspired by Crawford et al., 2020 [53]. Briefly, 293Ft cells (Invitrogen Cat # R70007) were maintained in 293 Media (Gibco DMEM Cat # 11965-092 supplemented with 2 mM L-Glutamine, 250 µg mL<sup>-1</sup> G418, 25 mM HEPES, and 10% Fetal Bovine Serum) and passaged once cells reached 70-100% confluency. The day prior to transfection, 293Ft cells were seeded at a density of approximately  $2.5 \times 10^6$  cells in 8-10 mL of 293 Media into a 100 mm tissue culture petri dish. Cells were allowed to recover for 12-16 hours in a humidified incubator at 37 °C and 5% CO<sub>2</sub>.

Petri dishes were then withdrawn from incubators and cells were assessed for confluency and adhesion. If the cells in petri dishes were 70% confluent and adherent, media was gently replaced with 8 mL of fresh 293 Media. The petri dish was returned to the incubator for approximately 45 minutes while the plasmids and transfection reagent were prepared. The following plasmids were mixed in 900 µL of serum-free commercial DMEM (Gibco DMEM Cat # 11965-092) in a sterile 1.5 mL centrifuge tube: 1 µg of lentiviral backbone Luciferase-IRES-ZsGreen (BRI Resources NR-52516) vector, 0.22 µg each of vectors HDM-Hgpm2 (BEI Resources NR-52517), pRC-CMV-Rev1b (BEI Resources NR-52519) and HDM-tat1b (BEI Resources NR-52518), and 0.34 µg of vector pCMV14-3X-Flag-SARS-CoV-2 S (Addgene Cat # 145780).

After adding all plasmids, the solution was mixed by pipetting up and down approximately 10 times before 30 µL of XtremeGENE HP Version 9 (Millipore Sigma, Burlington, MA, USA) was added directly to the solution. The contents of the tube were again mixed by pipetting up and down approximately 10 times before being allowed to incubate at room temperature for 25-30 minutes. The petri dish was then retrieved from the 37 °C incubator and the DNA- XtremeGENE HP mixture was dripped over the 293Ft cells. The petri dish was then returned to the incubator and allowed to recover for 12-18 hours overnight. After 12-18 hours, petri dishes were again removed from the incubator and the cell media was gently replaced with 10 mL of fresh prewarmed 293 Medium before petri dishes were returned to the incubator. After an additional 48 hours (60-66

hours total post-transfection), petri dishes were removed from the incubator and the medium was gently removed and transferred to a 15 mL tube. This 15 mL tube was then briefly centrifuged at 750 RPM (105 RCF) for 3 minutes to pellet any large cell clumps. The supernatant was filtered through a 0.45µm syringe filter and stored as 200 µL to 600 µL aliquots in low-binding 1.5 mL tubes (ThermoFisher Cat # 90410, Waltham, MA, USA). Aliquots were stored at -75 °C until use in future assays.

#### 4.6.2 Food Samples

Some of the most popular food samples in California were used in this study. Food samples were chosen from three categories of 1) fruits (apple (*Malus domestica*), strawberry (*Fragaria x ananassa*), and grapes (*Vitis vinifera*)), 2) vegetables (tomato (*Solanum lycopersicum*), cucumber (*Cucumis sativus L.*), lettuce (*Lactuca sativa L.*), Broccoli (*Brassica oleracea var. italica*), and parsley (*Petroselinum crispum L.*)), and 3) nuts (Brazil Nut (*Bertholletia excelsa*), almond (*Prunus amygdalus*), cashew (*Anacardium occidentale L.*), and hazelnut (*Corylus avellana L.*). All produce was purchased from local grocery stores. Before use, produce was rinsed thoroughly with tap water before a final deionized water rinse. Produce was then wiped down with lint-free wipes. Large produce (such as tomato, cucumber, and apple) was then sectioned into approximately 2 cm by 2 cm by 0.5 cm slices in the presence of a sterile flame. Thin produce (lettuce, parsley) was cut into approximately 2 cm by 2 cm squares. Produce not suitable for sectioning (Brazil Nuts, almonds, cashews, hazelnuts, grapes, strawberries) were split in half -or in the case of almonds, purchased as slivers- to ensure that samples did not tip over during the course of experimentation. Sections of produce were then sprayed thoroughly with 70% Ethanol and allowed to dry. For viral infectivity assays, produce was placed into a BSL2 Biosafety Cabinet (Thermo Fisher Scientific, Marietta, OH, USA) before ethanol was fully dry. The biosafety cabinet interior was sterilized with 70% ethanol and 30 minutes of UV-C irradiation prior to use.

#### 4.6.3 Artificial Contamination of Produce and Treatment with Ozone

Sections of produce were spotted with 75 µL of SARS-CoV-2 pseudotyped virus (from frozen aliquots as described above in section 2.1). Virus solution was allowed to dry in a biosafety cabinet with an air downflow of 63 ft min<sup>-1</sup> (0.320 m sec<sup>-1</sup>) and an air inflow of 103 ft min<sup>-1</sup> (0.523 m sec<sup>-1</sup>) for 1 hour. After samples were dry, virus was collected from surfaces by resuspending droplets in 90 µL of 293 Media. For ozone treatment experiments, produce with dried virus sample were placed into plastic Ziploc bags in preparation for transport to the gaseous ozone generator. Each sample that was treated with ozone had a corresponding matched negative control sample that was enclosed in a bag but not exposed to ozone. After samples were exposed to ozone (or solely kept in containment for control samples), samples were returned to biosafety cabinet and resuspended in 90 µL of 293 Media as described above.

Statistical analysis was performed to assess whether pseudovirus was, a) able to retain enough activity for a piece of produce to continue to be considered contaminated, and b) whether there was variability between pseudoviral survival on different surfaces. To assess whether a piece of produce is still considered contaminated, we looked for a 2-log reduction in viral activity, as inspired by existing literature [29, 54]. We performed a bootstrapped One-tailed t-test with a significance level  $\alpha = 0.05$  and 10000 re-sampling simulations. The null hypothesis asserted the mean normalized pseudoviral infectivity for the surface is greater than or equal to 0.01. To gauge whether there was a

difference in the retention of virus infectivity, we performed a One-Way ANOVA with a significance level  $\alpha = 0.001$ . Results were then assessed with a Tukey-Kramer Multiple Comparison Test (run at an  $\alpha = 0.05$  and  $\alpha = 0.001$ ). Since a Tukey-Kramer Multiple Comparison Test is more conservative, we ran two different  $\alpha$  values to judge the relationship between samples. High viral retention produce exhibited significant similarity to Positive Control viral infectivity for both  $\alpha = 0.05$  and  $\alpha = 0.001$ .

#### 4.6.4 Generation of Ozone

A commercial corona discharge ozone generator MP-8000 110V (A2Z Ozone Inc., Louisville, KY, USA) was used to provide gaseous ozone for exposure to the samples. To control the ozone concentration, samples were kept inside a 30 L Sterilitte weathertight gasket box. The ozone concentration in the box was then monitored by a BH-90A portable ozone detector (BOSEAN Inc., Zhengzhou, Henan, China). Throughout all experiments, the ozone concentration inside the box was kept within  $15 \text{ ppm} \pm 1 \text{ ppm}$ . For safety, we performed our experiment in a well-ventilated environment. The ozone generator along with the weathertight box were all placed under an F-103 5 Feet Benchtop Chemical Fume Hood (Jamestown Metal Products, Jamestown, NY, USA).

#### 4.6.5 Virus Infectivity Assays

Each well of a clear 96-well cell-culture plate was coated with  $25 \mu\text{L}$  poly-L-lysine (ScienCell Research Laboratories, Cat # 0413, Carlsbad, CA, USA) according to the manufacturer's instructions. The plate was returned to the  $37^\circ\text{C}$  incubator for 1 to 36 hours. After this time, the 96-well plate was removed from the incubator and the poly-L-lysine solution was pipetted out. Wells were then rinsed twice with  $45 \mu\text{L}$  of sterile, ultrapure deionized water before being set aside in preparation for seeding. Wells were then immediately seeded with  $1.5 \times 10^4$  293T-ACE2 cells (BEI NR-52511, Manassas, VA, USA) and the plate was returned to the humidified incubator so that cells may recover. 293T-ACE2 cells were passaged in identical conditions as 293Ft cells. After 12-16 hours, the plate was removed from the incubator and the wells were verified for cell adhesion. Supernatant media was gently pipetted out and immediately replaced with  $30 \mu\text{L}$  of 293t Infectivity Media (Gibco DMEM Cat # 11965-092 supplemented with 2 mM L-Glutamine,  $250 \mu\text{g mL}^{-1}$  G418, 25 mM HEPES, and 1% Fetal Bovine Serum).  $25 \mu\text{L}$  of virus (either directly from frozen stocks for positive control or from resuspended virus for produce tests) was then added to wells. The plate was then returned to the incubator. Each experimental infectivity condition was tested in triplicate per 96 well plate.

12-16 hours later, the 96-well plate was retrieved from the humidified incubator and  $150 \mu\text{L}$  of fresh, pre-warmed 293 Medium was added over the top of each well. This was to ensure that cells remained alive and viable for the duration of the experiment. The 96 well plate was returned to the  $37^\circ\text{C}$  incubator for an additional 36 to 48 hours. After 36 to 48 hours, the 96 well plate was retrieved from the humidified incubator. Bright-Glo Luciferase Reagent (Promega Corp., Cat #E2610, Madison, WI, USA) was thawed out and kept wrapped in foil until use.  $200 \mu\text{L}$  of the medium in each of the infectivity plate wells was pipetted out, leaving about  $30 \mu\text{L}$  of the medium in each well. Then  $30 \mu\text{L}$  of Bright-Glo reagent was added over the top of the wells and given 2-4 minutes to lyse cells. The contents of each well were then transferred to a white-backed

96-well plate and luciferase signal was read on a ClarioStar Plus microplate reader (BMG Labtech, Ortenberg, Germany) with a 3600 gain and a 1 second normalization time. All samples were run in triplicate with at least two separate biological replicates for each condition.

#### **4.6.6 Virion Capture Enzyme-Linked Immunosorbent Assay**

Nunc MaxiSorp™ high protein-binding capacity 96 well ELISA plates (ThermoFisher Scientific, Cat # 44-2404-21, Waltham, MA, USA) were coated overnight at 4 °C with 100 ng of anti-SARS-CoV-2 Spike monoclonal antibody (SinoBiological Cat # 40150-D001, Beijing, China). After overnight incubation, wells were then rinsed three times with 300 µL of commercial PBS each (Gibco, PBS, pH 7.2 Cat # 20012027). Wells were then blocked with 300 µL of 3% Bovine Serum Albumin (Sigma Chemical Company Cat # A-4503, St. Louis, MO, USA) dissolved in commercial PBS. The Nunc MaxiSorp capture plate was allowed to incubate at 37 °C for 1 hour.

During this time, tubes of pseudovirus aliquot (see section 2.2) were thawed at room temperature and then exposed to 15 ppm of ozone (generated by corona discharge as described in section 2.4) for either 15 minutes or 45 minutes. As a positive control, an aliquot of the virus was thawed and left capped in the fume hood to act as a non-ozone exposed control. ELISA Nunc MaxiSorp capture plate was then retrieved from 37 °C incubator and wells were rinsed once more with 300 µL of commercial PBS. Pseudovirus samples were then diluted tenfold with 293 Media and 50 µL of these virus samples were dispensed into wells. The plate was then incubated at 37 °C for 1 hour to allow for virus capture.

After 1 hour of incubation, 50 µL of PBS with 0.5% Triton X-100 (Sigma Chemical Company Cat # X100, St. Louis, MO, USA) was added to each well and allowed to sit for 5 minutes at ambient temperature to allow pseudovirions to lyse and release p24. After 5 minutes, 100 µL of PBS was added over the top. Then 10 µL of 10x XpressBio Lysis Buffer (provided in HIV-1 p24 ELISA Kit, XpressBio Cat # XB-1000, Frederick, MD, USA) was added over the top and allowed to sit for 5 minutes to ensure complete p24 release. 145 µL of lysed solution from each well was then transferred from Nunc MaxiSorp capture plate to an XpressBio p24 ELISA kit plate (XpressBio Cat # XB-1000, Frederick, MD, USA). The p24 capture assay was then carried out according to the manufacturer's instructions, and the levels of p24 in each well were measured on a ClarioStar Plus microplate reader set to 450 nm (BMG Labtech, Ortenberg, Germany). Data were analyzed by performing a One-Way ANOVA ( $\alpha = 0.10$ ) comparing experimental wells to each other. Results were verified with a Tukey-Kramer Multiple Comparison Test ( $\alpha = 0.10$ ).

#### **4.6.7 Bio-Layer Interferometry**

His-Tagged Griffithsin bearing the M78Q mutation (Q-Grft) as described in Chapter 3 of this dissertation were prepared. The Q-Grft was taken to 50 nM in commercial Q buffer (GatorBio Cat #120010) and then 200 µL of solution was aliquoted into wells of a Max plate (GatorBio Cat#130062). Then, Anti-His probes (GatorBio Cat#160009) were presoaked in Q-Buffer for 30 minutes before being run on a standard BLI Quantitation Protocol on a GatorBio Gator Prime BLI System. In brief, probes were functionalized with His-Tagged M78Q Griffithsin for 5.5 minutes before being allowed to

associate with ligand samples for 10 minutes. This was followed by dissociation for 10 minutes. Data was processed using GatorBio Software.

Ligands were taken up in a variety of solvents. In the case of samples with OptiMEM, we used Gibco™ Opti-MEM™ I Reduced Serum Medium (ThermoFisher Cat # 31-985-088, Waltham, MA, USA). For samples with NP-40, we used Thermo Scientific Chemicals NP-40 lysis buffer (Thermoscientific Cat # J60766-AP Waltham, MA, USA).

#### 4.7 References

- [1]: Mortazavi M, Bains A, Afsah-Hejri L, Ehsani R, LiWang PJ. SARS-CoV-2 pseudotyped virus persists on the surface of multiple produce but can be inactivated with gaseous ozone. *Heliyon*. 2022 Aug;8(8):e10280. doi: 10.1016/j.heliyon.2022.e10280. Epub 2022 Aug 15. doi: 10.1016/j.heliyon.2022.e10280.
- [2]: Walensky, R. P., Walke, H. T., & Fauci, A. S. (2021). SARS-CoV-2 variants of concern in the United States—Challenges and opportunities. *Jama*, 325, 1037–1038. <https://jamanetwork.com/journals/jama/article-abstract/2776739>.
- [3]: Yekta, R., Vahid-Dastjerdi, L., Norouzbeigi, S., & Mortazavian, A. M. (2020). Food products as potential carriers of SARS-CoV-2. *Food Control*, 107754. <https://doi.org/10.1016/j.foodcont.2020.107754>.
- [4]: Marquès, M., & Domingo, J. L. (2020). Contamination of inert surfaces by SARS-CoV-2: Persistence, stability and infectivity. A review. *Environmental Research*, 110559. <https://doi.org/10.1016/j.envres.2020.110559>.
- [5]: Miranda, R. C., & Schaffner, D. W. (2019). Virus risk in the food supply chain. *Current Opinion in Food Science*, 30, 43–48. <https://doi.org/10.1016/j.cofs.2018.12.002>.
- [6]: O’Shea, H., Blacklaws, B. A., Collins, P. J., McKillen, J., & Fitzgerald, R. (2019). Viruses associated with foodborne infections. Reference Module in Life Sciences, <https://www.ncbi.nlm.nih.gov/pmc/articles/PMC7157469/pdf/main.pdf>.
- [7]: Wang, M., Yan, M., Xu, H., Liang, W., Kan, B., Zheng, B., . . . others. (2005). SARS-CoV infection in a restaurant from palm civet. *Emerging infectious diseases*, 11, 1860. <https://dx.doi.org/10.3201%2Fid1112.041293>.
- [8]: Science Brief: SARS-CoV-2 and Surface (Fomite) Transmission for Indoor Community Environments. Centers for Disease Control and Prevention. 2021 Apr. <https://www.cdc.gov/coronavirus/2019-ncov/more/science-and-research/surface-transmission.html>
- [9]: Ong, S. W., Tan, Y. K., Chia, P. Y., Lee, T. H., Ng, O. T., Wong, M. S., & Marimuthu, K. (2020). Air, surface environmental, and personal protective equipment contamination by severe acute respiratory syndrome coronavirus 2 (SARS-CoV-2) from a symptomatic patient. *Jama*, 323, 1610–1612. <https://jamanetwork.com/journals/jama/article-abstract/2762692>.
- [10]: van Doremalen, N.; Bushmaker, T.; Morris, D.H.; Holbrook, M.G.; Gamble, A.; Williamson, B.N.; Tamin, A.; Harcourt, J.L.; Thornburg, N.J.; Gerber, S.I.; Lloyd-Smith, J.O.; de Wit, E.; Munster, V.J. Aerosol and Surface Stability of SARS-CoV-2 as

Compared with SARS-CoV-1. *N Engl J Med.* 2020 Apr 16;382(16):1564-1567. doi: 10.1056/NEJMc2004973. Epub 2020 Mar 17. PMID: 32182409; PMCID: PMC7121658.

[11]: Hu, X.; Chen, Z.; Su, Z.; Deng, F.; Chen, X.; Yang, Q.; Li, P.; Chen, Q.; Ma, J.; Guan, W.; Pei, R.; Wang, Y. Ozone Water Is an Effective Disinfectant for SARS-CoV-2. *Viol Sin.* 2021 Oct;36(5):1066-1068. doi: 10.1007/s12250-021-00379-7. Epub 2021 Mar 31. PMID: 33788169; PMCID: PMC8010484.

[12]: Khaneghah, A. M.; Abhari, K.; Eş, I.; Soares, M. B.; Oliveira, R. B.; Hosseini, H.; Rezaei, M.; Balthazar, C.F.; Silva, R.; Cruz A. G.; Ranadheera, S. C.; Sant'Ana, A. S. (2020). Interactions between probiotics and pathogenic microorganisms in hosts and foods: A review. *Trends in Food Science & Technology*, 95, 205–218. <https://doi.org/10.1016/j.tifs.2019.11.022>.

[13]: Di Cola, G. F. (2021). Foodborne transmission of hepatitis A and hepatitis E viruses: A literature review. *International Journal of Food Microbiology*, 338(108986). <https://doi.org/10.1016/j.ijfoodmicro.2020.108986>.

[14]: Ma, N.L.; Peng, W.; Soon, C.F.; Noor Hassim, M.F.; Misbah, S.; Rahmat, Z.; Yong, W.T.L.; Sonne, C. Covid-19 pandemic in the lens of food safety and security. *Environ Res.* 2021 Feb;193:110405. doi: 10.1016/j.envres.2020.110405. Epub 2020 Oct 29. PMID: 33130165; PMCID: PMC7598367.

[15]: Raj, V. S.; Lamers, M. M.; Smits, S. L.; Demmers, J. A.; Mou, H.; Bosch, B.-J.; Haagmans, B. L. (2015). Identification of protein receptors for coronaviruses by mass spectrometry. In *Coronaviruses* (pp. 165–182). Springer. [https://doi.org/10.1007/978-1-4939-2438-7\\_15](https://doi.org/10.1007/978-1-4939-2438-7_15).

[16]: Rodríguez, V.; Lagares, A.; Arteaga, H.; Mattar, S.; Ruiz, L. C. (2020). Viral emerging pathogen evolution. In *Emerging and reemerging viral pathogens* (pp. 35–51). Elsevier. <https://doi.org/10.1016/B978-0-12-819400-3.00003-X>.

[17]: Farahmandfar, R.; Asnaashari, M.; Hesami, B. (2021). Monitoring of new coronavirus (SARS-CoV-2): origin, transmission, and food preservation methods. *Journal of Food Processing and Preservation*, e15564. <https://doi.org/10.1111/jfpp.15564>.

[18]: Fecchi, K.; Anticoli, S.; Peruzzu, D.; Iessi, E.; Gagliardi, M. C.; Matarrese, P.; Ruggieri, A. (2020). Coronavirus interplay with lipid rafts and autophagy unveils promising therapeutic targets. *Frontiers in Microbiology*, 11, 1821. <https://doi.org/10.3389/fmicb.2020.01821>.

[19]: Blanco, A., de Borja Ojembarrena, F., Clavo, B., & Negro, C. (2021). Ozone potential to fight against SAR-COV-2 pandemic: facts and research needs. *Environmental Science and Pollution Research*, 1–15. <https://link.springer.com/article/10.1007/s11356-020-12036-9>.

[20]: Manjunath, S. N., Sakar, M., Katapadi, M., & Balakrishna, R. G. (2021). Recent case studies on the use of ozone to combat coronavirus: Problems and perspectives. *Environmental Technology & Innovation*, 21, 101313. <https://doi.org/10.1016/j.eti.2020.101313>.

- [21]: Huang, Y., Yang, C., Xu, X.-f., Xu, W., & Liu, S.-w. (2020). Structural and functional properties of SARS-CoV-2 spike protein: potential antiviral drug development for COVID-19. *Acta Pharmacologica Sinica*, 41, 1141–1149. <https://doi.org/10.1038/s41401-020-0485-4>.
- [22]: Afsah-Hejri, L., Hajeb, P., Ehsani, R. J. (2020). Application of ozone for degradation of mycotoxins in food: A review. *Comprehensive Reviews in Food Science and Food Safety*, 19, 1777–1808. <https://pubmed.ncbi.nlm.nih.gov/33336912/>.
- [23]: Fan, X. (2021). Gaseous ozone to preserve quality and enhance microbial safety of fresh produce: Recent developments and research needs. *Comprehensive Reviews in Food Science and Food Safety*, <https://doi.org/10.1111/1541-4337.12796>.
- [24]: Afsah-Hejri, L., Toudeshki, A., Homayouni, T., Mehrazi, S., Parez, A. G., Gordon, P., & Ehsani, R. (2021). Potential of ozonated-air (OA) application to reduce the weight and volume loss in fresh figs (*Ficus carica* L.). *Postharvest Biology and Technology*, 180, 111631. <https://www.sciencedirect.com/science/article/pii/S0925521421001708>.
- [25]: Emerson, M. A., Sproul, O. J., Buck, C. E. (1982). Ozone inactivation of cell-associated viruses. *Applied and environmental microbiology*, 43, 603–608. <https://doi.org/10.1128/aem.43.3.603-608.1982>.
- [26]: Shin, G.-A., Sobsey, M. D. (2003). Reduction of Norwalk virus, poliovirus 1, and bacteriophage MS2 by ozone disinfection of water. *Applied and environmental microbiology*, 69, 3975–3978.
- [27]: Thurston-Enriquez, J. A., Haas, C. N., Jacangelo, J., Gerba, C. P. (2005). Inactivation of enteric adenovirus and feline calicivirus by ozone. *Water research*, 39, 3650–3656. <https://doi.org/10.1016/j.watres.2005.06.006>.
- [28]: Predmore, A., Sanglay, G., Li, J., Lee, K. (2015). Control of human norovirus surrogates in fresh foods by gaseous ozone and a proposed mechanism of inactivation. *Food microbiology*, 50, 118–125. <https://www.sciencedirect.com/science/article/pii/S0740002015000775>.
- [29]: Brié, A., Boudaud, N., Mssihid, A., Loutreul, J., Bertrand, I., Gantzer, C. (2018). Inactivation of murine norovirus and hepatitis A virus on fresh raspberries by gaseous ozone treatment. *Food Microbiology*, 70, 1–6. <https://doi.org/10.1016/j.fm.2017.08.010>.
- [30]: Zhou, Z., Zuber, S., Cantergiani, F., Sampers, I., Devlieghere, F., Uyttendaele, M. (2018). Inactivation of foodborne pathogens and their surrogates on fresh and frozen strawberries using gaseous ozone. *Frontiers in Sustainable Food Systems*, 2, 51. <https://doi.org/10.3389/fsufs.2018.00051>.
- [31]: Cristiano, L. (2020). Could ozone be an effective disinfection measure against the novel coronavirus (SARS-CoV-2)? *Journal of Preventive Medicine and Hygiene*, 61, E301. <https://dx.doi.org/10.15167%2F2421-4248%2Fjpmh2020.61.3.1596>.
- [32]: Hirneisen, K. A. (2011). Ozone inactivation of norovirus surrogates on fresh produce. *Journal of food protection*, 74(5), 836-839. <https://meridian.allenpress.com/jfp/article/74/5/836/173503/Ozone-Inactivation-of-Norovirus-Surrogates-on>.



- [33]: Sridhar, A., Ponnuchamy, M., Kumar, P. S., Kapoor, A. (2021). Food preservation techniques and nanotechnology for increased shelf life of fruits, vegetables, beverages and spices: a review. *Environmental Chemistry Letters*, 19, 1715–1735. <https://doi.org/10.1007/s10311-020-01126-2>.
- [34]: Mazur-Panasiuk, N.; Botwina, P.; Kutaj, A.; Woszczyna, D.; Pyrc, K. Ozone Treatment Is Insufficient to Inactivate SARS-CoV-2 Surrogate under Field Conditions. *Antioxidants (Basel)*. 2021 Sep 16;10(9):1480. doi: 10.3390/antiox10091480. PMID: 34573110; PMCID: PMC8470094.
- [35]: Criscuolo, E.; Diotti, R.A.; Ferrarese, R.; Alippi, C.; Viscardi, G.; Signorelli, C.; Mancini, N.; Clementi, M.; Clementi, N. (2021). Fast inactivation of SARS-CoV-2 by UV-C and ozone exposure on different materials. *Emerging microbes & infections*, 10, 206–210. <https://doi.org/10.1080/22221751.2021.1872354>.
- [36]: Tizaoui, C. (2020). Ozone: a potential oxidant for COVID-19 virus (SARS-CoV-2). *Ozone: science & engineering*, 42, 378–385. <https://doi.org/10.1080/01919512.2020.1795614>.
- [37]: Bayarri, B.; Cruz-Alcalde, A.; López-Vinent, N.; Micó, M. M.; Sans, C. (2021). Can ozone inactivate SARS-CoV-2? A review of mechanisms and performance on viruses. *Journal of Hazardous Materials*, 415, 125658. <https://doi.org/10.1016/j.jhazmat.2021.125658>.
- [38]: Clavo B, Córdoba-Lanús E, Rodríguez-Esparragón F, Cazorla-Rivero SE, García-Pérez O, Piñero JE, Villar J, Blanco A, Torres-Ascensión C, Martín-Barrasa JL, González-Martin JM, Serrano-Aguilar P, Lorenzo-Morales J. (2020). Effects of Ozone Treatment on Personal Protective Equipment Contaminated with SARS-CoV-2. *Antioxidants*, 9(12), 1222. <https://www.mdpi.com/2076-3921/9/12/1222>.
- [39]: Murata T, Komoto S, Iwahori S, Sasaki J, Nishitsuji H, Hasebe T, Hoshinaga K, Yuzawa Y. (2021). Reduction of severe acute respiratory syndrome coronavirus-2 infectivity by admissible concentration of ozone gas and water. *Microbiology and Immunology*, 65, 10–16. <https://doi.org/10.1111/1348-0421.12861>.
- [40]: Valverde-Miranda, D.; Díaz-Pérez, M.; Gómez-Galán, M.; Callejón-Ferre, Á.-J. (2021). Total soluble solids and dry matter of cucumber as indicators of shelf life. *Postharvest Biology and Technology*, 180, 111603. <https://www.sciencedirect.com/science/article/pii/S0925521421001423>.
- [41]: Perveen, R. S. (2015). Tomato (*Solanum lycopersicum*) carotenoids and lycopenes chemistry; metabolism, absorption, nutrition, and allied health claims—A comprehensive review. *Critical reviews in food science and nutrition*, 55(7), 919-929. <https://www.tandfonline.com/doi/full/10.1080/10408398.2012.657809>.
- [42]: USDA. (2020). U.S. Department of Agriculture FoodData Central. apple, <https://fdc.nal.usda.gov/fdc-app.html#/food-details/1750340/nutrients>.
- [43]: Masters, P. S. (2019). Coronavirus Genomic RNA Packaging. *Virology*, 537, 198-207. <https://doi.org/10.1016/j.virol.2019.08.031>.
- [44]: Popova, D. S.-H. (2015). Representative mammalian cell culture test materials for assessment of primary recovery technologies: A rapid method with industrial

applicability. *Biotechnology journal*, 10(1), 162-170.  
<https://doi.org/10.1002/biot.201400294>.

[45]: Tait, A. S.-S. (2013). Differential response in downstream processing of CHO cells grown under mild hypothermic conditions. *Biotechnology progress*, 29(3), 688-696.  
<https://doi.org/10.1002/btpr.1726>.

[46]: Toyama, B. H. (2013). Protein homeostasis: live long, won't prosper. *Nature reviews Molecular cell biology*. *Nature reviews Molecular cell biology*, 14(1), 55-61,  
<https://doi.org/10.1038/nrm3496>.

[47]: Reed, G. F. (2002). Use of coefficient of variation in assessing variability of quantitative assays. *Clinical and Vaccine Immunology*, 9(6), 1235-1239.  
<https://doi.org/10.1128/cdli.9.6.1235-1239.2002>.

[48]: Wood, R. J. (1980). Reproducibility of serological titers. *Journal of clinical microbiology*, 11(6), 541-545. <https://doi.org/10.1128/jcm.11.6.541-545.1980>.

[49]: Maier, I.; Chu, T. (2016). Use of Ozone for Inactivation of Bacteria and Viruses in Cryostats. *Journal of Cytology & Histology*, 7(3), 428. <https://doi.org/10.4172/2157-7099.1000428>.

[50]: Hudson, J. B. (2009). Development of a Practical Method for Using Ozone Gas as a Virus Decontaminating Agent. *Ozone: Science & Engineering*, 31(3), 216-223.  
<https://doi.org/10.1080/01919510902747969>.

[51]: Grignani, E. M. (2021). Safe and effective use of ozone as air and surface disinfectant in the conjuncture of Covid-19. *Gases*, 1(1), 19-32.  
<https://doi.org/10.3390/gases1010002>.

[52]: Batakliiev, T.; Georgiev, V.; Anachkov, M.; Rakovsky, S.; Zaikov, G. E. (2014). Ozone decomposition. *Interdisciplinary Toxicology*, 7, 47–59.  
<https://sciendo.com/pdf/10.2478/intox-2014-0008>.

[53]: Crawford KHD, Eguia R, Dingens AS, Loes AN, Malone KD, Wolf CR, Chu HY, Tortorici MA, Veessler D, Murphy M, Pettie D, King NP, Balazs AB, Bloom JD. (2020). Protocol and Reagents for Pseudotyping Lentiviral Particles with SARS-CoV-2 Spike Protein for Neutralization Assays. *Viruses*, 12, 15. <https://doi.org/10.3390/v12050513>.

[54]: Tizaoui, C.; Stanton, R.; Statkute, E.; Rubina, A.; Lester-Card, E.; Lewis, A.; Holliman, P.; Worsley, D. (2022). Ozone for SARS-CoV-2 inactivation on surfaces and in liquid cell culture media. *Journal of Hazardous Materials*, 428, 128251.  
<https://doi.org/10.1016/j.jhazmat.2022.128251>.

[55]: Volkoff, S. J. (2021). Demonstrated SARS-CoV-2 Surface Disinfection Using Ozone. *Ozone: Science & Engineering*, 43(4), 296-305.  
<https://doi.org/10.1080/01919512.2020.1863770>.

[56]: Malka, S. K.-H. (2022). Fresh Produce Safety and Quality: Chlorine Dioxide's Role. *Frontiers in Plant Science*, 12. <https://doi.org/10.3389/fpls.2021.775629>.

[57]: Arslan M, Xu B, Gamal El-Din M. Transmission of SARS-CoV-2 via fecal-oral and aerosols-borne routes: Environmental dynamics and implications for wastewater management in underprivileged societies. *Sci Total Environ*. 2020 Nov 15;743:140709.

doi: 10.1016/j.scitotenv.2020.140709. Epub 2020 Jul 3. PMID: 32652357; PMCID: PMC7332911.

[58]: WHO. 2003b. Inadequate plumbing systems likely contributed to SARS transmission. in: Inadequate Plumbing Systems Likely Contributed to SARS Transmission: <https://www.who.int/mediacentre/news/releases/2003/pr70/en/> (Accessed 29th April, 2020).

[59]: Qu G, Li X, Hu L, and Jiang G. An Imperative Need for Research on the Role of Environmental Factors in Transmission of Novel Coronavirus (COVID-19). *Environ. Sci. Technol.* 2020;54(7);3730–3732. <https://doi.org/10.1021/acs.est.0c01102>.

[60]: Nova, N. Cross-Species Transmission of Coronaviruses in Humans and Domestic Mammals, What Are the Ecological Mechanisms Driving Transmission, Spillover, and Disease Emergence? *Front. Public Health.* 2021:9. <https://doi.org/10.3389/fpubh.2021.717941>

[61]: Payne S. Family Coronaviridae. *Viruses.* 2017:149–58. doi: 10.1016/B978-0-12-803109-4.00017-9. Epub 2017 Sep 1. PMCID: PMC7149805.

[62]: Hilgenfeld R, Peiris M. From SARS to MERS: 10 years of research on highly pathogenic human coronaviruses. *Antiviral Res.* 2013 Oct;100(1):286-95. doi: 10.1016/j.antiviral.2013.08.015. Epub 2013 Sep 6. PMID: 24012996; PMCID: PMC7113673.

[63]: “Rich n Chip’s Tips and Tricks for Best Quantitation and Kinetics Performance on a BLI system.” GatorBio. Uploaded Nov 24, 2021. <[https://www.youtube.com/watch?v=AhIAfCK\\_fEM](https://www.youtube.com/watch?v=AhIAfCK_fEM)> Accessed August 14, 2023.

[64]: Xue J, Hoorelbeke B, Kagiampakis I, Demeler B, Balzarini J, Liwang PJ. The griffithsin dimer is required for high-potency inhibition of HIV-1: evidence for manipulation of the structure of gp120 as part of the griffithsin dimer mechanism. *Antimicrob Agents Chemother.* 2013 Aug;57(8):3976-89. doi: 10.1128/AAC.00332-13. Epub 2013 Jun 10. PMID: 23752505; PMCID: PMC3719714.

## Chapter 5 Conclusion

### Future Directions and Closing Thoughts

The Covid-19 pandemic has profoundly impacted the profile Coronaviridae family viruses and the field of coronavirus research. More broadly, the Pandemic changed how science is conducted: researchers engaged in citizen-science, donating computing power to run simulations of the viral proteins, and numerous high-profile papers in the field acknowledge the contribution of consortiums of researchers in their authorship lists [1, 2, 3]. All of this kindled the rapid rise in the profile of coronavirus research, with the growth of Covid-19 research articles being called “unprecedented” and “transformed research publishing” [4, 5].

In this dissertation, we summarize our own work in contributing to the field of SARS-CoV-2 research. First, we orient the reader by summarizing the discovery of and evolutionary history of coronaviruses. Analysis of the mutation rates of coronavirus RNA replicase and phylogenetic analysis have led scientists to date the existence of the Family to date as far back as the late Jurassic to early Cretaceous periods, although formal discovery and classification of the Family only occurred in the early-to mid 20<sup>th</sup> century [6, 7]. The field itself underwent growth in the 21<sup>st</sup> century, with the emergence of several highly contagious human coronaviruses: SARS-CoV-1, MERS-CoV, and most recently, SARS-CoV-2 [8].

### 5.1 Future Directions of SARS-CoV-2 Spike S1 Domain Glycan Mutation Research

Our work on the role of S1 domain SARS-CoV-2 Spike N-linked glycosylation brings attention to the potential function of these glycans in regulating the hACE2-mediated infectivity of Spike pseudotyped lentivirions. The removal of the glycans N17, N61, N74, and N122 appeared to consistently decrease the hACE2-mediated infectivity of SARS-CoV-2 Spike lentivirions, while N234 appeared to increase the hACE2-mediated infectivity. Overall, these results are not inconsistent with existing literature: for instance, the removal of N234Q ranged from slightly decreasing infectivity to slightly increasing infectivity, while removing N17 and N61 consistently decreased infectivity [9, 10].

As a future step, we believe it would be of import to elucidate exactly how these N-linked glycans facilitate hACE2-Spike protein binding. Some phenomena to analyze would include: 1) whether the removal of these glycans affect the furin cleavage at the S1/S2 junction, 2) whether the removal of these glycans affect the TMPRSS2 or Cathepsin processing at the S2' cleavage site, 3) whether the removal of these glycans affect the number of Spike proteins that are expressed on the surface of the virion, 4) whether the removal of these glycans affect the processing of glycans at other N-linked sites on the SARS-CoV-2 Spike protein, and 5) whether the removal of these glycans affect the dynamics of the Receptor Binding Domain of the Spike protein. All of these questions would likely require different expertise and varied specialized equipment to test thoroughly, ranging from familiarity in Mass Spectroscopy (to characterize glycan processing), mammalian protein expression (to consistently produce enough protein for analysis), Transmission Electron Microscopy (to observe the number of Spike proteins

expressed on the surface of the virion), fluorophore or other labeling techniques (to characterize the dynamics of the RBD of the Spike protein), and computational molecular dynamics modeling (to assist in characterizing the dynamics of the Spike protein RBD), to name but a few. All of these techniques essentially would need the capabilities of a University-level biochemistry department, meaning that there are several collaborative projects that could branch out from our work on SARS-CoV-2.

Likewise, altering the glycans on the SARS-CoV-2 Spike protein also affected the ability of lentivirions to undergo DC-SIGN mediated Trans-infection. We believe an analysis of the SARS-CoV-2 Spike protein would be necessary to elucidate why this occurs (particularly a characterization of whether any of the glycan mutations affects the expression of the SARS-CoV-2 Spike on the viral surface). Out of all of the glycan mutants, we believe that it may be important to test whether the removal of the glycan site at N234 does increase the affinity of the Spike protein to DC-SIGN. To that end, it may be most expeditious for a successor in our lab to perform BLI experiments with DC-SIGN and Spike protein with and without the N234Q mutation. Given the predicted role of the N234 glycan in propping the Spike protein in the “up” or “open” conformation, it could be possible that the N234Q mutation leads the Spike protein to have a higher tendency in adopting the “closed”/down conformation. Thus, it could be possible that the “closed”/ “down” conformation of the Spike protein has higher affinity for attachment receptors like DC-SIGN. Ergo, it would be important and not too labor intensive to also assess the affinity of Spike protein locked in the “closed” conformation to DC-SIGN. Furthermore, the DC-SIGN C-terminal CRD should not be very hard to create in high quantities, as previous literature has shown that the CRD can be expressed in *E. coli* [11, 12]. Alternatively, N234 is the S1 glycan site that is most consistently decorated with high mannose glycans. Since complex and hybrid glycans have more representation of charged sugars- such as N-Acetyl-Neuraminic Acid or D-Glucosamine- while mannose is a neutral/uncharged sugar, it could be possible that the N234 glycan’s effect on SARS-CoV-2 virus infectivity could be due to charge characteristics [13, 14]. Given that researchers at our institution have already published papers reporting the effect of the Spike protein’s conformation on the electric field surrounding the protein, it would be feasible and academically appealing to assess how their model changes when the Spike glycans are taken into account [15].

Finally, the Omicron strains of SARS-CoV-2 contain numerous mutations on the Spike protein, leading to demonstrably different Spike conformational changes and furin cleavage than other strains of Covid-19 [16-19]. Since we have developed an efficient and relatively fast assay for lectin-receptor-mediated Trans-infection, it may be most expeditious to assess whether the same S1 domain spike mutations cause similar changes in Direct- and Trans- infectivity on our assay. Furthermore, NIH AIDS Reagent offers a paired cell line transduced to express another potential SARS-CoV-2 lectin attachment receptor called L-SIGN, meaning that it could be quite simple to perform similar experiments to determine whether the aforementioned Spike glycan mutations have the same effect when L-SIGN is used as the attachment receptor to mediate Trans-infection [20]. Over the course of the past 2 years, BEI Resources has also made available a set of HEK 293t cells that express Furin or TMPRSS2 in addition to hACE2 [21]. Thus, utilizing these cells can provide insight into whether the SARS-CoV-2 Spike glycan mutations are able to increase the susceptibility of Spike proteins to processing at the S1/S2 or the S2’ sites, respectively. Finally, it may be worthwhile to assess whether the S2 domain glycans can contribute to Direct- and Trans- infectivity, and more

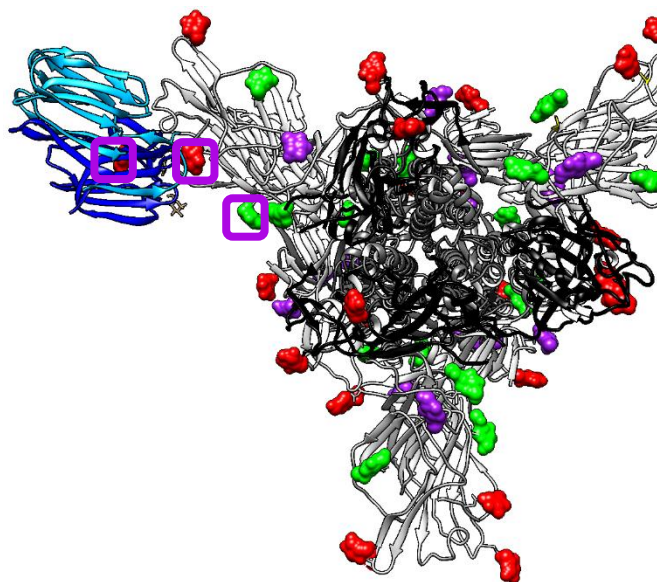
importantly, ascertain whether there is a more suitable cluster of glycans that can act as an epitope for the development of a strain-resistant Covid-19 entry inhibitor.

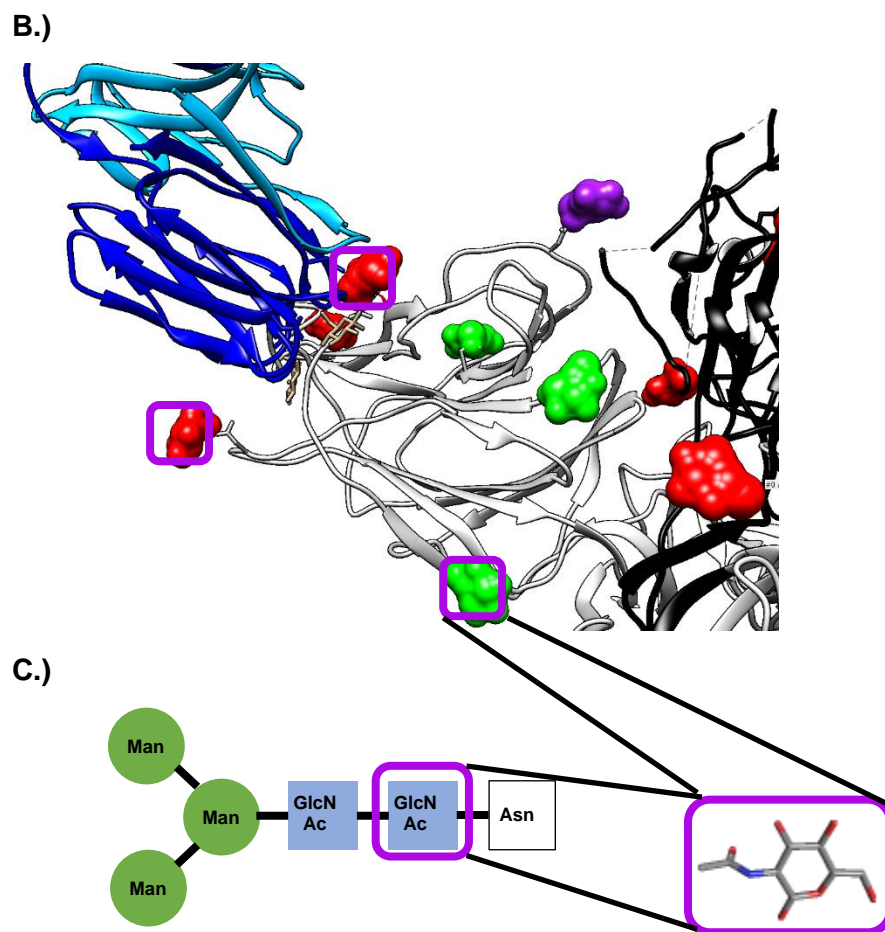
## 5.2 Future Directions on Lectin-Based Inhibitors of SARS-CoV-2 Coronavirus

Our work also showed that the antiviral lectin Griffithsin showed enhanced inhibitory capabilities when the SARS-CoV-2 Membrane Structural Protein was co-expressed in cells with lentiviral particles. However, this does not necessarily mean that Griffithsin preferentially binds to the M protein; for instance, the M protein could regulate Spike protein dynamics in such a way as to make them more susceptible to Griffithsin binding. Testing this should be a relatively easy task for a successor in our lab: either BLI, fluorescence anisotropy, or a virus capture ELISA could provide information to compare whether Griffithsin has higher binding affinity for M protein or SARS-CoV-2 Spike protein.

Furthermore, since Griffithsin has three putative glycan binding sites on each monomer of the protein, exhibits favorable pharmacokinetic properties, is highly stable and relatively easy to produce, Griffithsin could serve as a viable backbone or starting point in the development of a novel class of anti-Covid-19 prophylactics that bind to S1 domain glycan clusters that were identified in Chapter 2 [22-25]. Specifically, the glycan cluster N17/61/74 is probably the best epitope to leverage for the development of Griffithsin into a therapeutic. Not only was infectivity heavily decreased on the N17/61/74Q Spike protein- indicating that there is high evolutionary pressure to retain these glycans- but also these three glycans are in close proximity to each other, indicating that Griffithsin may not need much more alteration in its backbone structure to access the three glycans at once.

A.)





**D.)**

Residues	Estimated Distance (Angstroms)
Griffithsin D30-D70	11.1
Griffithsin D30-D112	12.1
Griffithsin D70-D112	10.5
SARS-CoV-2 Spike N17-N61	33.0
SARS-CoV-2 Spike N17-N74	21.4
SARS-CoV-2 Spike N61-N74	34.2

**Figure 5.1: Depiction of Griffithsin oriented to dock onto the glycans of the N17/61/74 cluster. A.)** View of the Spike protein from the top with the D112 sugar binding site of Griffithsin docked on top of the glycan at N17. To assist with visualizing the remaining sugar binding sites on Griffithsin, the sugars that are present in the PDB structure 2NUO are colored tan. **B.)** View of the Spike protein from the top with the D112 sugar binding site of Griffithsin docked on top of the

glycan at N17. To assist with visualizing the remaining sugar binding sites on Griffithsin, the sugars that are present in the PDB structure 2NUO are colored tan. Spike protein PDB ID: 7NT9 overlaid on 6VYB. Griffithsin PDB ID: 2NUO. Although Griffithsin does not appear to be able to bind to all 3 putative glycan sites that are part of the N17/61/74 cluster, we stress that our figure only depicts each glycan site as a monosaccharide. **C.)** We show the core pentasaccharide, Man3GlcNAc2, which is initially attached onto the N-linked glycan sites in the Endoplasmic Reticulum. The Man3GlcNAc2 is typically further processed to have more monosaccharides attached onto the sugar chain. For comparison, only a single GlcNAc (N-Acetyl Glucosamine, boxed in purple) is depicted on our SARS-CoV-2 Spike ribbon structures. **D.)** A table summarizing the distances of the aforementioned amino acid residues on each protein. For Griffithsin, we depict the distance between the sugar-binding Aspartic Acids. For SARS-CoV-2, we depict the distance between the N-linked glycans as Asparagines 17, 61, and 74.

### **5.3 Future Directions on Assessing the Stability of SARS-CoV-2 Pseudotyped Lentivirions**

Finally, our work on SARS-CoV-2 led to an increase in collaborative opportunities within our institution. Given that globally speaking, Covid-19 is likely to persist as a disease of concern, it is therefore likely that there will be ample opportunity to collaborate with colleagues in the future [26]. However, these collaborators come from varied scientific disciplines, meaning they have/will have a variety of systems and experimental setups that are not necessarily typical of microbiology and biochemistry labs, and which would thereby expose our virions, proteins, and other biological molecules in atypical experimental conditions. Indeed, there have been several collaborative projects the writer of this dissertation has worked on that have failed due to constraints relating to the instability of lentiviral particles.

Therefore, in the future, it would be useful to ascertain what aspects of the pseudotyped virions are susceptible to various environmental conditions that are typical of techniques in other realms of science. For example, our attempts at obtaining Transmission Electron Microscopy (TEM) images of the SARS-CoV-2 Spike pseudotyped virus typically failed due to damage to the enveloped virions, either during the process of flash-freezing or during negative staining with uranyl acetate. The author created virions in variations of standard media conditions, and it appeared that certain alterations to the media aided in stabilizing the virus (information is forthcoming, likely to be published in the works of Zachary Petrek, Chemistry and Biochemistry Graduate Group, University of California, Merced).

### **5.4 Final Thoughts**

One of the most important aspects of our work that was not explicitly stated was the expansion in experimental capabilities at our institution, the University of California, Merced. Over the course of the 2.5 years that this research was conducted, reagents and materials were made available by other academic institutions and the United States Government, allowing us to lay the foundations of our SARS-CoV-2 infectivity research [21, 27, 28]. New staff who join our lab should be able to theoretically work on model systems of any membrane-encapsulated virus that mediates infectious tropism via a Spike glycoprotein. Perhaps rather than looking forwards, it may be prudent for us to use our newfound capabilities to look backwards and study viruses that we were previously incapable of working on. For example, it could be worthwhile to apply our analysis of the glycosylation pattern of coronaviral Spike proteins to other human



coronaviruses like SARS-CoV-1, MERS-CoV and HCoV-NL63. Alternatively, being able to quickly test protein-protein interactions in a high-throughput manner via BLI could greatly assist in the screening of novel inhibitory proteins. In short, the research summarized in this dissertation should open the door to allowing our institution to perform broader screens for therapeutics against a variety of pathogenic viruses, identify methods of inhibiting those viruses, and develop ways to stabilize the structure of pseudotyped virions and cVLPs to allow us to analyze the virions on relatively uncommon assays, such as TEM and atomic force microscopy. The wealth of grants that allowed diverse labs to enter into SARS-CoV-2 research allowed us to foster relationships with varied staff at our institution, laying what should be the groundwork for many more unique and fruitful collaborations. Staff and students merely need to ensure that these relationships continue to persist and grow.

## 5.5 References

- [1]: Temming, M. You can help fight the coronavirus. All you need is a computer: Donating computing time can help create a virtual supercomputer that can search for a cure. *ScienceNews*. 2020 Mar 25; <https://www.sciencenews.org/article/coronavirus-covid-19-proteins-super-computer-fight-pandemic>.
- [2]: Fabius JM, Krogan NJ. Creating collaboration by breaking down scientific barriers. *Cell*. 2021 Apr 29;184(9):2271-2275. doi: 10.1016/j.cell.2021.02.022. Epub 2021 Mar 24. PMID: 33765441; PMCID: PMC8630979.
- [3]: Duan D, Xia Q. Evolution of scientific collaboration on COVID-19: A bibliometric analysis. *Learn Publ*. 2021 Jul;34(3):429-441. doi: 10.1002/leap.1382. Epub 2021 Apr 8. PMID: 34230773; PMCID: PMC8250802.
- [4]: Teixeira da Silva JA, Tsigaris P, Erfanmanesh M. Publishing volumes in major databases related to Covid-19. *Scientometrics* 126, 831–842 (2021). <https://doi.org/10.1007/s11192-020-03675-3>
- [5]: Else, H. How a torrent of COVID science changed research publishing — in seven charts. *Nature* 588, 553 (2020) doi: <https://doi.org/10.1038/d41586-020-03564-y>
- [6]: Claramunt, S.; Cracraft, J. A new time tree reveals Earth history's imprint on the evolution of modern birds. *Sci Adv*. 2015 Dec 11;1(11):e1501005. doi: 10.1126/sciadv.1501005. PMID: 26824065; PMCID: PMC4730849.
- [7]: Tsagkogeorga, G.; Parker, J.; Stupka, E.; Cotton, J. A.; Rossiter, S. J. Phylogenomic Analyses Elucidate the Evolutionary Relationships of Bats. *Current Biology*. Volume 23, Issue 22, 18 November 2013, Pages 2262-2267
- [8]: Singh, D., Yi, S.V. On the origin and evolution of SARS-CoV-2. *Exp Mol Med* 53, 537–547 (2021). <https://doi.org/10.1038/s12276-021-00604-z>
- [9]: Li, Q.; Wu, J.; Nie, J.; Zhang, L.; Hao, H.; Liu, S.; Zhao, C.; Zhang, Q.; Liu, H.; Nie, L.; Qin, H.; Wang, M.; Lu, Q.; Li, X.; Sun, Q.; Liu, J.; Zhang, L.; Li, X.; Huang, W.; Wang, Y. The Impact of Mutations in SARS-CoV-2 Spike on Viral Infectivity and Antigenicity. *Cell* 2020, 182,1284-1294.e9, <https://doi.org/10.1016/j.cell.2020.07.012>.

[10]: Huang, H.Y.; Liao, H.Y.; Chen, X.; Wang, S.W.; Cheng, C.W.; Shahed-Al-Mahmud, M.; Liu, Y.M.; Mohapatra, A.; Chen, T.H.; Lo, J.M.; Wu, Y.M.; Ma, H.H.; Chang, Y.H.; Tsai, H.Y.; Chou, Y.C.; Hsueh, Y.P.; Tsai, C.Y.; Huang, P.Y.; Chang, S.Y.; Chao, T.L.; Kao, H.C.; Tsai, Y.M.; Chen, Y.H.; Wu, C.Y.; Jan, J.T.; Cheng, T.R.; Lin, K.I.; Ma, C.; Wong, C.H. Vaccination with SARS-CoV-2 spike protein lacking glycan shields elicits enhanced protective responses in animal models. *Sci Transl Med* 2022, 14, eabm0899, <https://doi.org/10.1126/scitranslmed.abm0899>.

[11]: Hijazi K, Wang Y, Scala C, Jeffs S, Longstaff C, Stieh D, Haggarty B, Vanham G, Schols D, Balzarini J, Jones IM, Hoxie J, Shattock R, Kelly CG. DC-SIGN increases the affinity of HIV-1 envelope glycoprotein interaction with CD4. *PLoS One*. 2011;6(12):e28307. doi: 10.1371/journal.pone.0028307. Epub 2011 Dec 7. PMID: 22163292; PMCID: PMC3233575.

[12]: Mitchell DA, Fadden AJ, Drickamer K. A Novel Mechanism of Carbohydrate Recognition by the C-type Lectins DC-SIGN and DC-SIGNR: SUBUNIT ORGANIZATION AND BINDING TO MULTIVALENT LIGANDS. *JBC*. 2001;276(31):28939-28945. <https://doi.org/10.1074/jbc.M104565200>.

[13]: Symbol Nomenclature for Glycans (SNFG). National Library of Medicine: National Center for Biotechnology Information. Created: October 15, 2015; Last updated: August 20, 2023. Accessed August 24, 2023. <<https://www.ncbi.nlm.nih.gov/glycans/snfg.html>>

[14]: Molecule of the Week Archive: D-Glucosamine. American Chemical Society. July 27, 2020. Accessed August 24, 2023. <<https://www.acs.org/molecule-of-the-week/archive/g/d-glucosamine.html>>

[15]: Kucherova A, Strango S, Sukenik S, Theillard M. Computational modeling of protein conformational changes - Application to the opening SARS-CoV-2 spike. *J Comput Phys*. 2021 Nov 1;444:110591. doi: 10.1016/j.jcp.2021.110591. Epub 2021 Jul 26. PMID: 36532662; PMCID: PMC9749448.

[16]: Hui K.P.Y.; Ng, K-C.; Ho, J.C.W.; Yeung, H-Y.; Ching, R.H.H.; Gu, H.; Chung, J.C.K.; Chow, V.L.Y.; Sit, K-Y.; Hsin, M.K.Y.; Au, T.W.K.; Poon, L.L.M.; Peiris, M.; Nicholls, J.M.; Chan, M.C.W. Replication of SARS-CoV-2 Omicron BA.2 variant in ex vivo cultures of the human upper and lower respiratory tract. *eBioMedicine* 2022, 83, 104232, <https://doi.org/10.1016/j.ebiom.2022.104232>.

[17]: Willett, B.J.; Grove, J.; MacLean, O.A.; Wilkie, C.; De Lorenzo, G.; Furnon, W.; Cantoni, D.; Scott, S.; Logan, N.; Ashraf, S.; Manali, M.; Szemiel, A.; Cowton, V.; Vink, E.; Harvey, W.T.; Davis, C.; Asamaphan, P.; Smollett, K.; Tong, L.; Orton, R.; Hughes, J.; Holland, P.; Silva, V.; Pascall, D.J.; Puxty, K.; da Silva Filipe, A.; Yebra, G.; Shaaban, S.; Holden, M.T.G.; Pinto, R.M.; Gunson, R.; Templeton, K.; Murcia, P.R.; Patel, A.H.; Klenerman, P.; Dunachie, S.; PITCH Consortium; COVID-19 Genomics UK (COG-UK) Consortium; Haughney, J.; Robertson, D.L.; Palmarini, M.; Ray, S.; Thomson, E.C. SARS-CoV-2 Omicron is an immune escape variant with an altered cell entry pathway. *Nat Microbiol* 2022, 7, 1161-1179, <https://doi.org/10.1038/s41564-022-01143-7>.

[18]: Gobeil, S.M.; Henderson, R.; Stalls, V.; Janowska, K.; Huang, X.; May, A.; Speakman, M.; Beaudoin, E.; Manne, K.; Li, D.; Parks, R.; Barr, M.; Deyton, M.; Martin, M.; Mansouri, K.; Edwards, R.J.; Sempowski, G.D.; Saunders, K.O.; Wiehe, K.; Williams,

W.; Korber, B.; Haynes, B.F.; Acharya, P. Structural diversity of the SARS-CoV-2 Omicron spike. *Mol Cell* 2022, 82, 2050-2068.e6, <https://doi.org/10.1101/2022.01.25.477784>.

[19]: Yang, K.; Wang, C.; Kreuzberger, A.J.B.; White, K.I.; Pfuetzner, R.A.; Esquivies, L.; Kirchhausen, T.; Brunger, A.T. Structure-based design of a SARS-CoV-2 Omicron-specific inhibitor. *PNAS* 2023, 120, e2300360120, <https://doi.org/10.1073/pnas.2300360120>.

[20]: Lempp FA, Soriaga LB, Montiel-Ruiz M, Benigni F, Noack J, Park YJ, Bianchi S, Walls AC, Bowen JE, Zhou J, Kaiser H, Joshi A, Agostini M, Meury M, Dellota E Jr, Jaconi S, Cameroni E, Martinez-Picado J, Vergara-Alert J, Izquierdo-Useros N, Virgin HW, Lanzavecchia A, Veesler D, Purcell LA, Telenti A, Corti D. Lectins enhance SARS-CoV-2 infection and influence neutralizing antibodies. *Nature*. 2021 Oct;598(7880):342-347. doi: 10.1038/s41586-021-03925-1. Epub 2021 Aug 31. PMID: 34464958.

[21]: Baker R, Peacock S. BEI Resources: supporting antiviral research. *Antiviral Res*. 2008 Nov;80(2):102-6. doi: 10.1016/j.antiviral.2008.07.003. Epub 2008 Aug 23. PMID: 18675849; PMCID: PMC2614313.

[22]: Kramzer LF, Hamorsky KT, Graebing PW, Wang L, Fuqua JL, Matoba N, Lasnik AB, Moncla BJ, Zhang J, Palmer KE, Rohan LC. Preformulation Characterization of Griffithsin, a Biopharmaceutical Candidate for HIV Prevention. *AAPS PharmSciTech* 22, 83 (2021). <https://doi.org/10.1208/s12249-021-01931-0>

[23]: Siddiqui S, Ahmed A. Griffithsin; A Potential Therapeutic Agent for SARS-CoV-2. *Acta Scientific Microbiology*. 2022 Jan 27;5(2):82-87.

[24]: Moulaei T, Shenoy SR, Giomarelli B, Thomas C, McMahon JB, Dauter Z, O'Keefe BR, Wlodawer A. Monomerization of viral entry inhibitor griffithsin elucidates the relationship between multivalent binding to carbohydrates and anti-HIV activity. *Structure*. 2010 Sep 8;18(9):1104-15. doi: 10.1016/j.str.2010.05.016. PMID: 20826337; PMCID: PMC3399781.

[25]: Kouokam JC, Huskens D, Schols D, Johannemann A, Riedell SK, Walter W, Walker JM, Matoba N, O'Keefe BR, Palmer KE. Investigation of griffithsin's interactions with human cells confirms its outstanding safety and efficacy profile as a microbicide candidate. *PLoS One*. 2011;6(8):e22635. doi: 10.1371/journal.pone.0022635. Epub 2011 Aug 2. PMID: 21829638; PMCID: PMC3149051.

[26]: Murray CJL, Piot P. The Potential Future of the COVID-19 Pandemic: Will SARS-CoV-2 Become a Recurrent Seasonal Infection? *JAMA*. 2021 Apr 6;325(13):1249-1250. doi: 10.1001/jama.2021.2828. PMID: 33656519.

[27]: NIH AIDS Research and Reference Reagent Program. "HIV Reagent Program." National Institutes of Health. 10801 University Boulevard, Manassas, VA 20110-2209. <https://www.hivreagentprogram.org/>

[28]: Chen B, Fan K, Fan M. Addgene. 490 Arsenal Way, Suite 100, Watertown, MA 02472. January 2004. <<https://www.addgene.org/>>